DISTRIBUTION OF ANTIRETROVIRALS WITHIN THE BRAIN TISSUE AND
RELATIONSHIP WITH NEUROCOGNITIVE IMPAIRMENT DUE TO HIV

Nithya Srinivas

A dissertation submitted to the faculty of the University of North Carolina at Chapel Hill in
partial fulfillment of the requirements for the degree of Doctor of Philosophy in the
Pharmaceutical Sciences (the Division of Pharmacotherapy and Experimental Therapeutics)
from the Eshelman School of Pharmacy

Chapel Hill
2018

Approved by:

Angela DM Kashuba

Kim Brouwer

Elena Batrakova

Amanda Corbett

Kevin Robertson

Alan Forrest

ABSTRACT

Nithya Srinivas: Distribution of antiretrovirals within the brain tissue and relationship with
neurocognitive impairment due to HIV
(Under the direction of Angela DM Kashuba)

As of the year 2015, 36.7 million people worldwide were living with HIV infection. While

the introduction of highly active antiretroviral therapy (HAART) has greatly reduced the

morbidity and mortality of HIV infection, there is still no cure for this disease. In the central

nervous system (CNS), HIV RNA in the cerebrospinal fluid (CSF) has been found even in

patients who otherwise have viral suppression in the plasma. Further, HIV infection in the

brain may lead to the development of HIV-associated neurocognitive disorders (HAND).

Milder forms of cognitive decline in HAND remain highly prevalent in people taking

HAART and this may be a function of ineffective antiretroviral (ARV) distribution in the

brain tissue. However, existing methods only measure ARV pharmacokinetics (PK) in the

CSF and are insufficient to explain brain distribution of ARVs. Therefore, the goal of this

project was to conduct a comprehensive analysis of ARV penetration into the brain tissue in

preclinical models, evaluate the role of drug transporters in modulating ARV brain tissue

disposition across species, and develop a model to predict disposition of one ARV (efavirenz

[EFV]) in human brain tissue using PK data from preclinical models and determine the

relationship between model-predicted drug exposure in the brain and neurocognitive

impairment in a cohort of HIV-positive participants.

In the first aim of the study, the brain tissue concentration and brain tissue:plasma penetration ratio of six ARVs were determined across two humanized mouse models and one nonhuman primate (NHP) model by LC-MS/MS. ARV brain tissue:plasma concentrations were only preserved across all three species for raltegravir, and showed no differences based on infection status or sex (in the NHPs). In the NHPs, ARV concentrations in the CSF were >6-fold lower than brain tissue. The CSF concentrations were poorly predictive of the brain tissue concentrations for all ARVs except EFV (r=0.91, p<0.001). Mass-spectrometry imaging could only detect EFV distribution within the brain, and greater accumulation was noted in the white matter vs. gray matter. The total colocalization to HIV target cell (microglia and CD4+ T-cells) area in the brain ranged from 45-80%. EFV was the only ARV to achieve concentrations $>IC_{90}$ in the brain tissue across all NHPs, however, MSI showed that <3% of HIV-target cells contained EFV at concentrations$>IC_{50}$ of viral replication.

In the second aim of the study, we noted significant differences in the gene expression of drug-transporters in the brain tissue across all three species. For example, the gene expression of Abcb1 was ten-fold higher in the hu-HSC-RAG mice compared to the BLT mice. The concentration of only BCRP and P-gp proteins were quantified in the majority of the brain tissue samples and there was 16-fold higher BCRP protein in the NHPs relative to the humanized mouse models. There were no differences in the expression of drug transporters due to infection status, but female macaques showed >two-fold higher protein expression of BCRP and P-gp compared to male animals. The protein concentration of transporters in the brain tissue did not predict the brain tissue:plasma concentration of any of the ARVs.

In the final aim of the study, we developed an eight-compartment PK model to describe the distribution of EFV into the CSF and brain tissue in rhesus macaques. Using the preclinical model structure and human PK data from a small clinical trial, the brain tissue distribution of EFV was predicted in our cohort of HIV positive participants. At steady state, EFV profile in the brain tissue was predicted to be flat with a median concentration of 8,000 ng/mL. Model-predicted brain tissue exposure showed good agreement with plasma (r=0.99, p<0.001). However, due to the high variability in the CSF measurements, the correlation between brain tissue and CSF concentrations in humans was poor (r=0.34, p=0.11). A 1,000-replicate Monte Carlo simulation of the final clinical model was able to capture observed EFV brain tissue concentration data available from three participants in the National Neuro-AIDS Tissue Consortium (NNTC) repository, indicating the biological plausibility of our model predictions. The model-predicted brain tissue exposures did not show any correlation with neurocognitive score measurements that were collected from the study participants (rho<0.05, p>0.05).

Through these experiments, it was determined that ARV penetration into the brain tissue is highly variable across preclinical models. With the limited ARV concentration data that are available from the human brain tissue, drug concentrations achieved in the brain tissue of NHPs closely approximate what is seen clinically. The CSF is not an appropriate surrogate for brain tissue PK of all ARVs investigated except EFV, and our surrogate measures of efficacy for EFV indicate that although the drug achieves high concentrations in the brain tissue, a lack of adequate spatial coverage over HIV-target cells may lead to reduced efficacy. There are several inter-species differences in drug transporter expression in the brain tissue; however, brain tissue transporter expression was not predictive of ARV

brain tissue penetration. Finally, our data demonstrate that sparse preclinical and clinical data can be leveraged to predict human brain tissue exposure of ARVs by the use of novel Bayesian models. Our small study suggests that factors other than ARV brain tissue PK may influence HAND persistence.

This thesis is dedicated to the memory of Dr. Alan Forrest.

To Ma, Pa, and Sandhya

Pat is VRT.

ACKNOWLEDGEMENTS

I would like to express my gratitude to my advisor, Dr. Angela Kashuba. My first interview at UNC was with Dr. Kashuba and I remember being awestruck from the moment I first heard her speak. The passion that Dr. Kashuba has towards her research has definitely made an impact on me, and in the past 4 years I have gained research know-how, presentation skills and built a strong work ethic with her unwavering encouragement and support. Thank you so much Dr. Kashuba for making me the researcher I am today, I could definitely not have done this without your incredible mentorship.

I am thankful to have had incredible support and encouragement from my dissertation committee and wanted to thank all of them for their generosity with their time, especially during the past 6 months. I would like to thank Dr. Kim Brouwer for agreeing to chair my committee and for her thoughtful input and additions to my dissertation project. Dr. Amanda Corbett brought invaluable expertise in the clinical implications of my project and Dr. Kevin Robertson added in a wealth of knowledge on the diagnosis and presentation of HIV-associated neurocognitive disorder. They both allowed me to see the big picture translation and scope of my project. I am very grateful to Dr. Elena Batrakova for her expertise on the mechanistic aspects of my project. Throughout the years she has encouraged me to ask a lot of questions and probe more into the underlying mechanisms to better understand the big picture. Finally, I would like to express my heart-felt gratitude to Dr. Forrest for his guidance and support in these past three years. When I first started interacting with Dr. Forrest in my second year of

graduate school, it was at a time when I doubted my capabilities in pharmacokinetics and pharmacometric modeling. It was through the incredible guidance of Dr. Forrest that I regained my confidence in these skills, and evolved as an independent researcher. Dr. Forrest was a brilliant scientist, a passionate pharmacometrician, and an incredible mentor to me and many others. For my work on this dissertation and other pharmacokinetic/pharmacometric heavy projects, Dr. Forrest provided me with a very strong foundation in pharmacometrics and fostered the interest in me to pursue research questions that can be enriched with modeling and simulation. Above all else, he was a kind man who was incredibly generous with his time, and always willing to put the needs of his students above his own. His dedication and love for pharmacometrics inspired many, and I hope to also carry that passion for my work throughout my professional career. For all these reasons and so many more, my heartfelt thanks to Dr. Forrest. May his soul rest in peace.

I want to express my thanks to all the members of the Kashuba lab, both past and present, for time very well spent as colleagues, confidantes, and friends. Mackenzie Cottrell, you were my second mentor in lab and I will forever remember your generosity and the midnight pizza while writing my first review article. Nicole White, for all your help with sample analysis and for all our food adventures. Eli Rosen, for teaching me about MALDESI and being a sounding board for the often-extensive troubleshooting that followed, Jason Pirone for your guidance throughout the various statistical aspects of my project. None of this work would have been possible with the extensive expertise of the analytical scientists in the lab and I would like to thank all of them for their contributions to this work: Amanda Schauer, Kimberly Handy, Nicole White, Stephanie Malone, and Craig Sykes. I want to thank John Dohnal, our lab manager, for all that he does to ensure our safety in the lab. Special thanks to

the people I shared a "cube" with: Dr. William Gilliland Jr, Erin Burgunder and Dr. Aaron Devanathan. I wish you guys all the best for all your future endeavors. In the almost four years I have been here, I feel very lucky to have met so many talented individuals with a shared passion for HIV research and am glad to have learned so much from them. I would especially like to acknowledge Dr. Corbin Thompson, a recent graduate of the Kashuba lab who has never hesitated to help me out with my experiments or walk me through the challenging aspects of my research. I am grateful for his support and perspective as a senior graduate student, especially during my first two years in the program.

Finally, my immense gratitude to the Royster Society of Fellows for their generous support of my stipend for the past four years, as well as for providing me with several professionally enriching opportunities. Thank you to Dr. Steve Matson, Dean of the Graduate School, Dr. Marsha Collins and Dr. David Pfennig, our Royster Professors, Julie Montaigne, Dr. Sandra Hoeflich and Theresa Phan. In particular, I am very grateful to have been given the opportunity to collaborate with fellow Roysters Nikhil Tomar and Elena Casey to teach a FYS for Fall, 2017. Thank you, Nikhil and Elena for giving me the chance to share in this experience with you and for allowing me to learn more about teaching and administrating a course.

My special thanks to the DPET division. Not only did I receive a wealth of scientific knowledge through coursework and consultations on my research projects, but I also received invaluable guidance and perspective on my professional development. In this regard, I would really like to thank Dr. Daniel Gonzalez, for the incredible job he does as our divisional director of graduate studies (DDGS), and for his input as my collaborator and mentor. Thank you to Dr. Craig Lee for recruiting me into this program, and Dr. Tim Wiltshire for his guidance as our first DDGS and beyond. I would like to thank several faculty in the division: Dr. Dhiren Thakker, Dr. Gauri Rao, Dr. Yanguang Cao, and Dr. Herb Patterson for your encouragement and support throughout the years. Thank you to the administrative staff of our division, Arlo Brown, Liza Ashton, Sara Pettway, Jessie Bishop, Julie Leemkuil and Anna Crollman.

I would like to specially thank the other members of my "cohort" of PhD students – Dr. Izna Ali, Olivia Dong and Dr. Jingxian Chen. We travelled together, made mistakes on the pharmacogenomics assignments together, and grew up as researchers together. I am able to see my own growth through all of your achievements and am so glad I had such a great group of people to hang out and swap experiences with throughout graduate school. I would also like to

one of the bravest people I know, travelling across the world at 18 and living on her own, which was something I definitely could not have done. I admire her immensely for her maturity, for her style and for her wit (which she got from me) and I am so excited for the bright future ahead of her.

As I write this, I am incredibly humbled by the wealth of individuals I had the fortune to meet, learn from and spend the last four years with. You all made this journey more fruitful, more memorable and much more enjoyable. Thank you so much.

TABLE OF CONTENTS

LIST OF TABLES

LIST OF FIGURES

LIST OF ABBREVIATIONS

Abcb1	Mouse ATP-binding cassette subfamily B member 1
ABCB1	Rhesus macaque/human ATP-binding cassette subfamily B member 1
Abcc1	Mouse ATP-binding cassette subfamily C member 1
ABCC1	Rhesus macaque/human ATP-binding cassette subfamily C member 1
Abcc2	Mouse ATP-binding cassette subfamily C member 2
ABCC2	Rhesus macaque/human ATP-binding cassette subfamily C member 2
Abcc4	Mouse ATP-binding cassette subfamily C member 4
ABCC4	Rhesus macaque/human ATP-binding cassette subfamily C member 4
AIC	Akaike information criterion
AIDS	Acquired Immunodeficiency Syndrome
ANI	Asymptomatic neurocognitive impairment
ARV(s)	Antiretroviral(s)
ATZ	Atazanavir
BBB	Blood brain barrier
B-CSF-B	Blood CSF barrier
BCRP	Breast cancer resistance protein
BLQ	Below the limit of quantification
BLT	Bone marrow, liver, thymus humanized mouse model
cART	Combination antiretroviral therapy
CSF	Cerebrospinal fluid
CWRES	Conditional weighted residuals

CYP450	Cytochrome P450
DTG	Dolutegravir
DTT	Dithiothreitol
EFV	Efavirenz
ENT1	Equilibrative nucleoside transporter 1
ER	Estrogen receptor
ERE	Estrogen receptor element
FTC	Emtricitabine
FTC-tp	Emtricitabine triphosphate
HAART	Highly active antiretroviral therapy
HAD	HIV associated dementia
HAND	HIV associated neurocognitive disorder
HIV	Human Immunodeficiency Virus
IF	Immunofluorescence
IHC	Immunohistochemistry
IPRED	Individual model prediction
IR-MALDESI	Infrared matrix assisted laser desorption electrospray ionization
ISH	In-situ hybridization
IT2S	Iterative two-stage estimation
LC	Liquid chromatography

LCMS/MS	Liquid chromatography tandem mass spectrometry
LLOQ	Lower limit of quantification
MAP	Maximum-a-priori
MDR1	Multidrug resistant protein 1
ML	Maximum-likelihood
MND	Mild neurocognitive disorder
MRP1	Multidrug resistance-associated protein 1
MRP2	Multidrug resistance-associated protein 2
MRP4	Multidrug resistance-associated protein 4
MS	Mass-spectrometry
MSI	Mass-spectrometry imaging
MVC	Maraviroc
NCA	Non-compartmental analysis
NHP	Nonhuman primate
NONMEM	Non-linear mixed effects modeling
NPD	Naïve pooled data
NRTI	Nucleotide reverse transcriptase inhibitor
NNRTI	Non-nucleotide reverse transcriptase inhibitor

Oat3	Mouse organic anion transporter 3
OAT3	Rhesus macaque/human organic anion transporter 3
OATP1A2	Rhesus macaque/human organic anion transporting polypeptide 1A2
Oatp1a4	Mouse organic anion transporting polypeptide 1a4 (mouse isoform)
Oct2	Mouse organic cation transporter 2
OCT2	Rhesus macaque/human organic cation transporter 2
PBMC(s)	Peripheral blood mononuclear cell(s)
PD	Pharmacodynamics
PEG	Polyethylene glycol
P-gp	P-glycoprotein
PK	Pharmacokinetics
PRED	Model prediction
PrEP	Pre-exposure prophylaxis
PVDF	Polyvinylidene difluoride
qPCR	Quantitative polymerase chain reaction
QTAP	Quantitative targeted absolute proteomics
RAL	Raltegravir
SHIV	Simian-human (chimeric) immunodeficiency virus

Slc22a2	Mouse solute carrier family 22 member A2
SLC22A2	Rhesus macaque/human solute carrier family 22 member A2
Slc22a8	Mouse solute carrier family 22 member A8
SLC22A8	Rhesus macaque/human solute carrier family 22 member A8
Slc29a1	Mouse solute carrier family 29 member 1
SLC29A1	Rhesus macaque/human solute carrier family 29 member 1
SLCO1A2	Rhesus macaque/human solute carrier organic anion transporter protein family member 1A2
Slco1a4	Mouse solute carrier organic anion transporter protein family member 1A4
TBS-T	Tris-buffered saline with Tween 20
TDF	Tenofovir disoproxil fumarate
TFV	Tenofovir
TFV-dp	Tenofovir diphosphate
TPL	Translational Pathology Laboratory
WB	Western blot
ZDV	Zidovudine

CHAPTER-I: CLINICAL PHARMACOKINETICS AND PHARMACODYNAMICS OF DRUGS ACTING IN THE CENTRAL NERVOUS SYSTEM[1]

1.1. Summary

Despite significant advances in the treatment of human immunodeficiency virus (HIV) infection, HIV may still persist within the central nervous system (CNS) and can cause a spectrum of neurocognitive deficits known as HIV-associated neurocognitive disorders (HAND). While the continued persistence of HAND despite therapy may be related to the concentration of antiretrovirals achieved in the brain tissue, it is difficult to quantify brain tissue concentrations pre-mortem in humans. Animal models can be used to determine the pharmacokinetics (PK) of antiretrovirals in the brain tissue and translate the relationship with efficacy to humans. However, a focused assessment is required to identify the differences in pharmacokinetics/pharmacodynamics (PK/PD) between animal models and humans. In this review, we summarize available literature from human studies on the PK and pharmacodynamics (PD) in brain tissue, cerebrospinal fluid, and interstitial fluid for drugs used in the treatment of neuroHIV as well as psychosis and Alzheimer's disease and address critical questions in the field. We also explore newer methods to predict the clinical PK and better characterize PK/PD relationships at the CNS target site for these classes of drugs.

1.2.   Introduction

Disorders of the brain contribute significantly to global disease burden. Psychiatric, neurological, developmental and substance abuse disorders affect more than 1 billion people worldwide(1). As of 2010, these were the leading cause of years lived with disability (YLD) globally, accounting for approximately 30% of all YLDs(2). However, CNS drug development is extremely challenging. Compared to non-CNS drug development, these programs have a lower clinical approval rate (6% versus 13%) and a longer time to market (12 years versus 6-7 years)(3–6). This has led to several companies withdrawing drug development programs in the neurosciences(7–9) signaling an uncertain future for novel research in CNS disorders.

Difficulty selecting initial drug dosage, untoward toxicities and lack of efficacy are cited as some driving forces behind the high attrition rate of CNS therapies(10). A robust concentration-effect analysis can provide valuable, reproducible information regarding both the therapeutic as well as adverse effect drug profile over a wide range of doses and greatly aid the development of CNS-acting drugs. However, a report from 2007 indicated that there were very few sets of pharmacodynamic data generated from human studies over a wide range of doses or concentrations(11). Although concentration-effect relationships are assessed in animals, animal models do not always accurately predict human disease, especially in case of CNS disorders(12). Difference in blood-brain barrier (BBB) permeability, drug metabolizing enzymes and transporters can lead to differences in drug exposure in the human brain compared to animals(13) and only rarely can drug be sampled from the human brain for pharmacokinetic (PK) measures. Further, animal models may only mimic some mechanisms of human CNS disease or contain targets not seen in humans, challenging the translation of efficacy and/or toxicity of novel therapeutics. Therefore, to address these issues a focused

pharmacokinetic/pharmacodynamic (PK/PD) assessment is required in humans to identify differences from animal models and adjust dosing. This has been accomplished by employing alternate methodologies such as in-vitro systems, translational studies or in-silico modelling to supplement the understanding of pharmacology within the CNS.

This review is broadly divided into three parts. In section 1.3, existing methods to measure PK and PD in the brain tissue, cerebrospinal fluid (CSF) and interstitial fluid (ISF) are reviewed. While there is abundance of PK/PD information from animal models in the CNS, less complete information is available from human studies. In sections 1.4-1.6, we examine clinical PK/PD analyses at relevant target sites in the CNS for antipsychotics, anti-Alzheimer's drugs and antiretrovirals and examine the utility of available information and the need for more research to answer critical questions in the field. In the absence of clinical results, available animal data are presented and cautiously interpreted for clinical relevance. Finally, new methods to improve CNS drug development are examined in section 1.7.

1.3.   Methodology

An extensive literature search was performed to identify research articles and conference abstracts published in Embase (including articles in the MEDLINE® database) using terms for drugs used to treat disorders of the brain and CNS, combined with terms for PK or PD and terms for the brain and CNS. A full search strategy is provided in **Appendix 1.1**. These searches were augmented by targeted searches in PubMed, Google Scholar, and Google Books, which combined terms from the full search strategy, plus additional terms for PK or PD

measures or factors affecting these measures. The bibliographies of relevant review articles were also hand searched for additional relevant studies.

1.4. Pharmacokinetic and pharmacodynamic considerations for drugs acting in the CNS

1.4.1. Measures of drug pharmacokinetics in the CNS:

Drug distribution into the CNS has been characterized by several methods: measuring drug uptake into cultured brain cells (in-vitro), or measuring drug concentration in the brain tissue (ex-vivo) or CSF or ISF (in-vivo).

In-vitro models of the BBB are used as a first line-approach for determining the extent to which investigational agents cross into the brain(14). There are several validated models of the BBB from multiple species(15) and while no ideal cell line exists, the human cell line most widely used and well characterized is the human immortalized endothelial cell line hCMEC/D3. hCMEC/D3 experiments can quantify drug permeability, identify relevant drug-efflux transporter interactions, rapidly screen drug candidates for CNS activity and carry out initial PK studies. However, these models are a static measure of drug PK. For anti-infectives in particular, these models do not account for time-dependent killing and may be less clinically relevant. In-vitro systems also do not fully replicate all in-vivo features of the BBB. For example hCMEC/D3 is more "leaky" than the BBB, and can express lower levels of BBB-specific enzymes and drug transporters(15). Therefore, in-vitro systems may have to undergo modification such as co-culture with other brain cells to replicate tight junctions of BBB.(16)

Newer microfluidic technologies such as BBB-on-a-chip or neurovascular-unit-on-a-chip(17) hold promise to mimic the dynamic in-vivo environment.

There are several ex-vivo approaches to measuring drug concentrations in brain tissue either after surgical resection or necropsy. Most PK information comes from brain tissue homogenates using liquid chromatography-mass spectrometry (LC-MS) analysis. These measurements are then used to calculate ISF and intra-cellular fluid (ICF) concentrations(18). Though commonly used, these methods do not provide information about drug localization. Mass spectrometry (MS) imaging has emerged as a method to quantify drug molecules by MS and spatially visualize drug distribution in tissue slices(19). The advantage of MS imaging is that it can capture drug distribution patterns within different regions of a tissue(20). For example, using Matrix Assisted Laser Desorption Ionization (MALDI) imaging MS, the anti-tubercular drug pretomanid was found to localize predominantly in the corpus callosum of Sprague Dawley rats(21). By using serial sections collected at different time points, it was shown that pretomanid distributed into the corpus callosum 1-2 hours after an intraperitoneal dose of 20mg/kg and diffused into other parts of the brain at later time points. With advances in imaging technology, this technique may be used to image intracellular drug concentrations and can be coupled with PD targets through immunohistochemistry (IHC) or in-situ hybridization in contiguous slices. While this has not yet been demonstrated for brain cells, Aikawa et al. used hematoxylin and eosin (H&E) along with IHC staining for CD31 and multidrug resistance transporter 1 (MDR1) to show the colocalization of anti-cancer drug alectinib with blood vessels in murine brains(22). A drawback of ex-vivo imaging is that it is a static measurement, and a composite of multiple images from different animals is required to gain information across a dosing interval.

In-vivo imaging techniques, such as Positron Emission Tomography (PET), can provide longitudinal information on drug disposition. PET is a non-invasive imaging technique that relies on the detection of radio-labelled ligands over time. It has been used to measure absolute spatial concentration of drug and determine PK parameters as well as target occupancy of several CNS-acting drugs. While a detailed discussion of PET is beyond the scope of this review, the reader is directed to a 2013 review(23) for a detailed summary on estimating PK parameters using PET studies. Despite the spatial advantages and applicability to human studies, PET scans are expensive, generally limited to fewer patients because of the use of radioactivity and may not distinguish between parent compound and metabolites.

Other in-vivo drug estimation methods measure drug penetration into fluid compartments of the CNS. Microdialysis involves inserting a dialysis probe into the cerebral region of the brain to measure the protein-unbound concentration in the ISF. This technique is regularly used in animal models for continuous monitoring of drug concentration, but is only applicable during intra-operative procedures in humans(24). Further, this procedure might not be suitable to measure the concentration of highly lipophilic or protein bound drugs as there can be a high degree of non-specific binding to the microdialysis probe and poor recovery of drug from the fluid(24,25). Additionally, intracellular active metabolites are not captured using this technique.

The most common approach to generating PK data is drug sampling in CSF. This is done by lumbar puncture for a single sample and spinal catheterization in the subarachnoidal space for continuous sampling. While less invasive than microdialysis, lumbar punctures are painful and not without medical risks, and are not routinely performed. Also, concentrations measured by lumbar puncture can differ based on the location and time of measurement(13).

For example, using a mathematical model, phenytoin was predicted to reach 300% greater concentration in cranial CSF than spinal CSF(26). Generally, unbound CSF concentrations are used as surrogates for unbound brain tissue concentrations in animal models(27) based on the free drug hypothesis which stipulates that protein-unbound drug passively moves from the plasma through the BBB and blood-CSF barrier (BCSFB) into the brain and CSF(28). However, this generalization holds true for certain drugs(29,30) with two significant exceptions: i) Drugs that use membrane transporters for influx and efflux (Eg. antidepressants, antiretrovirals [ARVs]) and ii) Drugs with low permeability to cross through the BBB where CSF bulk flow exceeds passive diffusion of the compound into CSF(31). For substrates of efflux membrane transporters such as P-gp, CSF concentrations tend to overestimate ISF concentrations(32). While the exact reason for this observation remains unknown, some hypotheses include subapical or apical localization of P-gp on the choroid plexus that results in drug transfer and accumulation into the CSF(33), or non-functionality of P-gp at the BCSFB(34). Since the CSF is recycled at a faster rate than ISF, the CSF acts as a "sink" to clear drug(31). For high permeability compounds, this effect is negligible but for low-permeability compounds, CSF concentrations underestimate the brain or ISF concentrations (Eg. morphine 6-glucuronide). Therefore, the unbound concentration in the brain may differ from the CSF concentration and confound target site assumptions.

In case of in-vivo measurements made at a single time point, the concentration of drug in brain or CSF may be normalized to a simultaneously-collected plasma concentration. While this is a common means of estimating the extent of drug uptake into the CNS, and allows for comparisons of uptake between drugs, the rates of entry and elimination of the drug in plasma, CSF and brain compartments differ(35). For example, the CSF:plasma concentration ratio for

7

ciprofloxacin increases by as much as 1400% over 24 hours(35). One approach to avoid this confounding is to use sparse serial sampling in a group of animals or humans to characterize the drug's full PK profile in the CSF and plasma and calculate the ratio of drug exposure in the two compartments by measuring the area under the concentration-time curve. This approach has been performed for several anti-infective drugs(36) during ventricle catheterization when CNS infections need to be monitored(37) or excess CSF fluid needed to be drained(38,39). Due to difficulties in obtaining multiple CSF samples from patients, population PK modeling has been used with sparse CSF and plasma sampling in order to obtain exposure profiles of various drugs such as abacavir(40).

1.4.2. Intracellular vs. Extracellular drug concentrations:

When considering the site of action, it is important to distinguish between extracellular and intracellular CNS drug concentrations. For drugs that act on receptors on neuronal cell membranes such as anti-epileptic drugs (AEDs) and anti-Alzheimer's drugs, it is preferable to measure drug concentration in the ISF where the PD effect is exerted. Extracellular acting drugs have been measured in brain tissue homogenates, but this approach may be misleading. For AEDs and other basic drugs (pKa >7) where brain volume of distribution is greater than brain water volume (0.8 mL/g), ISF concentrations are over-estimated by brain tissue homogenate due to non-specific binding in brain tissue(41,42). For anti-infective and anti-cancer drugs which act on intracellular targets, the unbound intracellular drug concentration is the most appropriate PK measure linked with activity. Friden and colleagues demonstrated a method to indirectly estimate unbound intracellular drug concentration. Briefly, in-vitro volume of distribution of unbound drug in brain ($V_{u,brain}$) is measured in brain slices from drug-naïve animals incubated in drug containing buffer (brain slice method(43)) and fraction of

unbound drug in the brain ($f_{u,brain}$) is measured by adding drug to brain homogenates from drug-naïve animals(18). The ratio of intracellular to extracellular unbound drug concentration ($K_{p,uu,cell}$) is given by **Equation 1.1**.

$$K_{p,uu,cell} = V_{u,brain} * f_{u,brain} \tag{1.1}$$

Using this method, intracellular drug concentrations of gabapentin, oxycodone, morphine and codeine were found to be greater than extracellular concentrations(18).

1.4.3. Factors affecting pharmacokinetics of drugs in the CNS:

Many factors have been identified to affect drug exposure in the CNS. These are summarized in **Figure 1.1**. For an in-depth analysis on specific classes of drugs, the reader is referred to two excellent reviews(36,44).
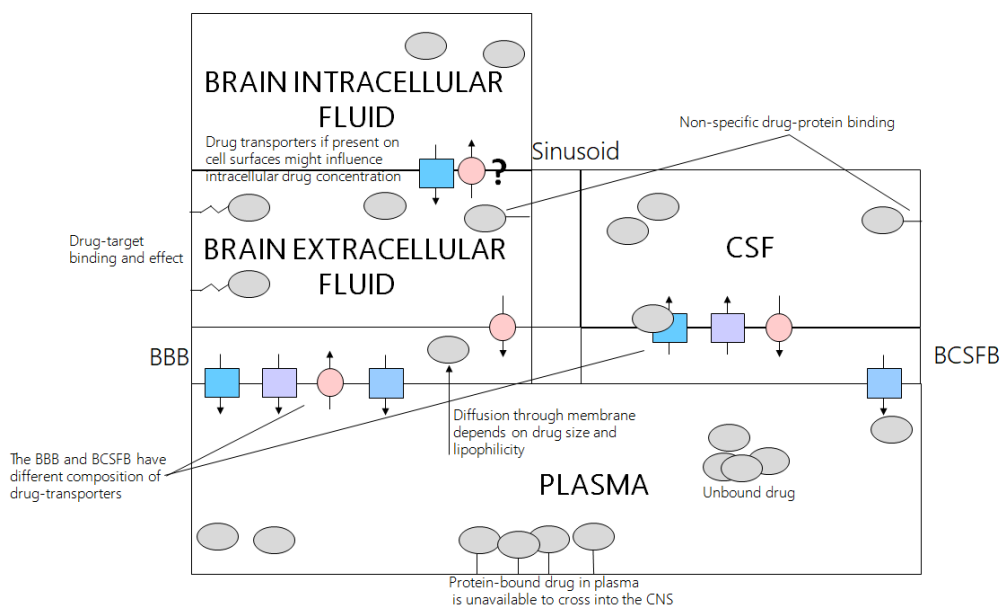
Figure 1.1. Factors affecting the pharmacokinetics and pharmacodynamics of drugs in central nervous system. This figure demonstrates various factors the influence pharmacokinetic and pharmacodynamic activity in CNS and highlights various compartments of drug action. Effect of drug transporters, physicochemical properties and specific and non-specific protein binding are illustrated. Drug transporters along the membranes may also co-localize which leads to bidirectional movement of drugs. Legend: BBB – blood brain barrier, BCSFB – blood CSF barrier

a) Protein Binding – Protein binding influences the entry and activity of drug into the CNS. Drugs that are highly protein bound in the plasma concentrate to a lesser extent in the CSF and brain tissue. Conversely, for drugs that accumulate intracellularly in brain tissue such as gabapentin and morphine, the degree of plasma protein binding is low (3% for gabapentin and 20% for morphine). The degree of protein binding varies between plasma, CSF and tissue, based on the concentration of drug-binding proteins. For albumin, concentrations range from 35-50g/L in plasma and are <250mg/L in CSF. For AAG, concentrations are approximately 0.77g/L in plasma and 8.4mg/L in CSF(31). These proteins can also be synthesized by microglial cells(45). Therefore, while highly protein-bound drugs (>95% protein binding) such as efavirenz and fluoxetine have lower total drug concentrations in the CSF compared to blood plasma, protein-unbound drug concentrations are similar in both fluids. In general, use of unbound drug concentrations in the CSF leads to mechanistic PK/PD relationships(46) and better translatability between species(47).

b) Drug Efflux Transporters – Drug efflux transporters such as MDR1 (P-glycoprotein), BCRP and MRP4 are highly expressed at the BBB(48–50). MDR1 and MRPs have also been identified on the surface of astrocytes(48). Studies using transporter knockout (KO) mice have shown that MDR1 KO increases brain concentrations of MDR1 substrates by 10-100 fold(51), while the KO of BCRP and MRP4 has minimal effect(52,53). Therefore, MDR1 inhibition should be a viable option to increase the CNS exposure of drugs in rodent models. Indeed, it has been shown that the co-administration of MDR1 inhibitors (eg. cyclosporin or zosuquidar) increases CNS brain penetration of MDR1 substrates such as nelfinavir or paclitaxel(54). For indinavir(55), increased CSF penetration was demonstrated in HIV-infected patients when MDR1 inhibitor ritonavir, was given

concomitantly. Although there was increase in plasma exposure, this was driven by a 5-fold increase in trough concentration. Linear regression analysis showed that increase in CSF concentrations (2.67 fold) was not explained by increase in plasma concentrations alone, and inhibition of efflux transporters at the BBB might also contribute to increased CSF exposure of indinavir.

c) Physicochemical properties– Lipophilic drugs show greater permeability through the lipophilic BBB. In a study of compounds ranging from highly polar (sucrose, logD = -4.49) to highly lipophilic (estradiol, logD = 4.14), the log brain uptake index (BUI) of estradiol in Sprague-Dawley rats was 232 times higher than sucrose[56]. However, a higher lipophilicity also results in a higher degree of non-specific tissue binding[57]. In a study of 7 compounds that ranged in BBB permeability by 160-fold, the highly lipophilic compound fluoxetine showed the greatest permeability through the BBB (evidenced by the highest permeability surface area product of 600 ml/kg*hr) of Sprague-Dawley rats but a free drug fraction (0.23%)[58] that was lower than plasma (6-15%). Similarly efavirenz has a permeability surface area product of 2.4 ml/kg*hr through the BBB and a free fraction of only 0.197%[59] in rat brain tissue, compared to 1% in blood plasma.

1.4.4. Measures of drug pharmacodynamics in the CNS:

Many PD targets are utilized in CNS disorders. In the following section, common clinical PD endpoints are summarized. The pros and cons of these measures are outlined in **Table 1.1**.

a) Receptor occupancy/ binding affinity:

Receptor occupancy and binding affinity are related in that receptor binding affinity is an in-vitro measure of the concentration of ligand resulting in a ligand-receptor complex while receptor occupancy is the proportion of receptors that have formed a ligand-receptor complex in-vivo relative to the baseline receptor density. The examples of the N-methyl-D-aspartate (NMDA) receptor agonists amantadine and memantine are illustrative of the binding affinity concept. Amantadine and memantine have weak affinity to the σ site of the NMDA receptor with binding affinities of 20.25 ± 16.48 uM and 19.98 ± 3.08 uM respectively[60]. The drugs showed higher affinity to the PCP binding site on the receptor (10.5 ± 6.1 uM for amantadine and 0.54 ± 0.23 uM for memantine). By taking into account the therapeutic concentrations of these drugs attained in the human brain[60], it was determined that amantadine acted at both the σ and PCP binding site, while memantine only acted at the PCP binding site. Receptor occupancy studies have been performed for several classes of drugs by means of PET scans and clinical data are available for dopamine D1 and D2 receptors (antipsychotics[61–63]), histamine H1 receptor (antidepressants[64]) and serotonin 5-HT 2 receptor (antipsychotics[63]).

b) Change in behavioral symptoms and clinical ratings scales:

For Parkinson's, depression and psychosis, the Unified Parkinson's Disease Ratings Scale (UPDRS)(65), Hamilton – Depression Rating Scale (HAM-D)(66) and Brief Psychiatric Rating Scale (BPRS)(67) respectively are widely used by clinicians to aid with diagnosis and progression of the disease as well as assess PD. In case of Alzheimer's, the Alzheimer's Disease Assessment Scale (ADAS) is commonly administered in almost all clinical trials of symptomatic Alzheimer's(68). However, several other ratings scales have been developed for Alzheimer's. A review published in 2010 identified 68 distinct, relevant scales(68), though only 5 of these scales met the requirements for a robust multi-domain assessment of the disease.

c) Neuroimaging markers:

Neuroimaging modalities can be used for several different PD measures. For example, in case of anti-depressants(69), PET scans have been used to derive receptor abundance and occupancy profiles in-vivo while functional magnetic resonance imaging (fMRI) provides information about changes in brain structure and white matter integrity.

d) PD endpoints for anti-infectives:

Common PD endpoints include time to mitigation of neurological symptoms such as headache, confusion and muscle weakness and lowering of antimicrobial load (eg. bacterial count, HIV viral RNA) in the CSF. Antibiotics are used to target CNS infections on the basis of in-vitro MIC and IC_{50} (drug concentration that yields 50% inhibition of microbial growth). Similarly, antiretrovirals may be selected for activity in the CNS on the basis of in-vitro IC50 values(70). HIV also causes a spectrum of neurocognitive deficits in patients

and in such instances, neurocognitive test scores, such as the global deficit score (GDS) have been developed as a PD measure to provide a baseline of neurocognitive impairment and track disease progression(71).

Table 1.1: Commonly used pharmacodynamic measures for CNS drugs and the advantages and disadvantages of each technique

Class of drugs / pharmacodynamic measure	Advantages	Disadvantages
I. Drugs used in psychiatric and neurological disorders		
1. Receptor occupancy/ binding affinity	+ Direct measure of efficacy of drug + Can be used for interacting drugs on different receptor sites	+ Discrepancy between in-vitro and in-vivo values + Species differences may result in difficulties in translation
2. Change in behavioral symptoms and clinical ratings scales	+ Are easy to understand clinically + Non-expensive + Can be made longitudinally to track progression of the disorder + Non-invasive	+ Difficult to translate between animal models and humans + Some disorders (Alzheimer's) present with several ratings systems which may not always agree. This causes issues with interpretation
3. Neuroimaging markers	+ Can provide more detailed information than subjective tests	+ PET scans are expensive + With fMRI, there is exposure to high-intensity magnetic fields
II. Anti-infectives		
1. Mitigation of symptoms	+ Easy to make PD measurement	+ May be subjective + May be difficult to interpret PK/PD relationship
2. Bacterial count/ viral load in CSF	+ Straight-forward correlation	+ Invasive procedure which can be painful

Class of drugs / pharmacodynamic measure	Advantages	Disadvantages
		+ Not enough information on whether CSF measurements approximates brain tissue measurements
3. Neurocognitive scores for HAND	+ Non-invasive procedure +Technique accounts for comorbidities	+ Research tool that is not used clinically

The following three sections examines currently available target site clinical pharmacology data for three disease states: Psychosis/Schizophrenia, Alzheimer's disease and neuro-HIV. The reader is referred to **Table 1.2** for more detailed information on the studies that are referenced in this manuscript.

1.5.   Clinical pharmacokinetics and pharmacodynamics of antipsychotics in the CNS:

Since chlorpromazine was approved over 60 years ago, there are now 21 FDA-approved first- and second-generation antipsychotics for the treatment of pediatric and adult psychosis. Despite significant advances in the field, a critical area that is yet to be fully addressed with these drugs is the variability in PD response required for efficacy, and the relationship to target site exposure. There is also lack of consensus on the appropriate PK target measure to correlate to anti-psychotic efficacy.

Anti-psychotic drugs are known to penetrate readily into the brain. For example, haloperidol is found in the brain tissue at concentrations that are 10-30 times higher than serum concentrations(72). Further reports of brain tissue concentration of antipsychotics are available

from autopsy tissue: a 2012 analysis in the prefrontal cortex tissue from 18 human autopsy samples noted high concentration of several drugs such as olanzapine (33,378 ng/g) and quetiapine (16,769 ng/g)(73). However, such reports often include no supporting information such as plasma concentrations and post-mortem interval of collection and are therefore difficult to interpret. Given that olanzapine and the other drugs showed a range from undetectable (<2ng/g) to high concentrations, the authors postulated that the exceedingly high concentrations were the result of overdose. Therefore, such studies may not provide accurate information about the therapeutic range of concentrations of antipsychotics. For the newer antipsychotics aripiprazole, lurasidone, and perospirone, clinical brain PK is unknown(74). However, extensive tissue distribution is evidenced by their large apparent volume of distribution of 400-6000 L(74). In the absence of brain tissue concentration data, CSF concentration may be predictive of unbound brain tissue PK(27), although this has not been verified in humans. Antipsychotics extensively enter the CSF(31) and historical estimates of total CSF:plasma protein-unbound concentration ratios for the older agents are indicative of significant binding to CSF proteins. For example, from a study of thioridazine in 48 patients, lumbar puncture followed by venipuncture was performed to obtain ratios of parent drug and metabolite in CSF compared to plasma. The average total CSF:unbound plasma ratio of thioridazine was determined to be 6 and ranged from 1.9 – 16.9(75), although it is unknown if all the patients in this analysis were under steady state conditions or what the time of sampling of CSF and plasma were relative to the dose(75). From the same analysis, mean free fraction of thioridazine in the CSF was 49% and the unbound concentration in CSF was twice that in plasma, possibly on account of passive diffusion of thioridazine across BBB. A significant correlation (p=0.002) was shown between the unbound concentration of thioridazine in plasma

and CSF(75), suggesting that unbound concentrations in plasma could potentially be used as a surrogate for CSF concentrations or neuroleptic efficacy. In a later study, the plasma from 53 patients newly started on 200mg/day thioridazine was sampled 12 hours post-dose 6 times over the course of two weeks. However, this analysis did not establish any link between plasma concentrations of thioridazine and anti-psychotic efficacy(76).

Substrates of drug efflux transporters (eg risperidone and P-gp affinity), may show a lack of correlation between plasma and CSF concentrations. In these cases, other correlates of efficacy such as unbound CSF drug concentrations need to be used. More recent PK/PD analyses have explored the relationship between CSF concentration of anti-psychotics and receptor occupancy data(77,78). In general, while CSF concentrations of antipsychotics correlated with efficacy (eg chlorpromazine)(79,80), this is not always the case due to difficulties in quantifying low CSF drug concentrations (eg. haloperidol)(79,81). Another potential confounder in the relationship between drug concentration and efficacy occurs if there is metabolism to a moiety with anti-psychotic effect. For example, the active metabolite of risperidone, 9-hydroxyrisperidone (paliperidone) is itself a marketed antipsychotic.

The importance of combined PK/PD modeling compared to PD alone has been demonstrated for anti-psychotics. Aripiprazole was dosed in 18 subjects from 2mg to 30mg, and PET scans were taken pre-dose and 3, 4, 5, and 120 hours post-dose(82). Hysteresis was present in the relationship between dopamine receptor occupancy and plasma concentrations due to delayed effect site equilibration. This resulted in the EC50 value changing based on the type of modeling performed. With the combined PK/PD analysis of predicted effect site concentration versus receptor occupancy, the EC50 was 8.6ng/ml(82). However, considering only PD, the EC50 was slightly higher (11.1 ng/mL) due to hysteresis causing a change in the

concentration-response slope. Therefore, for drugs where there is discrepancy between the time course of measured plasma concentration and receptor occupancy(82,83), a combined PK/PD analysis results in more reliable estimates of activity and accurate PD endpoints.

1.6. Clinical pharmacokinetics and pharmacodynamics of drugs used to treat Alzheimer's disease in the CNS

In the fall of 2017, interpedine and verubecestat were the latest drug failures for Alzheimer's disease(84). An examination of the clinical pharmacology of the currently approved drugs for Alzheimer's identifies several potential sources for failure of clinical trials. Alzheimer's is a progressive disease where deteriorating brain pathology may lead to altered drug concentrations in the brain. This may be challenging when interpreting PK results from healthy volunteers or animal models. For example, a recent PET scan analysis performed 2.5-3 hour (Tmax) after a single oral dose of 1mg or 30ug ^{11}C-donepezil in four healthy women(85) showed that the mean standardized unit value for mean intensity of pixels imaged (SUV$_{mean}$) was 0.9 in the brain for both doses which is indicative of an almost even distribution of radioactivity in the brain compared to the rest of the body. However, in a study of donepezil in patients with Alzheimer's, despite achieving concentrations in the CSF that were ten times lower than plasma, higher concentrations at 24 hours post-dose compared to 12 hours post-dose was observed in CSF but not plasma(86,87). This is thought to be due to the degradation of P-gp protein in the progressive pathogenesis of Alzheimer's (donepezil is a substrate of P-gp) that reduces the efflux of drug from CSF(87). Given the localization of P-gp in BBB and its role in the efflux of drugs from the brain tissue, one might expect similar accumulation of donepezil to occur in brain tissue of Alzheimer's patients as well, however, this is unknown. Another consideration is the suitability of surrogate PK measurements and their relationship

with target site concentrations. For the NMDA receptor antagonist memantine, concentrations in the CSF from six patients (0.05-0.3uM) were 50% lower than serum concentrations(88) while the brain tissue concentration of memantine measured from a single autopsy patient (5.7 mg/kg) was 2.7-times higher than the heart blood concentration (2.1 ug/ml) and 6.9-times higher than the femoral blood concentration (0.83 ug/ml)(89). While such data may be too sparse to interpret, memantine is a basic compound (pKa = 10.7)(88), and sequestering within acidic lysosomes via pH partitioning and lysosomal trapping may be responsible for the enhanced brain accumulation of the drug compared to CSF. While clinical brain tissue concentrations are unknown for the acetyl cholinesterase (AChE) inhibitor rivastigmine(90), continuous CSF sampling in 18 patients at steady state for up to 12 hours post-dose(91) demonstrated that rivastigmine exhibited differential PK in plasma and CSF. The Cmax in CSF was lower than plasma by 2- to 4-fold and Tmax in CSF was longer than plasma (1.4-3.8 hours compared to 0.5-1.67 hours).

There is limited data on the utility of PD measures in patients with Alzheimer's disease. For example, an earlier review noted complications of using AChE activity measurements as an outcome measure due to confounding by a number of factors such as diet, concomitant medication or time of lumbar puncture(92), making the effect size of PK/PD analyses more difficult to interpret. Further, while there are some studies that utilize plasma concentrations to correlate with treatment outcomes(93), plasma concentrations must first be validated as an appropriate surrogate for the target site.

1.7.   Clinical pharmacokinetics and pharmacodynamics of antiretrovirals in the CNS

In 2007, research nosology in the field of HIV was updated(71) to provide guidance on the neurocognitive disorders caused due to HIV – collectively called HIV-associated neurocognitive disorders (HAND). Since this time, the CNS has been implicated as an anatomical reservoir for HIV(94–97), capable of harboring latent viral infection in macrophage and microglia cells in the brain. To advance our understanding of both the treatment and potential cure for HIV in the CNS, it is imperative to understand the PK of antiretrovirals (ARVs) in the CNS and their relationship with neurocognition and latent reservoirs.

ARV PK has been extensively studied in the CSF and the reader is referred to two reviews summarizing this topic(44,98). Using measures of CSF PK of ARVs along with physicochemical properties of the drugs and clinical utility, Letendre and colleagues devised a CNS-penetration effectiveness (CPE) score that accounts for efficacy of ARVs and extent of penetration into the CNS(99). The scores range from 1-4 with 1 being less effective (having lowest CNS penetration), and 4 being most effective (having highest CNS penetration)(99). ARVs having higher CPE score cause greater reduction in viral load in the CSF in HIV patients(100). However, the correlation between CPE score and degree of neurocognitive impairment in patients with HAND is variable. For example, while improvement in neurocognitive function was noted by using agents with a higher CPE score in some studies(101), there are instances where higher CPE was not associated with neurocognitive improvement(102), or where higher CPE was associated with poorer functioning(103,104).

Given the contradicting PK/PD results, one hypothesis is that brain tissue concentration of ARVs may be a better predictor of neurocognitive impairment in patients with HAND. However, there are sparse clinical data on the agreement between CSF and brain tissue

concentrations of ARVs. In a small study by Bumpus and colleagues, sub-compartmental brain tissue concentration of ARVs were evaluated in nine HIV-positive adults who had AIDS at the time of death(105). Concentrations in white matter, cortical gray matter and globus pallidus regions of the brain were taken from necropsy samples, and compared to historical CSF concentration data(105). No difference in brain and CSF concentration was found for efavirenz, emtricitabine, atazanavir and lamivudine. However, for tenofovir, the overall brain concentration of 206 ng/g was 37-fold higher than CSF. For lopinavir, a protease inhibitor, greater accumulation was found in white matter (>400 ng/g) compared to other brain regions (<25 ng/g). Contrary to these data, a recent in-silico model(59) predicted that efavirenz accumulates in brain tissue, with a median tissue-plasma penetration ratio of 15.8. Data recently published in 12 nonhuman primates(106) showed that tenofovir, emtricitabine, efavirenz, raltegravir, maraviroc, and atazanavir all reached higher total concentrations in brain tissue compared to CSF at trough. For efavirenz, the brain tissue to CSF concentration ratio was highest (769-fold) and brain tissue-plasma penetration ratio ranged from 3-5.7, indicating accumulation of efavirenz. Since information on patient adherence was not available for the Bumpus study and comparisons between brain tissue and CSF concentrations were made with historical CSF estimates, low adherence to an ARV regimen before death could explain why efavirenz concentrations were equivalent to the CSF measurements and much lower in these samples than that demonstrated in the nonhuman primates or predicted in the model.

A critical area for future investigation is PK/PD correlations as they relate to development of latent reservoirs in target cells of the brain tissue. With advances in mass spectrometry imaging, this work may be able to determine specific distribution patterns of ARVs in the brain(20) that can lead to differential viral growth or establish latency if there is

insufficient ARV coverage. Another area of research is to understand the optimal range of intracellular concentration that can prevent HIV cellular infection without CNS toxicity(107).

Table 1.2: Summary of pharmacokinetic and pharmacodynamic measurements made in the CSF and brain tissue for anti-psychotic drugs, anti-Alzheimer's drugs and antiretrovirals in human studies

Authors	Study population	Sample size	Drug(s)	Parameters and Results	Reference
I. Psychosis					
Pharmacokinetics					
Wode-Helgodt et al.	Humans with a psychotic disorder	44	Chlorpromazine	CSF and plasma were analyzed. Clinical improvements in patients with drug concentrations greater than 1ng/ml in CSF and 40ng/ml in plasma	(80)
Kornhuber et al.	Postmortem brain tissue of humans treated with Haloperidol	11	Haloperidol	Liquid chromatography was used to measure concentrations in 5 brain regions. Drug concentrations were 10x higher than serum concentrations optimal to treat schizphrenia. Elimination $T_{1/2}$ from brain tissue was estimated by population PK analysis and was 6.8 days	(72)

Authors	Study population	Sample size	Drug(s)	Parameters and Results	Reference
Rimón et al.	Humans with chronic schizophrenia	12	Haloperidol	At steady-state, CSF and serum concentrations 12 hours post-dose were compared. CSF concentrations were 4.3% of serum	(81)
Sampedro et al.	Postmortem brain tissue	18	Amisulpiride, haloperidol, levomepromazine, norclozapine, olanzapine, paliperidone, quetiapine, risperidone, Sulpiride, triapride, ziprasidone	Liquid chromatography tandem mass spectroscopy was used to measure concentration of 17 antipsychotics in the prefrontal cortex. Concentrations below lower limit of quantification noted in ten samples. Some samples had high drug concentrations indicating drug overdose	(73)
Nyberg et al.	Humans with a psychotic disorder	48	Thioridazine	Paired CSF and blood samples were obtained. Collection time-point is unclear. Mean total concentration was 19.4nmol/L in CSF Free fraction in CSF = 49.1%	(75)
Pharmacodynamics					
Kim et al.	Healthy volunteers	18	Aripiprazole	PET was used to measure dopamine receptor	(82)

Authors	Study population	Sample size	Drug(s)	Parameters and Results	Reference
				occupancy at 3, 45 and 120 hours post-dose. EC50 = 11.1ng/ml from PD modeling. EC50 = 8.63ng/mL from PK-PD modeling	
Yokoi et al.	Healthy volunteers	15	Aripiprazole	PET was used to measure D2 and D3 occupancy after two weeks of daily dosing. Dose dependent receptor occupancy from 40-95% observed	(61)
Farde et al.	Humans with a psychiatric disorder	14	Chlorpromazine, Clozapine, flupentixol, haloperidol, melperone, perphenazine, pimozide, raclopride, sulpride, thioridazine, thioxanthene, trifluperazine hydrochloride	PET was used to measure dopamine receptor occupancy at steady-state, 6 hours post-dose 65-85% D2 receptor occupancy across the 11 drugs	(62)
Mamo et al.	Humans with schizophrenia	16	Ziprasidone	PET was used to measured dopamine and serotonin occupancy after 3 weeks of administration at trough. Occupancy at 5-HT2 was 76% and at D2 was 56%	(63)
II. Alzheimer's disease					

Authors	Study population	Sample size	Drug(s)	Parameters and Results	Reference
Pharmacokinetics					
Mochida et al.	Healthy women	4	^{11}C-Donepezil	Women were orally administered 1mg and 30ug ^{11}C-Donepezil and underwent PET scan 2.5 hours post-dose Mean standardized unit value for mean intensity of pixels imaged was 0.9 in the brain, indicating even distribution of radioactivity in brain as the rest of the body	(85)
Valis et al.	Humans with Alzheimer's	16	Donepezil	Donepezil concentrations in CSF were measured via liquid chromatography. CSF concentration higher at 24h (7.54ng/ml) vs 12hr (5.19ng/ml). No accumulation in plasma	(86)
Darreh-shori et al.	Humans with Alzheimer's	104	Donepezil	CSF and blood AChE measured via Ellman's colrimetric assay. Collection timepoint is unclear, but all patients were at steady-state. CSF concentrations	(87)

Authors	Study population	Sample size	Drug(s)	Parameters and Results	Reference
				were 10x lower than plasma. CSF AChE-S inhibition was 30-40% after 5mg dose and 45-55% after 10mg dose.	
Kornhuber et al.	Humans with mild to moderate dementia	6	Memantine	Plasma and CSF measured 2-3 hours after dose in 4 patients CSF concentration was 0.05-0.3uM and 50% lower than in serum	(88)
Rohrig et al.	Postmortem human brain tissue	1	Memantine	Brain tissue concentration was 5.7 mg/kg which was 2.7-times higher than the heart blood concentration (2.1 ug/ml) and 6.9-times higher than the femoral blood concentration (0.83 ug/ml)	(89)
Cutler et al.	Humans with Alzheimer's	18	Rivastigmine	Cmax in CSF was lower than plasma by 2-4-fold and Tmax in CSF (1.4-3.8 hours) was longer than plasma (0.5-1.67 hours)	(91)
Pharmacodynamics					
Wattmo et al.	Humans with Alzheimer's	84	Galantamine	Alzheimer's Disease Assessment Scale - cognitive subscale (ADAS-cog)	(93)

Authors	Study population	Sample size	Drug(s)	Parameters and Results	Reference
				Mini-Mental State Examination (MMSE) instrumental activities of daily living (IADL) Plasma concentrations did not correlate with any of the PD measures	
III. Neuro-HIV					
Pharmacokinetics					
Yilmaz et al.	HIV-positive humans	1	Efavirenz	Liquid chromatography tandem mass spectoscopy was used to quantify drug concentrations. Median concentration in plasma was 3,718ng/ml and in CSF was 16.3ng/ml. CSF penetration was 0.44% of plasma	(37)
Bumpus et al.	Postmortem human brain tissue	21	Atazanavir, Efavirenz, Emtricitabine, Lamivudine, Lopinavir, Tenofovir	Drug concentrations were assessed by liquid chromatography and compared to historical CSF measures. Concentrations varied by brain regions and lower in cortical grey matter than other	(105)

Authors	Study population	Sample size	Drug(s)	Parameters and Results	Reference
				regions for lopinavir (p=0.01) No difference for other drugs and tenofovir had higher concentration in brain tissue than CSF	
Curley et al.	Virtual cohort of humans	NA/100 virtual simulations	Efavirenz	CNS distribution predicted using permeability-limited PBPK model. Median Cmax was 3,184ng/ml, 49.9ng/ml, and 50,343ng/ml in plasma, CSF, and brain tissue. Brain tissue to plasma ratio was 15.8.	(59)
Pharmacodynamics					
Smurzynski et al.	HIV-positive humans	2,636	Combination ARV therapy	Neuropsychiatric testing scores (NPZ3) – better scores associated with higher CPE for more than 3 ARV drug regimens. No association for regimens less than 3 ARVs	(101)
Baker et al.	HIV-positive humans	64	Combination ARV therapy	Neuropsychiatric testing scores (NPZ4) – no relationship with CPE Brain volumetric changes – no relationship with CPE	(102)

Authors	Study population	Sample size	Drug(s)	Parameters and Results	Reference
Caniglia et al.	HIV-positive humans	61,938	Combination ARV therapy	"intention-to-treat" hazard ratios of 4 neuro-AIDS conditions – high CPE associated with increased risk of dementia	(104)

1.8.   Optimization of Pharmacokinetics/Pharmacodynamics:

1.8.1. Study of biomarkers:

In Alzheimer's disease, abnormal aggregation of protein can manifest as cognitive impairment or dementia(108). Often, protein accumulation processes begin before clinical manifestations. Therefore, the search for quantifiable proteins or biomarkers in the CSF or blood is important for diagnosis. Biomarkers may also have utility as PD endpoints and a recent review identified amyloid and tau in the CSF as commonly used biomarker outcome measures in ongoing clinical trials for Alzheimer's disease(109). As previously demonstrated(110) the utility of these measures comes from the stability of these biomarkers over time and significant differences in concentrations attained between patients with Alzheimer's and healthy volunteers. Utility of biomarkers to aid in anti-depressant drug development was recently demonstrated by Kielbasas et al. In an indirect response analysis, plasma PK concentrations of the antidepressants atomoxetine, duloxetine and edivoxetine were modeled against the CSF concentration of 3,4-dihydroxyphenylglycol (DHPG)(111), the deaminated form of norepinephrine, as a biomarker. The analysis showed that the antidepressants all had a maximal inhibition of rate of formation of DHPG (Imax) of 33-37% in plasma and that edivoxetine was most potent. However, when in CSF, Imax was much greater for edivoxetine (75%) compared

to atomoxetine (53%) and duloxetine (38%). Further investigation of such biomarkers in the clinic can assist in the discovery of novel drug candidates.

Identification of novel biomarkers may also be useful in the field of neuro-HIV as a surrogate measure for neurocognitive impairment(112) to avoid the possibility of confounding with subjective psychiatric tests. In this regard, neurofilament light chain (NFL) has shown promise as a biomarker relating to HAND, although there have been no clinical studies evaluating the correlation of ARV and biomarker concentrations in HIV patients. Similarly, biomarkers should also be explored as a surrogate for establishment of latent HIV reservoir in the brain(113).

1.8.2. Modeling and simulation:

Several modeling tools have been developed to predict drug disposition within brain. Both a top-down approach (population PK modeling)(78) and a bottom-up approach (PBPK modeling)(26,77,114,115) have been used to predict the brain penetration of various drugs in humans using in-vitro and animal data. Gaohua and colleagues recently developed an extensive PBPK model that incorporated four additional compartments of the brain(26): brain blood, brain mass and cranial and spinal CSF. The model was well suited to describe anatomy and physiology of the brain including passive and active transport mechanisms through the BBB. The model was validated with measured clinical concentrations and in-vitro data for phenytoin and paracetamol and was used to simulate various scenarios that mimicked transporter mediated mechanisms and CSF turnover. A recently developed generic PBPK model that incorporated five CSF compartments, including the extravascular drainage from CSF as well as intracellular and extracellular brain compartments was utilized to predict the human brain and CSF PK of nine diverse drugs, including antipsychotics and antidepressants(116). Such

efforts will greatly improve our understanding of CNS target site approximations in humans. Modeling techniques further benefit from incorporating both the PK profile as well as the concentration and effect of endogenous substances. For example, a mechanistic monkey PK/PD model was developed using plasma and CSF concentrations from the cisterna magna of two novel BACE-1 inhibitors with beta-amyloid and secreted amyloid-precursor protein biomarkers(117). This model could predict in-vivo inhibition of BACE-1 and effect on amyloid precursor processing by the BACE-1 inhibitors using in-vitro cellular inhibition and enzyme activities as well as drug concentration data.

1.8.3. PK/PD translation from preclinical models:

Developing innovative animal models for CNS research could address issues in clinical PK/PD such as the relationship between effect site drug concentrations and novel biomarkers, as well as allow for the discovery of novel targets. Zebrafish models have been refined to study several neuro-behavioral disorders such as depression, Parkinson's disease and attention-deficit hyperactive disorder (ADHD)(118). They offer the advantages of low cost and genetic manipulation over traditional lab species such as rodents, and show a high degree of genetic and physiologic homology to mammals(119). Novel rodent models have also been explored for pediatric epilepsy(120) and CNS involvement in HIV infection(121).

For current animal models, their clinical applicability must be carefully examined. For example, certain animals may lack receptors or drug targets available in humans. Animal models may also differ in expression or activity of drug metabolizing enzymes and transporters. Comprehensive work by Terasaki and colleagues in quantitative targeted absolute proteomics (QTAP) have quantified transporter protein concentrations on the BBB of several species, including humans(50,122) and found interspecies differences in several important

transporters. For instance, humans have a greater absolute concentration (fmol/ug of protein) of BCRP compared to mice, while mice have a greater absolute concentration of P-gp, OATP1A2, MRP4 and OAT3. Similarly, absolute transporter concentrations in cynomolgus monkeys track more closely with humans than mice. Since multiple transporters contribute to both the uptake and efflux of drugs at the BBB, the relationship between transporter expression/activity and PK is not straight forward in the CNS. Therefore, while transporter differences at BBB are not currently considered in allometry, models that account for differential transporter-activity between species in CNS are needed to understand if this warrants changes in human dose.

1.9. Conclusions

Understanding the extent of drug penetration and concentration-effect relationship at the various sites of the CNS is essential for neuro-active drug development. Currently, information on brain and CSF drug distribution exists for anti-psychotics, Alzheimer's drugs and anti-infectives. However, the interaction between drug concentration and effect is still not clearly defined across these areas.

This thesis provides a framework to understand PK/PD of ARVs in the brain tissue as this relates to the treatment of HIV in the brain. Three well-characterized *preclinical models* of HIV infection were utilized to compare the inter-species differences in the extent of ARV penetration into the brain tissue and CSF. The gene expression and protein concentration of drug transporters across the three species were measured to explore if inter-species differences in transporter concentration were associated with differential penetration of ARVs into the

brain across the three models. Finally, *modeling and simulation* was used to predict clinical PK in the brain tissue and CSF of efavirenz using data collected from a nonhuman primate model. The model-predicted brain exposure in humans was then correlated with the extent of neurocognitive impairment in a cohort of HIV-positive participants in order to explore PK/PD relationships.

Integration of PK/PD information for ARVs in the CNS can provide valuable information on clinical concentration-effect relationships in the brain tissue and can lead to better precision medicine in HIV-positive individuals with neurocognitive disorders. In support of this, better utilization of clinical pharmacology tools can help pave the way for more rigorous explanation of clinical brain PK/PD.

1.10.   REFERENCES

1.   Neurological Disorders: Public Health Challenges. 2006.

2.   Patel V, Chisholm D, Parikh R, Charlson FJ, Degenhardt L, Dua T, et al. Addressing the burden of mental, neurological, and substance use disorders: key messages from Disease Control Priorities, 3rd edition. Lancet. 2016;387(10028):1672–85.

3.   Cummings JL, Morstorf T, Zhong K. Alzheimer's disease drug-development pipeline : few candidates , frequent failures. Alzheimer's Res Ther. 2014;6(July):1–7.

4.   Benedetti F, Carlino E, Piedimonte A. Increasing uncertainty in CNS clinical trials : the role of placebo , nocebo , and Hawthorne effects. Lancet Neurol. 2016;15(7):736–47.

5.   Kesselheim AS, Hwang TJ, Franklin JM. Two decades of new drug development for central nervous system disorders. Nat Rev. 2015;14(12):815–6.

6.   Pangalos MN, Schechter LE, Hurko O. Drug development for CNS disorders: strategies for balancing risk and reducing attrition. Nat Rev Drug Discov. 2007;6(July):521–32.

7.   Miller G. Is Pharma Running Out of Brainy Ideas ? Science (80-). 2012;329(July 2010).

8.   Choi DW, Armitage R, Brady LS, Coetzee T, Fisher W, Hyman S, et al. Perspective Medicines for the Mind : Policy-Based "' Pull '" Incentives for Creating Breakthrough CNS Drugs. Neuron. 2013;84(3):554–63.

9.   Goetghebeur PJD, Swartz JE. True alignment of preclinical and clinical research to enhance success in CNS drug development : a review of the current evidence. J Psychopharmacol. 2016;586(July 2016):1–9.

10.   de Lange ECM, Hammarlund-Udenaes M. Translational aspects of blood-brain barrier transport and central nervous system effects of drugs: from discovery to patients. Clin Pharmacol Ther. 2015;97(4):380–94.

11.   Aronson JK. Concentration-effect and dose-response relations in clinical pharmacology. Br J Clin Pharmacol. 2007;63(3):255–7.

12.   Markou A, Chiamulera C, Geyer MA, Tricklebank M. Removing obstacles in neuroscience drug discovery: The future path for animal models. Neuropsychopharmacology. 2009;34(1):74–89.

13.   Deo AK, Theil FP, Nicolas JM. Confounding parameters in preclinical assessment of blood-brain barrier permeation: An overview with emphasis on species differences and effect of disease states. Mol Pharm. 2013;10(5):1581–95.

14.   Alavijeh MS, Chishty M, Qaiser MZ, Palmer AM. Drug Metabolism and Pharmacokinetics , the Blood-Brain Barrier , and Central Nervous System Drug Discovery. 2005;2(October):554–71.

15.   Helms HC, Abbott NJ, Burek M, Cecchelli R, Couraud P-O, Deli MA, et al. In vitro models of the blood-brain barrier: An overview of commonly used brain endothelial cell culture models and guidelines for their use. J Cereb Blood Flow Metab.

2016;0271678X16630991.

16. Appelt-Menzel A, Cubukova A, Günther K, Edenhofer F, Piontek J, Krause G, et al. Establishment of a Human Blood-Brain Barrier Co-culture Model Mimicking the Neurovascular Unit Using Induced Pluri- and Multipotent Stem Cells. Stem Cell Reports. 2017;8(4):894–906.

17. Palmiotti CA, Prasad S, Naik P, Abul KMD, Sajja RK, Achyuta AH, et al. In vitro cerebrovascular modeling in the 21st century: Current and prospective technologies. Pharm Res. 2014;31(12):3229–50.

18. Fridén M, Gupta A, Antonsson M, Bredberg U H-UM. In Vitro Methods for Estimating Unbound Drug Concentrations in the brain interstitial and intracellular fluids. Drug Metab Dispos. 2007;35(9):1711–9.

19. Wiseman JM, Ifa DR, Zhu Y. Desorption electrospray ionization mass spectrometry: Imaging drugs and metabolites in tissues. Proc …. 2008;2–7.

20. Thompson CG, Bokhart MT, Sykes C, Adamson L, Fedoriw Y, Luciw PA, et al. Mass spectrometry imaging reveals heterogeneous efavirenz distribution within putative HIV reservoirs. Antimicrob Agents Chemother. 2015;59(5):2944–8.

21. Shobo A, Bratkowska D, Baijnath S, Naiker S, Somboro AM, Bester LA, et al. Tissue distribution of pretomanid in rat brain via mass spectrometry imaging. Xenobiotica. 2016;46(3):247–52.

22. Aikawa H, Hayashi M, Ryu S, Yamashita M, Ohtsuka N, Nishidate M, et al. Visualizing spatial distribution of alectinib in murine brain using quantitative mass spectrometry imaging. Sci Rep. 2016;6(October 2015):23749.

23. Varnäs K, Varrone A, Farde L. Modeling of PET data in CNS drug discovery and development. J Pharmacokinet Pharmacodyn. 2013;40(3):267–79.

24. Shannon RJ, Carpenter KLH, Guilfoyle MR, Helmy A, Hutchinson PJ. Cerebral microdialysis in clinical studies of drugs: Pharmacokinetic applications. J Pharmacokinet Pharmacodyn. 2013;40(3):343–58.

25. Lindberger, M; Tomson, T; Lars S. Microdialysis sampling of carbamazepine, phenytoin and phenobarbital in subcutaneous extracellular fluid and subdural cerebrospinal fluid in humans: an in vitro and in vivo study of adsorption to the sampling device. J Pharmacol Toxicol. 2002;158–65.

26. Gaohua L, Neuhoff S, Johnson TN, Rostami-hodjegan A, Jamei M, Centre BE, et al. Development of a permeability-limited model of the human brain and cerebrospinal fluid (CSF) to integrate known physiological and biological knowledge: Estimating time varying CSF drug concentrations and their variability using in vitro data. Drug Metab Pharmacokinet. 2016;31(3):1–49.

27. Liu X, Smith BJ, Chen C, Callegari E, Becker SL, Chen X, et al. Evaluation of cerebrospinal fluid concentration and plasma free concentration as a surrogate measurement for brain free concentration. Drug Metab Dispos. 2006;34(9):1443–7.

28. Smith DA, Di L, Kerns EH. The effect of plasma protein binding on in vivo efficacy: misconceptions in drug discovery. Nat Rev Drug Discov. 2010;9(DECEmbER):929–39.

29. Fridén M, Winiwarter S, Jerndal G, Bengtsson O, Hong W, Bredberg U, et al. Structure-brain exposure relationships in rat and human using a novel data set of unbound drug concentrations in brain interstitial and cerebrospinal fluids. J Med Chem. 2009;52(20):6233–43.

30. Kodaira H, Kusuhara H, Fujita T, Ushiki J, Fuse E, Sugiyama Y. Quantitative evaluation of the impact of active efflux by p-glycoprotein and breast cancer resistance protein at the blood-brain barrier on the predictability of the unbound concentrations of drugs in the brain using cerebrospinal fluid concentration as a. J Pharmacol Exp Ther. 2011;339(3):935–44.

31. Shen DD, Artru AA, Adkison KK. Principles and applicability of CSF sampling for the assessment of CNS drug delivery and pharmacodynamics. Adv Drug Deliv Rev. 2004;56(12):1825–57.

32. De Lange ECM. Utility of CSF in translational neuroscience. J Pharmacokinet Pharmacodyn. 2013;40(3):315–26.

33. Kassem NA, Deane R, Segal MB, Chen R, Preston JE. Thyroxine (T4) transfer from CSF to choroid plexus and ventricular brain regions in rabbit: Contributory role of P-glycoprotein and organic anion transporting polypeptides. Brain Res. 2007;1181(1):44–50.

34. Westerhout J, Smeets J, Danhof M, De Lange ECM. The impact of P-gp functionality on non-steady state relationships between CSF and brain extracellular fluid. J Pharmacokinet Pharmacodyn. 2013;40(3):327–42.

35. Nau R, Zysk G, Thiel A, Prange HW. Pharmacokinetic quantification of the exchange of drugs between blood and cerebrospinal fluid in man. Eur J Clin Pharmacol. 1993;45(5):469–75.

36. Nau R, Sörgel F, Eiffert H. Penetration of drugs through the blood-cerebrospinal fluid/blood-brain barrier for treatment of central nervous system infections. Clin Microbiol Rev. 2010;23(4):858–83.

37. Yilmaz A, Watson V, Dickinson L, Back D. Efavirenz pharmacokinetics in cerebrospinal fluid and plasma over a 24-hour dosing interval. Antimicrob Agents Chemother. 2012;56(9):4583–5.

38. Chicano-Piá P V, Cercós-Lletí AC, Romá-Sánchez E. Pharmacokinetic model for tobramycin in acinetobacter meningitis. Ann Pharmacother. 2002;36(1):83–6.

39. Kühnen E, Pfeifer G, Frenkel C. Penetration of fosfomycin into cerebrospinal fluid across non-inflamed and inflamed meninges. Infection. 1987;15(6):422–4.

40. Capparelli E V, Letendre SL, Ellis RJ, Patel P, Holland D, Mccutchan JA. Population Pharmacokinetics of Abacavir in Plasma and Cerebrospinal Fluid Population Pharmacokinetics of Abacavir in Plasma and Cerebrospinal Fluid. Antimicrob Agents

Chemother. 2005;49(6):2504–6.

41. Rambeck B, Jürgens UH, May TW, Wolfgang Pannek H, Behne F, Ebner A, et al. Comparison of brain extracellular fluid, brain tissue, cerebrospinal fluid, and serum concentrations of antiepileptic drugs measured intraoperatively in patients with intractable epilepsy. Epilepsia. 2006;47(4):681–94.

42. Hammarlund-Udenaes M. Active-site concentrations of chemicals - Are they a better predictor of effect than plasma/organ/tissue concentrations? Basic Clin Pharmacol Toxicol. 2010;106(3):215–20.

43. Kakee A, Terasaki T, Sugiyama Y. Brain efflux index as a novel method of analyzing efflux transport at the blood-brain barrier. J Pharmacol Exp Ther. 1996;277(3):1550–9.

44. Calcagno A, Di Perri G, Bonora S, A. C, G. DP, S. B. Pharmacokinetics and Pharmacodynamics of Antiretrovirals in the Central Nervous System. Clin Pharmacokinet. 2014;53(10):891–906.

45. Ahn SM, Byun K, Cho K, Kim JY, Yoo JS, Kim D, et al. Human microglial cells synthesize albumin in brain. PLoS One. 2008;3(7):4–9.

46. Read KD, Braggio S. Assessing brain free fraction in early drug discovery. Expert Opin Drug Metab Toxicol. 2010;6(3):337–44.

47. Di L, Umland JP, Chang G, Huang Y, Lin Z, Scott DO, et al. Species independence in brain tissue binding using brain homogenates. Drug Metab Dispos. 2011;39(7):1270–7.

48. Lee G, Dallas S, Hong M, Bendayan R. Drug Transporters in the Central Nervous System : Brain Barriers and Brain Parenchyma Considerations. 2001;53(4):569–96.

49. Hartz AMS, Bauer B. ABC Transporters in the CNS – An Inventory. 2011;656–73.

50. Uchida Y, Ohtsuki S, Katsukura Y, Ikeda C, Suzuki T, Kamiie J, et al. Quantitative targeted absolute proteomics of human blood-brain barrier transporters and receptors. J Neurochem. 2011;117(2):333–45.

51. Löscher W, Potschka H. Blood-brain barrier active efflux transporters: ATP-binding cassette gene family. NeuroRX. 2005;2(1):86–98.

52. Zhao R, Raub TJ, Sawada GA, Kasper SC, Bacon JA, Bridges AS, et al. Breast cancer resistance protein interacts with various compounds in vitro, but plays a minor role in substrate efflux at the blood-brain barrier. Drug Metab Dispos. 2009;37(6):1251–8.

53. Leggas M, Adachi M, Scheffer G, Sun D, Wielinga P, Du G, et al. MRP4 confers resistance to topotecan and protects the brain from chemotherapy. Mol Cell Biol. 2004;24(17):7612–21.

54. Kalvass JC, Polli JW, Bourdet DL, Feng B, Huang S-M, Liu X, et al. Why clinical modulation of efflux transport at the human blood-brain barrier is unlikely: the ITC evidence-based position. Clin Pharmacol Ther. 2013;94(1):80–94.

55. van Praag RM, Weverling GJ, Portegies P, Jurriaans S, Zhou XJ, Turner-Foisy ML, et al. Enhanced penetration of indinavir in cerebrospinal fluid and semen after the addition

of low-dose ritonavir. AIDS. 2000;14(9):1187–94.

56. Toda R, Kawazu K, Oyabu M, Miyazaki T, Kiuchi Y. Comparison of drug permeabilities across the blood-retinal barrier, blood-aqueous humor barrier, and blood-brain barrier. J Pharm Sci. 2011;100(9):3904–11.

57. Liu X, Chen C. Strategies to optimize brain penetration in drug discovery. Curr Opin Drug Discov Devel. 2005;8(4):505–12.

58. Liu X, Smith BJ, Chen C, Callegari E, Becker SL, Chen X, et al. Use of a physiologically based pharmacokinetic model to study the time to reach brain equilibrium: an experimental analysis of the role of blood-brain barrier permeability, plasma protein binding, and brain tissue binding. J Pharmacol Exp Ther Donepezil Cerebrospinal Fluid AD Patients Eval Dos Suffic Stand Treat Strateg. 2005;313(3):1254–62.

59. Curley P, Rajoli RKR, Moss DM, Liptrott NJ, Letendre S, Owen A. Efavirenz Is Predicted To Accumulate in Brain Tissue: and In Silico, In Vitro and In Vivo Investigation. Antimicrob Agents Chemother. 2017;61(1):1–10.

60. Kornhuber J, Schoppmeyer K, Riederer P. Affinity of 1-aminoadamantanes for the sigma binding site in post-mortem human frontal cortex. Neurosci Lett. 1993;163(2):129–31.

61. Yokoi F, Grunder G, Biziere K, Stephane M, Dogan AS, Dannals RF, et al. Dopamine D2 and D3 receptor occupancy in normal humans treated with the antipsychotic drug aripiprazole (OPC 14597): a study using positron emission tomography and [11C]raclopride. Neuropsychopharmacology. 2002;27(2):248–59.

62. Farde L, Wiesel F a, Halldin C, Sedvall G. Central D2-dopamine receptor occupancy in schizophrenic patients treated with antipsychotic drugs. Arch Gen Psychiatry. 1988;45(1):71–6.

63. Mamo D, Sc M, Papatheodorou G, Mann S, Therrien F, Pharm D, et al. A PET Study of Dopamine D 2 and Serotonin 5-HT 2 Receptor Occupancy in Patients With Schizophrenia Treated With Therapeutic Doses of Ziprasidone. 2004;(May):818–25.

64. Sato H, Ito C, Tashiro M, Hiraoka K, Shibuya K, Funaki Y, et al. Histamine H1 receptor occupancy by the new-generation antidepressants fluvoxamine and mirtazapine: A positron emission tomography study in healthy volunteers. Psychopharmacology (Berl). 2013;230(2):227–34.

65. Goetz CG, Tilley BC, Shaftman SR, Stebbins GT, Fahn S, Martinez-Martin P, et al. Movement Disorder Society-Sponsored Revision of the Unified Parkinson's Disease Rating Scale (MDS-UPDRS): Scale presentation and clinimetric testing results. Mov Disord. 2008;23(15):2129–70.

66. Hamilton M. A rating scale for depression. J Neurol Neurosurg Psychiatry. 1960;23:56–62.

67. Overall JE, Gorham DR. The Brief Psychiatric Rating Scale. Psychol Rep. 1962;10(3):799–812.

68.   Robert P, Ferris S, Gauthier S, Ihl R, Winblad B, Tennigkeit F. Review of Alzheimer's disease scales: is there a need for a new multi-domain scale for therapy evaluation in medical practice? Alzheimers Res Ther. 2010;2(4):24.

69.   Dunlop BW, Mayberg HS. Neuroimaging-based biomarkers for treatment selection in major depressive disorder. Dialogues Clin Neurosci. 2014;16(4):479–90.

70.   Ene L, Duiculescu D, Ruta SM. How much do antiretroviral drugs penetrate into the central nervous system? J Med Life. 2011;4(4):432–9.

71.   Antinori A, Arendt G, Becker JT, Brew BJ, Byrd DA, Cherner M, et al. Updated research nosology for HIV-associated neurocognitive disorders. Neurology. 2007;69(18):1789–99.

72.   Kornhuber J, Schultz A, Wiltfang J, Meineke I, Gleiter CH, Zöchling R, et al. Persistence of haloperidol in human brain tissue. Am J Psychiatry. 1999;156(6):885–90.

73.   Sampedro MC, Unceta N, Gómez-Caballero A, Callado LF, Morentin B, Goicolea MA, et al. Screening and quantification of antipsychotic drugs in human brain tissue by liquid chromatography-tandem mass spectrometry: Application to postmortem diagnostics of forensic interest. Forensic Sci Int. 2012;219(1–3):172–8.

74.   Caccia S. Pharmacokinetics and metabolism update for some recent antipsychotics. Expert Opin Drug Metab Toxicol. 2011;7(7):829–46.

75.   Nyberg G, Axelsson R, Mftrtensson E. Cerebrospinal Fluid Concentrations of Thioridazine and Its Main Metabolites in Psychiatric Patients. 1981;148:139–48.

76.   Cohen BM, Lipinski JF, Waternaux C. A fixed dose study of the plasma concentration and clinical effects of thioridazine and its major metabolites. Psychopharmacology (Berl). 1989;97(4):481–8.

77.   Alqahtani S, Kaddoumi A. Development of a Physiologically Based Pharmacokinetic/Pharmacodynamic Model to Predict the Impact of Genetic Polymorphisms on the Pharmacokinetics and Pharmacodynamics Represented by Receptor/Transporter Occupancy of Central Nervous System Drugs. Clin Pharmacokinet. 2016;55(8):957–69.

78.   Li CH, Stratford RE, Velez de Mendizabal N, Cremers TI, Pollock BG, Mulsant BH, et al. Prediction of brain clozapine and norclozapine concentrations in humans from a scaled pharmacokinetic model for rat brain and plasma pharmacokinetics. J Transl Med. 2014;12(1):203.

79.   Garver DL. Neuroleptic Drug Levels and Antipsychotic Effects: A difficult Correlation; Potential Advantage of Free (or Derivative) versus Total Plasma Levels. J Clin Psychopharmacol. 1989;9(4):277–81.

80.   Wode-Helgodt BB. Clinical effects and drug concentrations in plasma and cerebrospinal fluid in psychotic patients treated with fixed doses of chlorpromazine. Acta Psychiatr Scand. 1978;58(2):149–73.

81. Rimón R, Averbuch I, Rozick P, Fijman-Danilovich L, Kara T, Dasberg H, et al. Serum and CSF levels of haloperidol by radioimmunoassay and radioreceptor assay during high-dose therapy of resistant schizophrenic patients. Psychopharmacology (Berl). 1981;73(2):197–9.

82. Kim E, Howes OD, Kim B-H, Jeong JM, Lee JS, Jang I-J, et al. Predicting brain occupancy from plasma levels using PET: superiority of combining pharmacokinetics with pharmacodynamics while modeling the relationship. J Cereb Blood Flow Metab. 2012;32(4):759–68.

83. Greenblatt DJ, von Moltke LL, Ehrenberg BL, Harmatz JS, Corbett KE, Wallace DW, et al. Kinetics and dynamics of lorazepam during and after continuous intravenous infusion. Crit Care Med. 2000;28(8):2750–7.

84. Carrol J. Another Alzheimer's drug flops in pivotal clinical trial. Science. 2017;

85. Mochida I, Shimosegawa E, Kanai Y, Naka S, Isohashi K, Horitsugi G, et al. Whole-Body Distribution of Donepezil as an Acetylcholinesterase Inhibitor after Oral Administration in Normal Human Subjects : A C-donepezil PET Study. Asia Ocean J Nucl Med Biol. 2017;5(1):3–9.

86. Valis M, Masopust J, Vysata O, Hort J, Dolezal R, Tomek J, et al. Concentration of Donepezil in the Cerebrospinal Fluid of AD Patients: Evaluation of Dosage Sufficiency in Standard Treatment Strategy. Neurotox Res. 2016;

87. Darreh-Shori T, Meurling L, Pettersson T, Hugosson K, Hellström-Lindahl E, Andreasen N, et al. Changes in the activity and protein levels of CSF acetylcholinesterases in relation to cognitive function of patients with mild Alzheimer's disease following chronic donepezil treatment. J Neural Transm. 2006;113(11):1791–801.

88. Kornhuber J, Quack G. Cerebrospinal fluid and serum concentrations of the N-methyl-d-aspartate (NMDA) receptor antagonist memantine in man. Neurosci Lett. 1995;195(2):137–9.

89. Rohrig TP, Hicks CA. Brain tissue: A viable postmortem toxicological specimen. J Anal Toxicol. 2015;39(2):137–9.

90. Noetzli M, Eap CB. Pharmacodynamic, pharmacokinetic and pharmacogenetic aspects of drugs used in the treatment of alzheimer's disease. Clin Pharmacokinet. 2013;52(4):225–41.

91. Cutler NR, Polinsky RJ, Sramek JJ, Enz A, Jhee SS, Mancione L, et al. Dose-dependent CSF acetylcholinesterase inhibition by SDZ ENA 713 in Alzheimer's disease. Acta Neurol Scand. 1998;97(4):244–50.

92. Talesa VN. Acetylcholinesterase in Alzheimer's disease. Mech Ageing Dev. 2001;122(16):1961–9.

93. Wattmo C, Jedenius E, Blennow K, Wallin AK. Dose and plasma concentration of galantamine in Alzheimer's disease - clinical application. Alzheimers Res Ther. 2013;5(1):1–9.

94. Fois AF, Brew BJ. The Potential of the CNS as a Reservoir for HIV-1 Infection: Implications for HIV Eradication. Curr HIV/AIDS Rep. 2015;299–303.

95. Avalos CR, Price SL, Forsyth ER, Pin JN, Shirk EN, Bullock BT, et al. Quantitation of Productively Infected Monocytes and Macrophages of Simian Immunodeficiency Virus-Infected Macaques. J Virol. 2016;90(12):5643–56.

96. Gama L, Abreu CM, Shirk EN, Price SL, Li M, Laird GM, et al. Reactivation of simian immunodeficiency virus reservoirs in the brain of virally suppressed macaques. Aids. 2017;31(1):5–14.

97. Desplats P, Dumaop W, Smith D, Adame A, Everall I, Letendre S, et al. Molecular and pathologic insights from latent HIV-1 infection in the human brain. Neurology. 2013;80:1415–23.

98. Decloedt EH, Rosenkranz B, Maartens G, Joska J. Central nervous system penetration of antiretroviral drugs: pharmacokinetic, pharmacodynamic and pharmacogenomic considerations. Clin Pharmacokinet. 2015;54(6):581–98.

99. Letendre S. Validation of the CNS Penetration-Effectiveness Rank for Quantifying Antiretroviral Penetration Into the Central Nervous System. Arch Neurol. 2008;65(1):65.

100. Marra CM, Zhao Y, Clifford DB, Letendre S, Evans S, Henry K, et al. Impact of combination antiretroviral therapy on cerebrospinal fluid HIV RNA and neurocognitive performance. AIDS. 2009;23(11):1359–66.

101. Smurzynski M, Wu K, Letendre S, Robertson K, Bosch RJ. Effects of Central Nervous System Antiretroviral Penetration on Cognitive Functioning in the ALLRT Cohort. AIDS. 2012;25(3):357–65.

102. Baker LM, Paul RH, Heaps-Woodruff JM, Chang JY, Ortega M, Margolin Z, et al. The Effect of Central Nervous System Penetration Effectiveness of Highly Active Antiretroviral Therapy on Neuropsychological Performance and Neuroimaging in HIV Infected Individuals. J Neuroimmune Pharmacol. 2015;487–92.

103. Marra CM. HIV-associated neurocognitive disorders and central nervous system drug penetration: what next? Antivir Ther. 2015;

104. Caniglia EC, Cain LE, Justice A, Tate J, Logan R, Sabin C, et al. Antiretroviral penetration into the CNS and incidence of AIDS-defining neurologic conditions. Neurology. 2014;83(2):134–41.

105. Bumpus N, Ma Q, Best B, Moore D, Ellis RJ, Crescini M, et al. Antiretroviral Concentrations in Brain Tissue Are Similar to or Exceed Those in CSF. 2015;92103.

106. Srinivas N, Fallon JK, Sykes C, White N. SHIV Infection and Drug Transporters Influence Brain Tissue Concentrations of efavirenz. In: International AIDS Society. Paris, France; 2017.

107. Robertson K, Liner J, Meeker RB. Antiretroviral neurotoxicity. J Neurovirol. 2012;18(5):388–99.

108. Llorens F, Schmitz M, Ferrer I, Zerr I. CSF biomarkers in neurodegenerative and vascular dementias. Prog Neurobiol. 2016;138–140:36–53.

109. Cummings J, Lee G, Mortsdorf T, Ritter A, Zhong K. Alzheimer's disease drug development pipeline: 2017. Alzheimer's Dement Transl Res Clin Interv. 2017;3(3):367–84.

110. Le Bastard N, Aerts L, Sleegers K, Martin J-J, Van Broeckhoven C, De Deyn PP, et al. Longitudinal Stability of Cerebrospinal Fluid Biomarker Levels: Fulfilled Requirement for Pharmacodynamic Markers in Alzheimer's Disease. J Alzheimer's Dis. 2013;33(3):807–22.

111. Kielbasa W, Lobo E. Pharmacodynamics of norepinephrine reuptake inhibition: Modeling the peripheral and central effects of atomoxetine, duloxetine, and edivoxetine on the biomarker 3,4-dihydroxyphenylglycol in humans. J Clin Pharmacol. 2015;55(12):1422–31.

112. McGuire J, Gill A, Douglas S, Kolson D. Central and peripheral markers of neurodegeneration and monocyte activation in HIV-associated neurocognitive disorders. J Neurovirol. 2013;19:S57.

113. Gray LR, Brew BJ, Churchill MJ. Strategies to target HIV-1 in the central nervous system. Curr Opin HIV AIDS. 2016;11(4):371–5.

114. Ball K, Bouzom F, Scherrmann J-M, Walther B, Declèves X. Physiologically Based Pharmacokinetic Modelling of Drug Penetration Across the Blood-Brain Barrier-Towards a Mechanistic IVIVE-Based Approach. AAPS J. 2013;15(4):913–32.

115. Trapa PE, Belova E, Liras JL, Scott DO, Steyn SJ. Insights from an Integrated Physiologically Based Pharmacokinetic Model for Brain Penetration. J Pharm Sci. 2016;105(2):965–71.

116. Yamamoto Y, Välitalo PA, van den Berg DJ, Hartman R, van den Brink W, Wong YC, et al. A Generic Multi-Compartmental CNS Distribution Model Structure for 9 Drugs Allows Prediction of Human Brain Target Site Concentrations. Pharm Res. 2017;34(2):333–51.

117. Liu X, Wong H, Scearce-Levie K, Watts RJ, Coraggio M, Shin YG, et al. Mechanistic Pharmacokinetic-Pharmacodynamic Modeling of BACE1 Inhibition in Monkeys: Development of a Predictive Model for Amyloid Precursor Protein Processings. Drug Metab Dispos. 2013;41(7):1319–28.

118. Kalueff A V., Stewart AM, Gerlai R. Zebrafish as an emerging model for studying complex brain disorders. Trends Pharmacol Sci. 2014;35(2):63–75.

119. Nguyen M, Yang E, Neelkantan N, Mikhaylova A, Arnold R, Poudel MK, et al. Developing "integrative" zebrafish models of behavioral and metabolic disorders. Behav Brain Res. 2013;256:172–87.

120. Auvin S, Pineda E, Shin D, Gressens P, Mazarati A. Novel Animal Models of Pediatric Epilepsy. Neurotherapeutics. 2012;9(2):245–61.

121. Honeycutt JB, Sheridan P a., Matsushima GK, Garcia JV. Humanized mouse models for HIV-1 infection of the CNS. J Neurovirol. 2015;21(3):301–9.

122. Ito K, Uchida Y, Ohtsuki S, Aizawa S, Kawakami H, Katsukura Y, et al. Quantitative membrane protein expression at the blood-brain barrier of adult and younger cynomolgus monkeys. J Pharm Sci. 2011;100(9):3939–50.

SPECIFIC AIMS

AIM 1: Quantify the penetration of antiretrovirals (ARVs) within the brain tissue in nonhuman primates (NHPs) and humanized mouse models using IR-MALDESI imaging and LC-MS/MS methods.

(Discussed in Chapter-II)

1a: Use IR-MALDESI imaging technique to visualize and quantify the distribution of ARVs from five therapeutic classes within the brain tissue of two species of humanized mice and NHPs.

1b: Colocalize the drug exposure by IR-MALDESI imaging with the distribution of target cells in the brain tissue of humanized mouse models and NHPs

1c: Quantify ARV concentrations in the brain tissue collected in Aim 1a using traditional LC-MS/MS in humanized mouse models and NHPs and determine brain tissue:plasma penetration ratio of ARVs and 90% inhibitory quotients in the brain tissue of NHPs.

AIM 2: Determine the expression patterns of five efflux transporters and four uptake transporters involved in ARV distribution in the brain tissue of NHPs and humanized mouse models. Identify if inter-species differences in expression of transporters affects the disposition patterns of ARVs.

(Discussed in Chapter-III)

2a: Quantify and evaluate inter-species differences in the gene expression by quantitative polymerase chain reaction (qPCR) and protein expression by western blotting and quantitative

44

targeted absolute proteomics (QTAP) of relevant drug transporters in the brain tissue of humanized mouse models and NHPs.

2b: Determine if inter-species differences in the expression of transporters is correlated with the disposition of ARVs in the brain tissue of humanized mouse models and NHPs.

2c: Visualize the distribution of BCRP, P-gp, MRP4, MRP1, and OATP1A2 in the brain tissue of humanized mouse models and NHPs using immunohistochemistry (IHC) staining.

AIM 3: Develop a PK model in NHPs and humans to predict the exposure of efavirenz in brain tissue and explore the relationship between the model-predicted concentration of efavirenz in brain tissue and neurocognitive outcome in HIV positive participants.

(Discussed in Chapter-IV)

3a: Develop a PK model for penetration of efavirenz into the cerebrospinal fluid (CSF) and brain tissue of NHPs using data generated in Aim 1c.

3b: Develop a human PK model from the NHP PK model developed in Aim 3a to predict efavirenz penetration into the brain using sparse plasma and CSF concentrations from patients in the THINC Clinical Study (PO1 grant no. MH094177).

3c: Perform correlation analysis between model-predicted exposure of efavirenz in the brain tissue and neurocognitive scores data from the THINC study in 24 HIV-positive participants.

CHAPTER-II: ANTIRETROVIRAL CONCENTRATIONS IN THE BRAIN TISSUE AND CEREBROSPINAL FLUID IN HUMANIZED MOUSE MODELS AND NONHUMAN PRIMATES[1]

2.1. Summary

Antiretroviral (ARV) concentrations in the cerebrospinal fluid (CSF) are used as a surrogate for brain tissue, although sparse data support this. Here, we quantified ARV concentrations in the brain tissue across preclinical models commonly used to study HIV infection, compared them to CSF, and calculated 90% inhibitory quotients (IQ_{90}) in the brain tissue of nonhuman primates (NHPs). Spatial distribution of efavirenz was performed with mass spectrometry imaging (MSI) and the colocalization of efavirenz distribution with the distribution of microglia and CD4+ T-cell target cell populations was explored. HIV or RT-SHIV-infected and uninfected animals from two humanized mouse models (hemopoietic-stem cell/RAG2- [Hu-HSC-Rag, number of animals = 36] and the bone marrow-liver-thymus [BLT, number of animals = 13]) and an NHP model (rhesus macaque, number of animals = 18) were dosed to steady state with tenofovir, emtricitabine, efavirenz, raltegravir, maraviroc, and atazanavir. Brain tissue, CSF (NHPs only) and plasma were collected at necropsy. Drug concentrations were measured by liquid chromatography tandem mass spectroscopy (LC-MS/MS). Rapid equilibrium dialysis was used to determine protein binding of ARVs in the NHP brain. MSI was by infrared matrix-assisted laser desorption electrospray ionization (IR-

MALDESI). CD11b and CD4 staining were performed by immunofluorescence in order to identify the microglia and T-cell populations in the brain tissue. Colocalization of the MSI and immunofluorescence images was performed in Matlab. ARV brain tissue concentrations normalized to plasma concentrations were >ten-fold lower ($p<0.02$) in the humanized mouse models than NHPs for all ARVs except raltegravir. Brain tissue concentrations in NHPs were >6-fold higher ($p<0.02$) than CSF concentrations. Most ARVs were less than 25% bound in the brain tissue except for efavirenz that was highly protein-bound (97%). Despite the high protein binding in the brain tissue, efavirenz was the only ARV which achieved $IQ_{90}>1$ in all animals. Efavirenz showed a 1.1- to 3-fold greater penetration into the white matter compared to the grey matter and the fractional coverage of CD11b cells and CD4+ T-cells that contained efavirenz at a concentration above the IC_{50} was only 3%. This analysis revealed that brain tissue penetration varied widely across animal models for all ARVs except raltegravir, and extrapolating brain tissue concentrations between models should be avoided. With the exception of efavirenz, CSF is not a suitable surrogate for brain tissue concentrations of ARVs. Our two surrogate measures of efficacy for efavirenz show that despite a high concentration of free drug, inadequate coverage of efavirenz at relevant target cells may contribute to HIV persistence in the brain, and this should be investigated further.

---

[1]This chapter was previously published as an article in the journal Xenobiotica. The original citation is as follows: Srinivas N, Rosen EP, Gilliland WM Jr, Kovarova M, Remling-Mulder L, De La Cruz G, White N, Adamson L, Schauer AP, Sykes C, Luciw P, Garcia JV, Akkina R, & Kashuba ADM, Xenobiotica, 2018. https://doi.org/10.1080/00498254.2018.1539278

2.2.   Introduction

HIV invades the central nervous system (CNS) early after infection. HIV RNA can be detected in the cerebrospinal fluid (CSF) of acutely infected patients eight days after exposure(1), and may be detected in the CSF even when undetectable in the plasma(2,3). In the brain, HIV replication occurs in long lived cells such as macrophages and astrocytes(4) and the resulting immune activation is hypothesized to cause neuronal death and decline in neurological functioning(5,6). Before combination antiretroviral (ARV) therapy, almost 60% of patients with AIDS developed a debilitating form of neurological disease called HIV associated dementia (HAD)(7). Currently, the prevalence of HAD has been reduced to 5%, although milder forms of neurocognitive impairment remain high at 20-50%(8). This may be related to the extent of antiretroviral (ARV) penetration into the CNS(9). While our understanding of ARV exposure/response relationships in the CSF has greatly improved in the past decade, some key knowledge gaps still exist.

The first critical knowledge gap is the extent of ARV penetration into the brain tissue and the agreement between the CSF and brain tissue concentration of ARVs. The brain is the relevant target site for HIV replication in the CNS, however, a paucity of information exists on ARV concentrations achieved in the brain tissue. Furthermore, while CSF concentrations are often considered as a surrogate for brain tissue exposure, little data support this for ARVs. For several classes of drugs acting in the CNS, CSF concentrations are either much lower than, or not predictive of, brain tissue concentrations(10,11). This may also be the case for ARVs due to their affinity for the drug uptake and efflux transporters at the blood-brain barrier (BBB) and the blood-CSF barrier (B-CSF-B). Active transport of ARVs along the BBB and B-CSF-B disturbs the equilibrium of passive protein-unbound drug movement(12), which may result

in different relationships between plasma, CSF and brain tissue concentrations for different ARVs.

The second critical gap is related to defining an appropriate efficacy target for drug exposure in the CNS. An efficacy target that is commonly employed is the drug concentration required to inhibit HIV viral replication by 50% (IC_{50}). While achieving drug concentration >IC_{50} has been generally considered optimal in the CSF(13,14), having coverage at IC_{50} concentrations may not be enough to avoid the onset of resistance mutations(15). In a recent analysis by Calcagno(15), inhibitory quotients (IQ) were calculated for commonly used ARV regimens in the CSF by using a standardized wild-type IC_{95} for HIV clinical isolates(16). The investigators were able to demonstrate the utility of this measurement in optimizing CNS-penetrating ARV regimens by showing that an IQ_{95}>1 was associated with better viral control in the CSF. While such an approach could provide a standardized drug efficacy target across studies, the wild-type IC_{95} estimates utilized in this analysis were corrected for protein binding in the plasma and not the CSF. Since drugs usually exhibit a higher extent of protein binding in the plasma compared to the CSF(17,18), it is likely that some of the final IQ estimates may have been underestimated. Furthermore, these values have not been determined for brain tissue.

Since it is not practical to obtain robust human brain tissue pharmacokinetic (PK) data, animal models can be used to address the knowledge gaps detailed above. However, there is no consensus in the field as to which animal model would best approximate human brain tissue PK. Therefore, in this work, we measure the penetration of ARVs across three commonly used HIV preclinical models – two humanized mouse models and one nonhuman primate (NHP) model(19,20). In the NHPs, we evaluate the agreement between total ARV concentrations in

the brain tissue and CSF and measure unbound ARV brain tissue concentrations in order to calculate the IQ_{90} estimates. To provide a measure of spatial brain tissue distribution of ARVs in the brain tissue, we use mass spectrometry imaging (MSI). These results were then combined with immunohistochemistry (IHC), to determine the colocalization of ARV distribution in the brain tissue with the distribution of relevant HIV target cells as a second surrogate measure of efficacy of ARVs within the brain tissue.

2.3. Materials and Methods

2.3.1. Animal models:

This analysis utilized three commonly used animal models: two species of humanized mouse models [human stem cell hemopoietic/RAG 2- (hu-HSC-Rag, number of animals = 36) and bone marrow-liver-thymus (BLT, number of animals = 13)] and one species of NHP (rhesus macaques, number of animals = 18). Humanization of the mice was by protocols that have been previously described(21,22). The extent of humanization for the humanized mouse models was assessed by quantifying the human T-cell populations using flow cytometry. All the humanized mice were female, while six (33.3%) of the NHPs were female. Half of the animals were left uninfected while the other half were infected with 200 µL 2.1 x 10^6 IU/mL of $HIV_{Bal\,D7}$ intraperitoneally (hu-HSC-RAG), or 200 µL 90,000 tissue culture infectious units (TCIU) of HIV_{JRcsf} intravenously (BLT), or $10^{4.5}$ tissue culture infective dose (TCID50) RT-SHIV intravenously (macaques)(23,24) for four weeks. The hu-HSC-RAG and BLT mice underwent humanization when aged three to six months and were then dosed with various ARV regimens for a period of ten days. Hu-HSC-RAG mice were dosed with EFV 10 mg/kg only (six uninfected and six infected animals), or atazanavir (ATZ) 140 mg/kg only (six

uninfected and six infected animals), or a combination of tenofovir (TFV) 208 mg/kg, emtricitabine (FTC) 240 mg/kg, raltegravir (RAL) 56 mg/kg, and maraviroc (MVC) 62 mg/kg (six uninfected and six infected animals). BLT mice were dosed with a combination of TFV, FTC, RAL, MVC, and ATZ at equivalent doses but not EFV due to toxicity concerns (personal communication from J. Victor Garcia). All drugs were administered by oral gavage once a day, and dosing solutions were prepared by solubilizing formulated drug. Dosing regimens for each of the animal models are summarized in **Table 2.1**. The dosage selection for all the drugs in the animal models was based on standard doses used for the treatment of HIV in these animal models, and to minimize the potential for drug-drug interactions. ARVs were dosed for ten days to achieve PK steady-state conditions in tissues based on known half-lives of these drugs.

Table 2.1. Sample size and dosage regimens for the preclinical models

Dosing Regimen	Humanized Mice				Rhesus macaques			
	Hu-HSC-RAG		BLT		Male		Female	
	HIV-	HIV+	HIV-	HIV+	RT-SHIV+	RT-SHIV-	RT-SHIV+	RT-SHIV-
EFV	N=6	N=6						
ATZ	N=6	N=6						
TFV/FTC/RAL/MVC	N=6	N=6						
TFV/FTC/RAL/MVC/ATZ			N=6	N=7				
TFV/FTC/EFV/RAL					N=3	N=3	N=1	N=2

Dosing Regimen	Humanized Mice				Rhesus macaques			
	Hu-HSC-RAG		BLT		Male		Female	
	HIV-	HIV+	HIV-	HIV+	RT-SHIV+	RT-SHIV-	RT-SHIV+	RT-SHIV-
TFV/FTC/MVC/ATZ					N=3	N=3	N=1	N=2

The macaques were dosed with a backbone of TFV 30 mg/kg administered subcutaneously and FTC 16 mg/kg administered subcutaneously, with a combination of either EFV 200 mg/day and RAL 200 mg/day (four uninfected and five infected animals) given orally with food, or MVC 150 mg/day and ATZ 270 mg/kg (four uninfected and five infected animals) given orally with food. Similar to the humanize mouse models, the doses and regimens in the rhesus macaques were chosen based on standard doses used for the treatment of HIV in these animal models and to minimize the potential for drug-drug interactions. One infected female macaque dosed with TFV, FTC, EFV, and RAL developed liver failure before necropsy and the measured drug concentrations in the plasma, CSF, and tissue matrices in this animal were >100-fold higher than in the other NHPs. As a result, the drug concentration data from this animal were excluded from the final liquid chromatography mass spectrometry (LC-MS/MS) analysis. All animal studies were performed in concordance with institutional animal care and use committee (IACUC) protocols from the University of North Carolina at Chapel Hill (protocol 15-168), Colorado State University (protocol 16-6998A) and the University of California at Davis (protocol 18345).

2.3.2. Fluid and tissue collection from animal models:

The humanized mice were euthanized by isoflurane overdose and underwent necropsy one day after the final ARV dose was administered by a trained veterinary pathologist. Whole blood was collected via retroorbital or cardiac puncture and centrifuged at 2,500 RPM for 15 minutes to separate out the plasma. CSF was not collected in the animals because of the small CSF volume and risk of plasma contamination. For the NHPs, animals were sedated with ketamine hydrochloride one day after the final ARV dose and CSF was collected. The animals were then euthanized by a barbiturate overdose and whole blood was collected via venipuncture, and centrifuged for 15 minutes at 2500 RPM to separate out the plasma. All animals underwent necropsy by trained veterinary pathologists. The plasma and CSF fluid samples were stored at -80°C within a few hours after collection.

At necropsy, several potential tissue reservoirs for HIV persistence were collected from all animals, including the brain tissue. After removal from the body, the humanized mouse brain tissue was cut in half longitudinally and placed into separate aluminum foil pouches and snap frozen on dry ice. In case of the NHPs, four distinct regions of the brain tissue were collected – the frontal cortex, the cerebellum, the basal ganglia, and the parietal cortex. These regions were snap frozen with dry-ice and then placed into aluminum foil. The brain regions chosen for investigation were both cortical (frontal and parietal lobes) and sub-cortical (cerebellum and basal ganglia). These were chosen to evaluate morphologically different areas and to select the areas that had more extensive involvement in HIV injury to the brain. The total time from euthanization to tissue freezing was less than one hour for all tissues. After freezing, tissues were stored at -80°C within a few hours of collection, until further analysis.

2.3.3. Tissue preparation for LC-MS/MS:

Brain tissue was mounted on optimal cutting temperature (OCT) compound and sliced frozen at 10 μm thickness using a cryostat (Leica Biosystems, Wetzlar, Germany) in order to obtain serial sections needed for the various analyses (LC-MS/MS, mass spectrometry imaging and immunofluorescence). The 10 μm thick sections were then thaw mounted onto glass microscope slides in the following order: eight slices for IHC and three slices for MSI (one for analysis and two for backup). Three slices of brain tissue at 40 μm thickness were placed in an Eppendorf tube and subsequently homogenized for the LC-MS/MS analysis. The glass slides and Eppendorf tubes were stored at -80°C until the time of analysis. For the analysis of ARV active metabolites, tissue slices could not be used for the LC-MS/MS analysis as all the analytes were below the limit of quantification (BLQ). Therefore, for these analyses 10-15 mg of tissue was homogenized for further analysis by LC-MS/MS.

2.3.4. Sample analysis for antiretroviral concentrations in the brain tissue:

Plasma and CSF samples were extracted by protein precipitation using stable, isotopically labeled internal standards as described previously(25). The extracts were analyzed on a Shimadzu HPLC system with a Waters Atlantis T3 (50 mm x 2.1 mm, 3 μm particle size) column, with an API 5000 mass spectrometer (SCIEX, Framingham, MA) detector equipped with a TurboIonSpray interface. The lower limit of quantification (LLOQ) was 1 ng/mL. The inter- and intra-day precision and accuracy of the assays (two separate assays for TFV/FTC and for EFV/RAL/MVC/ATZ) were within 15%.

Brain samples were homogenized in a Precelly's tube with metal beads (Precelly's tissue homogenizer) in one mL of 70:30 acetonitrile:1 mM ammonium phosphate (pH 7.4) and

then extracted by protein precipitation with stable, isotopically labeled internal standards. TFV and FTC were analyzed by the method described for plasma and CSF, while ATZ, EFV, MVC, and RAL were separated using an Agilent Pursuit XRs 3 Diphenyl (50 mm x 2 mm, 3 µm particle size) HPLC column. The LLOQs were 0.002 ng/mL (FTC and MVC), 0.005 ng/mL (ATZ, EFV, and RAL), and 0.01 ng/mL (TFV), respectively. These concentrations in ng/mL were converted to ng/g using a density of 1.06 g/m^3(26). The intracellular active metabolites of TFV (tenofovir diphosphate: TFV-dp) and FTC (emtricitabine triphosphate: FTC-tp) were also quantified in the brain tissue. TFV-dp and FTC-tp were extracted by homogenizing the tissue with 70:30 acetonitrile:1 mM ammonium phosphate (pH 7.4). An aliquot of the resulting homogenate was mixed with acetonitrile containing an isotopically-labelled internal standard, 13C5-TFV-dp, (Moravek Biochemicals, Brea, CA). The extracts were evaporated to dryness, reconstituted with 1 mM ammonium phosphate (pH 7.4), and transferred to a 96-well plate for analysis. TFV-dp and FTC-tp were analyzed using anion exchange chromatography on a Thermo BioBasic AX (50 x 2.1 mm, 5 µm particle size) analytical column (Waters, Milford, MA) followed by detection under positive ion electrospray conditions. Data were collected using an AB Sciex API-5000 triple quadrupole mass spectrometer. The dynamic range was 0.300–300 ng/mL homogenate (rhesus macaques) and 0.0200 – 300 ng/mL homogenate (humanised mouse models) for both TFV-dp and FTC-tp. The inter- and intra-day precision and accuracy of the assays were within 15%.

2.3.5. Determination of protein binding in the NHP brain tissue

The protein binding of EFV, RAL, MVC, and ATZ in the brain tissue was determined by rapid equilibrium dialysis (RED). Briefly, 5 to 10 mg of frontal cortex brain tissue samples were homogenized in Precelly's tubes and incubated at 37°C for 18 hours in RED cartridges

(Thermo Scientific, Pittsburg, PA). The samples subsequently underwent liquid-liquid extraction with methyl tert-butyl ether (MTBE) (Fisher Scientific, Norcross, GA, USA). An Agilent 1200 series HPLC System and an Agilent 1100 MSD (Agilent Technologies, New Castle, DE) in positive ESI mode were used. Analytes were separated on an Agilent Zorbax Eclipse XDB-C8 (3.0 mm × 50 mm, 1.8 m) column. Assay sensitivity was two ng/ml and inter- and intra-day precision was within 15%. The median fraction unbound value was used to determine the unbound ARV concentration across all NHP brain tissue samples.

2.3.6. Calculation of 90% Inhibitory Quotients in the NHP brain tissue

IQ_{90} was calculated as a measure of ARV efficacy in brain tissue using the protein-unbound brain tissue concentrations and the protein-unbound IC_{90} for the RT-SHIV strain of virus, when available. Since the RT-SHIV viral strain has the reverse transcriptase (RT) enzyme from HIV-1 clinical isolates, the IC_{90} values of ARV classes targeting this enzyme: nucleoside reverse transcriptase inhibitors (NRTI) and non-nucleoside reverse transcriptase inhibitors (NNRTI) were taken from the values for HIV-1 clinical isolates from various sources[16,27,28]. MVC IC_{90} values for RT-SHIV were available from Pal[29] and RAL IC_{90} values for RT-SHIV were available from Hassounah[30]. IC_{90} value of ATZ against RT-SHIV (12,750 ng/g) was calculated from concentration-response data provided by Z. Ambrose (personal communication, September 18th, 2018). All values were corrected for protein binding as described by Yilmaz[31] The formula for ARV IQ_{90} in brain tissue is given by **Equation 2.1**.

$$IQ_{90} = \frac{ARV\ protein-unbound\ concentration\ in\ the\ brain\ tissue}{Protein-free\ wild-type\ IC90\ of\ RT-SHIV} \tag{2.1}$$

2.3.7. Mass-spectrometry imaging:

We chose to investigate EFV concentrations by MSI due to its accumulation in brain tissue(25) and its well-known clinical toxicity profile. Methods for the Infrared Matrix-Assisted Laser Desorption Electrospray Ionization (IR-MALDESI) MSI analysis have been published previously(25,32). Frozen slices (10 μm) of discrete tissue regions (NHPs) or whole brain (humanized mouse models) were thaw-mounted onto a glass slide and placed in the source chamber maintained at -10°C. Humidity inside the chamber was reduced to <6% with liquid nitrogen for ten minutes, following which the humidity was then increased to deposit a layer of ice across the entire stage. Tissues were ablated with two mid-IR laser pulses (IR-Opolette 2371, Opotek, Carlsbad, CA) with a 100 μm spot-to-spot distance. Ablated molecules were ionized by electrospray and sampled into a Thermo Fisher Scientific Q Exactive mass spectrometer (Bremen, Germany) for analysis. Raw data from each volumetric pixel (voxel) were converted to the mzXML format with MS Convert (ProteoWizard) and then imzML format to evaluate using MSiReader(33). Both the mzXML and imzML formats are widely used for the processing of mass spectrometry data. Images were ultimately converted and stored in the imzML format due to the smaller file size and greater efficiency in storage. Since the .RAW mass spectrometry file could not be directly converted to imzML, the mzXML format was first generated before converting to imzML. ARV concentrations were quantified by spotting calibration standards of known concentration onto a non-dosed tissue slice from identical matrix (Bioreclamation IVT, Baltimore, MD). The resulting ng/slice concentrations were converted to ng/g using the area of each slice, the tissue thickness, and a density of 1.06 g/mL(26).

2.3.8. Immunofluorescence (IF):

Dual IF on frozen sections of humanized mouse and NHP brain tissue were performed at the UNC Tissue Pathology Laboratory with the Bond fully-automated slide staining system (Leica Microsystems) using the Bond Polymer Refine Detection kit (DS9800). The slides remained at room temperature for 15 minutes and were then fixed in 10% neutral buffered formalin for 15 minutes. Following this, slides were placed in Bond wash solution (AR9590) and antigen retrieval was done at 100°C in Bond-epitope retrieval solution 2 (pH9.0, AR9640) for ten minutes. Staining was performed for two distinct subsets of cells: CD3/CD4 staining for the CD4+ T-cells and CD45/CD11b for the microglial cells. For the CD3/CD4 cellular subset, staining was first performed using a CD4 EPR6855 antibody (Abcam, Cambridge, UK) at 1:1000 dilution for one hour with Bond Polymer reagents and then Cy5 fluorochrome (Perkin Elmer) for 15 minutes. Antigen retrieval was done at 100°C in Bond-epitope retrieval solution 2, while Bond-epitope retrieval solution 1 was used between protocols. Slides were then stained with CD3 LN10 (Leica, Wetzlar, Germany) ready-to-use antibody for 15 minutes with Bond Polymer and Post-Primary reagents for 30 minutes. Cy3 fluorochrome (Perkin Elmer) was applied for 15 minutes. Slides were counterstained with Hoechst 33258 (Invitrogen, Carlsbad, CA) and mounted with ProLong Gold antifade reagent (P36934, Life Technologies). Similarly, for the CD45/CD11b cellular subset, the tissue section was first stained with CD11b NB110-89474 antibody (Novus Biologicals, Littleton, CO) at a 1:1000 dilution for one hour with Bond Polymer reagents and then Cy5 fluorochrome for 15 minutes. Antigen retrieval was done at 100°C in Bond-epitope retrieval solution 1 during the first stain. Following this, the slides were stained with CD45 NCL-LCA at 1:500 dilution with Bond Polymer and Post-Primary reagents for 30 minutes followed by Cy3 fluorochrome for 15

minutes. A background 4′,6-diamidino-2-phenylindole (DAPI) stain was used for cellular staining.

2.3.9. Image Colocalization:

Manipulation and co-registration of images were performed using the Matlab v. R2015a Image Processing Toolbox (Mathworks, Natick, MA). For MSI, pixel intensity matrices for cholesterol, heme, and each ARV of interest were exported into Matlab across the entire tissue slice using MSi Reader. The cellular IF samples were scanned as described above and down sampled from the one μM (cellular) resolution in order to match the 100 μM resolution of the MSI data and facilitate image overlay. The cholesterol signal was used to mask any off-tissue ARV response, and a heme distribution mask was applied to show only the ARV signal that localized outside of the microvasculature, to account for blood contamination. Co-registration of images was performed on the cholesterol image using the background DAPI staining as a reference to ensure that the MSI and IF images were aligned appropriately before colocalization. A transform variable that resulted from aligning the orientation of the DAPI and cholesterol map images was then applied to all ARV images so that every image was oriented in an identical direction. Finally, the heme-corrected transformed ARV images were overlaid with the variable of interest (CD4 or CD11b) to generate a fused image containing both the ARV (in red) and the cellular variable of interest (in green). After image overlay was performed, the fractional coverage of the total cellular area that contained detectable drug concentration and drug concentrations above IC_{50} and IC_{90} were calculated by masking the cellular area with the EFV drug distribution maps at various concentrations.

2.3.10. Statistical analysis:

To compare the CSF and brain tissue concentrations between species, ARV concentrations were normalized to plasma to give either a CSF: plasma penetration ratio or a brain tissue: plasma penetration ratio. Comparisons between species, sex, and brain tissue and CSF compartments were made using the Kruskal-Wallis test. The Spearman rank-order correlation was used to determine the relationship between the ARV concentrations in the brain tissue and the CSF. Data were analyzed using SigmaPlot 13.0 (Systat Software Inc., San Jose, CA); the significance was set at $p<0.05$. Data are presented as median (range) unless otherwise noted.

2.4.   Results

2.4.1. Concentration of ARVs in the plasma of the animal models:

The ARV trough concentrations in the plasma that were collected at necropsy were measured in order to ensure consistency in ARV exposure across the animal models. ARV plasma concentrations were detectable in >90% of samples. **Figure 2.1** compares plasma exposure between infected and uninfected animals from each model. Since there were no significant differences in plasma exposure between these groups, the data were combined in **Figure 2.2**, which shows plasma data across all three animal models. There were no statistically significant differences in plasma concentrations between the two humanized mouse models for any of the ARVs. The NHPs had plasma concentrations that were not significantly different than the humanized mouse models for most ARVs, with the exception of RAL which was 7- to 70-fold higher in NHPs relative to the humanized mice ($p<0.02$).

Plasma concentrations in NHPs were usually within two- to ten-fold of human concentrations

from the literature(34–38).
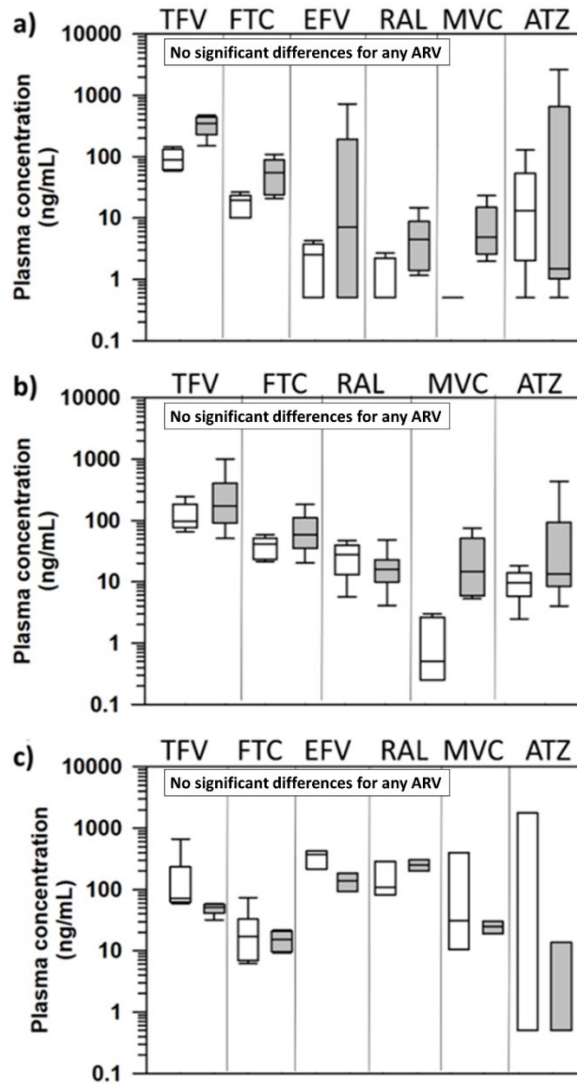
Figure 2.1. Antiretroviral concentrations in the plasma of the (a) hu-HSC-RAG mice, (b) BLT mice, and (c) NHPs stratified by infection status. The plasma trough concentrations of antiretrovirals are shown in the uninfected animals (white bars) and infected animals (gray bars). There were no differences in ARV concentrations on the basis of infection status. Boxes represent 1st and 3rd quartile with median line. Whiskers represent 10th and 90th percentile and open circles represent outliers. BLT mice were not dosed with efavirenz due to prior toxicity concerns (personal communication, JV Garcia).
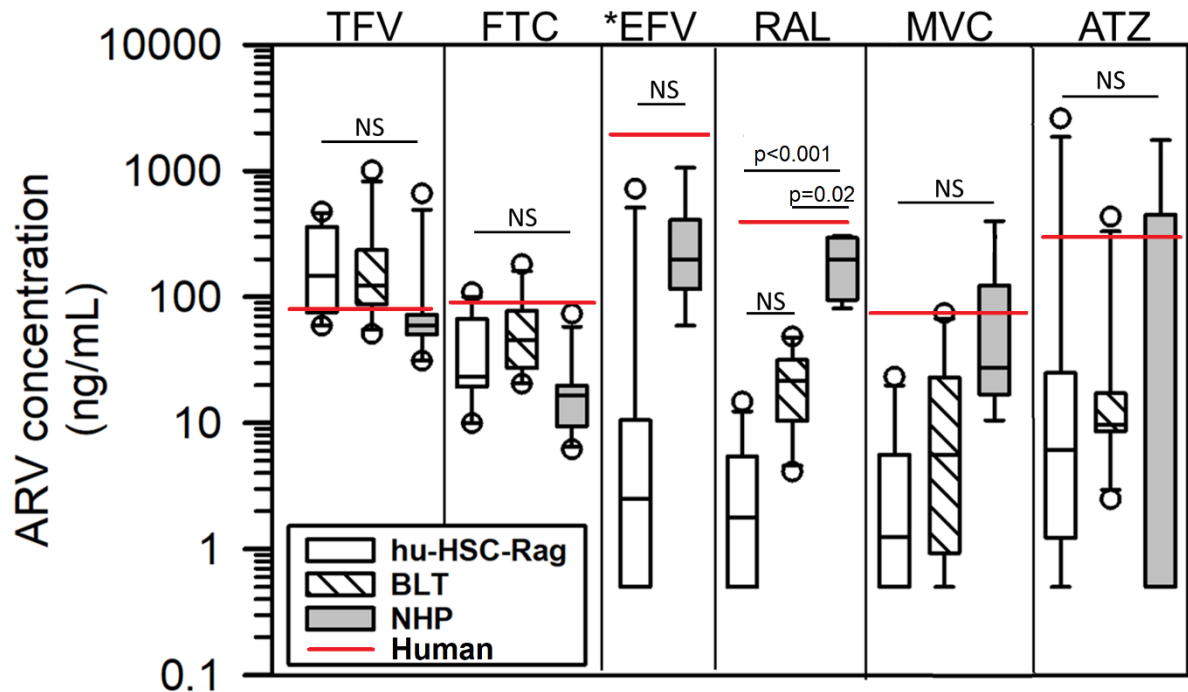
Figure 2.2. Antiretroviral concentrations in the plasma of the hu-HSC-RAG mice, BLT mice and NHPs and comparison to concentrations achieved in humans. There were no differences in the plasma concentration of ARVs in across the preclinical models for all ARVs except RAL. RAL concentration was ten-fold higher in the NHPs relative to the BLT mice, and 100-fold higher compared to the hu-HSC-RAG mice. Boxes represent 1st and 3rd quartile with median line. Whiskers represent 10th and 90th percentile and open circles represent points outside the 10th and 90th percentile. Human ARV concentrations were from the literature. Legend: NS – not significant. *BLT mice were not dosed with EFV due to prior toxicity concerns (personal communication, JV Garcia).

2.4.2. Concentration of ARVs in the brain tissue of humanized mice:

The brain tissue concentrations of all ARVs were <150 ng/g for most of the humanized mice, except for one hu-HSC-RAG mouse where the brain tissue concentration of EFV was 1,400 ng/g **(Figure 2.3a).** The brain tissue:plasma penetration ratio ranged from 0.001 (TFV and FTC) to 100 (ATZ) **(Figure 2.3b)** and was five-fold higher in the BLT mice compared to the hu-HSC-RAG mice for MVC (p=0.002) and three- to five-fold higher in the BLT mice compared to the hu-HSC-RAG mice for TFV and FTC (p>0.15), respectively. RAL brain tissue:plasma penetration ratios were 0.13 in both humanized mouse models and the ratio of

ATZ concentration in the brain tissue:plasma were 0.12 and 0.13 in the hu-HSC Rag mice and

BLT mice respectively. Infection status did not impact ARV concentrations or ratios (p=1.0,

data not shown).
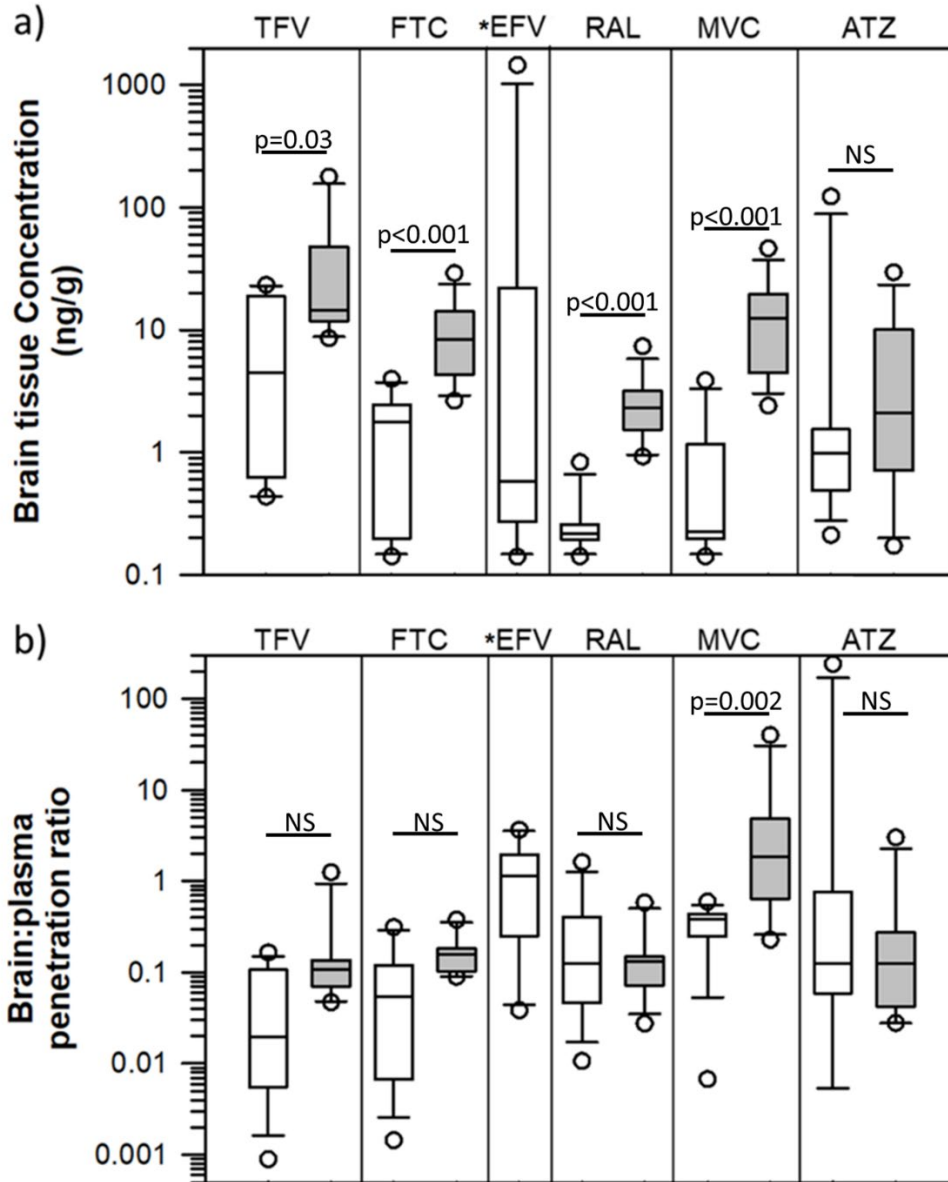
Figure 2.3. (a) Antiretroviral concentrations in the brain tissue and (b) brain tissue: plasma antiretroviral concentrations in humanized-mice. The penetration of antiretrovirals into the brain tissue of the hu-HSC-RAG mice (white bars) was generally lower than in the BLT mice (gray bars). Penetration of antiretrovirals into the brain tissue of BLT mice was significantly higher for MVC (p=0.002). Boxes represent 1st and 3rd quartile with median line. Whiskers represent 10th and 90th percentile and open circles represent points outside the 10th and 90th percentile. *BLT mice were not dosed with efavirenz due to prior toxicity concerns (personal communication, JV Garcia).

2.4.3. Concentration of ARVs in the CSF and brain tissue of NHPs:

ARV concentrations across the four brain regions that were sampled in the NHPs did not differ by LC-MS/MS **(Figure 2.4; p>0.08)**. Therefore, these concentrations were combined for one concentration measure per animal.
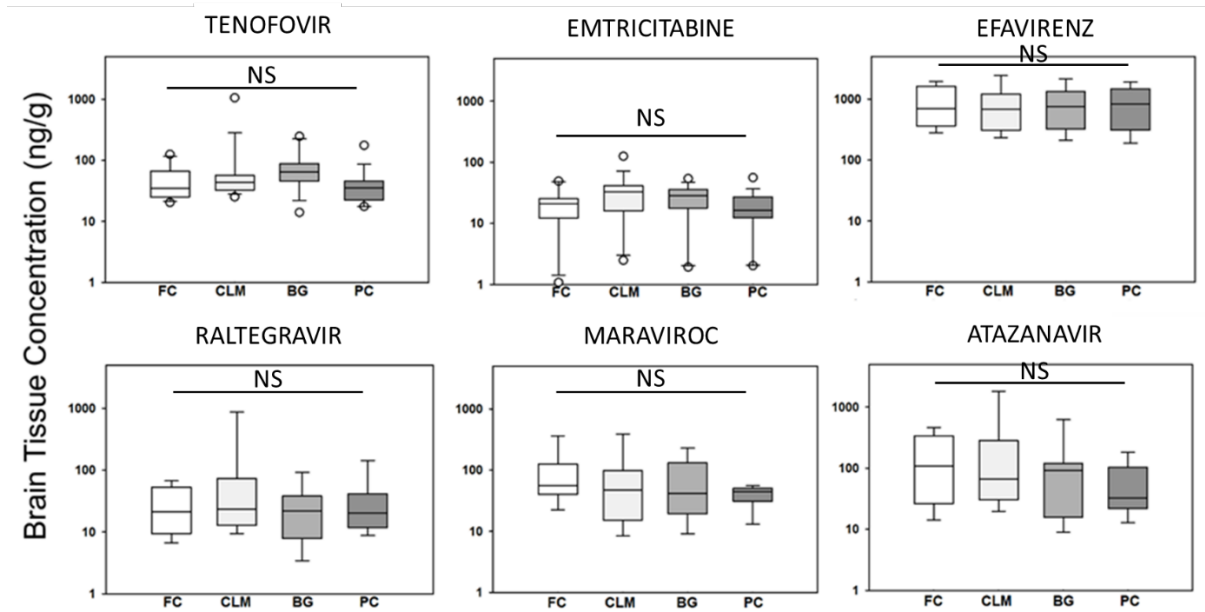
Figure 2.4. Antiretroviral concentrations in different parts of the nonhuman primate brain. ARV concentration was not significantly different across the various parts of the brain (p>0.08). FC – frontal cortex, CLM – cerebellum, BG – basal ganglia, PC – Parietal cortex.

EFV reached the highest concentration in the brain tissue (775 [240-1982] ng/g), which was >9-fold higher than all other ARVs, where median concentrations were <100ng/g **(Figure 2.5a)**. The lowest brain tissue concentrations were found for FTC (26.29 [2-69.2] ng/g) and RAL (21.8 [11.5-264.9] ng/g). Brain tissue:plasma concentration ratio was highest for EFV (4.2 [4-4.6], **Figure 2.5b**) and lowest for RAL (0.09 [0.02-0.21]). Brain tissue ARV concentrations were >6-fold higher (p<0.02) than the CSF. EFV concentration in the CSF strongly correlated with brain tissue (r=0.91, p<0.001) but this was not the case (r<0.5) for other ARVs **(Figure 2.6)**. EFV concentrations in the brain tissue also showed strong

correlation with the plasma concentrations (r=0.97, p<0.001), which was not the case for the other ARVs (data not shown). For EFV and RAL, the brain tissue:plasma concentration ratio was two- to four-fold lower in infected animals relative to uninfected animals, although this difference was not statistically significant (p=0.15). We also noted a two-fold increase in brain tissue:plasma concentration in female NHPs for RAL, but this did not reach statistical significance (p=0.15).
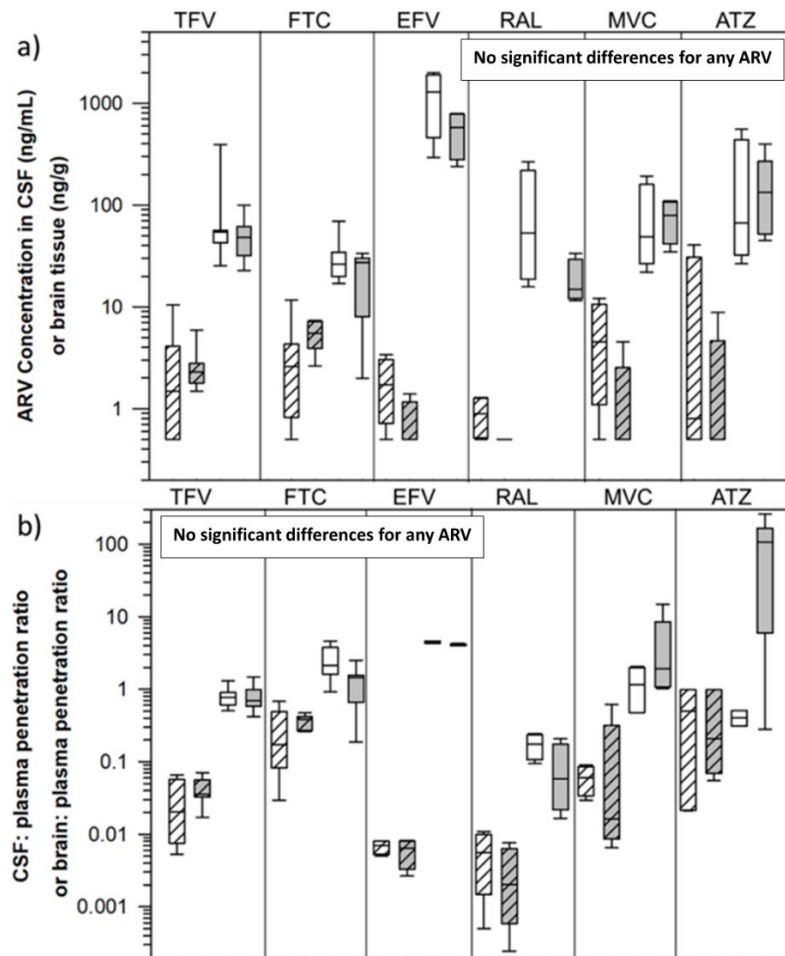
Figure 2.5. (a) Antiretroviral concentrations in the CSF and brain tissue and (b) the penetration ratio of CSF or brain tissue: plasma concentrations in NHPs. ARV concentrations and penetration ratios are shown in the CSF (stripes) and brain tissue (solid fill) stratified by infection status (uninfected animals in white and infected animals in gray). Brain tissue concentrations were higher than CSF for all ARVs (p<0.01). Tissue penetration ratios were higher than CSF penetration ratios for all ARVs except ATZ (p<0.01). Infection did not alter brain and CSF distribution of ARVs (p>0.15). Boxes represent 1st and 3rd quartile with median line. Whiskers represent 10th and 90th percentile.
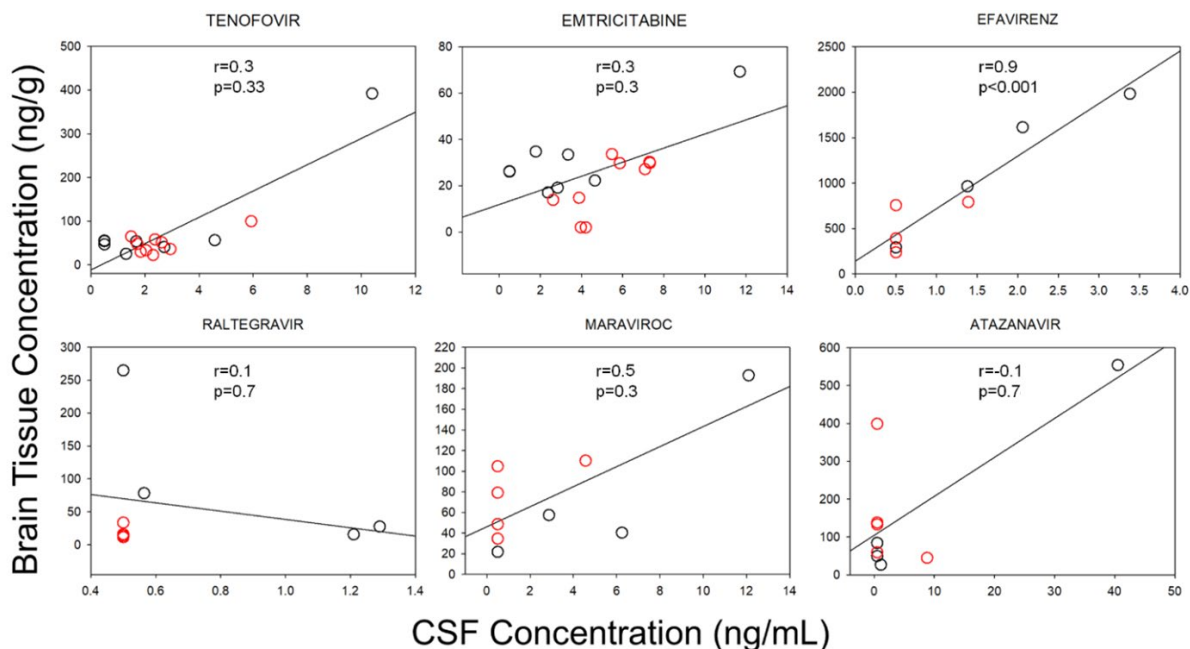
Figure 2.6. Correlation analysis between antiretroviral concentrations in the brain tissue and cerebrospinal fluid in the NHPs. Significant correlations between the brain tissue and CSF concentrations were only noted for efavirenz (r=0.91; p<0.001). Black open circles – uninfected animals and red open circles – RT-SHIV-infected animals. Legend: CSF – cerebrospinal fluid.

2.4.4. Inter-species comparison of the brain tissue:plasma concentration of ARVs and brain tissue concentration of active metabolites:

For most ARVs, brain tissue:plasma concentration ratio in the NHPs was 10- to 100-fold higher than the BLT mice (p<0.006), and 5- to 100-fold higher than the hu-HSC-RAG (p<0.02). Often, this result was due to lower ARV concentrations in the brain tissue and plasma of both humanized mouse models **(Figure 2.7 and Appendix 2.1)**. However, in the case of TFV and FTC, the low brain tissue penetration in the two humanized mouse models was a result of lower brain tissue concentrations and higher plasma concentrations in the mice compared to NHPs. Only the brain tissue: plasma penetration ratio of RAL (median of 0.132; p=0.6) was preserved across all three species while the MVC brain tissue: plasma penetration ratio (median of 1.86; p=1.0) was preserved across the BLT mice and NHPs **(Figure 2.7)**. RAL

was the only ARV that showed strong positive correlation between brain tissue and plasma concentrations across all animal models (r=0.85, p<0.001, data not shown). The concentration of ARVs in the plasma, CSF, and brain tissue across all the individual animals is shown in **Appendix 2.2**.
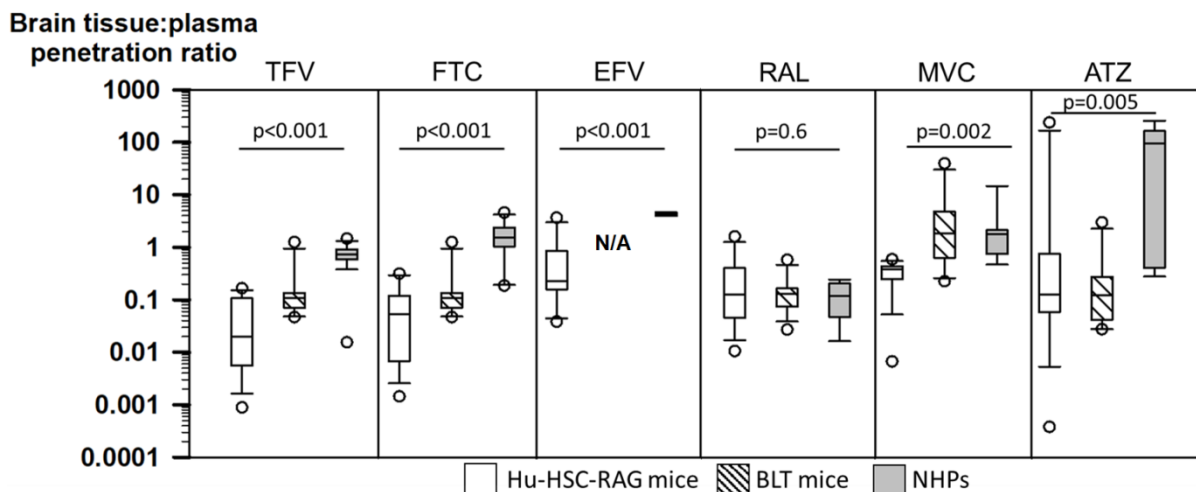
Figure 2.7. Antiretroviral brain tissue:plasma penetration ratio in the hu-HSC-RAG mice (n=26), BLT mice (n=13) and nonhuman primates (n=17). Only the brain tissue:plasma penetration ratio of RAL was preserved across all three species (p=0.6). MVC brain tissue:plasma penetration ratio did not differ between the BLT mice and NHPs (p=1.0) and ATZ penetration did not differ between the hu-HSC-RAG and BLT mice (p=0.8). For all other ARVs, the order of brain tissue penetration ratio was hu-HSC-RAG<BLT<NHP. Boxes represent the 1st and 3rd quartile of the data with median line. Whiskers represent the 10th and 90th percentile of the data and open circles represent outliers. The BLT mice were not dosed with EFV due to toxicity issues.

The active metabolite of TFV, TFV-dp, was quantifiable in all brain tissue samples, with concentrations ranging from 851 to 179,000 fmol/g of tissue. Median brain tissue concentrations of TFV-dp were 10-fold higher in the hu-HSC-RAG mice (14,700 fmol/g) compared to the BLT mice (1440 fmol/g), despite TFV concentrations being lower in the hu-HSC-RAG mice, though this did not reach statistical significance (p=0.29). TFV-dp concentration in the NHP brain was 34,800 (15,000-179,000) fmol/g. Due to the low concentration of FTC in the brain tissue for both the humanized mouse models (3.31 ng/g [0.14

ng/g to 29.1 ng/g] and NHPs (26.3 ng/g [2.0 ng/g to 69.3 ng/g]), its active metabolite FTC-tp was not quantifiable across all three animal models **(Figure 2.8)**. TFV-dp concentrations across the individual animals are shown in **Appendix 2.3**.
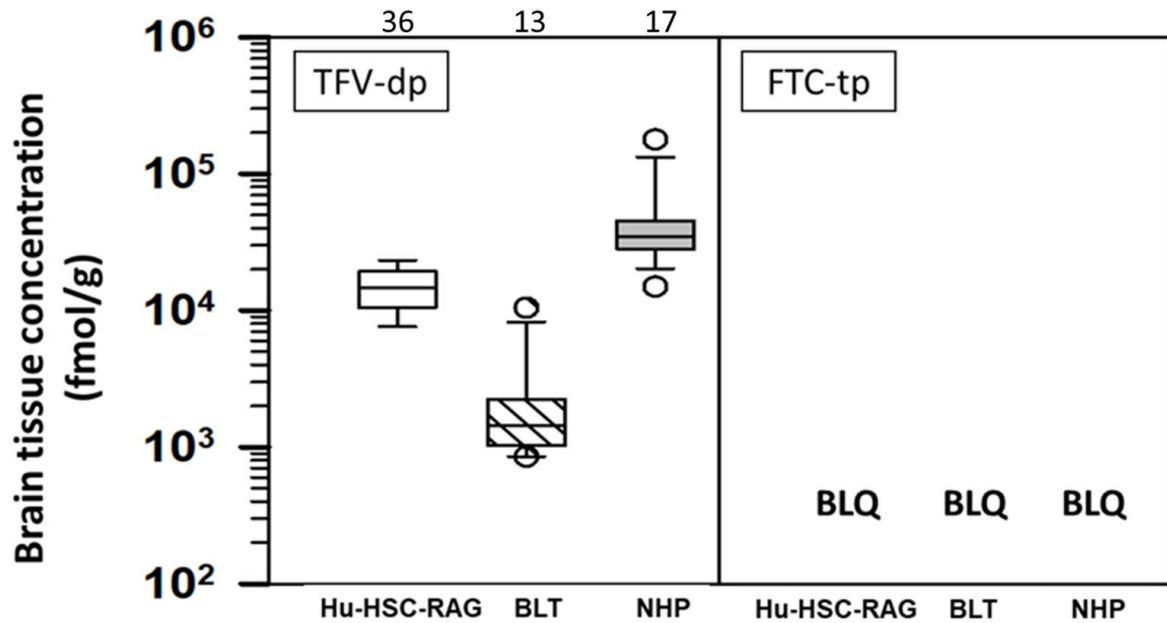
Figure 2.8. Concentration of active metabolites of tenofovir and emtricitabine in the brain tissue of hu-HSC-RAG mice, BLT mice and nonhuman primates. Emtricitabine triphosphate (FTC-tp) was not detected in the brain tissue of any of the animal models. Median brain tissue concentrations of tenofovir diphosphate (TFV-dp) were 10-fold higher in the hu-HSC-RAG mice compared to the BLT mice (14371 fmol/g vs 1443 fmol/g, p=0.29). TFV-dp concentration in the NHP brain was 34,840 fmol/g**.**

2.4.5. Protein binding of ARVs in the brain tissue of nonhuman primates and IQ$_{90}$ calculation:

Protein binding in the brain tissue for EFV was 97% (91%, 98%), whereas it was lower for ATZ, (24% [0%, 39%]) and negligible for MVC (3%, [0%, 19%]). Due to low concentrations of RAL in brain tissue, the fraction unbound could only be estimated for one of the samples (24%, n=1).

The IQ$_{90}$ calculated using the unbound brain tissue drug concentration (EFV, MVC, ATZ, and RAL) and unbound IC$_{90}$ values, are shown in the open circles in **Figure 2.9**. Only EFV was consistently above an IQ$_{90}$ of one in all of the animals. One animal showed RAL IQ$_{90}$ of 1.1 while one other animal showed a TFV-dp IQ$_{90}$ of 1.1. For MVC, ATZ, TFV, and FTC none of the animals had IQ$_{90}$ >1. IQ values across the individual NHPs are shown in **Appendix 2.4**.
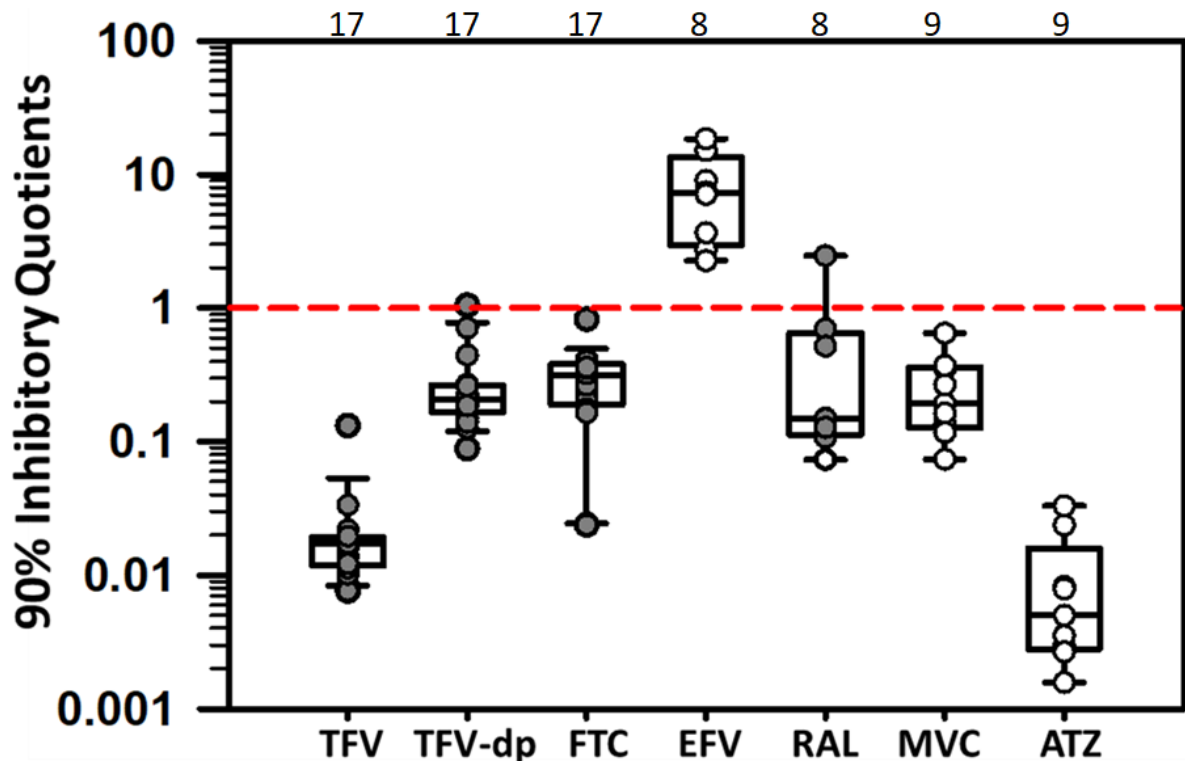
Figure 2.9. 90% inhibitory quotients (IQ$_{90}$) for antiretrovirals and metabolites in the brain tissue of nonhuman primates. EFV had the highest IQ$_{90}$ values in the nonhuman primates, which was above one for all eight animals. In case of TFV, TFV-dp, FTC, MVC, and ATZ none of the animals had IQ$_{90}$ above one. Boxes represent the 1st and 3rd quartile of the data with median line. Whiskers represent the 10th and 90th percentile of the data. Dot-plot overlay represents individual values; the open circles represent values that were derived from the unbound brain tissue concentrations while the grey filled circles represent values that were derived from the total brain tissue concentrations. The numbers at the top of the graph represent total number of NHPs

2.4.6. Mass-spectrometry imaging to visualize spatial distribution of ARVs in the brain tissue:

With the exception of EFV, all other ARVs were not detected in the brain tissue of the humanized mice and NHPs by IR-MALDESI as the median concentration of these ARVs were <100 ng/g in the brain tissue by LC-MS/MS.

The MSI results in **Figure 2.10** show response to EFV and endogenous marker cholesterol **(Figure 2.10, left-pane)** which was used to delineate regions of WM and GM, and heme **(Figure 2.10, middle-pane)**, which was used as a surrogate for blood contamination in the brain tissue samples. EFV distribution **(Figure 2.10, right-pane)** was masked based on the heme distribution in order to show the EFV response that did not colocalize with heme. EFV distribution was visualized in only one hu-HSC-RAG mouse with the highest EFV concentration measured by LC-MS/MS (1,400 ng/g) (**Figure 2.10a**). In this animal, drug distribution was relatively homogeneous across the brain structures and heme distribution accounted for 30% of the summed EFV MSI response across the tissue. EFV was not detected in the other mice, where concentrations were <35 ng/g. In the NHPs, EFV was detected in all tissues. In the uninfected animals (**Figure 2.10b**), EFV concentrations were up to 2-fold higher in the WM relative to the GM. The variability (as defined by CV%) of concentration/voxel in the uninfected animals was approximately 85% in the GM and 78% in the WM. Infected animals showed 86% lower EFV concentration (**Figure 2.10c**) compared to uninfected animals, and no morphological differences in EFV distribution pattern were evident. The variability (CV%) of concentration/voxel in the infected NHPs was similar to the uninfected NHPs; 77% in the GM and 83% in the WM. The heme response was negligible in the

uninfected and SHIV-infected NHPS and accounted for only 1% of the summed EFV MSI response across the tissue.
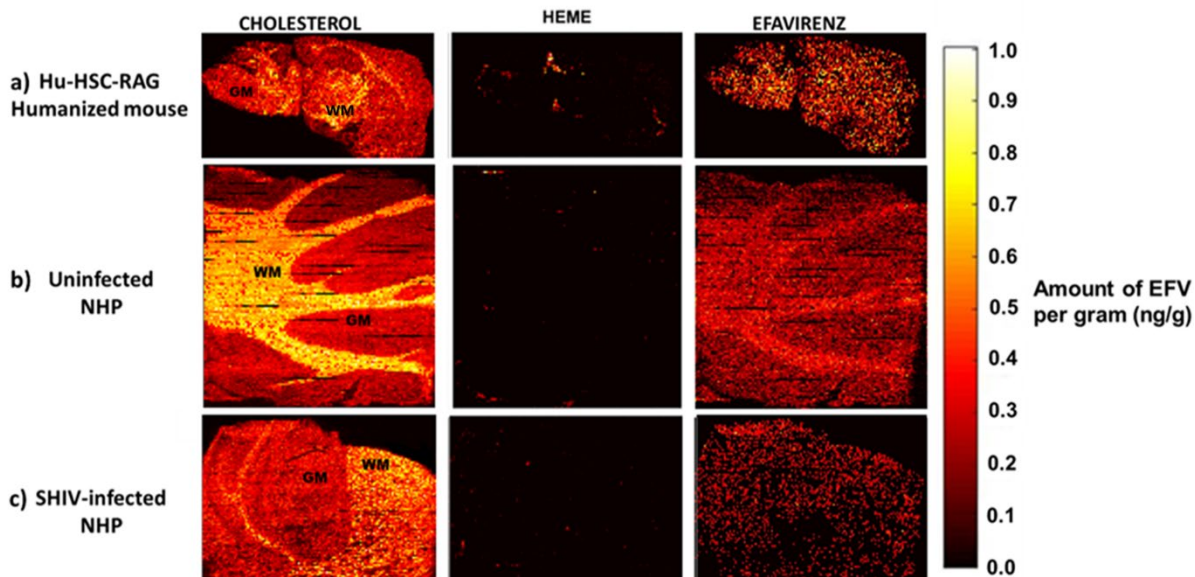
Figure 2.10. Mass-spectrometry imaging of the cholesterol and heme distribution and the concentration of efavirenz per volumetric pixel in the brain tissue of preclinical species. The cholesterol heat maps shown on the left-pane were used to indicate morphological differences in the brain tissue between the WM and the GM. The heme distribution maps shown in the middle-pane were used as a marker of blood contamination in the brain tissue. The efavirenz heat maps shown on the right-pane were masked with the heme distribution to show efavirenz response outside of the blood contamination.

(a) Efavirenz was detected in only one infected hu-HSC-RAG mouse with homogenous distribution throughout the tissue. The blood contamination in this animal accounted for 30% of the total efavirenz response in the brain tissue (b) In the cerebellum tissue of uninfected NHPs, preferential distribution of efavirenz was noted in the WM compared to the GM. (c) In the RT-SHIV-infected NHPs, there was 86% lower concentration of efavirenz in the brain tissue. Heme distribution in all NHPs was minimal, accounting for ~1% of the efavirenz response. Legend: WM – white matter, GM – grey matter, NHP – nonhuman primate.

In the infected female macaque that developed liver failure, the median brain tissue concentrations were 3600, 280, 5610, and 230 ng/g for TFV, FTC, EFV, and RAL, respectively. However, despite these concentrations being 10- to 100-fold higher than the other animals, the brain tissue distribution of only TFV and EFV were detected in this animal by IR-

MALDESI. **Figure 2.11** shows the drug distribution images in the cerebellum tissue. The median concentration of EFV across the four regions of the brain tissue by IR-MALDESI was 23,151 ng/g (four-fold higher than the LC-MS/MS results) while the median concentration of TFV was 915 ng/g (four-fold lower than the LC-MS/MS results). EFV showed slight preferential distribution in the white matter (WM) versus gray matter (GM) in the cerebellum while TFV was preferentially distributed in the GM in the cerebellum and frontal cortex regions.
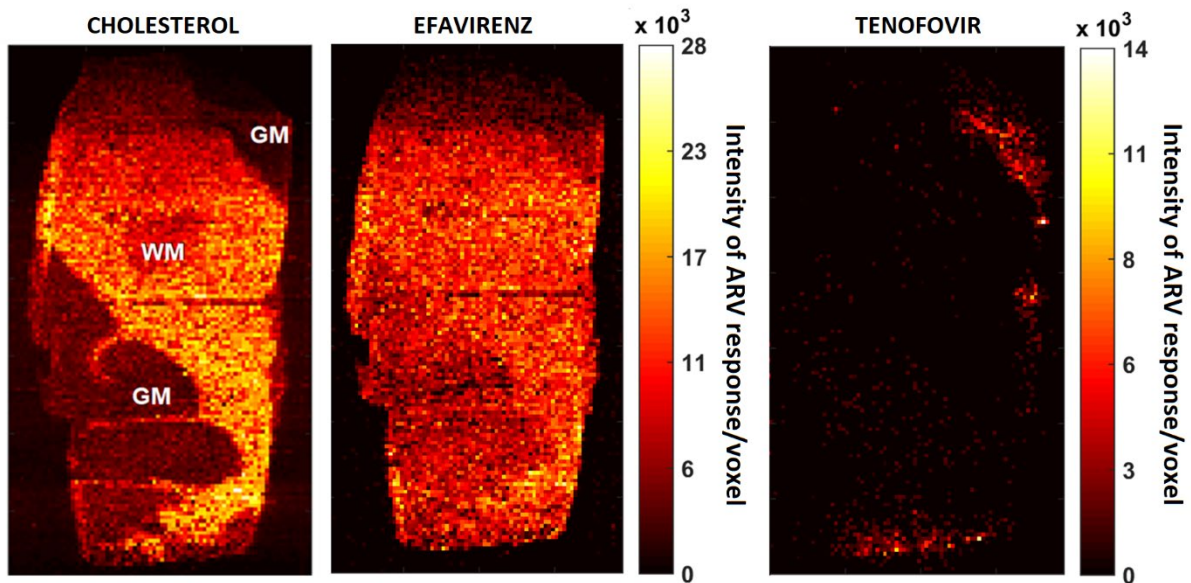
Figure 2.11. Mass spectrometry imaging of cholesterol, efavirenz and tenofovir distribution in one RT-SHIV infected female macaque. The cholesterol heat maps shown on the left-pane are used to indicate morphological differences in the cerebellum tissue between the white matter and the gray matter. The efavirenz and tenofovir heat maps show drug signal intensity per volumetric pixel. For the two antiretrovirals detected in this animal, slight preferential distribution of efavirenz was noted in the white matter versus gray matter. For tenofovir, there appeared to be slightly higher drug distribution in the gray matter relative to the white matter. Increase in signal intensity represents increase drug concentrations. Legend: WM – white matter, GM – gray matter.

Finally, the MSI drug distribution heat maps of EFV were overlaid with the CD11b cell and CD4+ T-cell distribution maps in the brain tissue. In **Figure 2.12**, the overlay of CD11b

cells is shown with EFV in the cerebellum of uninfected (**Figure 2.12a**) and RT-SHIV-infected NHPs (**Figure 2.12b**). For uninfected animals, the fraction of total CD11b cell or CD4+ T-cell cellular area with detectable EFV concentrations ranged from 50-80%. For the infected animals, the fractional coverage of cells was even lower from 45-70%. However, the fractional coverage of cells that contained EFV at a concentration above the IC_{50} target was only ~3% for both uninfected and infected animals.
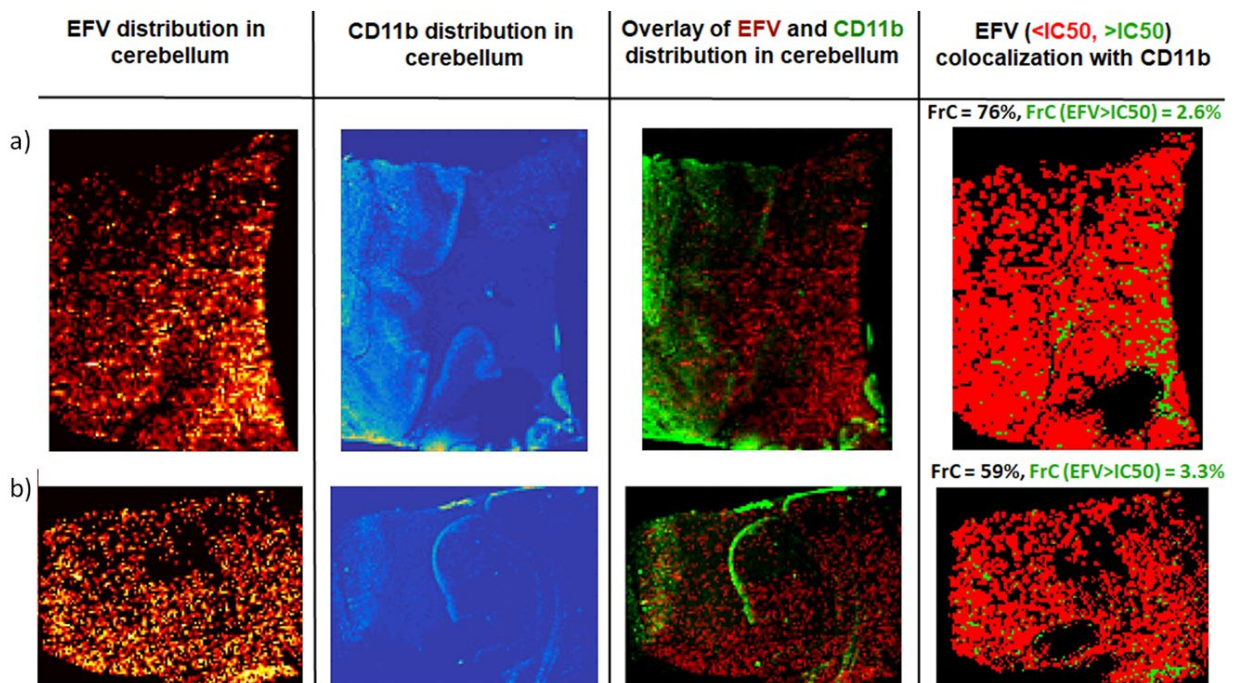
Figure 2.12. Overlay between efavirenz MSI and CD11b+ cell distribution in the cerebellum tissue in a) uninfected and b) RT-SHIV-infected animals. Distribution of EFV and CD11b+ cells in the cerebellum and the overlay of distribution are shown in (a) uninfected and (b) RT-SHIV-infected animals. In the far-left panel, brighter colors represent higher concentration of EFV. In the panel second from the left, light color represents greater density of cells, increasing form light blue to yellow. In the panel second from the right, overlay between EFV MSI and cell distribution is shown. In far-right panel, only the target cells containing detectable EFV or EFV above IC50 are shown. Fractional coverage of the CD11b+ cells with detectable EFV was higher in the uninfected animals compared to the RT-SHIV infected animals. Coverage with EFV concentration >IC50 was only 3% regardless of infection status.

2.5.   Discussion

In this analysis we present a comprehensive overview of brain tissue concentrations of ARVs across three commonly used HIV preclinical models. We show that ARV brain tissue penetration by LC-MS/MS is highly variable between the ARVs (50-150%), and between the animal models for a given ARV. This variability is consistent, albeit greater, than the variability shown with ARV LC-MS/MS concentration data in human CSF (~35%)(15).

Comparing drug exposure between the species, brain tissue penetration rank order distinctively increased from hu-HSC-RAG mice to BLT mice to NHPs for TFV and FTC. For ATZ, the brain tissue penetration was similar in hu-HSC-RAG and BLT humanised mouse models, but was 100-fold lower higher in NHPs. For MVC, brain tissue penetration was lower in the hu-HSC-RAG model and similar in the BLT mice and NHPs. RAL penetration into the brain was similar across all three species and this may be a result of the increased plasma concentration of RAL in the NHPs relative to the BLT and the hu-HSC-RAG mice. For the other ARVs that showed a large degree of overlap in plasma concentrations between the preclinical models, underlying drug-transporter interactions or physicochemical properties may play a role in the variability in brain tissue concentrations. For example, the greater brain tissue:plasma penetration of TFV, FTC, and MVC in the BLT mice relative to the hu-HSC-RAG mice may be due to co-administration of these ARVs with ATZ in the BLT model, which inhibits drug efflux by P-gp, BCRP, and MRP1(39). While we were not able to avoid drug-drug interactions due to the limited number of animals, such interactions are clinically unavoidable as well since multiple drugs constitute HIV treatment regimens. In such cases, we can use these preclinical models to also test how different ARV combinations may affect tissue distribution.

In this study, we found that CSF ARV concentrations in NHPs approximate human concentrations as reported by Calcagno(40). FTC was the one exception, where CSF concentrations were approximately three-fold lower in NHPs. While there are fewer human brain tissue studies to compare to our preclinical models, one recent study by Nicol provides some insights(41). Three African men with AIDS taking EFV and TFV had brain tissue concentrations measured post-mortem. The median concentrations of EFV and TFV were 900 ng/g and 80 ng/g, respectively, which agree with the values we report in the NHPs (775 ng/g and 65 ng/g, respectively).

To address the current gap of whether CSF exposures of ARVs are an appropriate surrogate for brain tissue exposure, we compared ARV concentrations between the brain tissue and CSF in the NHPs. Our data show that the total brain tissue concentrations are consistently higher than CSF concentrations. This was shown across all classes of drugs, irrespective of drug lipophilicity, pKa, drug transporter affinity, or other physicochemical properties, and agrees with what has been shown in the literature for several classes of CNS-acting drugs. For example, anti-epileptics like carbamazepine that are moderately lipophilic (pKa=2) showed C_{CSF}/C_{brain}=0.2(11), while poorly lipophilic CNS stimulant theophylline showed CSF to brain tissue exposure ratio of 0.74(10). For the low permeability ARVs such as TFV and MVC (both ARVs are BCS class III), CSF concentrations may have underpredicted brain tissue concentrations due to the fast recycling rate of the CSF that acts like a 'sink' to clear drug(42). For other ARVs that have higher permeability, underlying interactions between ARVs and drug transporters might also play a role in the discrepancy between drug concentration measurements. For example, FTC is a highly permeable drug (BCS class I) and is a substrate of MRP1(43), an efflux transporter that is localized on the basolateral membrane of the B-

CSF-B. MRP1 effluxes drug-substrates out in the direction of CSF to blood(44,45) at the B-CSF-B but is not localized on the BBB(45). Thus, the presence of MRP1 on the B-CSF-B but not on the BBB could result in lower FTC concentrations in the CSF relative to the brain tissue. For the remaining ARVs: EFV, RAL, and ATZ, which are highly permeable (BCS class I or class II) and substrates of either P-gp or BCRP, our results may appear to contradict conventional understanding, since P-gp and BCRP are both localized on the apical membrane of the BBB (direction of drug-efflux is brain to blood) and the B-CSF-B (direction of drug-efflux is blood to CSF)(45). However, many of these ARVs (FTC, EFV, MVC, and ATZ) are also inhibitors of P-gp and BCRP(46). As previously discussed, co-administration of multiple ARVs may have resulted in significant inhibition of the function of P-gp and BCRP and accumulation of ARVs in the brain tissue relative to the CSF. These data suggest that deriving concentration-efficacy relationships in the CNS using only CSF concentrations may be inaccurate.

This is the first study to define ARV IQ_{90} in the brain tissue using protein-unbound brain tissue concentrations. We chose to calculate IQ values since they have previously demonstrated utility in studying the relationship between drug exposure and efficacy(47,48). Targeting $IQ_{90}>1$ in plasma has been associated with improvement in virologic control and clinical outcomes(47,48). Importantly, recent work by Calcagno(15) suggested that the CSF IQ_{95} may guide the rational selection of CNS-targeted ARV regimens. In order to derive the IQ_{90}, we measured the unbound concentration in the brain tissue for EFV, RAL, MVC, and ATZ. Since TFV and FTC protein binding in plasma is <10%, we used the total concentrations in brain tissue for their IQ_{90} estimation This analysis provided a few novel findings regarding brain tissue protein binding and surrogate measures of efficacy using IQ_{90} estimation. First,

we showed that the extent of drug binding in the brain tissue was low (0-24%) for all ARVs except EFV (91-99%). The degree of brain tissue binding for all ARVs was lower than the blood plasma protein binding that has been previously reported for these drugs. For example, ATZ has been shown to be highly bound in the blood plasma (86%)(49), however, the median binding of ATZ in the brain tissue was only 24%. Similarly, while MVC has been shown to be moderately bound in the blood plasma (~76%)(50), the binding of MVC to the brain tissue was negligible (<3%) in this analysis. These results can be explained by the very low concentration of drug binding proteins in the brain tissue, relative to the plasma. For example, albumin concentration ranges from 35 to 50 g/L in the plasma, but is <1 mg/L in the brain tissue(51). The relatively high protein binding of EFV (97%) in the brain tissue, comparable to the plasma (99.5%)(49), may be due to the high lipophilicity of EFV (logP=4.6) and the binding affinity of EFV for CYP46A1 (cholesterol hydroxylase), an enzyme localized to the endoplasmic reticulum of neurons(52,53).

These data may also be useful for understanding drug toxicity in the CNS. For example, ATZ has been shown to cause neuronal toxicity, both in pig-tail macaques (with the same dosage regimen of ATZ that we used in this study), as well as in an in-vitro system of human cells(54). While ATZ concentrations in the CSF of our NHPs ranged from 0.5 ng/mL to 40 ng/mL, we found the unbound brain tissue concentrations of ATZ (38 ng/g to 418 ng/g) to be at least two-fold higher than the total ATZ concentrations that caused neuronal toxicity in the human in-vitro system, potentially explaining the macaque toxicity finding. Our data are among the first that can be used to make this connection, since previous analyses relied on CSF concentrations of ATZ which are low clinically (ranged from 5-21 ng/mL)(55). High ATZ

concentrations in the human brain tissue may also explain the clinical cases of CNS toxicity that have been reported due to ATZ(56).

We further demonstrate that for most ARVs, the IQ_{90} was <1 for all but two of the animals. For RAL, the IQ_{90} in the one animal where we could measure unbound brain tissue concentration was 0.07. Even when using total brain tissue concentrations, the IQ_{90} of RAL was <1 for six of the remaining seven animals. This shows that despite brain tissue concentrations being 16- to 1000-fold greater than the CSF, very few animals achieve ARV concentrations >IC_{90} of RT-SHIV replication. We also show that despite having a high degree of protein binding in the brain tissue, EFV still achieves an IQ_{90} of >1, in all eight animals. This suggests that by the IQ method, free EFV concentrations are high enough in the brain to achieve efficacy.

The results above were based on our LC-MS/MS analysis, whereby tissue homogenate was assessed for drug concentrations. However, the results of our MSI analysis indicated that there was heterogeneity in EFV distribution into the brain tissue that led to a different estimation of surrogate efficacy. In uninfected NHPs, EFV had a relatively heterogeneous distribution across brain tissue, accumulating up to three-fold higher in the cerebellar WM versus GM. Given recent evidence that EFV binds to CYP46A1 (cholesterol hydroxylase; an enzyme localized to the endoplasmic reticulum of neurons)(52,53), widespread EFV distribution may be a function of neuronal binding with a very low fraction unbound (~3%) as described above. In the case of RT-SHIV infected NHPs, the brain tissue concentrations were seven-fold lower than the uninfected animals, which made it more difficult to detect regional differences in drug localization. Interestingly, the regional coverage of HIV target cells with EFV concentrations >IC_{50} in this analysis was only 3%, in all animals. Despite all animals

having EFV concentrations >the IC_{90} by tissue homogenate, none of the areas where the target cells were located contained EFV at these concentrations. Rather, preferential accumulation of EFV was in the WM, whereas an increased density of microglial cells or CD4+ T-cells (target cells for HIV replication) is found in the GM(57). Taken together with the high brain tissue protein binding, these preliminary results indicate the potential for suboptimal coverage of active EFV within the brain tissue and active viral replication despite high IQs as measured by tissue homogenate. These results may help explain why CSF escape may still occur in patients who are treated with EFV(2,58), despite the high concentrations of drug that are achieved in the CNS. Future experiments imaging viral replication in the CNS along with drug concentrations should be performed to understand the clinical implications of these findings.

There were a few limitations to this investigation. Sex differences in the plasma PK of laboratory animals have been observed with several classes of anti-infective and CNS-acting drugs(59). Although we were unable to secure male humanised mice for this investigation, we evaluated the CNS distribution of ARVs in male and female NHPs and did not find any substantive differences in CSF or brain tissue concentrations between males and females. Another limitation of this study is the missing information on IC_{90} values against the RT-SHIV strain of virus for several of the ARVs in our analysis. As mentioned earlier, in case of the NRTIs and NNRTIs, using the IC_{90} for the clinical HIV-1 isolates was a reasonable estimate, as has been shown for the IC_{50} for viral replication(60). Finally, the IC_{90} values against RT-SHIV were 20-fold (RAL), 100-fold (MVC), and 1,000-fold (ATZ) higher than against the clinical HIV-1 isolates, respectively. If unbound exposures in the human brain tissue approximate the NHP exposures, MVC and ATZ would achieve IQ_{90} >1 in the human brain,

although this may not the case for RAL (IQ_{90} would be 0.9 based on the unbound exposures from one NHP).

2.6.   Conclusions

For the ARVs examined in this study, penetration into the brain tissue relative to plasma was only preserved across all three species for RAL and was otherwise 10- to 100-fold higher in NHPs compared to the humanized mice. NHP brain tissue penetration of TFV, EFV, RAL and MVC were 6- to 1000-fold higher than the CSF. Because of this variable and increased concentration of ARVs in brain tissue, the CSF may not be a global surrogate for brain tissue concentrations. Except for EFV, all ARVs were >75% unbound in the brain tissue and only EFV showed unbound concentrations in the brain tissue above an IQ_{90} in all the animals. Contrary to the IQ results, our IR-MALDESI investigations found that EFV poorly colocalized with HIV-target cells in the brain as a result of preferential accumulation in the white matter. These results show that despite a high concentration of free drug, lack of adequate EFV spatial coverage at the target cells of interest may contribute to HIV persistence in the brain[58] and this should be investigated further.

2.7.   REFERENCES

1.   Valcour V, Chalermchai T, Sailasuta N, Marovich M, Lerdlum S, Suttichom D, et al. Central nervous system viral invasion and inflammation during acute HIV infection. J Infect Dis. 2012;206(2):275–82.

2.   Edén A, Fuchs D, Hagberg L, Nilsson S, Spudich S, Svennerholm B, et al. HIV-1 viral escape in cerebrospinal fluid of subjects on suppressive antiretroviral treatment. J Infect Dis. 2010;202(12):1819–25.

3.   Farhadian S, Patel P, Spudich S. Neurological complications of HIV infection. Curr Infect Dis Rep. 2017;19(50):1–7.

4.   Joseph SB, Arrildt KT, Sturdevant CB, Swanstrom R. HIV-1 target cells in the CNS. J Neurovirol. 2014;276–89.

5.   New DR, Maggirwar SB, Epstein LG, Dewhurst S, Gelbard HA. HIV-1 Tat induces neuronal death via tumor necrosis factor-α and activation of non-N-methyl-D-aspartate receptors by a NFκB-independent mechanism. J Biol Chem. 1998;273(28):17852–8.

6.   Zayyad Z, Spudich S. Neuropathogenesis of HIV: From Initial Neuroinvasion to HIV-Associated Neurocognitive Disorder (HAND). Curr HIV/AIDS Rep. 2015;12(1):16–24.

7.   Ances BM, Ellis RJ. Dementia and neurocognitive disorders due to HIV-1 infection. Semin Neurol. 2007;27(1):86–92.

8.   Marra CM. HIV-associated neurocognitive disorders and central nervous system drug penetration: what next? Antivir Ther. 2015;20(4):365–7.

9.   Letendre S. Central Nervous System Complications in HIV Disease : HIV-Associated Neurocognitive Disorder. Top Antivir Med. 2011;19(4):137–42.

10.   Liu X, Smith BJ, Chen C, Callegari E, Becker SL, Chen X, et al. Evaluation of cerebrospinal fluid concentration and plasma free concentration as a surrogate measurement for brain free concentration. Drug Metab Dispos. 2006;34(9):1443–7.

11.   Rambeck B, Jürgens UH, May TW, Wolfgang Pannek H, Behne F, Ebner A, et al. Comparison of brain extracellular fluid, brain tissue, cerebrospinal fluid, and serum concentrations of antiepileptic drugs measured intraoperatively in patients with intractable epilepsy. Epilepsia. 2006;47(4):681–94.

12.   Smith DA, Di L, Kerns EH. The effect of plasma protein binding on in vivo efficacy: misconceptions in drug discovery. Nat Rev Drug Discov. 2010;9(12):929–39.

13.   Best BM, Koopmans PP, Letendre SL, Capparelli E V., Rossi SS, Clifford DB, et al. Efavirenz concentrations in CSF exceed IC50 for wild-type HIV. J Antimicrob Chemother. 2011;66(2):354–7.

14.   Croteau D, Letendre S, Best BM, Ellis RJ, Breidinger S, Clifford D, et al. Total raltegravir concentrations in cerebrospinal fluid exceed the 50-percent inhibitory

concentration for wild-type HIV-1. Antimicrob Agents Chemother. 2010;54(12):5156–60.

15. Calcagno A, Simiele M, Alberione MC, Bracchi M, Marinaro L, Ecclesia S, et al. Cerebrospinal fluid inhibitory quotients of antiretroviral drugs in HIV-infected patients are associated with compartmental viral control. Clin Infect Dis. 2015;60(2):311–7.

16. Acosta EP, Limoli KL, Trinh L, Parkin NT, King JR, Weidler JM, et al. Novel method to assess antiretroviral target trough concentrations using in vitro susceptibility data. Antimicrob Agents Chemother. 2012;56(11):5938–45.

17. Nguyen A, Rossi S, Croteau D, Best BM, Clifford D, Collier AC, et al. Etravirine in CSF is highly protein bound. J Antimicrob Chemother. 2013;68(5):1161–8.

18. Avery LB, Sacktor N, McArthur JC, Hendrix CW. Protein-free efavirenz concentrations in cerebrospinal fluid and blood plasma are equivalent: Applying the law of mass action to predict protein-free drug concentration. Antimicrob Agents Chemother. 2013;57(3):1409–14.

19. Denton PW, Garcia JV. Novel humanized mouse models for HIV research. Curr HIV/AIDS Rep. 2009;6:13–9.

20. Hatziioannou T, Evans DT. Animal models for HIV/AIDS research. Nat Rev Microbiol. 2012;10(12):852–67.

21. Melkus MW, Estes JD, Padgett-Thomas A, Gatlin J, Denton PW, Othieno FA, et al. Humanized mice mount specific adaptive and innate immune responses to EBV and TSST-1. Nat Med. 2006;12(11):1316–22.

22. Berges BK, Wheat WH, Palmer BE, Connick E, Akkina R. HIV-1 infection and CD4 T cell depletion in the humanized Rag2-/-gamma c-/- (RAG-hu) mouse model. Retrovirology. 2006 Jan;3:76.

23. North TW, Rompay KKA Van, Higgins J, Matthews TB, Wadford DA, Pedersen NC, et al. Suppression of Virus Load by Highly Active Antiretroviral Therapy in Rhesus Macaques Infected with a Recombinant Simian Immunodeficiency Virus Containing Reverse Transcriptase from Human Immunodeficiency Virus Type 1. J Virol. 2005;79(12):7349–54.

24. North TW, Higgins J, Deere JD, Hayes TL, Villalobos A, Adamson L, et al. Viral sanctuaries during highly active antiretroviral therapy in a nonhuman primate model for AIDS. J Virol. 2010 Mar;84(6):2913–22.

25. Thompson CG, Bokhart MT, Sykes C, Adamson L, Fedoriw Y, Luciw PA, et al. Mass spectrometry imaging reveals heterogeneous efavirenz distribution within putative HIV reservoirs. Antimicrob Agents Chemother. 2015;59(5):2944–8.

26. Srinivasan VJ, Atochin DN, Radhakrishnan H, Jiang JY, Ruvinskaya S, Wu W, et al. Optical coherence tomography for the quantitative study of cerebrovascular physiology. J Cereb Blood Flow Metab. 2011;31(6):1339–45.

27. Rompay KKAVAN, Cherrington JM, Marthas ML, Berardi CJ, Mulato AS, Spinner A, et al. 9- [2- (Phosphonomethoxy) Propyl] Adenine Therapy of Established Simian Immunodeficiency Virus Infection in Infant Rhesus Macaques. 1996;40(11):2586–91.

28. Mathez D, Schinazi RF, Liotta DC, Leibowitch J. Infectious amplification of wild-type human immunodeficiency virus from patients' lymphocytes and modulation by reverse transcriptase inhibitors in vitro. Antimicrob Agents Chemother. 1993;37(10):2206–11.

29. Pal R, Galmin L, Pereira LE, Li B, Zhang J, Li D, et al. Virological and molecular characterization of a simian human immunodeficiency virus (SHIV) encoding the envelope and reverse transcriptase genes from HIV-1. Virology. 2012;432(1):173–83.

30. Hassounah SA, Mesplede T, Quashie PK, Oliveira M, Sandstrom PA, Wainberg MA. Effect of HIV-1 Integrase Resistance Mutations When Introduced into SIVmac239 on Susceptibility to Integrase Strand Transfer Inhibitors. J Virol. 2014;88(17):9683–92.

31. Yilmaz A, Price RW, Gisslén M. Antiretroviral drug treatment of CNS HIV-1 infection. J Antimicrob Chemother. 2012;67(2):299–311.

32. Barry JA, Robichaud G, Bokhart MT, Thompson C, Sykes C, Kashuba ADM, et al. Mapping antiretroviral drugs in tissue by IR-MALDESI MSI coupled to the Q Exactive and comparison with LC-MS/MS SRM assay. J Am Soc Mass Spectrom. 2014;25(12):2038–47.

33. Robichaud G, Garrard KP, Barry JA, Muddiman DC. MSiReader: An open-source interface to view and analyze high resolving power MS imaging files on matlab platform. J Am Soc Mass Spectrom. 2013;24(5):718–21.

34. Csajka C, Marzolini C, Fattinger K, Décosterd L, Fellay J, Telenti A, et al. Population pharmacokinetics and effects of efavirenz in patients with human immunodeficiency virus infection. Clin Pharmacol Ther. 2003;73(1):20–30.

35. Lahiri CD, Reed-Walker K, Sheth AN, Acosta EP, Vunnava A, Ofotokun I. Cerebrospinal fluid concentrations of tenofovir and emtricitabine in the setting of HIV-1 protease inhibitor-based regimens. J Clin Pharmacol. 2015;56(4):492–6.

36. Cattaneo D, Gervasoni C, Meraviglia P, Landonio S, Fucile S, Cozzi V, et al. Inter- and intra-patient variability of raltegravir pharmacokinetics in HIV-1-infected subjects. J Antimicrob Chemother. 2012;67(2):460–4.

37. Crutchley RD, Ma Q, Sulaiman A, Hochreitter J, Morse GD. Within-patient atazanavir trough concentration monitoring in HIV-1-infected patients. J Pharm Pract. 2011;24(2):216–22.

38. Abel S, Van Der Ryst E, Rosario MC, Ridgway CE, Medhurst CG, Taylor-Worth RJ, et al. Assessment of the pharmacokinetics, safety and tolerability of maraviroc, a novel CCR5 antagonist, in healthy volunteers. Br J Clin Pharmacol. 2008;65(1):5–18.

39. Griffin T, Anneart P, Brouwer K. Influence of drug transport proteins on the pharmacokinetics and drug interactions of HIV protease inhibitor. J Pharm Sci.

2011;100(9):3636–54.

40. Calcagno A, Di Perri G, Bonora S, A. C, G. DP, S. B. Pharmacokinetics and Pharmacodynamics of Antiretrovirals in the Central Nervous System. Clin Pharmacokinet. 2014;53(10):891–906.

41. Nicol M, Taylor J, Pastick K, Fisher J, Karuganda C, Rhein J, et al. Differential Brain Tissue Penetration of Antiretrovirals and Fluconazole. In: Conference on Retroviruses and Opportunistic Infections (CROI); Abtract number: 474; Available from: https://www.croiconference.org/sessions/differential-brainissue- penetration-antiretrovirals-and-fluconazole [Accessed 10 August 2018]. Boston, Massachusetts; 2018.

42. Shen DD, Artru AA, Adkison KK. Principles and applicability of CSF sampling for the assessment of CNS drug delivery and pharmacodynamics. Adv Drug Deliv Rev. 2004;56(12):1825–57.

43. Bousquet L, Pruvost A, Didier N, Farinotti R, Mabondzo A. Emtricitabine: Inhibitor and substrate of multidrug resistance associated protein. Eur J Pharm Sci. 2008;35(4):247–56.

44. Wijnholds J, DeLange E, Scheffer G, van den Berg D, Mol C, van der Valk, M Schinkel A, et al. Multidrug resistance protein 1 protects the choroid plexus epithelium and contributes to the blood-cerebrospinal fluid barrier. J Clin Invest. 2000;105(3):279–85.

45. Strazielle N, Ghersi-Egea JF. Efflux transporters in blood-brain interfaces of the developing brain. Front Neurosci [Internet]. 2015;9. Available from: https://www.frontiersin.org/articles/10.3389/fnins.2015.00021/full. Last accessed: September 1st, 2018

46. Alam C, Whyte-Allman S-K, Omeragic A, Bendayan R. Role and modulation of drug transporters in HIV-1 therapy. Adv Drug Deliv Rev. 2016;103:121–43.

47. Hoefnagel J, Koopmans P, Burger D, Schuurman R, Galama J. Role of the inhibitory quotient in HIV therapy. Antivir Ther. 2005;10(8):879–92.

48. Winston A, Khoo S. Clinical application of the inhibitory quotient: is there a role in HIV protease inhibitor therapy? Curr Opin HIV AIDS. 2008;3(6):608–11.

49. Boffito M, Back DJ, Blaschke TF, Rowland M, Bertz RJ, Gerber JG, et al. Protein binding in antiretroviral therapies. AIDS Res Hum Retroviruses. 2003;19:825–35.

50. MacArthur M, Novak R. Maraviroc: The first of a new class of antiretroviral agents. Clin Infect Dis. 2008;47(2):236–41.

51. Srinivas N, Maffuid K, Kashuba ADM. Clinical Pharmacokinetics and Pharmacodynamics of Drugs in the Central Nervous System. Clin Pharmacokinet. 2018;57(9):1059–74.

52. Anderson KW, Mast N, Hudgens JW, Lin JB, Turko I V., Pikuleva IA. Mapping of the allosteric site in cholesterol hydroxylase CYP46A1 for efavirenz, a drug that

stimulates enzyme activity. J Biol Chem. 2016;291(22):11876–86.

53.   Mast N, Li Y, Linger M, Clark M, Wiseman J, Pikuleva IA. Pharmacologic stimulation of Cytochrome P450 46A1 and Cerebral Cholesterol Turnover in Mice. J Biol Chem. 2014;289(6):3529–38.

54.   Robertson K, Liner J, Meeker RB. Antiretroviral neurotoxicity. J Neurovirol. 2012;18(5):388–99.

55.   Best BM, Letendre SL, Brigid E, Clifford DB, Collier AC, Gelman BB, et al. Low atazanavir concentrations in cerebrospinal fluid. AIDS. 2009;23(1):83–7.

56.   Martina T. Atazanavir Causing CNS Toxicity? Unexplained Neurological Symptoms in Two Patients Recently Started on Atazanavir. J AIDS Clin Res. 2013;4(3):3–4.

57.   Lawson LJ, Perry VH, Dri P, Gordon S. Heterogeneity in the distribution and morphology of microglia in the normal adult mouse brain. Neuroscience. 1990;39(1):151–70.

58.   Mukerji SS, Misra V, Lorenz DR, Uno H, Morgello S, Franklin D, et al. Impact of Antiretroviral Regimens on CSF Viral Escape in a Prospective Multicohort Study of ART-Experienced HIV-1 Infected Adults in the United States. Clin Infect Dis [Internet]. 2018; Available from: https://doi.org/10.1093/cid/ciy267 [Epub ahead of print] [Accessed 1 September 2018]

59.   Czerniak R. Gender-based differences in pharmacokinetics in laboratory animal models. Int J Toxicol. 2001;20(3):161–3.

60.   Witrouw M, Pannecouque C, Switzer WM, Folks T, De Clercq E, Heneine W. Susceptibility of HIV-2, SIV and SHIV to various anti-HIV-1 compounds: implications for treatment and postexposure prophylaxis. Antivir Ther. 2004;9(1):57–65.

CHAPTER-III: INTER-SPECIES DIFFERENCES IN THE EXPRESSION OF DRUG TRANSPORTERS IN THE BRAIN TISSUE AND RELATIONSHIP WITH ANTIRETROVIRAL PENETRATION INTO THE BRAIN[1]

3.1. Summary

The persistence of HIV in the brain may be related to the limited penetration of antiretroviral (ARV) drugs into the brain tissue. At the blood brain barrier (BBB), several efflux transporters limit the entry of ARVs. However, the relationship between transporter expression within the brain tissue and ARV disposition into this compartment is complex and difficult to study clinically. While preclinical species could be used to better determine this relationship, there are no definitive studies examining transporter gene and protein expression in the brain tissue across the commonly used animal models for HIV infection. Further, while there have been several reports on transporter expression at the BBB, there are fewer studies examining drug transporter expression within the brain parenchyma, which serves as an important secondary barrier for the entry of ARVs into HIV target cells such as the microglia. The aims of this analysis were to measure the gene and protein expression as well as localization of drug transporters in the brain tissue, determine if factors such as sex and infection status led to alterations in transporter expression and examine the ability of transporter data in the brain tissue to predict the brain tissue:plasma penetration ratio of six ARVs across three preclinical species. Brain tissue samples were collected from two

humanized mouse (hu-HSC-Rag [36 animals]; BLT [13 animals]) models and one nonhuman primate (rhesus macaque, [NHP, 18 animals]) model and analyzed for gene (qPCR) and protein (liquid chromatography mass spectroscopy [LC-MS/MS] proteomics and Western blot) expression and localization (immunohistochemistry) of five efflux and four uptake transporters. ARV penetration into the brain tissue was determined by LC-MS/MS. The Kruskal-Wallis test was used to compare transporter expression across the preclinical species. Pearson's correlation test was used for the correlation analysis between ARV penetration into the brain and transporter expression. All transporter genes were detected in the brain tissue, and there were several significant differences in transporter expression detected across the preclinical species. For example, the gene expression of efflux transporter P-gp (Abcb1) was 100-fold lower ($p < 0.001$) in the BLT mice compared to the hu-HSC-Rag mice, while the uptake transporter Oatp1a4 (Slco1a4) was five-fold lower in the BLT mice compared to the hu-HSC-RAG mice. The transporter protein measurements showed that only P-gp and BCRP were detected in >85% of the brain tissue samples. There were no inter-species differences in the protein concentration of P-gp in the brain tissue ($p = 0.08$), however, there was a 16-fold higher BCRP protein concentration in the brain tissue of the NHPs compared to both the humanized mouse models ($p < 0.001$). Infection status did not alter transporter expression patterns in humanized mouse models or NHPs ($p > 0.1$), however sex differences did influence transporter expression. Male macaques had higher gene expression but lower protein concentration of BCRP and P-gp relative to female macaques ($p < 0.05$). Although the concentrations of P-gp and BCRP in the brain tissue showed a similar relative abundance as compared to the BBB, protein concentrations in the brain tissue were not a true surrogate for the BBB and did not have any utility in predicting the penetration of ARVs into the brain tissue.

From these analyses, we can conclude that uninfected animals can be used as preclinical models to study ARV transporters in the brain tissue since HIV infection status did not lead to differences in transporter expression across the preclinical models. While measurement of transporter expression in the brain tissue provides valuable information on the secondary transporter barrier in the brain tissue, drug transporter expression in the brain tissue appeared to only be a surrogate for the BBB expression of P-gp and not BCRP, possibly due to more extensive P-gp localization in the brain cells that comprise the neurovascular unit. Therefore, the integration of our results with drug transporter measurements at the BBB may provide more insight into the role of drug transporters in modulating ARV entry into the brain.

---

[1]This work has been presented, in part, at the 2017 IAS Meeting, Paris, France, July 23 – 26, 2017.

3.2.   Introduction

Of the nearly 37 million people worldwide living with HIV infection, approximately 53% are currently on antiretroviral (ARV) therapy[1]. With an increased access to ARV coverage, what was once a deadly disease has been transformed into a chronic, manageable illness with lifespan in HIV-infected individuals approaching that in uninfected individuals. However, despite the general effectiveness of ARV therapy in suppressing HIV viral load in the plasma, virus may continue to persist in various anatomical reservoirs in the body despite therapy[2–4] and this creates additional challenges to overcome for the treatment and cure of HIV.

Alongside other compartments such as the lymphatic system and genital tract, the central nervous system (CNS) has long been considered an anatomical reservoir for the persistence of HIV. Evidence for this comes from several studies within the cerebrospinal fluid (CSF), where there is poor exchange of viral genetic information with other sites of the body[5] that leads to a distinct evolution of macrophage and microglia derived virus (M-tropic virus) in the CSF despite a phenotype of CD4+ T-cell derived virus in the plasma[6]. HIV may continue to replicate in the CSF of patients who otherwise exhibit viral suppression in the plasma, a phenomenon termed "CSF escape"[7,8]. HIV RNA has also been detected in autopsy brain tissue from patients treated with ART and with undetectable HIV viral load in the plasma[9,10]. Clinically, the continued persistence of HIV and low-level viral replication in the CNS has been associated with the high prevalence (20-50%)[11], of mild forms of HIV-associated neurocognitive impairment[12] as well as the emergence of drug resistance to ARVs[13]. Since the events described above occur in the presence of ARV concentrations that suppress virus in the plasma, it is hypothesized that the inadequate penetration of ARVs into

the brain tissue results in ongoing HIV viral replication within this compartment. Sparse data exist on ARV concentrations and penetration into the brain tissue, and we have explored this across commonly used preclinical models for HIV infection in *Chapter II*. In *Chapter IV*, we explored the relationship between the model-predicted brain tissue concentrations of efavirenz (EFV) in HIV-positive patients and neurocognitive impairment scores. The objectives of this Chapter were to explore if there were differences in drug transporter expression in the brain tissue across the preclinical models and if any differences in transporter expression were associated with alterations in ARV PK in the brain tissue.

The CNS is regarded as a sanctuary site because the entry of ARVs into the brain tissue and CSF is highly regulated by two barriers: the blood brain barrier (BBB) and the blood-CSF-barrier (B-CSF-B). A combination of factors influences drug passage through the BBB and B-CSF-B. For example, highly lipophilic drugs are more likely to cross through the barriers and accumulate within the fat-rich brain tissue(14). Affinity for drug transporters might also influence ARV concentrations within the CNS since ARVs are substrates for several efflux transporters that are highly expressed along the barrier membranes (e.g. P-glycoprotein [P-gp] and breast cancer resistance protein [BCRP])(15,16). Several uptake and efflux drug transporters are found to be localized at the BBB(17,18), and there are marked inter-species differences in the protein concentration of these transporters at the BBB(17,19). The influence of other factors such as infection(20) and sex may also contribute to differences in transporter expression and have not been well characterized. Furthermore, drug transporters located within the brain tissue parenchyma could present a second barrier to cellular ARV permeability, however there is no clear consensus across the field on the differences in drug transporter expression between the brain tissue parenchyma and BBB. In this work, the gene expression

and protein concentration of drug transporters in the brain tissue of two species of humanized mice and rhesus macaques(21,22) were measured and correlation analyses were performed between transporter expression measurements in the brain tissue and brain tissue:plasma penetration ratio of six different ARV drugs. Finally, immunohistochemistry (IHC) staining was conducted to determine localization patterns of drug transporters within the brain tissue.

3.3.   Materials and Methods

3.3.1.   Antiretroviral dosing and tissue collection in preclinical models:

Animal dosing and tissue collection were described in detail in *Chapter II*, but briefly, three commonly used animal models were employed in this study: the hemopoietic stem-cell/RAG2- (hu-HSC-Rag; number of animals=36) and bone marrow-liver-thymus (BLT; number of animals=13) humanized mouse models, and a nonhuman primate model (rhesus macaque, [NHP]; number of animals=18), with half of each cohort infected with HIV or SHIV as described previously. The hu-HSC-RAG mice were dosed orally with one of several ARV regimens for ten days: EFV 10 mg/kg (six uninfected and six infected animals) alone; atazanavir (ATZ) 140 mg/kg (six uninfected and six infected animals) alone; or tenofovir (TFV) 208 mg/kg, emtricitabine (FTC) 240 mg/kg, raltegravir (RAL) 56 mg/kg, and maraviroc (MVC) 62 mg/kg (six uninfected and six infected animals) in combination. The BLT mice were dosed with all ARVs (at similar doses as in the hu-HSC-RAG mice) except for EFV, due to concerns of neurotoxicity of EFV in these animal models (personal communication with JV Garcia). The NHPs were dosed for ten days with a backbone of TFV 30 mg/kg subcutaneously and FTC 16 mg/kg subcutaneously with one of the following regimens added on: MVC 270 mg/kg twice daily (BID) with ATZ 150 mg/kg BID (four uninfected animals and five infected

animals) or EFV 200 mg once daily with RAL 100 mg/kg BID (four uninfected animals and five infected animals). Doses for all drugs were chosen based on commonly used treatment doses for HIV infection in these models(23–27). Brain tissue was collected at necropsy, snap frozen and stored at -80˚C until further analysis. All experiments were performed in accordance with locally-approved institutional animal care and use committee (IACUC) protocols.

3.3.2. Gene expression of drug transporters in the brain tissue:

The gene expression of five efflux and four influx transporters were analyzed by quantitative PCR. These transporters were chosen based on relevance to the ARVs chosen in this analysis and the expression in the BBB **(Table 3.1 and Figure 3.1)**. Approximately 30 mg of tissue was homogenized in QIAzol lysis buffer using a Precellys Tissue Homogenizer (Bertin Technologies, Montigny-le-Bretonneux, France) and RNA was extracted by using Qiagen RNAeasy Lipid Mini Kit (Qiagen, Valencia, CA). VILO Superscript cDNA Synthesis Kit (Thermo Fisher) was used to reverse-transcribe 200 ng of RNA. A ten-cycle pre-amplification step was performed to obtain a large enough volume of cDNA using Taqman Pre-amplification Master Mix (Life Technologies, Carlsbad, CA) and Taqman Gene Expression Assays (**Appendix 3.1**). This was followed by a 40-cycle quantitative PCR performed using Taqman primers and probes in QuantStudio7 (Life Technologies). Transporter expression was normalized to the GAPDH gene using the 2-ΔCT method(28). In the humanized mouse models, separate assays were run to detect mouse and human transporter genes. The extent of humanization of the drug transporters was expressed as a ratio by subtracting the mouse transporter CT threshold value in the logarithmic scale from the human

transporter CT threshold value in the logarithmic scale for each brain tissue sample, in order

to get the equivalent ratio of mouse transporter/human transporter in the linear scale.
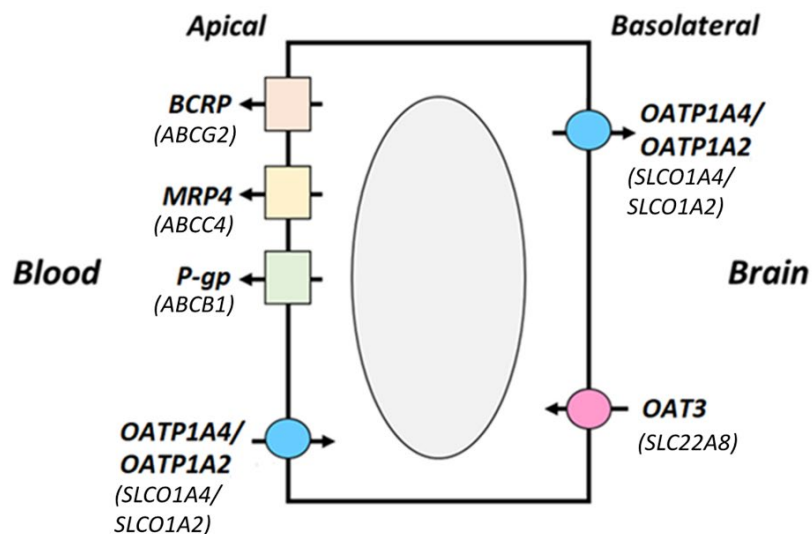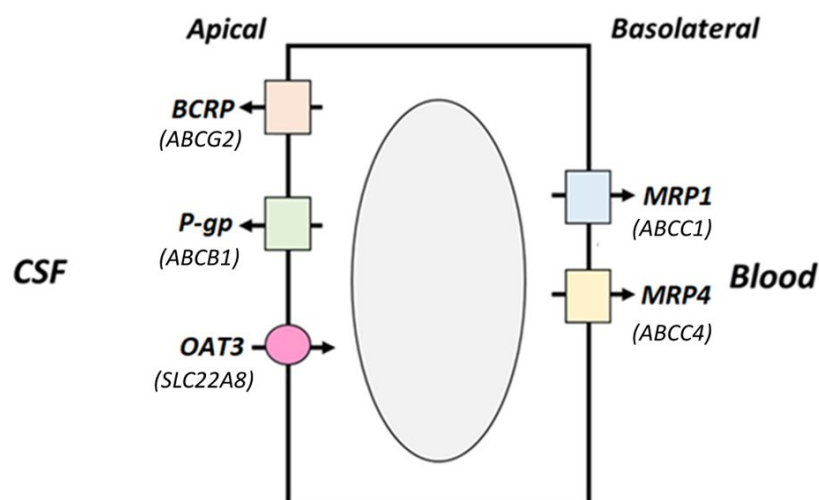
Figure 3.1. Localization of drug transporters (gene name in italics) at the (a) blood-brain-barrier and (b) blood-CSF-barrier. At the (a) blood-brain-barrier, efflux transporters P-gp, BCRP and MRP4 on the apical side of the membrane efflux drug out from the brain into the blood, while the uptake transporter OATP1A4 (mouse) or OATP1A2 (human) facilitates drug entry into the brain. OAT3 is localized on the basolateral membrane and effluxes drug out of the brain into the cell. At the (b) blood-CSF-barrier, BCRP and P-gp localized on the apical side of the membrane actively efflux drug out from the blood into the CSF, while MRP1 and MRP4 present on the basolateral side of the membrane actively efflux drug out into the blood. OAT3 is localized on the apical membrane and effluxes drug out from the CSF into the cell.

Table 3.1. Efflux and uptake transporters that were analyzed in the brain tissue of the preclinical models and antiretroviral (ARV) substrates and inhibitors of these transporters. Transporters are listed as gene (transporter) name.

TRANSPORTERS	SUBSTRATES	INHIBITORS[1]	REFERENCES
EFFLUX TRANSPORTERS ABCC1 (Multi-drug resistance-associated protein-1 [MRP1])	ATZ, FTC	TFV, FTC, ATZ	(15)
ABCC2 (Multi-drug resistance-associated protein-2 [MRP2])	ATZ	TFV, FTC	(15)
ABCC4 (Multi-drug resistance-associated protein-4 [MRP4])	TFV	-	(29)
ABCB1 (P-glycoprotein [P-gp])	TFV, RAL, MVC, ATZ	FTC, EFV, MVC, ATZ	(30)
ABCG2 (Breast cancer resistance protein [BCRP])	TFV, EFV, RAL	EFV, ATZ	(31)
UPTAKE TRANSPORTERS Slco1a4/SLCO1A2	ATZ	-	(32)

TRANSPORTERS	SUBSTRATES	INHIBITORS[1]	REFERENCES
(Organic anion transporting polypeptide 1a4/1A2 [Oatp1a4/OATP1A2])			
SLC29A1 (Equilibrative nucleoside transporter 1 [ENT1])	TFV, FTC	-	(15)
SLC22A2 (Organic cation transporter 2 [OCT2])	-	TFV, FTC	(33)
SLC22A8 (Organic anion transporter 3 [OAT3])	TFV	-	(34)

[1] – indicates that the information on inhibitors of the transporter are unknown.

3.3.3. Protein extraction and expression by western blot:

Transporter protein that was used for Western blot and LC-MS/MS proteomics analyses was isolated using a modified version of an extraction method optimized for proteomics as described previously(35,36). Briefly, tissue samples (10 to 100 mg) were homogenized in 1.3 mL hypotonic buffer containing 10 mM NaCl, 1.5 mM $MgCl^2$, 10 mM Tris HCl pH 7.4, and 150 µL of Complete Protease Inhibitor Solution (Sigma-Aldrich, St. Louis, MO) using the Precellys tissue homogenizer. Tissue homogenates were left on ice for 30 minutes, then sonicated for five minutes and centrifuged for ten minutes at 10,000 g. The supernatant was saved and subjected to high-speed centrifugation at 55,000 rpm for one hour. Supernatant was then discarded and the pellet was resuspended in cOmplete™ Protease

Inhibitor solution. Protein concentrations were quantified using the BCA protein assay (Pierce, Rockford, IL). The total protein isolated from each tissue was split between the western blot and proteomics analyses. A fraction of the isolated protein (30 μg) was reserved for proteomics, while the remaining protein was used for western blot.

For the western blot analysis, up to 10 μg of protein was combined with 7.5 μL sample buffer (NuPage, ThermoFisher) and 0.5 M dithiothreitol (DTT, Sigma-Aldrich) and heated at 70˚C for 10 minutes. Then, samples were loaded onto a 4-12% electrophoresis gel (NuPage) and run for 110 minutes at 180 V. Transfer onto a PVDF membrane (NuPage) occurred over 90 minutes at 30 V. Once the transfer was completed, membranes were rinsed with tris-buffered saline with tween-20 (TBS-T) and blocked for one hour at room temperature in 5% milk. After blocking, primary antibody was added for one of the six following drug transporter proteins: P-gp (1:4000, ab170904; Abcam, Cambridge, MA), MRP2 (1:200, ALX-801-037-C125; Enzo Life Sciences, Farmingdale, NY), MRP1 (1:200, ALX-801-007-C125; Enzo), BCRP (1:1000, ab3380; Abcam), OATP1A2 (1:500, ab105124; Abcam) and GAPDH (1:2000, sc-25778; Santa Cruz Biotechnology, Dallas, TX). Membranes were incubated in primary antibody for one to three hours, then rinsed with TBS-T and incubated in milk with appropriate secondary antibody (anti-rabbit, 1:2000, ab16284, Abcam; anti-mouse, 1:10000, ab112458 Abcam; anti-goat, 1:5000, sc2020, Santa Cruz) for one to two hours, then rinsed again with TBS-T. Development was performed using Clarity ECL reagents (Bio-Rad, Hercules, CA) with a Chemi-Doc XRS+ Imager (Bio-Rad) with a five-minute exposure. The densitometry relative to GAPDH was calculated using ImageLab 5.2.1 (Bio-Rad). P-gp and GAPDH were analyzed during the same exposure, and then each membrane was stripped and re-probed for MRP2 and BCRP, then MRP1, with all densitometry being compared to the initial five-minute

GAPDH exposure. A combination of 15 µg each of mouse brain extract (six µL), liver extract (two µL), and T98G cell lysate (six µL, Santa Cruz) was used as a positive control sample for the efflux transporters. For OATP1A2, a separate positive control of 15 µL MDA-Mb-468 cell lysate was employed.

3.3.4. Absolute protein concentration of drug transporters in the brain tissue:

The absolute protein concentration of drug transporters was determined by quantitative targeted absolute proteomics (QTAP). Total protein (30 µg) was isolated(35,36) and digested for 18 hours with trypsin after adding one pmol of stable isotope labeled (SIL) peptide standards, obtained from Theracode JPT Inc (Acton, MA)(35). The transporter sequences were loaded into the uniport software and SIL peptides were chosen on the basis of electrospray efficiency, hydrophobic index and specificity across mice, macaques, and humans. Sample analysis was conducted with a nanoACQUITY system (Waters, Milford, MA) coupled to a QTRAP 5500 mass spectrometer (SCIEX) equipped with a Nanospray III source. Around 0.06 to 0.12 µg of membrane microsomal protein was loaded onto a C18 trap column (180 µm x 20 mm, 5 µm particle size, Waters) connected to a BEH130 C18 main separation column (150 µm x 100 mm, 1.7 µm particle size, Waters). Analyst 1.5 software (SCIEX) was used for multiple reaction monitoring (MRM) data acquisition within a detection window of 90 seconds and a pause time of three milliseconds between MRMs. Data analysis was performed using MultiQuant 2.0 software (SCIEX). Area ratios of unlabeled/SIL peptides were determined using the MRM sums. The limit of detection for the peptides was 0.1 pmol/mg protein. The list of standard peptide sequences used for the drug transporters are provided in **Appendix 3.2.**

3.3.5. Antiretroviral concentrations in the plasma and brain tissue:

Analytical techniques for quantifying ARV concentrations in the plasma and brain tissue have been described in detail in *Chapter II*. In brief, plasma samples were extracted by protein precipitation with methanol containing stable, isotopically-labeled internal standards. Samples were vortexed and centrifuged, then the supernatant was diluted with water prior to the LC-MS/MS analysis. The lower limit of quantitation (LLOQ) was one ng/mL for each analyte. The precision and accuracy of the calibration standards and quality control samples were within the acceptable range of 15%.

Tissue samples were placed in a Precellys tube (Precellys 2 mL Hard Tissue Metal Beads Kit) containing one mL of ice-cold 70:30 acetonitrile:water. Samples were homogenized using a Precellys 24 benchtop homogenizer. A portion of the homogenate was then mixed with methanol containing stable, isotopically labeled internal standards. Following centrifugation, the supernatant was evaporated to dryness and reconstituted with water (for TFV and FTC analysis) or 25:75 methanol:water (for ATZ, EFV, MVC, and RAL analysis). The LLOQs for the tissue analysis were 0.002 ng/mL (FTC and MVC), 0.005 ng/mL (ATZ, EFV, and RAL), and 0.01 ng/mL (TFV). Tissue concentrations were ultimately converted into ng/g tissue units by assuming a brain tissue density of 1.06 g/cm^3(37) and the brain tissue:plasma penetration ratio was calculated by dividing the trough concentration in the brain tissue by the trough concentration in the plasma.

3.3.6. Immunohistochemistry (IHC) for localization of drug transporters:

Briefly, tissues were sliced frozen at ten μm thickness using a cryostat (Leica Biosystems, Wetzlar, Germany) and thaw mounted onto glass microscope slides as described previously in *Chapter II*. The frozen tissues were stained with primary antibody for P-gp (1:50

dilution; Abcam), BCRP (1:50 dilution; Santa Cruz) or OATP1A2 (1:20 dilution; Santa Cruz) for 15 to 60 minutes followed by pH antigen retrieval (Leica). 3,3'-diaminobenzidine (DAB) was used as a substrate-chromogen for detection. All staining was performed on a Leica Bond automated tissue stainer (Leica). Staining protocols were optimized using mouse and NHP liver as a positive control for the antibodies against all transporters except OATP1A2. For OATP1A2, human tonsil tissue was used as a positive control for protocol optimization. Samples were visually evaluated for transporter localization.

Quantification of transporter response was performed using FiJi ImageJ software (www.imagej.net). Five unique focal viewpoints at 20X magnification and of one mm^2 area were captured from the raw brain tissue scanned slides loaded into the ImageScope software. These images were loaded onto Fiji and thresholded by color in order to separate out the transporter stain from the background. Following this, the image was converted into grayscale and thresholded in order to calculate the fractional area of the transporter protein, which was the quantitative endpoint.

3.3.7. Statistical analysis:

Comparisons between the gene and protein expression stratified by species, infection and sex (in the rhesus macaques) were made using one-way Kruskal-Wallis ANOVA on ranks. Dunn's post-test was used for pairwise multiple comparisons when significant differences ($p<0.05$) were detected.

Spearman rank-order correlation test was used to determine the relationship between brain tissue:plasma penetration ratio of the ARVs and transporter measurements. All statistical tests were conducted using SigmaPlot 13.0 (Systat Software Inc., San Jose, CA).

3.4. Results

3.4.1 Gene expression of drug transporters:

In the humanized mouse models, human transporter gene expression of several uptake transporters represented <10% of total transporter expression. For example, human SLC22A8 was detected in only one hu-HSC-RAG mouse and one BLT mouse, and human SLC22A2 and SLCO1A4 were undetectable in all samples. Human SLC29A1, however, was detected in 70% of the samples. Efflux transporters were generally detected in more samples, although human ABCC2 was only detected in six hu-HSC-RAG mice (out of 36 mice, 16%) and five BLT mice (out of 13 mice, 38%). Uninfected and infected BLT mice had higher human gene expression of only one efflux transporters (ABCC1, 5-fold higher; $p<0.05$) relative to the hu-HSC-RAG mice. Infected BLT mice had higher gene expression of one efflux transporter (ABCC4, 10-fold higher; $p<0.001$) and one uptake transporter (SLC29A1, 9-fold higher; $p<0.001$), relative to the hu-HSC-RAG mice. Generally, the mouse gene expression of all the drug transporters was greater than the human gene expression for uninfected (**Figure 3.2a**) and infected animals (**Figure 3.2b**).

The mouse transporter gene expression was similar between the hu-HSC-RAG and BLT mice for most efflux and uptake transporters (**Figure 3.3 and Figure 3.4**). However, significantly higher gene expression ($p<0.001$) was noted in the hu-HSC-RAG mice compared to the BLT mice for the efflux transporter ABCB1 (100-fold greater), and the uptake transporter Slco1a4 (five-fold greater). Comparisons of transporter gene expression between the humanized mice cohorts are shown in **Appendix 3.3**.
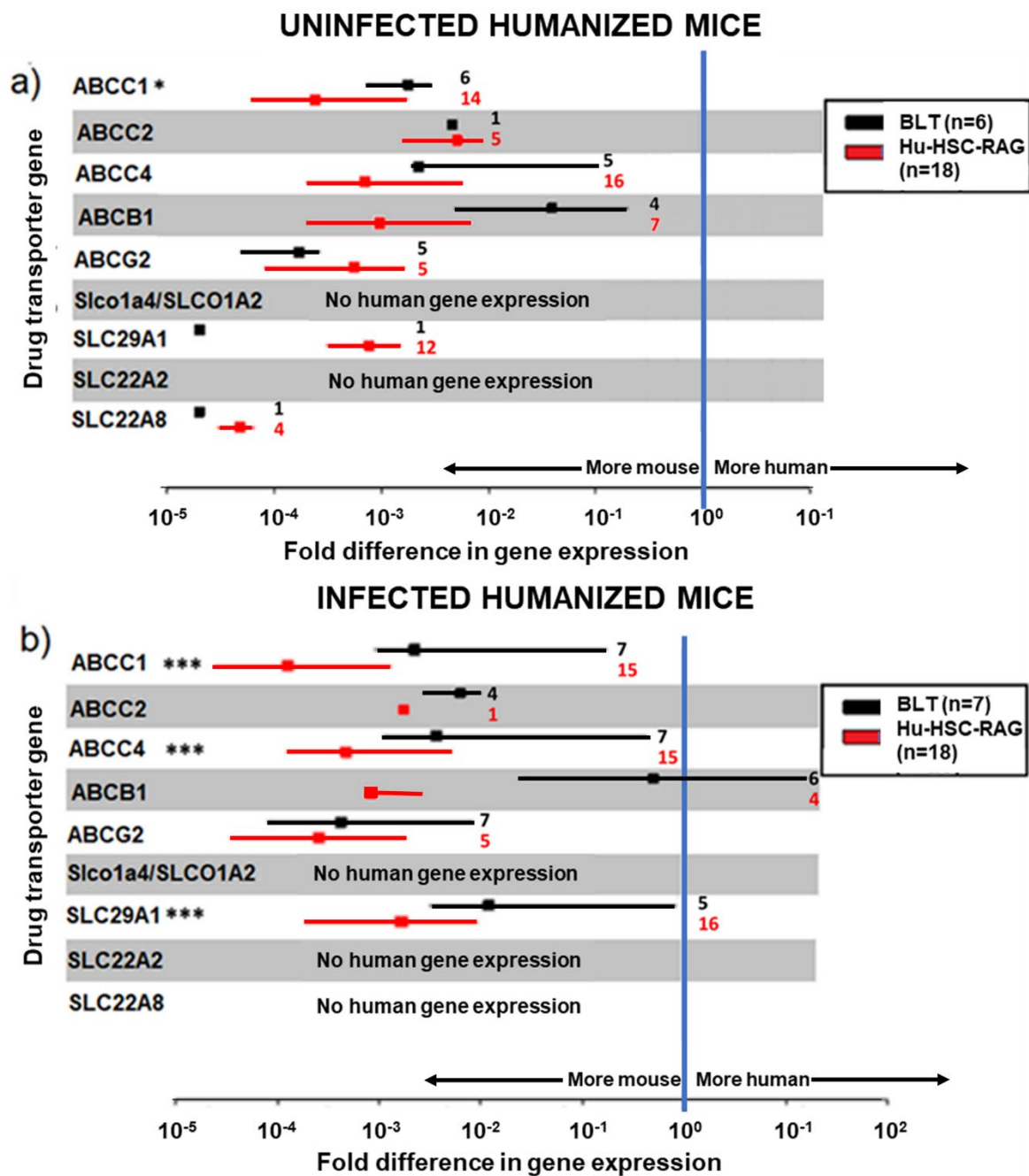
Figure 3.2. Human gene expression in the brain tissue of humanized mouse models by qPCR in (a) uninfected humanized mouse models and (b) infected humanized mouse models. The extent of human gene expression relative to mouse gene expression is shown for the efflux and uptake transporters. The number of animals having detectable transporter concentrations in the brain tissue is shown to the right of the graph. Slco1a4/SLCO1A2 and SLC22A2 were not detected in any of the humanized mice while SLC22A8 was not detected in the infected mice. Data are shown as median (range). * p<0.05, ***p<0.001

Considering the expression of the efflux transporters in the brain tissue, there were several interspecies differences in the gene expression that are summarized in **Figure 3.3**. Of note, both the hu-HSC-RAG mice and the BLT mice showed a four-fold higher expression of Abcg2/ABCG2 ($p<0.001$) compared to the NHPs. The BLT mice showed 100-fold lower expression of Abcb1/ABCB1 compared to both the hu-HSC-RAG mice and the NHPs ($p<0.001$).

When considering the gene expression of the uptake transporters, only the gene expression of Slc29a1/SLC29A1 was similar across all three animal models (**Figure 3.4**). The expression of Slc22a2/SLC22A2 and Slc22a8/SLC22A8 was >100-fold higher in both the hu-HSC-RAG and the BLT humanized mouse models, compared to the NHPs ($p<0.001$), while Oatp1a4/OATP1A2 expression was five-fold higher in the hu-HSC-RAG mice compared to the NHPs ($p<0.001$). The transporter gene expression measurements across all the individual animals are summarized in **Appendix 3.4**.

Sex differences were shown to influence gene expression as the male NHPs had >two-fold higher gene expression ($p<0.05$) of three efflux transporters (ABCC4, ABCB1, ABCG2) and two uptake transporters (SLCO1A2, SLC29A1) compared to the female animals (**Figure 3.5**). However, there were no significant differences in gene expression of drug transporters in either of the humanized mouse models or the NHPs on the basis of infection status ($p=0.3$, **Figure 3.6**).
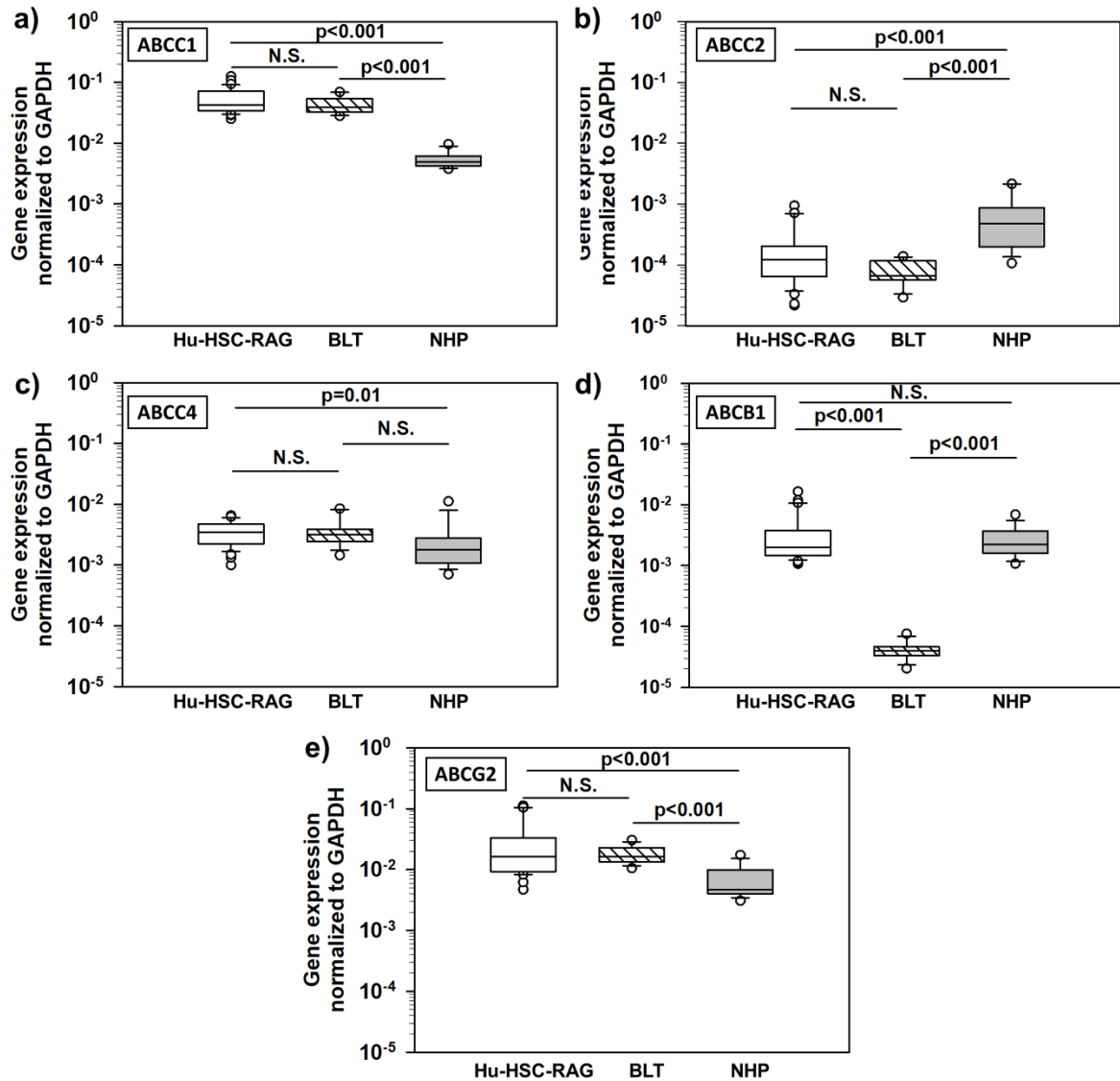
Figure 3.3. Gene expression of efflux transporters in the brain tissue of humanized mouse models and rhesus macaques by qPCR. There were several inter-species differences in the transporter gene expression normalized to the expression of GAPDH. Difference in gene expression between the humanized mouse models was only noted for the efflux transporter ABCB1 (100-fold higher in the hu-HSC-RAG mice compared to BLT mice; $p < 0.001$). For the other transporters, the transporter gene expression did not differ between the humanized mouse models. The hu-HSC-RAG mice and BLT mice showed a 10-fold higher gene expression of ABCC1 ($p < 0.001$) and a 4-fold higher gene expression of ABCG2 ($p < 0.001$) relative to the NHPs. ABCC2 expression was 3-fold lower ($p < 0.001$) in the hu-HSC-RAG mice and BLT mice compared to the NHPs. Boxes represent the 1st and 3rd quartile of the data with median line. Whiskers represent the 10th and 90th percentile of the data and the open circles represent outliers. Legend: qPCR – quantitative polymerase chain reaction
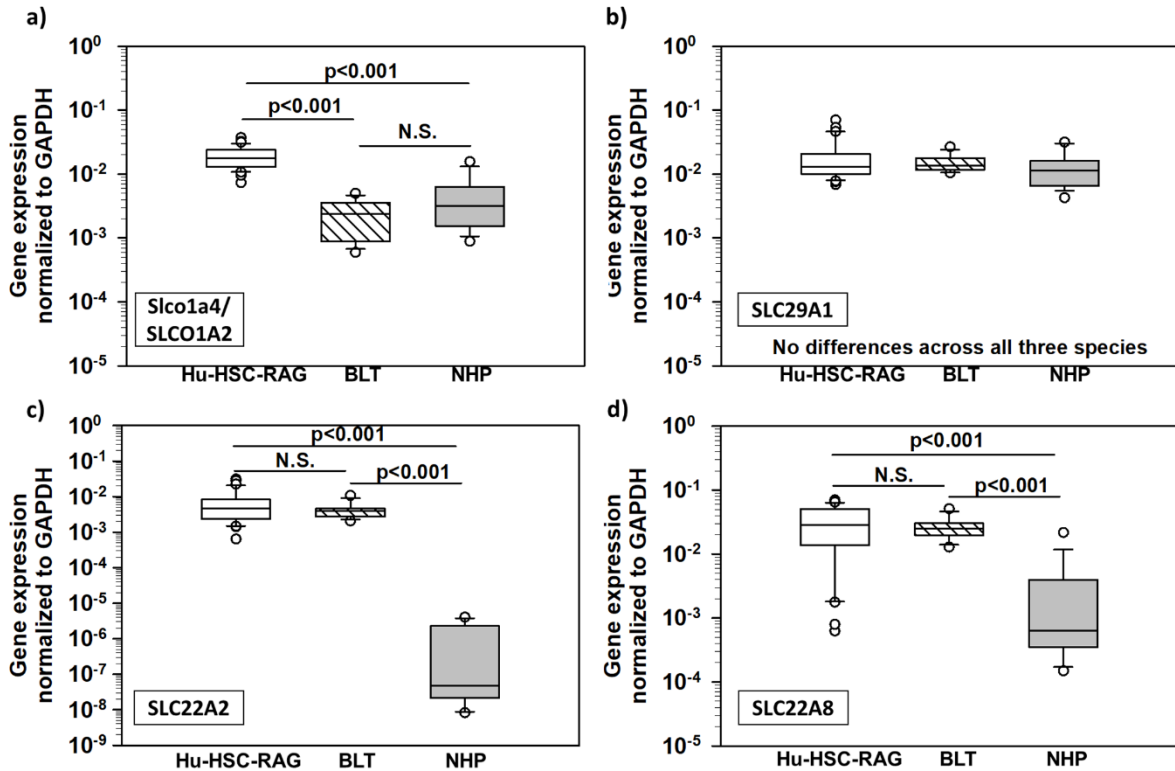
Figure 3.4. Gene expression of uptake transporters in the brain tissue of humanized mouse models and rhesus macaques by qPCR. There were several inter-species differences in the gene expression of uptake transporters normalized to the expression of GAPDH. Differences in gene expression between the humanized mouse models was only noted for the Slco1a4/SLCO1A2 transporter, with hu-HSC-RAG mice showing five-fold higher gene expression compared to the BLT mice ($p<0.001$). The gene expression of SLC29A1 was similar across all three preclinical species ($p=0.15$). The gene expression of SLC22A2 and SLC22A8 were >100-fold higher in both the humanized mouse models as compared to the NHPs ($p<0.001$). Boxes represent the 1st and 3rd quartile of the data with median line. Whiskers represent the 10th and 90th percentile of the data and the open circles represent outliers. Legend: qPCR – quantitative polymerase chain reaction
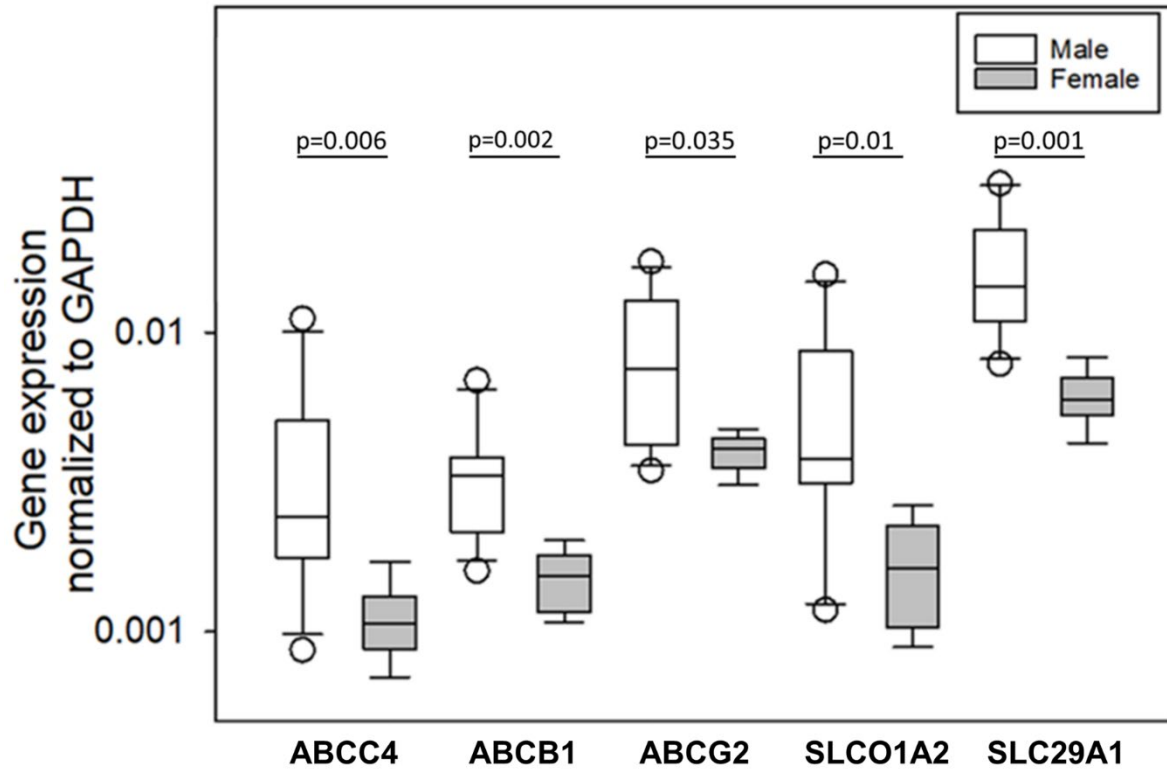
Figure 3.5. Significant differences in the gene expression of efflux and uptake transporters in the brain tissue of rhesus macaques due to sex differences. The gene expression of the efflux transporters ABCC4, ABCB1, and ABCG2 and uptake transporters SLCO1A2 and SLC29A1 were >2-fold lower in female macaques compared to male macaques ($p<0.05$). The boxes represent the 1st and 3rd quartile of the data with median line. The whiskers represent the 10th and 90th percentile of the data and the open circles represent outliers.
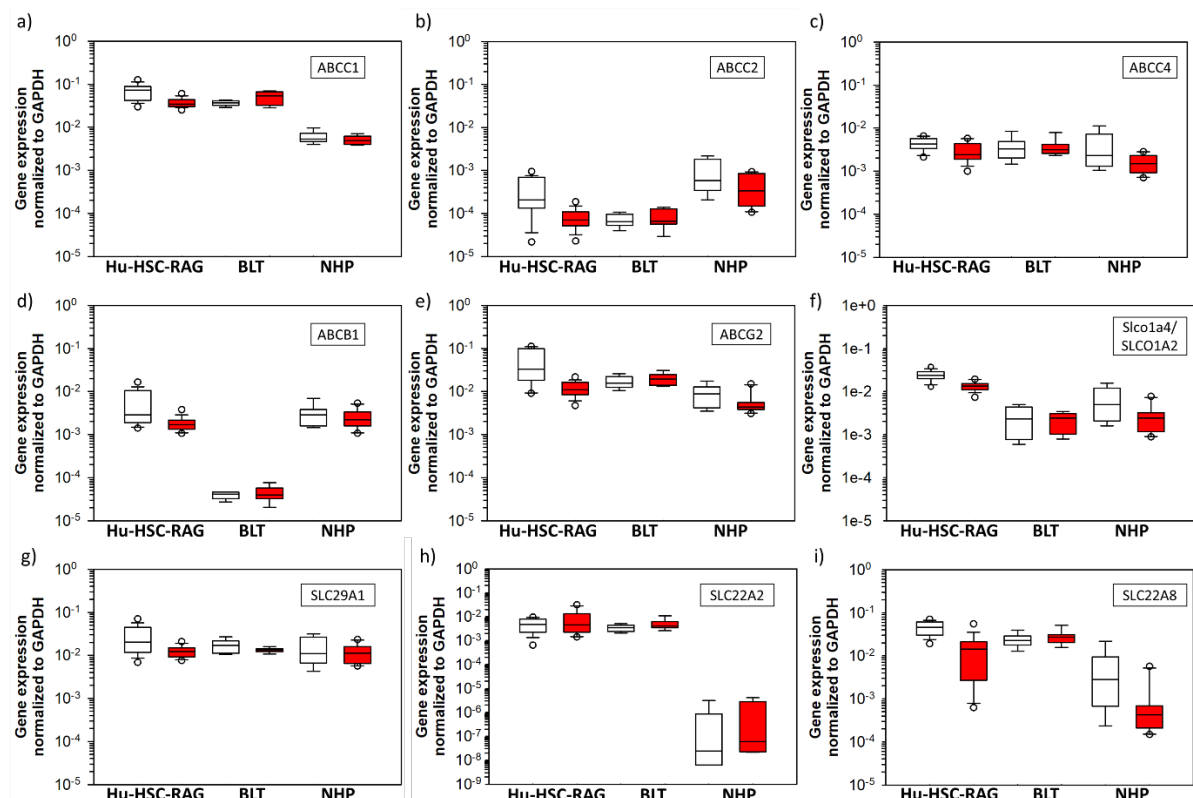
Figure 3.6. Effect of infection status on the gene expression of drug transporters across the preclinical species. Infection status did not appreciably alter the gene expression of drug transporters across any of the preclinical models. The uninfected animals are shown in white and infected animals are shown in red. The boxes represent the 1st and 3rd quartile of the data with median line. The whiskers represent the 10th and 90th percentile of the data and the open circles represent outliers.

3.4.2. Protein expression of drug transporters by western blot:

BCRP was detected in the majority of the brain tissue samples (96%) across all the preclinical models by western blot analysis. Both the monomer (72 kDa) and dimer (144 kDa) forms of BCRP were detected in the humanized mouse models (0.62 [0.0-18.1] fold change over GAPDH; **Figure 3.7a**) and the male rhesus macaques (1.32 [0.62-6.21] fold change over GAPDH; **Figure 3.7b**). P-gp was only detected in 34% of the brain tissue samples, while Oatp1a4/OATP1A2 was detected in 25% of the samples. Given the limited number of

transporters that were detected by the western blot analysis, QTAP was used as the only measure of transporter protein expression.
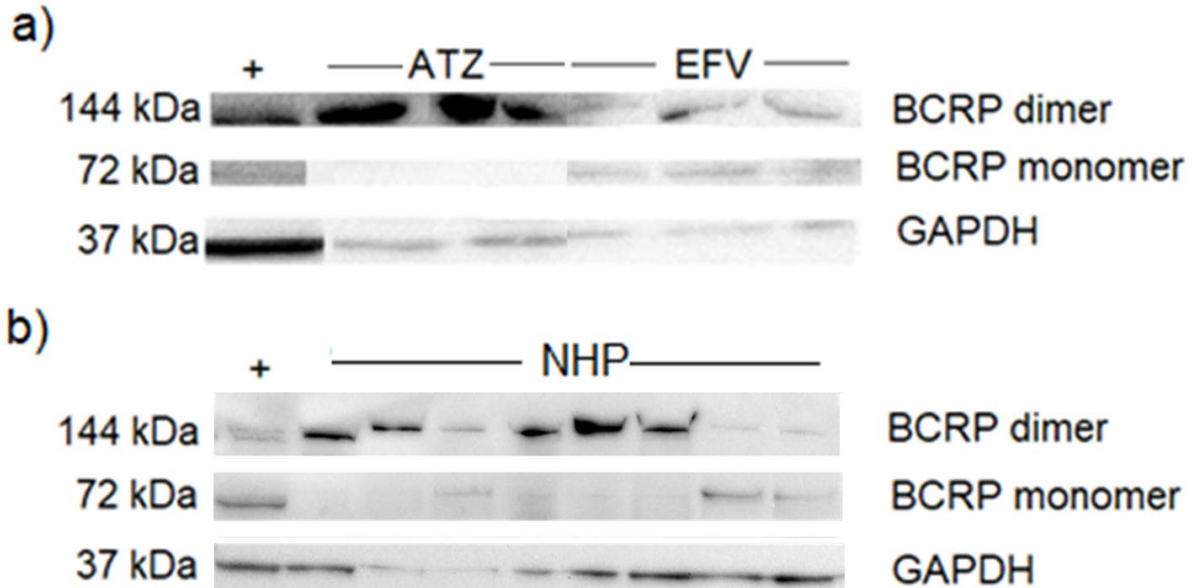
Figure 3.7. BCRP transporter protein expression relative to GAPDH by western blot. Western blots for BCRP expression in the (a) six hu-HSC-RAG mice from the atazanavir and efavirenz dosing cohorts, and (b) eight uninfected male nonhuman primates dosed with efavirenz and raltegravir. + represents the positive control samples. Both the dimer and monomer forms of BCRP were detected in the brain tissue samples. Legend: ATZ – atazanavir, EFV – efavirenz, NHP – nonhuman primate.

3.4.3. Protein concentration of drug transporters by QTAP:

Across the preclinical models, MRP1 and MRP2 were undetectable in all samples and Mrp4/MRP4, Oatp1a4/OATP1A2, Oat3/OAT3 and Oct3/OCT3 were undetectable in 60-94% of the samples. P-gp and BCRP were undetectable in <15% of the samples. Therefore, only the QTAP data for BCRP and P-gp are reported.

P-gp was found at higher concentrations in the hu-HSC-RAG mice (2.0 [0.8-6.6] pmol/mg protein) and BLT mice (0.76 [0.7-5.7] pmol/mg of protein), than Bcrp (p<0.01). This contrasted the gene expression results where the gene expression of P-gp was >10-fold lower

than Bcrp in both the humanized mouse models. Bcrp protein concentrations were similar in both the humanized mouse models (**Figure 3.8,** 0.14 [0.1-0.47] pmol/mg protein in the hu-HSC-RAG mice and 0.2 [0.1-0.61] pmol/mg protein in the BLT mice; p=0.25) and P-gp protein was higher in the hu-HSC-RAG compared to BLT mice (2- to 2.7-fold, p<0.01). Comparisons of transporter protein expression between the humanized mouse cohorts are shown in **Appendix 3.5**.

In the NHPs, BCRP was found at a higher concentration (1.8 [0.7-4.3] pmol/mg protein) than P-gp (1.24 [0.1-4.46] pmol/mg protein). The protein concentration of BCRP in the brain tissue of the NHPs was 16-fold higher than in the brain tissue of the BLT and hu-HSC-RAG humanized mouse models (p<0.001). The P-gp concentration was 4.5-fold lower in the NHP brain tissue compared to the hu-HSC-RAG mice, however, this was not statistically significant (p=0.08). The protein concentrations of BCRP and P-gp across all the preclinical species are shown in **Appendix 3.6**.
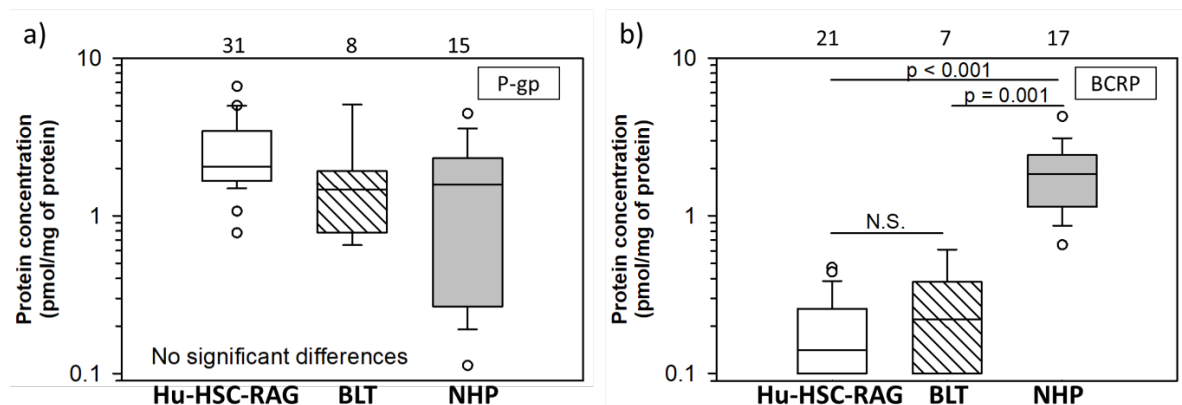
Figure 3.8. Multispecies absolute protein concentration of (a) P-gp and (b) BCRP efflux transporters in the brain tissue by QTAP. There were no differences in the concentration of (a) P-gp transporter between the preclinical models (p=0.08). (b) BCRP protein concentration was 16-fold higher in the NHPs compared to the hu-HSC-RAG mice and the BLT mice (p<0.001). The number of animals with detectable transporter concentrations in the brain tissue are listed above the graphs. The boxes represent the 1st and 3rd quartile of the data with median line. The whiskers represent the 10th and 90th percentile of the data and the open circles represent outliers. Legend: QTAP – quantitative targeted absolute proteomics

Female macaques showed >2-fold higher absolute protein concentrations of BCRP and P-gp (p≤0.002) in the brain tissue compared to the male animals **(Figure 3.9)**. No significant differences in BCRP or P-gp protein concentrations were noted in either the humanized mouse models or NHPs on the basis of infection status (**Figure 3.10**).
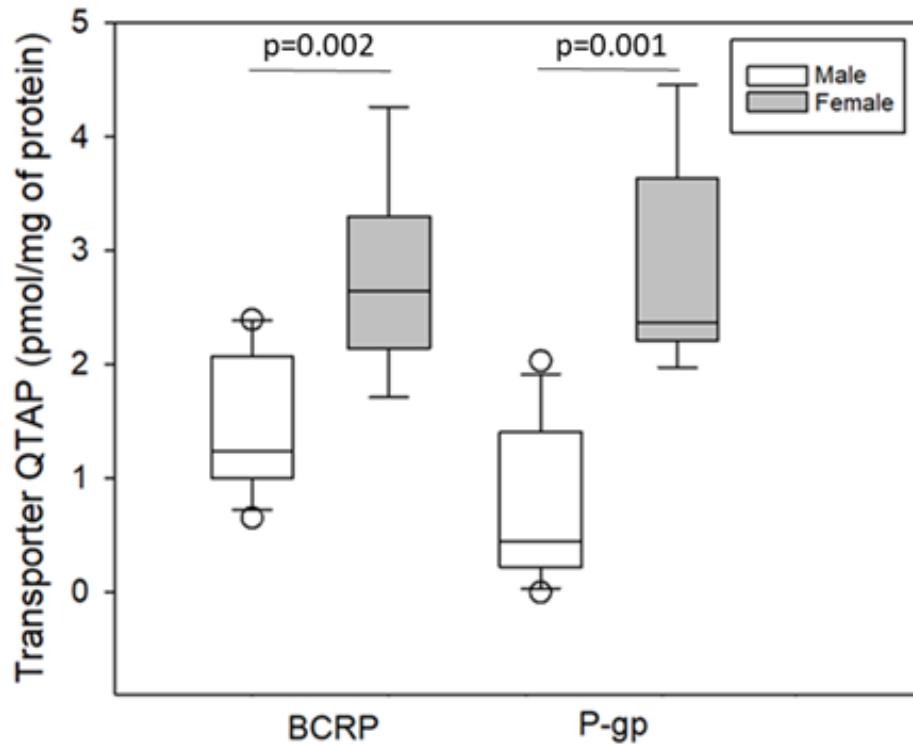
Figure 3.9. Significant differences in the absolute protein concentration of efflux transporters in the brain tissue by QTAP due to sex difference. Sex differences in the protein concentration of transporters were noted in the rhesus macaques. The protein concentration of efflux transporters BCRP and P-gp were 1.9-fold higher (p=0.002) and 5.2-fold higher (p=0.001) in female macaques compared to male macaques, respectively. The boxes represent the 1st and 3rd quartile of the data with median line. The whiskers represent the 10th and 90th percentile of the data and the open circles represent outliers. Legend: QTAP: quantitative targeted absolute proteomics
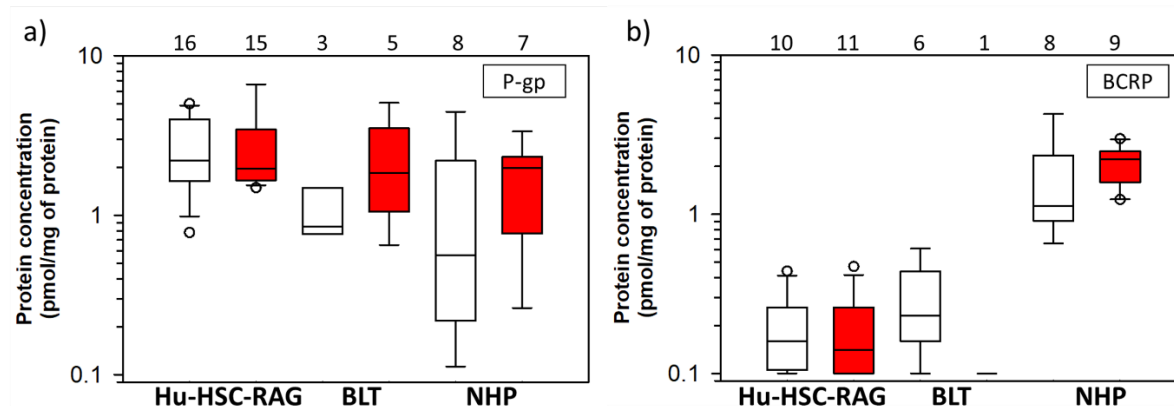
Figure 3.10. Effect of infection status on absolute protein expression of drug transporters. Infection status did not appreciably alter the protein expression of (a) P-gp or (b) BCRP across both the species of humanized mice and NHPs. The number of animals with detectable transporter concentrations are listed above the graphs. The uninfected animals are shown in white and infected animals are shown in red.

3.4.4. Comparison of drug transporter protein and gene expression evaluation methods:

Figure 3.11 shows correlation plots between the gene expression relative to GAPDH and protein concentration of P-gp and Bcrp/BCRP across the animal models. There was no correlation noted between the gene expression and protein expression of the P-gp transporter (rho=0.01) (**Figure 3.11a**). In case of Bcrp/BCRP (**Figure 3.11b**), an increase in transporter gene expression relative to GAPDH expression was associated with a weak decrease in the protein concentration of BCRP (rho = -0.26, p=0.01).
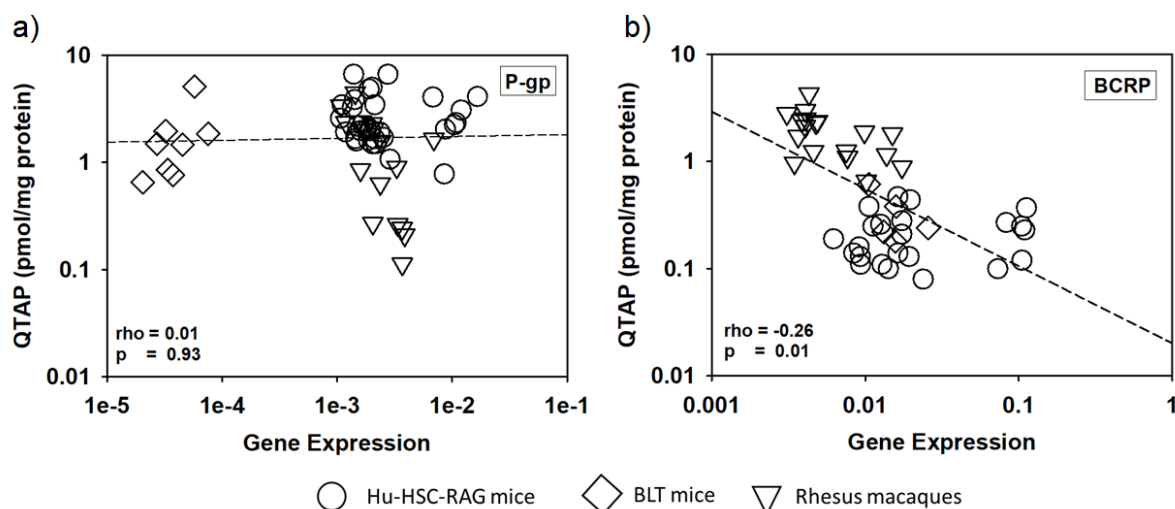
Figure 3.11. Correlation plots between protein concentration by QTAP and gene expression of (a) P-gp and (b) BCRP transporters across preclinical species. The relationship between the absolute protein concentration by QTAP (pmol/mg of protein) and gene expression normalized to GAPDH are shown across the preclinical models for (a) P-gp (rho=0.01; p=0.93) and (b) BCRP (rho=-0.26; p=0.01). Legend: QTAP – quantitative targeted absolute proteomics

3.4.5. Correlation between the protein concentration of drug transporters in the brain tissue and brain tissue:plasma penetration of ARVs:

The QTAP measurements of two efflux transporters (Bcrp/BCRP and P-gp) were retained in the correlation analysis with ARV brain tissue:plasma penetration ratio. The gene expression measurements for the drug transporters were not utilized in the analysis since the gene expression results poorly correlated with the QTAP (**Figure 3.11**). Significance was set at p<0.025, to account for the multiple comparisons of the ARV brain tissue:plasma penetration ratio with the two drug transporters. In **Table 3.2**, the results of the correlation analyses between the six ARVs and the two efflux transporters are summarized.

Table 3.2. Results of the correlation analysis between the two efflux transporters and six antiretrovirals. Correlation coefficients (rho) are listed in the table. The significant relationships are shown in the bold text.

Antiretroviral Drug	BCRP transporter	P-gp transporter
Tenofovir	**0.65**	-0.26
Emtricitabine	**0.68**	-0.34
Efavirenz	**0.64**	-0.26
Raltegravir	0.10	0.32
Maraviroc	0.42	-0.32
Atazanavir	0.53	-0.19

The penetration of TFV, FTC, and EFV into the brain tissue appeared to show a modest increase with the increase in concentration of Bcrp/BCRP transporter in the brain tissue (r=0.65, 0.68, and 0.64, respectively). However, on visual examination of the data **(Figure 3.12a-c)**, it appeared that the ARV brain tissue penetration ratio plateaued at the higher concentrations of BCRP transporter measured in the NHPs. When this relationship was re-examined with the humanized mouse data alone, there was no longer any correlation between BCRP transporter concentration and the penetration of these three ARVs into the brain **(insets of Figure 3.12a-c)**.

In the case of P-gp, there were only weak correlations noted between transporter concentrations and ARV penetration into the brain (rho ranged from -0.34 to 0.32), and these relationships did not reach statistical significance for any of the ARVs **(Figure 3.13)**.
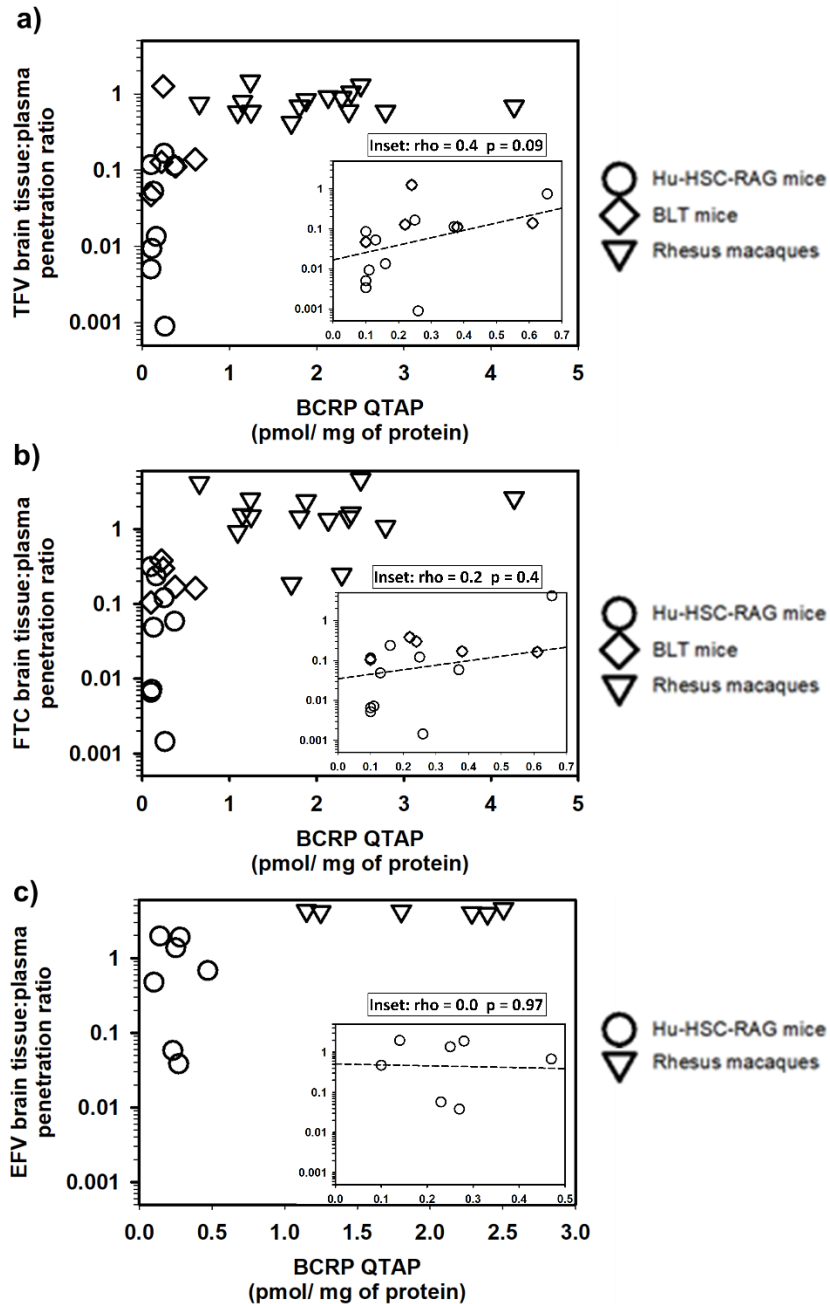
Figure 3.12. Relationship between BCRP protein concentrations and ARV penetration into the brain tissue. Brain tissue:plasma penetration ratio versus BCRP concentration by QTAP is shown stratified by species for (a) TFV, (b) FTC, and (c) EFV. At the higher BCRP concentrations measured in the NHPs, the brain tissue:plasma penetration ratios plateaued for all three ARVs, and appeared to drive the positive correlation noted between transporter concentration and ARV brain tissue:plasma ratio. The inset shows the relationship between BCRP transporter concentrations and brain tissue:plasma penetration ratio for the humanized mouse brain tissue samples alone. Considering these data alone, there was no longer any correlation between BCRP transporter concentration and the penetration of ARVs into the brain. Legend: QTAP – quantitative targeted absolute proteomics
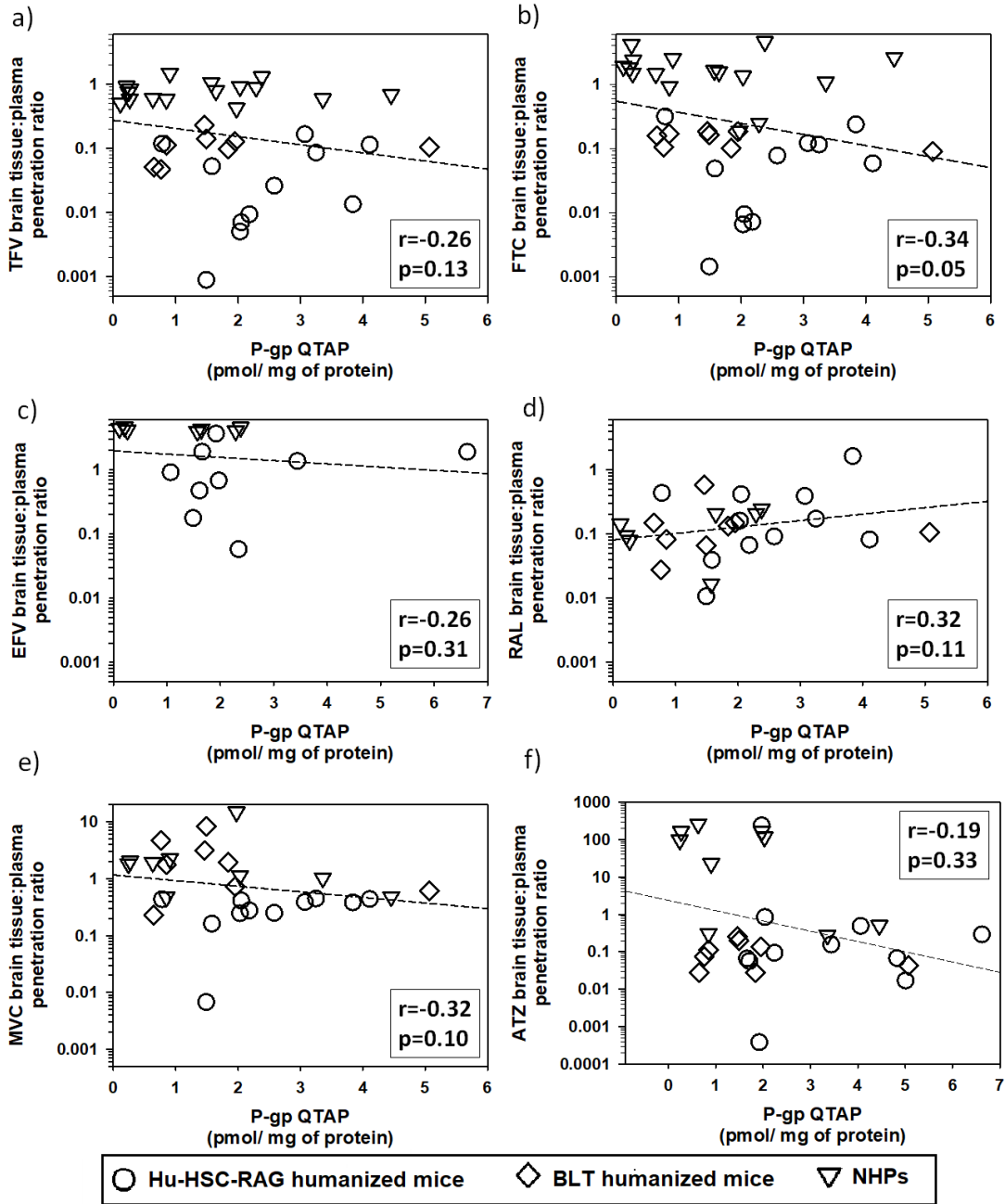
Figure 3.13. Relationship between P-gp protein concentrations and ARV penetration into the brain tissue. Brain tissue:plasma penetration ratios versus P-gp concentration by QTAP are shown stratified by species for (a) TFV, (b) FTC, (c) EFV, (d) RAL, (e) MVC, and (f) ATZ. There were no significant relationships noted between P-gp concentration and brain tissue penetration for any of the six ARVs. Legend: QTAP – quantitative targeted absolute proteomics

3.4.6. Localization of drug transporters in the brain tissue by immunohistochemistry:

In the case of the hu-HSC-RAG mice, cells stained more extensively for P-gp than BCRP across both uninfected (5X fractional area of P-gp staining relative to BCRP, p=0.02) as well as infected animals (7X fractional area of P-gp staining relative to BCRP, p=0.002) (**Figure 3.14**). BCRP staining was often diffuse in these sections with more scattered positive cells throughout the tissue section. Oatp1a4 transporter distribution (data not shown) was minimal in the humanized mice (~2 cells per square millimeter of tissue at 20X magnification). Infection status did not lead to differences in IHC staining of either BCRP or P-gp.
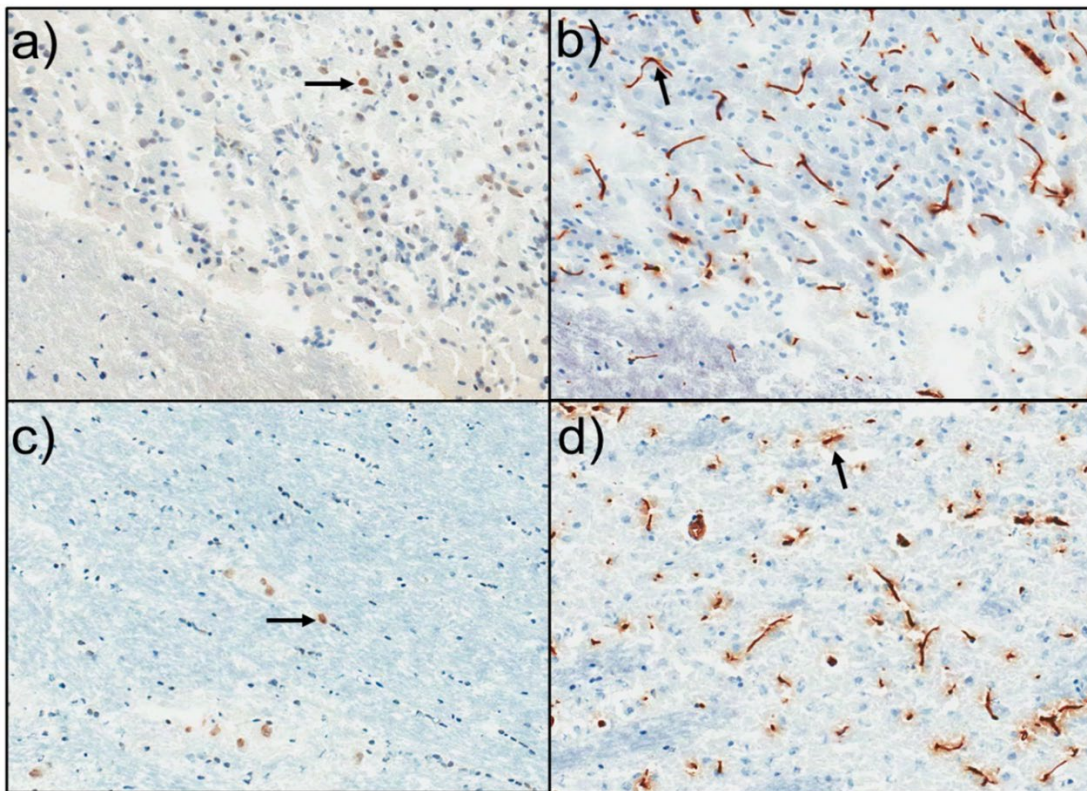
Figure 3.14. Immunohistochemistry staining of P-gp and BCRP drug transporters in the brain tissue of hu-HSC-RAG mice. Representative transporter immunohistochemistry images of 20X magnification in the brain tissue for BCRP in (a) uninfected and (c) infected, and P-gp in (b) uninfected and (d) infected hu-HSC-RAG humanized mouse models. The arrows represent cells stained positive for the transporter stain.

BCRP and P-gp were extensively distributed throughout the cerebellar tissue sections of both uninfected and RT-SHIV infected rhesus macaques (**Figure 3.15**). OATP1A2 was found more sparingly with an average of two to five stained cells per square-millimeter at 20X magnification (data not shown). The fractional area of BCRP was similar across both uninfected and RT-SHIV infected macaques (1.1% and 1.4% respectively, p=0.24). Similarly, the fractional area of P-gp also showed no difference based on RT-SHIV infection status (0.74% and 0.86% in uninfected and RT-SHIV infected macaques, p=0.4).
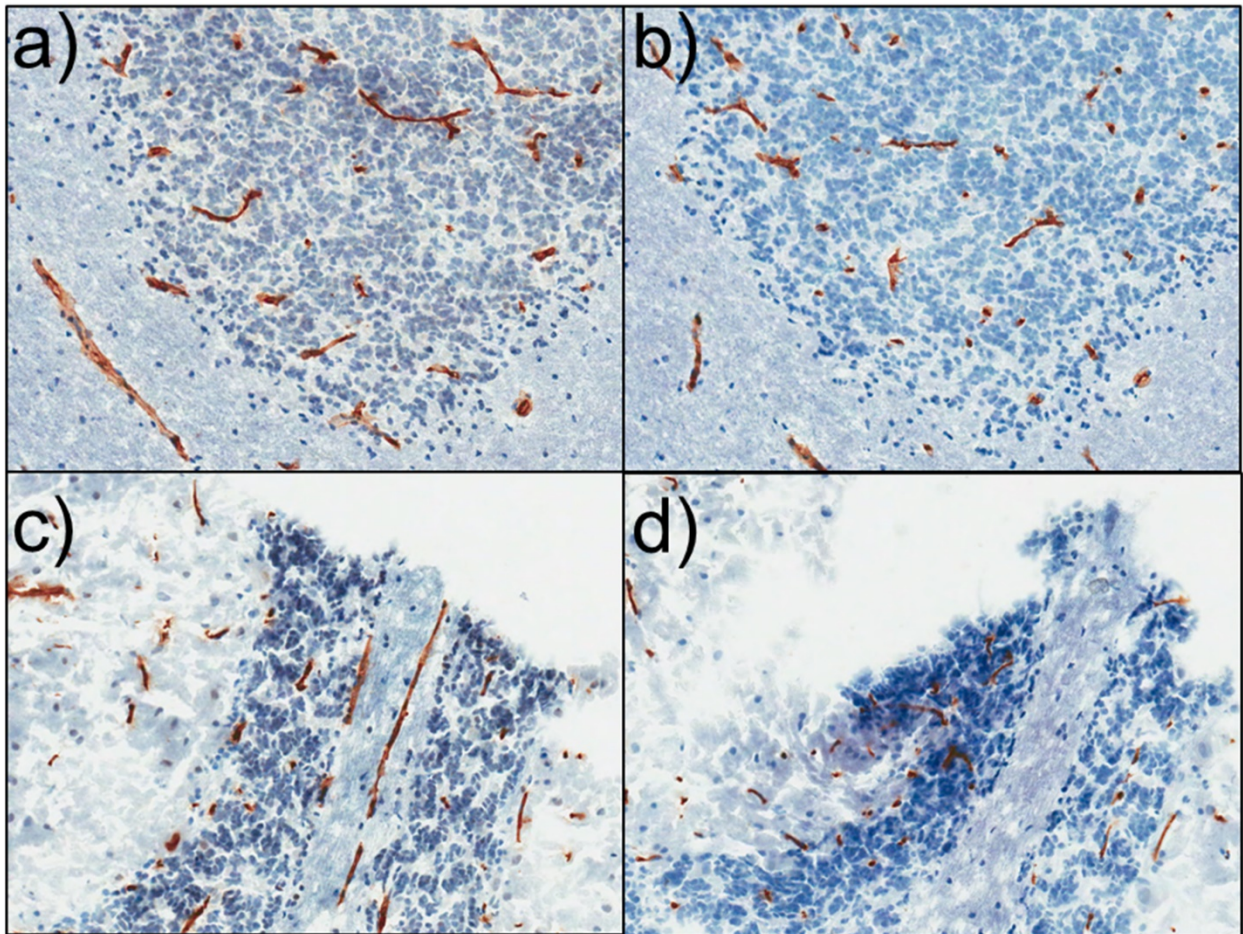
Figure 3.15. Immunohistochemistry staining of P-gp and BCRP drug transporters in the cerebellum of rhesus macaques. Representative transporter immunohistochemistry images of 20X magnification in the cerebellum tissue for BCRP in (a) uninfected and (c) infected, and P-gp in (b) uninfected and (d) infected rhesus macaques.

Finally, transporter images generated from the IHC analyses were overlaid with the EFV drug distribution maps that were generated from mass-spectrometry imaging (MSI) in *Chapter II* (**figure 3.16**). Correlation between drug transporter and EFV distribution was low (r ranged from 0.1 to 0.3), regardless of infection status. Despite transporter distribution throughout the tissue, there was notably less transporter staining in regions of white matter in uninfected animals, where EFV was shown to preferentially accumulate (*Chapter II*). In the infected animals, EFV was found at lower concentrations in the brain tissue and differences in localization were less readily apparent across different parts of the tissue.
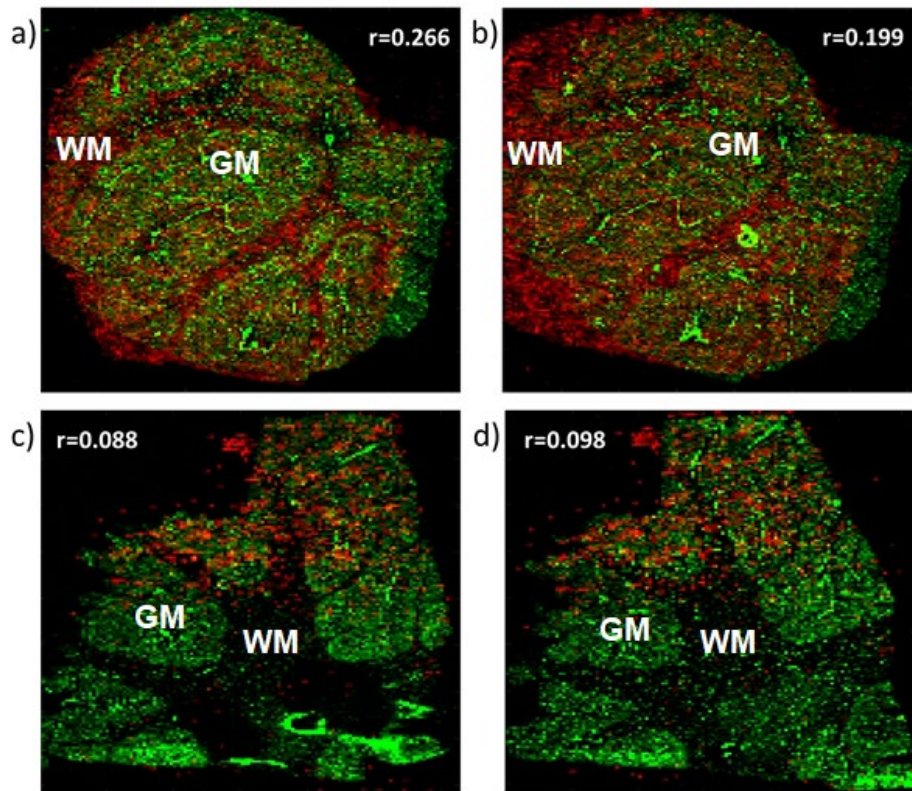
Figure 3.16. Colocalization between immunohistochemistry staining of drug transporters and mass spectrometry imaging of efavirenz distribution in cerebellum of uninfected and infected rhesus macaques. Representative transporter immunohistochemistry images (green color) were overlaid with the distribution maps of EFV (red color) in the cerebellum tissue for BCRP in (a) uninfected and (c) infected and P-gp in (b) uninfected and (d) infected rhesus macaques. Legend: GM – gray matter, and WM – white matter.

3.5.   Discussion

The aim of this study was to evaluate the gene and protein expression of drug transporters across three commonly used HIV preclinical models. We chose to evaluate drug transporters that are known to be present in the brain tissue and involved in the disposition of ARVs. We noted several inter-species differences in transporter gene expression across the preclinical models. BLT mice had five-fold and 100-fold lower gene expression of the uptake transporter Slco1a4 and the efflux transporter Abcb1, respectively, compared to the hu-HSC-RAG mice. Similarly, both the hu-HSC-RAG mice and the BLT mice showed higher gene expression of Abcc1/ABCC1, Abcg2/ABCG2, Slc22a8/SLC22A8 and Slc22a2/SLC22A2 ($p<0.01$) compared to the NHPs.

When considering the protein expression of drug transporters, however, both the western blot as well as the QTAP analyses were able to detect fewer transporters of interest compared to gene expression. From the QTAP analysis, only two efflux transporters (BCRP and P-gp) were detected in greater than 85% of all brain tissue samples. In case of the western blot analysis, BCRP was detected in 96% of the brain tissue samples, however, P-gp and Oatp1a4/OATP1A2 were only detected in 35% and 25% of the brain tissue samples, respectively. These results may seem surprising since antibody-based analyses have historically been considered to be more sensitive than LC-MS/MS proteomics analyses(38). However, with the proper optimization of standard peptides, LC-MS/MS proteomics assays can be as sensitive or even more sensitive than western blot(36,39,40). For our LC-MS/MS proteomics analyses, we initially optimized three to four standard peptide sequences per transporter and chose our final peptides based on the most optimal response shown across multiple samples. While our western blot assays were also previously optimized by our

laboratory, these conditions could have potentially been refined even further in order to improve the signal:noise ratio for the low-abundance transporters (for e.g. by choosing a more sensitive chemiluminescent substrate). While we ultimately excluded results from the western blot analysis for the inter-species comparisons, the detection of predominant BCRP bands within the brain tissue at a higher molecular weight was an interesting result. It has been shown that anti-BCRP antibodies are also capable of co-precipitating structural proteins called caveolins that function to link BCRP molecules into dimeric and tetrameric forms in the presence of cholesterol(41). Interestingly, these polymeric forms of BCRP are also associated with higher transporter activity as a 50% reduction in cholesterol can result in a 40% reduction in transporter activity(42). In fact, the modest positive correlation (r=0.6) that we noted between absolute BCRP transporter protein concentration and the penetration of the very lipophilic drug EFV into the brain tissue may be a result of high extent of accumulation of both the drug and transporter within the cholesterol-rich environment of the brain, though further studies are needed to confirm this.

Similar to the gene expression results, there were some interspecies differences in our QTAP data across the three preclinical models; for example, BCRP was 16-fold higher in the NHPs than the humanized mouse models. One caveat with our QTAP results is that the absolute protein concentration of BCRP and P-gp that we measured in this study were >two-fold lower than previously published measurements made from concentrated BBB samples in mice and cynomolgus monkeys.(19,43) This is due to our use of whole brain tissue resulting in diluted concentrations compared to the measurements made from a transporter-rich concentrated sample of the BBB. For similar reasons, only BCRP and P-gp could be quantified in the brain tissue samples, although MRP4, OATP1A2 and ENT1 were previously detected

in the BBB of cynomolgus monkeys(19). Since these other transporters were detected at lower concentrations in the BBB, they were below the limit of quantification (BLQ) in our brain tissue samples. Similar to the BBB measurements(19,43), our brain tissue samples also showed a differential gradient of transporter concentrations (**Table 3.3**) across the preclinical models. For example, P-gp was the predominant transporter detected in both the brain tissue and BBB in mice, while BCRP was the most abundant transporter in the NHPs. However, the transporter measurements in our brain tissue samples did not perfectly correlate with the BBB transporter measurements. For BCRP, the brain tissue protein concentrations were 8- to 40- fold lower than the BBB transporter protein concentrations, while for P-gp the brain tissue protein concentrations were 4- to 5-fold lower relative to the protein concentrations at the BBB. These results indicate that BCRP protein concentrations in the brain parenchyma are much lower than P-gp protein concentrations. This may be due to the more pronounced expression of P-gp on various cell types in the brain tissue such as astrocytes, microglia, and neurons(44,45). In contrast, previous studies have shown that BCRP appears to only be localized to the microglial cells in the brain parenchyma(44). Therefore, while our results do show similarities between the relative abundance of transporter protein concentrations in the brain tissue and at the BBB, the brain tissue is not an appropriate surrogate for BBB for all drug transporters.

Table 3.3. Concentration of efflux and uptake transporters measured in the blood brain barrier from previous studies and in the brain tissue of our preclinical models by QTAP. P-gp and BCRP drug transporters were predominantly detected by QTAP in the BBB from previously published studies, as well as in the brain tissue samples (data generated in this thesis). Generally, transporters detected at low concentrations (<2 pmol/mg protein) in the BBB were not detected in the brain tissue. Data are shown as means.

Transporter	Mouse BBB(17)	Mouse Brain Tissue	Monkey BBB(19)	NHP Brain Tissue	Human BBB(17)
BCRP (pmol/mg protein)	4.41	0.12	14.2	1.8	8.1
P-gp (pmol/mg protein)	14.1	2.6	4.7	1.2	6.1
MRP4 (pmol/mg protein)	1.6	<0.1	0.30	<0.1	0.2
OATP1A2 (pmol/mg protein)	2.0	<0.1	0.73	0.2 (n=26)	<0.2
ENT1 (pmol/mg protein)	0.9	<0.1	0.54	<0.1	0.6

We also explored the effect of factors that could alter drug transporter measurements in the three preclinical models. Overall, infection status did not alter the gene or protein expression of drug transporters across any of the individual dosing cohorts or animal models. However, we did note significant differences in both the gene as well as the protein concentration of transporters based on sex in the NHPs. While the gene expression of P-gp and

BCRP were lower in female macaques compared to males, the QTAP results showed the opposite result; BCRP was 1.9-fold higher in female macaques while P-gp was 5.2-fold higher in females. Higher protein expression of drug transporters in females compared to males has been shown before(46), and may be due to the effects of the female sex hormones. Estrogen, estradiol, and other female sex hormones bind to the estrogen receptor (ER), and activate the downstream estrogen receptor elements (ERE) that are located in the promoter region of target genes such as MDR1 and ABCG2 to increase transporter expression and ultimately the efflux of substrates(47–49). The ER proteins also interact with other transcription factors such as nuclear factor-kβ (NF-kβ)(48) that can induce the gene and increase the protein expression of P-gp and BCRP.

As shown previously by our laboratory with the intestinal tissue(36), poor agreement was demonstrated between the gene expression and protein concentration by QTAP analysis for P-gp (rho=0.1). While these results differ from a previous study that demonstrated a strong, positive relationship (r^2=0.8) between the gene expression, protein concentration and function of P-gp(50), it should be noted that this result was derived from an in-vitro cell line system, which provides a more controlled environment for transporter studies. With the brain tissue collected from our in-vivo experiments, the interplay of complex processes involved in the synthesis and degradation of RNA and protein might have affected the extent of agreement between gene and protein expression. We also noted a weak negative correlation between the gene expression and protein concentration of BCRP (rho=-0.26, p=0.01). Though such a negative relationship might just be an artefact of our sparse and variable proteomics data, a few other studies have also shown negative relationships between the gene message and protein concentration of cytokines(51,52). Such data may be explained by the difference in half-lives

between RNA and protein, post-translational modifications to proteins that lead to enhanced stability compared to RNA, or a negative-feedback loop that results in degradation of RNA with higher concentrations of protein(53).

We performed a correlation analysis between our QTAP drug transporter measurements and the brain tissue:plasma penetration ratio across our preclinical models to determine if drug transporter concentration in the brain tissue had any utility in predicting ARV penetration into the brain. Given the large number of transporter concentration values that were BLQ in our brain tissue samples and the imperfect correlation between drug transporter concentrations in the brain tissue and the BBB, the correlation analysis may have been more informative if we were able to correlate drug transporter measurements at the BBB with the plasma:brain tissue ratio of ARVs. However, given the methodological complexities in isolating the BBB, such as the need to pool brain tissue samples across multiple animals and the destructive nature of this technique, we were unable to isolate transporter protein at the BBB. However, despite this important limitation, there is still significant utility in the measurement of drug transporters in the brain tissue(54). The brain cells such as microglia, astrocytes, and neurons make up 80% of the total brain tissue volume(55), and drug transporters present on these cells are important regulators for drug uptake into cells(16,56).

Our correlation analysis showed a surprising modest increase (rho ranged from 0.64 to 0.68) in the brain tissue:plasma penetration ratio of TFV, FTC and EFV with an increase in BCRP transporter concentrations. However, on visual examination of our data, it became clear that this positive relationship was only driven by the plateau in ARV penetration into the brain tissue at higher BCRP transporter concentrations that were measured in the NHPs. When we re-examined this relationship with the data from the humanized mouse models alone, there was

no longer any significant relationship between transporter concentrations and brain tissue penetration for any of the three ARVs. This suggests that differences in BCRP transporter concentrations have no relationship with ARV penetration into the brain tissue. This finding agrees with previously generated in-vivo data that shows that the inhibition of BCRP does not significantly alter the brain tissue distribution of several known substrates of this transporter(57).

Our results also showed that there was no relationship between P-gp transporter concentrations in the brain tissue and the penetration of ARVs into the brain tissue, although there seemed to be a very weak trend between increased P-gp concentrations and lower ARV penetration into the brain for most of the ARV substrates except RAL. A careful review of our brain tissue transporter measurements relative to previously generated BBB measurements indicated that the brain parenchyma P-gp transporter measurements were a surrogate for the BBB, although future studies are needed to confirm this. Such a result could be explained by the pronounced localization of P-gp in various brain cells(44,45) that comprise the neurovascular unit. Therefore, the quantification of P-gp in this secondary barrier may not only inform ARV penetration into the brain by could also be important to inform the cellular penetration of ARVs. Although we did not measure intracellular drug concentrations in this analysis, future work employing methods as described by Fridén(58) or Guo(59) could be used to measure the intracellular concentrations of ARVs in the relevant HIV target cells (such as the microglia) and determine the ability of transporter concentrations in the brain parenchyma to predict these concentrations.

Finally, we performed IHC analyses to determine the localization of drug transporters within the brain tissue. Our IHC results showed good agreement with the QTAP results. For

example, only BCRP and P-gp were predominantly detected, with very minimal detection of OATP1A2. Further, BCRP transporter was predominantly expressed in the NHP tissue, while in the humanized mouse models, P-gp was more widely expressed. There were no differences in the transporter expression profiles between uninfected and infected animals and this was consistent across all the measures of transporter detection. The drug transporter IHC images for both P-gp and BCRP showed a poor correlation ($r<0.2$) with the distribution of EFV by MSI. Furthermore, in the uninfected animals it appeared that the transporter distribution was denser in the gray matter, while EFV distribution was more concentrated in the white matter, an observation that we noted in *Chapter II.* With the RT-SHIV infected animals, this was not as readily apparent due to the lower concentrations of EFV that were detected by MSI. Since we did not have the ability to co-stain for multiple transporters across one tissue slice, but used concomitantly sliced tissue for each individual transporter stain, we were not able to show the co-staining of multiple transporters or overlay images of cellular markers and transporters. Because of our experimental set-up, we used frozen tissue sections for IHC and these sections were not as strongly bound to the glass slide as compared to formalin-fixed paraffin-embedded tissue. Therefore, the multiple heating steps that were involved in multiplexing resulted in stripping of the tissue section from the glass slide.

There are some other important limitations to this work. Only BCRP was predominantly detected in the brain tissue samples in the western blot analysis and showed poor correlation to the absolute transporter protein concentrations as measured by the QTAP analysis. Further, although we used the QTAP analysis for our transporter protein concentrations, there were several limitations with this technique such as low sensitivity resulting in BLQ values for most transporters, and high variability in peptide measurements.

Finally, while we measured the differences in transporter absolute protein concentrations across the preclinical species, we were not able to measure the differences in the transporter function across the species, which might also considerably influence the penetration of ARVs into the brain tissue.

3.6.   Conclusions

From the results presented in this study, important inter-species differences in drug transporters were detected between commonly used models for HIV-infection, such as 16-fold higher protein concentration of BCRP in NHPs compared to humanized mouse models. While the two measures of drug transporter protein expression (localization and concentration) generally agreed with each other, there was poor correlation noted between the gene expression and protein expression measurements. BCRP and P-gp showed similarities in relative abundance in the brain tissue and the BBB, however an imperfect correlation between the protein concentrations of both these transporters at the two different sites suggests that brain tissue transporter protein concentrations may not be a suitable surrogate for the protein concentrations at the BBB. We noted no significant relationship between transporter concentrations in the brain tissue and ARV brain tissue:plasma penetration ratio. While these data provide an important proof-of-concept for examining the relationship between transporter differences and PK of ARVs in the brain tissue, the lack of significant findings may be due to the limited number of samples we had for this analysis and the imperfect correlation between transporter concentrations measured in our brain tissue samples and the BBB. Future work measuring the intracellular concentration of ARVs in relevant HIV target cells in the brain tissue would further elucidate the importance of the secondary barrier of drug transporters in

the brain parenchyma. Integration of our data with transporter measurements made at the BBB would allow for a better translation of the mechanistic differences in transporter expression and activity between the preclinical models and could be a useful tool to predict clinical brain tissue concentrations.

3.7.   REFERENCES

1.   UNAIDS. Global summary of the AIDS epidemic. 2016. Available at: http://www.who.int/hiv/data/en/. (Accessed April, 2018).

2.   Lorenzo-Redondo R, Fryer HR, Bedford T, Kim EY, Archer J, Kosakovsky Pond SL, et al. Persistent HIV-1 replication maintains the tissue reservoir during therapy. Nature. 2016;530(7588):51–6.

3.   Fois AF, Brew BJ. The Potential of the CNS as a Reservoir for HIV-1 Infection: Implications for HIV Eradication. Curr HIV/AIDS Rep. 2015;299–303.

4.   Persidsky Y, Poluektova L. Immune privilege and HIV-1 persistence in the CNS. Immunol Rev. 2006;213(Oct):180–94.

5.   Marban C, Forouzanfar F, Ait-Ammar A, Fahmi F, El Mekdad H, Daouad F, et al. Targeting the brain reservoirs: Toward an HIV cure. Front Immunol. 2016;7(SEP):1–13.

6.   Pratt RD, Nichols S, McKinney N, Kwok S, Dankner WM, Spector SA. Virologic markers of human immunodeficiency virus type 1 in cerebrospinal fluid of infected children. J Infect Dis. 1996;174(2):288–93.

7.   Peluso MJ, Ferretti F, Peterson J, Lee E, Fuchs D, Boschini A, et al. Cerebrospinal fluid HIV escape associated with progressive neurologic dysfunction in patients on antiretroviral therapy with well controlled plasma viral load. AIDS. 2012;26(14):1765–74.

8.   Edén A, Fuchs D, Hagberg L, Nilsson S, Spudich S, Svennerholm B, et al. HIV-1 viral escape in cerebrospinal fluid of subjects on suppressive antiretroviral treatment. J Infect Dis. 2010;202(12):1819–25.

9.   Canestri A, Lescure F, Jaureguiberry S, Moulignier A, Amiel C, Marcelin AG, et al. Discordance Between Cerebral Spinal Fluid and Plasma HIV Replication in Patients with Neurological Symptoms Who Are Receiving Suppressive Antiretroviral Therapy. Clin Infect Dis. 2010;50(5):773–8.

10.   Kumar AM, Borodowsky I, Fernandez B, Gonzalez L, Kumar M. Human immunodeficiency virus type 1 RNA levels in different regions of human brain: Quantification using real-time reverse transcriptase-polymerase chain reaction. J Neurovirol. 2007;13(3):210–24.

11.   Marra CM. HIV-associated neurocognitive disorders and central nervous system drug penetration: what next? Antivir Ther. 2015;20(4):365–7.

12.   Lamers SL, Salemi M, Galligan DC, Morris A, Gray R, Fogel G, et al. Human immunodeficiency virus-1 evolutionary patterns associated with pathogenic processes in the brain. J Neurovirol. 2010;16(3):230–41.

13.   Strain MC, Letendre S, Pillai SK, Russell T, Ignacio CC, Gu HF, et al. Genetic Composition of Human Immunodeficiency Virus Type 1 in Cerebrospinal Fluid and

Blood without Treatment and during Failing Antiretroviral Therapy. J Virol. 2005;79(3):1772–88.

14.   de Lange ECM, Ravenstijn PGM, Groenendaal D, van Steeg TJ. Toward the prediction of CNS drug-effect profiles in physiological and pathological conditions using microdialysis and mechanism-based pharmacokinetic-pharmacodynamic modeling. AAPS J. 2005;7(3):532–43.

15.   Kis O, Robillard K, Chan GNY, Bendayan R. The complexities of antiretroviral drug-drug interactions: role of ABC and SLC transporters. Trends Pharmacol Sci. 2010 Jan;31(1):22–35.

16.   Alam C, Whyte-Allman S-K, Omeragic A, Bendayan R. Role and modulation of drug transporters in HIV-1 therapy. Adv Drug Deliv Rev. 2016;103:121–43.

17.   Uchida Y, Ohtsuki S, Katsukura Y, Ikeda C, Suzuki T, Kamiie J, et al. Quantitative targeted absolute proteomics of human blood-brain barrier transporters and receptors. J Neurochem. 2011;117(2):333–45.

18.   Ohtsuki S, Schaefer O, Kawakami H, Inoue T, Liehner S, Saito A, et al. Simultaneous absolute protein quantification of transporters, cytochromes P450, and UDP-glucuronosyltransferases as a novel approach for the characterization of individual human liver: comparison with mRNA levels and activities. Drug Metab Dispos. 2012 Jan;40(1):83–92.

19.   Ito K, Uchida Y, Ohtsuki S, Aizawa S, Kawakami H, Katsukura Y, et al. Quantitative membrane protein expression at the blood-brain barrier of adult and younger cynomolgus monkeys. J Pharm Sci. 2011;100(9):3939–50.

20.   Hayashi K, Pu H, András IE, Eum SY, Yamauchi A, Hennig B, et al. HIV-TAT protein upregulates expression of multidrug resistance protein 1 in the blood–brain barrier. J Cereb Blood Flow Metab. 2005;26(8):1052–65.

21.   Denton PW, Garcia JV. Novel humanized mouse models for HIV research. Curr HIV/AIDS Rep. 2009;6:13–9.

22.   Hatziioannou T, Evans DT. Animal models for HIV/AIDS research. Nat Rev Microbiol. 2012;10(12):852–67.

23.   Massud I, Aung W, Martin A, Bachman S, Mitchell J, Aubert R, et al. Lack of prophylactic efficacy of oral maraviroc in macaques despite high drug concentrations in rectal tissues. J Virol. 2013 Aug;87(16):8952–61.

24.   Shytaj IL, Norelli S, Chirullo B, Della Corte A, Collins M, Yalley-Ogunro J, et al. A highly intensified ART regimen induces long-term viral suppression and restriction of the viral reservoir in a simian AIDS model. PLoS Pathog. 2012;8(6).

25.   Neff PC, Ndolo T, Tandon A, Habu Y, Akkina R. Oral pre-exposure prophylaxis by anti-retrovirals raltegravir and maraviroc protects against HIV-1 vaginal transmission in a humanized mouse model. PLoS One. 2010;5(12):1–7.

26.   Denton PW, Krisko JF, Powell DA, Mathias M, Kwak YT, Martinez-Torres F, et al.

Systemic administration of antiretrovirals prior to exposure prevents rectal and intravenous HIV-1 transmission in humanized BLT mice. PLoS One. 2010;5(1).

27. Veselinovic M, Yang KH, LeCureux J, Sykes C, Remling-Mulder L, Kashuba ADM, et al. HIV pre-exposure prophylaxis: Mucosal tissue drug distribution of RT inhibitor Tenofovir and entry inhibitor Maraviroc in a humanized mouse model. Virology. 2014;464–465:253–63.

28. Schmittgen TD, Livak KJ. Analyzing real-time PCR data by the comparative CT method. Nat Protoc. 2008;3(6):1101–8.

29. Ray AS, Cihlar T, Robinson KL, Tong L, Vela JE, Fuller MD, et al. Mechanism of active renal tubular efflux of tenofovir. Antimicrob Agents Chemother. 2006;50(10):3297–304.

30. Sankatsing SUC, Beijnen JH, Schinkel AH, Lange JM a, Prins JM. P glycoprotein in human immunodeficiency virus type 1 infection and therapy. Antimicrob Agents Chemother. 2004;48(4):1073–81.

31. Peroni RN, Di Gennaro SS, Hocht C, Chiappetta D a, Rubio MC, Sosnik A, et al. Efavirenz is a substrate and in turn modulates the expression of the efflux transporter ABCG2/BCRP in the gastrointestinal tract of the rat. Biochem Pharmacol. 2011;82(9):1227–33.

32. Hartkoorn RC, Kwan WS, Shallcross V, Chaikan A, Liptrott N, Egan D, et al. HIV protease inhibitors are substrates for OATP1A2, OATP1B1 and OATP1B3 and lopinavir plasma concentrations are influenced by SLCO1B1 polymorphisms. Pharmacogenet Genomics. 2010;20(2):112–20.

33. Jung N, Lehmann C, Rubbert A, Knispel M, Hartmann P, van Lunzen J, et al. Relevance of the organic cation transporters 1 and 2 for antiretroviral drug therapy in human immunodeficiency virus infection. Drug Metab Dispos. 2008;36(8):1616–23.

34. Bam RA, Yant SR, Cihlar T. Tenofovir alafenamide is not a substrate for renal organic anion transporters (OATs) and does not exhibit OAT-dependent cytotoxicity. Antivir Ther. 2014;19(7):687–92.

35. Fallon JK, Smith PC, Xia CQ, Kim MS. Quantification of Four Efflux Drug Transporters in Liver and Kidney Across Species Using Targeted Quantitative Proteomics by Isotope Dilution NanoLC-MS/MS. Pharm Res. 2016;33(9):2280–8.

36. Thompson CG, Fallon JK, Mathews M, Charlins P, Remling-Mulder L, Kovarova M, et al. Multimodal analysis of drug transporter expression in gastrointestinal tissue. AIDS. 2017;31(12):1669–78.

37. Srinivasan VJ, Atochin DN, Radhakrishnan H, Jiang JY, Ruvinskaya S, Wu W, et al. Optical coherence tomography for the quantitative study of cerebrovascular physiology. J Cereb Blood Flow Metab. 2011;31(6):1339–45.

38. Uchida Y, Tachikawa M, Ohtsuki S, Terasaki T. Blood–Brain Barrier (BBB) Pharmacoproteomics: A New Research Field Opened Up by Quantitative Targeted Absolute Proteomics (QTAP). In: Drug Delivery to the Brain AAPS Advances in the

Pharmaceutical Sciences Series, vol 10. 2014. p. 63–100.

39.   Li N, Nemirovskiy O V., Zhang Y, Yuan H, Mo J, Ji C, et al. Absolute quantification of multidrug resistance-associated protein 2 (MRP2/ABCC2) using liquid chromatography tandem mass spectrometry. Anal Biochem. 2008;380(2):211–22.

40.   Prasad B, Unadkat JD. Optimized Approaches for Quantification of Drug Transporters in Tissues and Cells by MRM Proteomics. AAPS J. 2014;16(4):634–48.

41.   Xu J, Liu Y, Yang Y, Bates S, Zhang JT. Characterization of Oligomeric Human Half-ABC Transporter ATP-binding Cassette G2. J Biol Chem. 2004;279(19):19781–9.

42.   Hartz AMS, Mahringer A, Miller DS, Bauer B. 17-B-Estradiol: A powerful modulator of blood-brain barrier BCRP activity. J Cereb Blood Flow Metab. 2010;30(10):1742–55.

43.   Ohtsuki S, Uchida Y, Kubo Y, Terasaki T. Quantitative targeted absolute proteomics-based ADME research as a new path to drug discovery and development: Methodology, advantages, strategy, and prospects. J Pharm Sci. 2011;100(9):3547–59.

44.   Sanchez-Covarrubias L, Slosky L, Thompson B, Davis T, Ronaldson P. Transporters at CNS Barrier Sites: Obstacles or Opportunities for Drug Delivery? Curr Pharm Des. 2014;20(10):1422–49.

45.   Ashraf T, Robillard K, Chan GNY, Bendayan R. Role of CNS transporters in the pharmacotherapy of HIV-1 associated neurological disorders. Curr Pharm Des. 2014;20(10):1543–63.

46.   Torres L, Bynoe MS. Influence of gender on blood brain barrier permeability and adenosine receptor signaling. FASEB J. 2017;31(1):1042–3.

47.   Shi J, Yang N, Ding H, Zhang J, Hu M, Leng Y, et al. ERα directly activated the MDR1 transcription to increase paclitaxel-resistance of ERα-positive breast cancer cells in vitro and in vivo. Int J Biochem Cell Biol. 2014;(53):35–45.

48.   Björnström L, Sjöberg M. Mechanisms of Estrogen Receptor Signaling: Convergence of Genomic and Nongenomic Actions on Target Genes. Mol Endocrinol [Internet]. 2005;19(4):833–42. Available from: https://academic.oup.com/mend/article-lookup/doi/10.1210/me.2004-0486

49.   Chang FW, Fan HC, Liu JM, Fan TP, Jing J, Yang CL, et al. Estrogen enhances the expression of the multidrug transporter gene ABCG2—increasing drug resistance of breast cancer cells through estrogen receptors. Int J Mol Sci. 2017;18(1):1–15.

50.   Taipalensuu J, Tavelin S, Lazorova L, Svensson AC, Artursson P. Exploring the quantitative relationship between the level of MDR1 transcript, protein and function using digoxin as a marker of MDR1-dependent drug efflux activity. Eur J Pharm Sci. 2004;21(1):69–75.

51.   Shebl FM, Pinto LA, García-Piñeres A, Lempicki R, Williams M, Harro C, et al. Comparison of mRNA and protein measures of cytokines following vaccination with human papillomavirus-16 L1 virus-like particles. Cancer Epidemiol Biomarkers Prev.

2010;19(4):978–81.

52. Tian Q, Stepaniants SB, Mao M, Weng L, Feetham MC, Doyle MJ, et al. Integrated Genomic and Proteomic Analyses of Gene Expression in Mammalian Cells. Mol Cell Proteomics. 2004;3(10):960–9.

53. Greenbaum D, Colangelo C, Williams K, Gerstein M. Comparing protein abundance and mRNA expression levels on a genomic scale. Genome Biol [Internet]. 2003;4(9). Available from: https://genomebiology.biomedcentral.com/articles/10.1186/gb-2003-4-9-117. Last accessed: October 1st, 2018.

54. Wang Q, Zuo Z. Impact of transporters and enzymes from blood–cerebrospinal fluid barrier and brain parenchyma on CNS drug uptake. Expert Opin Drug Metab Toxicol. 2018;14(9):961–72.

55. Wong AD, Ye M, Levy AF, Rothstein JD, Bergles DE, Searson PC. The blood-brain barrier: an engineering perspective. Front Neuroeng [Internet]. 2013;6. Available from: http://journal.frontiersin.org/article/10.3389/fneng.2013.00007/abstract. Last Accessed October 10th, 2018

56. Morris ME, Rodriguez-Cruz V, Felmlee MA. SLC and ABC Transporters: Expression, Localization, and Species Differences at the Blood-Brain and the Blood-Cerebrospinal Fluid Barriers. AAPS J. 2017;19(5):1317–31.

57. Kalvass JC, Polli JW, Bourdet DL, Feng B, Huang S-M, Liu X, et al. Why clinical modulation of efflux transport at the human blood-brain barrier is unlikely: the ITC evidence-based position. Clin Pharmacol Ther. 2013;94(1):80–94.

58. Fridén M, Gupta A, Antonsson M, Bredberg U H-UM. In Vitro Methods for Estimating Unbound Drug Concentrations in the brain interstitial and intracellular fluids. Drug Metab Dispos. 2007;35(9):1711–9.

59. Guo Y, Chu X, Parrott NJ, Brouwer KLR, Hsu V, Nagar S, et al. Advancing Predictions of Tissue and Intracellular Drug Concentrations Using In Vitro, Imaging and Physiologically Based Pharmacokinetic Modeling Approaches. Clin Pharmacol Ther. 2018;104(5):865–89.

CHAPTER-IV: PREDICTING THE EXPOSURE OF EFAVIRENZ IN THE HUMAN BRAIN TISSUE AND RELATIONSHIP TO NEUROCOGNITIVE IMPAIRMENT IN HIV-INFECTED INDIVIDUALS[1]

4.1. Summary

Sparse data exist in the literature on the penetration of antiretrovirals into the brain tissue. In this work, we present a modeling framework to use efavirenz (EFV) pharmacokinetic (PK) data in the plasma, cerebrospinal fluid (CSF), and brain tissue of eight rhesus macaques to predict the brain tissue exposure of EFV in a cohort of 24 HIV-infected participants from a clinical trial. We then perform exposure-response analysis with the model-predicted EFV brain tissue exposure and neurocognitive scores that were obtained from the study participants. Adult rhesus macaques were dosed with 200 mg EFV (as part of a four-drug regimen) for ten days and then sacrificed. Plasma was collected at eight time points over ten days and at necropsy, while CSF and brain tissue were collected at necropsy. In the clinical study, data were obtained from one paired plasma and CSF sample from participants who were prescribed EFV, and neuropsychological test evaluations were administered across 15 domains. PK modeling was performed using ADAPT v5.0 with the iterative two-stage analysis estimation method. An eight-compartment model best described EFV distribution in the plasma, CSF and brain tissue in rhesus macaques and humans. EFV was predicted to have a flat profile in the CSF and brain tissue with a median concentration of 31 ng/mL and 8,000 ng/mL, respectively. Model-

predicted brain tissue exposure of EFV was highly correlated with the plasma exposure (rho=0.99, p<0.001) but not with the CSF exposure (rho=0.34, p=0.1) and did not show any relationship with neurocognitive scores (rho<0.05, p>0.05). This analysis provides an approach to estimate PK in the brain tissue using sparse data in order to perform pharmacokinetic-pharmacodynamic analyses at the target site.

---

[1]This work has been submitted as a manuscript to the journal Clinical and Translational Sciences.

4.2. Introduction

HIV-associated neurocognitive disorders (HAND) are a spectrum of neurocognitive deficits in people living with HIV that remain highly prevalent despite the introduction of highly active antiretroviral therapy (HAART). Although the prevalence of HIV-associated dementia (HAD) has dramatically declined from 60% at end-stage disease in the pre-HAART era to 5% currently[1], the milder forms of HAND – asymptomatic neurocognitive impairment (ANI) and mild neurocognitive disorder (MND) - remain highly prevalent in 20-50% of HIV positive participants[1].

While the exact cause of HAND is unknown, it is hypothesized that HAND in HAART-treated individuals is a result of irreversible damage to neurons and other brain cells in the central nervous system (CNS), resulting from uncontrolled HIV replication and inflammation that occurred before the initiation of antiretroviral (ARV) therapy (also called a "legacy effect")[2]. The extent of ARV penetration into the CNS may also contribute to HAND in two ways. Restricted ARV penetration into the brain tissue could lead to ongoing viral replication and inflammation in the brain tissue[3]. Alternatively, for ARVs that reach high concentrations within the brain tissue, potential neurotoxicity may contribute to the onset of HAND[4,5]. Several studies have investigated neurocognitive impairment as a function of ARV cerebrospinal fluid (CSF) pharmacokinetics (PK)[4,6–8], but have been inconclusive. A possible explanation for this might be that neurocognitive impairment was only assessed as a function of drug exposure in the CSF. With the inability to obtain brain tissue in humans premortem for PK sampling, either CSF concentrations of ARVs or the CNS-penetration effectiveness (CPE) scores are used as surrogates[3]. The CPE scores are derived from a combination of the ability of the ARVs to control HIV replication in the CSF, the concentration

of the ARVs achieved in the CSF, and physicochemical properties of the ARVs(9). Since the site of action of ARVs is either within or on the surface of HIV target cells (for e.g. macrophages, microglia, and CD4+ T-cells) found in the brain, the brain tissue is the relevant target for PK assessment.

Modeling and simulation techniques may be useful to predict the pattern of drug distribution in the brain tissue(10). Non-linear mixed effects modeling (NLMEM), most frequently applied to 'population' pharmacokinetic/pharmacodynamic (PK/PD) analyses, can also provide better estimates at the individual subject level, when population inference is not relevant. Bayesian estimation methods such as the iterative two-stage (IT2S) method are particularly useful to describe individuals with sparse data(6). In such an approach, parameter estimates are initially defined from a prior distribution as in other Bayesian analyses, with an iterative estimation of the parameters to provide refined estimates for each individual. Such an NLMEM method allows data to be leveraged from all study samples, in order to better describe the PK in each study subject.

In this work, we apply NLMEM to predict the exposure of efavirenz (EFV) in human brain tissue based on PK data (plasma, CSF and brain tissue concentrations) obtained from rhesus macaques, combined with sparse plasma and CSF concentrations obtained from a clinical trial. EFV is part of a fixed dose combination regimen (Atripla®; a fixed dose regimen of 600 mg EFV, 200 mg emtricitabine [FTC] and 300 mg tenofovir disoproxil fumarate given once daily) that is a part of the World Health Organization's list of essential medicines(11) and is used in several developing regions of the world where the HAND prevalence is comparable to, or higher than, rates in the western world(12). Given the clinical relevance and established link of EFV usage with HAND prevalence(13) we investigated whether a relationship could

be established between model-predicted EFV brain tissue concentrations and neurocognitive impairment.

4.3. Materials and Methods

4.3.1. Antiretroviral dosing in rhesus macaques and preclinical study design:

Details on the PK evaluation of ARVs in the CSF and brain tissue in rhesus macaques have been previously reported in Chapter II. Briefly, nine (six male and three female) adult rhesus macaques (Macaca mulatta) were dosed for ten days with tenofovir (TFV) 30 mg/kg subcutaneously daily, FTC 16 mg/kg subcutaneously daily, EFV 200 mg orally daily, and raltegravir (RAL) 100 mg orally twice a day in order to achieve steady-state conditions. Animals were dosed in the morning, and the second dose of RAL was administered in the afternoon. For the morning dose, EFV and RAL were fed orally by mixing the contents of a 200 mg Sustiva® (EFV) capsule and a 100 mg Isentress® (RAL) chewable tablet with a peanut butter sandwich. For the afternoon dose, the Isentress® tablet was fed to the animals with strawberry jam. Five of the animals were first infected with 104.5 median tissue culture infective dose (TCID$_{50}$) of RT-SHIVmac239 intravenously in order to determine if infection status influenced EFV concentrations in the brain. Plasma HIV RNA was measured every week after inoculation up to four weeks in order to confirm infection. Plasma was sampled at the following time points in all animals: 0 hours, 4 hours, 10 hours and 24 hours after the first dose, then 24 hours after the dose on days four, six, nine, and ten (necropsy). All animals were sedated 24 hours after the last dose with ketamine hydrochloride, and plasma and CSF were collected. The macaques were then given a lethal dose of pentobarbital and euthanized. Brain tissue was collected at necropsy, snap frozen, and stored at -80°C until further analysis. Four

distinct regions of the brain tissue were collected for the measurement of EFV concentrations: the frontal cortex, the parietal cortex, the cerebellum and the basal ganglia. All animal experiments were performed in accordance with a locally-approved Institutional Animal Care and Use Committee (IACUC) protocol from the University of Davis, California (protocol 18345). One RT-SHIV-infected macaque developed liver failure during the course of the study, with measured concentrations in the plasma, CSF, and brain tissue matrices over 100-fold higher than in the other macaques, and was excluded from the analysis.

4.3.2. Clinical Study Participants:

The "Tropism of HIV, Persistence, Inflammation and Neurocognition in Therapy Initiation Cohort" (THINC, grant PO1 MH094177) study was conducted in full accordance with the Declaration of Helsinki. The study protocol was approved by the Institutional Review Boards at all three participating sites and participants provided informed consent before screening and study enrollment.

This multi-center study was conducted to provide a better understanding of the mechanisms behind the persistence of neurocognitive impairment in HIV-infected participants during ARV therapy. This large study included several interlinked projects that enrolled HIV-positive participants into two distinct observational cohorts based on their length of time on ARV therapy. Cohort A was comprised of individuals who were newly diagnosed, naïve to treatment, or who were off ARV therapy for at least three months. Cohort B was comprised of treatment-experienced individuals, who were on therapy for at least one year before study enrollment, and for whom viral replication was suppressed in the plasma and CSF. All participants were on drug regimens chosen by their primary care physician. While these two distinct cohorts were enrolled to evaluate two distinct hypotheses under the main THINC

study, participants from both cohorts provided PK samples that were combined for the PK sub-study analysis. The PK sub-study had two main objectives. The first objective was to use modeling and simulation in order to predict ARV exposure in the plasma, CSF and brain tissue after collection of sparse PK samples from the plasma and CSF. The second objective of the PK sub-study was to determine if model-derived brain tissue exposure predicted in each individual participant correlated with neurocognitive impairment scores obtained from the study participants.

This study enrolled HIV-infected men and women above the age of 18, who had a nadir CD4 count <400 cells/µL at some point prior to study enrollment. Participants were excluded if they had a physician-identified contraindication to lumbar punctures, had an active psychiatric illness, currently abused alcohol or drugs, or had a brain infection besides HIV that required acute or chronic therapy. The complete list of inclusion and exclusion criteria for the THINC study are provided in **Appendix 4.1**.

4.3.3. Clinical study design:

The design of the THINC study is shown in **Figure 4.1** for cohorts A and B. A longitudinal analysis was conducted for the participants in cohort A. Subjects were enrolled, initiated on ARVs (as per their primary care physician, with regimens not determined by the clinical study investigators) and followed for one year with four distinct study visits at various time points: the study baseline, two weeks, six months and one-year post enrollment. At the baseline, six-month and one-year visits, neurocognitive tests were administered by trained research assistants under the supervision of a neuropsychologist. At the two-week and one-year study visits, blood was drawn to measure ARV concentrations in plasma, and a lumbar puncture was performed to measure CSF concentrations. Participants were followed for one

year so that changes in cognitive function could be tracked over time from high viral load (at study entry) to no detectable viral replication (at the one-year visit). Cognitive tests were performed every six months to reduce memory bias. The blood draw and lumbar puncture procedures were scheduled within two to three hours of each other, and samples were collected based on subject and technician availability, with no pre-selected sampling time post-dose.

Time since starting study drug

	2 weeks	6 months	1 year	Post 1 year
COHORT A* (treatment naïve)	• Plasma collected for 1 PK time point • CSF collected for 1 PK time point	• Neuropsychiatric tests administered	• Plasma collected for 1 PK time point • CSF collected for 1 PK time point • Neuropsychiatric tests administered	N/A
COHORT B (treatment experienced)	N/A	N/A	N/A	• Plasma collected for 1 PK time point • CSF collected for 1 PK time point • Neuropsychiatric tests administered

Figure 4.1. Study design for the two cohorts of the THINC study. Cohort A were treatment-naïve and were followed for one year. One single paired PK sample was obtained in the plasma and CSF, at two-weeks and one-year post study enrollment. Neuropsychiatric tests were administered at baseline, and six months and one-year post enrollment into the study. Cohort B participants were treatment-experienced and enrolled into the study at least one year after initiating therapy. PK samples in the plasma and CSF were collected soon after study enrollment and neuropsychiatric tests were administered. The double red line indicates the time of enrollment into the study. CSF: cerebrospinal fluid *Neurocognitive tests were administered at study baseline for individuals enrolled into cohort A.

A cross-sectional (single time point) analysis was conducted for participants in cohort B. In this cohort, participants with neurocognitive impairment were enrolled into the study and had a PK visit within two weeks of enrollment. At this visit, plasma and CSF were sampled at a single time point as described for cohort A and neuropsychological tests were administered. There were no follow-up visits for this cohort, unless participants were viremic in the CSF.

4.3.4. Neuropsychological test evaluations:

Neuropsychological performance was assessed in the following domains (tests): premorbid verbal/language (Wide Range Achievement Test 4 - Reading Subtest(14)), learning (Hopkins Verbal Learning Test – Revised (HVLT-R)(15)), verbal memory (HVLT-R), speed of information processing (Trailmaking Test A(16,17) and Stroop Color Test(18)), WAIS-III Digit Symbol Test(19)), attention/working memory (WAIS-III Symbol Search Test(19) and Stroop word(18), fine motor (Grooved Pegboard Test(20)), gross motor (Timed Gait Test(21)) and executive functioning (Trailmaking Test B, Stroop interference test, and Letter and Category Fluency Test(22)).

For each participant and each individual domain/test, z-scores were computed from the normative scores that were demographically corrected by adjusting for age, education, gender, and race where appropriate. This was done by subtracting the raw test score from the corrected score followed by dividing by the normative standard deviation(23). The total z-score for each participant was calculated by averaging the individual z-scores across the 15 tests. A score of zero reflected average performance, positive scores denoted better than average and negative scores denoted lower than average performance. The global deficit score (GDS)(24) was computed by taking individual test scores across the neuropsychological battery, and converting them to deficit scores. The deficit scores ranged from zero (normal or above normal performances) to five (severe impairment)(25). The GDS was determined by averaging the deficit scores.

4.3.5. Quantification of efavirenz concentration in the fluid and tissue matrices:

Analytical methods for quantification of EFV in fluid and tissue samples of the rhesus macaques have been previously described.(26) EFV concentrations in the brain tissue

homogenate were expressed in ng/ml by using a density of 1.06 g/cm^3. In the clinical samples, EFV concentrations in the plasma and the CSF were analyzed by liquid chromatography tandem mass spectroscopy (LC-MS/MS) assays available at the UNC Center for AIDS Research Clinical Pharmacology and Analytical Chemistry Laboratory at the University of North Carolina at Chapel Hill(27). The lower limit of quantification (LLOQ) for EFV was 50 ng/ml in the plasma and 1 ng/ml in the CSF, with an intra- and inter-day precision and accuracy that was within 15%. For the brain tissue, the LLOQ of EFV was 0.005 ng/mL of tissue homogenate, and the inter- and intra-day precision and accuracy of the assay were within 20%.

4.3.6. Development of the preclinical pharmacokinetic model:

EFV concentrations in the plasma, CSF, and brain tissue of the rhesus macaques were fit in a sequential approach in ADAPT version 5.0 (Biomedical Simulation Resource, Los Angeles).(28) First, plasma concentrations alone were fit in each macaque using the iterative two-stage analysis (IT2S) NLMEM approach(29). The starting values for model parameters were derived from a previously published noncompartmental analysis (NCA) in rhesus macaques and empiric estimates of variability (coefficients of variation [CV%]) were made for all the plasma parameters(29). Bayesian priors were then updated based on the fitted values. After obtaining reasonable plasma fits, individual plasma parameters were fixed and CSF and brain tissue drug concentrations from all eight animals were added into the model. The CSF and brain tissue distributional parameters were then fit using a naïve pooled analysis by a maximum likelihood (ML) estimation method. This approach was used because the plasma data were sufficient to obtain macaque-specific estimates, but the CSF and brain data were limited. Because of issues with identifiability, the volume of distribution within the CSF was fixed in all animals to 0.015 L – which is the physiologic volume of the CSF in rhesus

macaques.(30) The CSF and brain tissue distributional parameters from the best fit were then used as initial estimates of the Bayesian prior means (with empiric variances) for the final PK model where the plasma, CSF and brain tissue exposure data from all eight animals (79 concentrations in all three matrices) were co-modelled by IT2S. **Table 4.1** includes detailed modeling methods, including the total number of data points available at each step. Weighting of the plasma, CSF, and brain tissue data was by the inverse of the estimated variance, which was composed of both additive and proportional components. Model discrimination was by Akaike's Information Criterion (AIC(31)). Bias and precision were evaluated based on the objective function, relative standard error (RSE%), and other goodness-of-fit diagnostic plots such as the observation versus individual model prediction plot.

Table 4.1: Modeling methods for the preclinical and clinical efavirenz PK models

Step	Modeling Methods	Data available	Source
Preclinical Model			
1) Step I	Iterative two-stage analysis to estimate plasma PK parameters in each macaque (fit individually in each animal)	Eight plasma concentrations to determine seven parameters in each animal	Initial estimates were from noncompartmental analysis(29)
2) Step II	Iterative two-stage analysis with refined estimates from Step I to estimate plasma PK parameters in each	Eight plasma concentrations to determine seven parameters in each animal	Refined estimates from Step I (geometric mean of parameter estimates)

Step	Modeling Methods	Data available	Source
	macaque (fit individually in each animal)		
3) Step III	Mixed likelihood naïve pooled data Analysis to estimate CNS parameters after fixing plasma parameters for individual macaques (fit with data combined from all eight animals)	16 CSF and brain tissue trough concentrations to determine seven CNS PK parameters in eight animals	Parameters defined from sensitivity analysis
4) Step IV	Maximum *a-priori* Bayesian analysis to refine plasma and CNS parameters in each macaque (fit individually in each animal)	Ten plasma, CSF, and brain tissue concentrations from each animal to determine 14 parameters in eight animals	Plasma model estimates from Step I and CNS model estimates from Step III
5) Step V	Iterative two-stage analysis with refined estimates from Step IV to determine final plasma and CNS PK parameters (fit with data	79 plasma, CSF and brain tissue concentrations to determine 14	Geometric mean of parameter estimates determined in step IV

Step	Modeling Methods	Data available	Source
	combined from all eight animals)	parameters in eight animals	
Clinical Model			
1) Step VI	Iterative two-stage analysis to estimate plasma PK parameters	24 plasma concentrations to determine six plasma PK parameters in 24 participants	Initial estimates from EFV population PK model by Kappelhoff et al. (32)
2) Step VII	Iterative two-stage analysis with refined estimates from Step I to estimate plasma PK parameters	24 plasma concentrations to determine six plasma PK parameters in 24 participants	Geometric mean of parameter estimates from Step VI (refined estimates)
3) Step VIII	Iterative two-stage analysis to estimate CNS parameters after fixing plasma parameters in each individual	24 CSF concentrations to determine seven CNS PK parameters in 24 participants	CNS PK parameter estimates from the macaque model determined in Step V

4.3.7. Development of the clinical pharmacokinetic model:

A sequential approach was also employed to fit the clinical data. The plasma data were initially fit alone by the IT2S method(33,34). Because of the sparseness of the clinical data, the structural model for EFV disposition in the clinical model was the same as for the rhesus macaques. However, the initial estimates for the plasma parameters, including the absorption parameters, were derived from a previously published EFV population PK model(32). The individual plasma PK parameters were then fixed in each participant and the CSF concentrations were added in to the model to fit the CSF exposures and predict the brain tissue exposures. The volume of distribution in the CSF (V_{CSF}) was fixed to a physiologically relevant volume of 0.15 L(35), that was allometrically scaled from the macaque CSF volume. The initial estimate of the brain tissue volume of distribution (V_{brain}) was allometrically scaled from the macaque model. The initial estimates of the distributional rate constants describing EFV movement between the plasma, CSF, and brain tissue were the same values from the final macaque model, using the assumption that the structural model of EFV distribution was the same in macaques and humans. All these parameters were then re-estimated by IT2S. The final PK model was used to simulate EFV concentrations at steady state over a 24-hour dosing interval in the plasma, CSF, and brain tissue in the study participants. Model discrimination and residual variance weighting was as described for the rhesus macaque model. The model was validated by measuring EFV in brain tissue samples that were available from the National Neuro-AIDS Tissue Consortium (NNTC) repository. Postmortem brain tissue concentrations from three HIV-positive participants were overlaid with the implications of the final model that were obtained by performing a 1000-replicate Monte-Carlo simulation.

4.3.8. Pharmacokinetic/pharmacodynamic correlation analysis:

Individual concentration versus time profiles over the 24-hour dosing interval at steady state were simulated post-hoc from the final model parameters in the plasma, CSF, and brain tissue. The trough concentration of EFV at the end of the dosing interval (C24h) and the exposure of EFV over the dosing interval (AUC$_{0-24h}$) were determined in the various matrices. Correlation analyses were performed between the model-predicted C24h and AUC$_{0-24h}$ parameters in the plasma, CSF, and brain tissue. Finally, the individual PK parameters were correlated with the relevant neurocognitive scores – the Z score and GDS.

4.3.9. Statistical analysis:

Comparison of EFV concentrations between the different regions of the brain tissue, and between sex and infection status in the rhesus macaques was performed by the Kruskal Wallis test; $p < 0.05$ was considered significant. Tests for correlation were performed using the Spearman correlation test. The PK estimates are presented as geometric means and the model-predicted C24h, AUC$_{0-24h}$ and brain tissue:plasma AUC$_{0-24h}$ ratio and brain tissue:CSF AUC$_{0-24h}$ ratio values are presented as median (range) unless noted otherwise. Data were analyzed using SigmaPlot 13.0 (Systat Software Inc., San Jose, CA); $p < 0.05$ was considered significant.

4.4.   Results

4.4.1. Pharmacokinetic model for efavirenz in the plasma, cerebrospinal fluid and brain tissue in rhesus macaques

In the rhesus macaques, the median concentration (range) of EFV was 691 ng/g (280-1929 ng/g) in the frontal cortex, 687 ng/g (232-2440 ng/g) in the cerebellum, 758 ng/g (213-2139 ng/g) in the basal ganglia, and 834 ng/g in the parietal cortex (190-1890 ng/g),

respectively. The concentration of EFV was similar across all regions of the brain (p=0.95) and averaged to give one brain tissue concentration per animal. There were no statistically significant differences in EFV concentrations by sex (p=0.9) or infection status (p=0.1). The disposition of EFV in the plasma, CSF, and brain tissue in the animals was best described by an eight-compartment model with a log-normal error model which included the central plasma compartment, one peripheral compartment and three transit absorption compartments to accommodate the delayed absorption of EFV **(Figure 4.2)**. Models that did not include a peripheral compartment were also tested and the total number of transit compartments were determined by adding in these compartments sequentially until the best fit (based on r^2 value of the model fit) and successful run diagnostics for all eight animals were obtained **(Table 4.2)**.
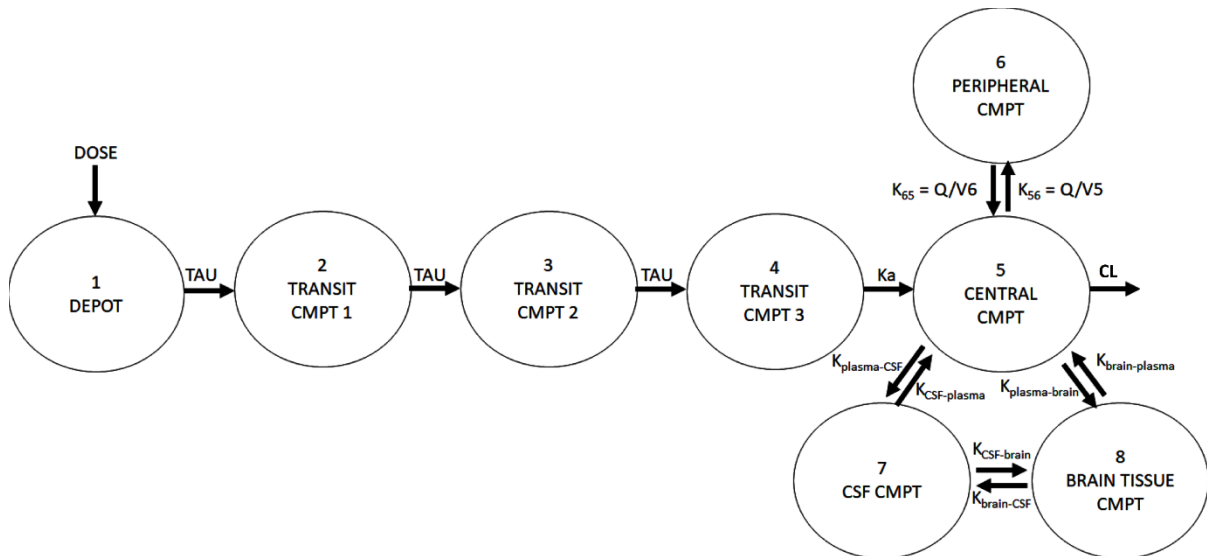
Figure 4.2. Structure of the pharmacokinetic model for efavirenz in rhesus macaques and humans. An eight-compartment model with first-order absorption and linear elimination, best described efavirenz disposition in the plasma, CSF, and brain tissue. Three transit compartments were used to describe the delayed peak of efavirenz in the plasma. Drug movement between the plasma, CSF, and the brain tissue were described by rate constants. The CSF volume of distribution was fixed to physiologically relevant values in rhesus macaques and humans (0.015 and 0.15 L respectively). Legend – CMPT: compartment, CSF: cerebrospinal fluid

Table 4.2: Evaluation of absorption models for efavirenz PK model in rhesus macaques

Animal Number	One Transit Compartment		Two Transit Compartments		Three Transit Compartments	
	Model fit r^2	Diagnostics[1]	Model fit r^2	Diagnostics	Model fit r^2	Diagnostics
Macaque 1	0.962	Pass	0.894	Pass	0.957	Pass
Macaque 2	0.981	Pass	0.944	Pass	0.820	Pass
Macaque 3	0.992	Pass	0.967	Pass	0.701	Pass
Macaque 4	0.999	Pass	0.993	Pass	0.995	Pass
Macaque 5	0.413	Fail	0.797	Pass	0.960	Pass
Macaque 6	0.784	Pass	0.262	Fail	0.828	Pass
Macaque 7	0.903	Pass	0.897	Pass	0.898	Pass
Macaque 8	0.931	Pass	0.990	Pass	0.996	Pass

[1] A failed run was defined as a near singular matrix and high standard errors

In four out of the eight macaques, plasma C24h values measured from day four until necropsy were 4- to 40-fold lower than the C24h values after the first dose **(Figure 4.3)**. This type of inter-occasion variability was accommodated by incorporating a multiplicative term (M) on clearance such that the oral clearance (CL/F) after 24 hours was given by the product of clearance for the first 24 hours and M (if time > 24h, then CL/F = CL/F·M). Four macaques had observed EFV concentrations that were below the limit of quantification (BLQ) in the CSF. The BLQ data were censored by the M5 (BLQ values imputed as LLOQ/2) method. This simple approach was considered appropriate to censor our data since we used a Bayesian

iterative estimation method (inferences are based on assumed prior distribution and are not sensitive to missing values). The parameter estimates from the M5 method were also similar to the the M1 (BLQ values ignored) and the M7 (BLQ values imputed as 0) methods.
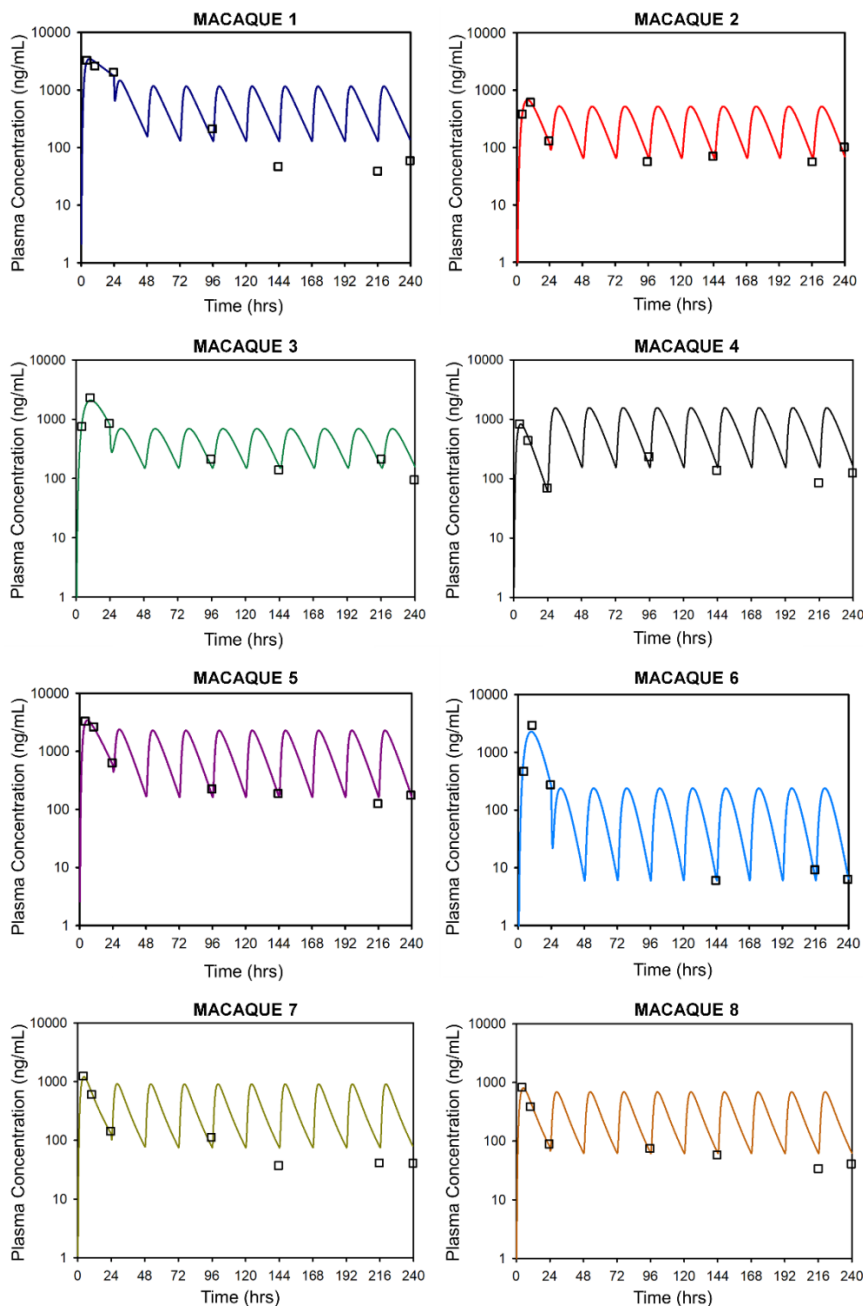
Figure 4.3. Individual model-predictions versus observations in the plasma in rhesus macaques. The model predictions for efavirenz pharmacokinetics in the plasma are shown over the 10 days in which the drug was administered in the eight rhesus macaques. The solid model prediction lines are overlaid with the observations in the open squares.

In the fits of individual macaques, the median RSEs were generally small (<30%) with moderate RSEs (30-50%) for the peripheral volume of distribution (V6/F), $K_{plasma-CSF}$, $K_{CSF-brain}$, and $K_{brain-CSF}$. The CL/F was 8.7 L/hr, V5/F was 6.5 L, and Ka was 0.18 1/hr. The V_{brain} (conditioned on the fixed estimate for V_{CSF}) of distribution was 0.037 L. The geometric mean of the parameter estimates and standard deviation of the parameter estimates (RSE%) are listed in **Table 4.3**.

Table 4.3: Model parameters from the final efavirenz pharmacokinetic model in rhesus macaques and humans

Rhesus Macaques

Parameter[1]	Geometric Mean	Median	CV%
CL/F (L/hr)	8.70	10.74	89.8
V5/F (L)	6.45	5.00	51.2
Ka (1/hr)	0.183	0.17	36.4
V6/F (L)	14.6	13.69	155.0
Q/F (L/hr)	4.66	5.9895	89.1
TAU (1/hr)	0.95	1.16	48.5
M[1]	2.63	2.07	103.0
$K_{plasma-CSF}$ (1/hr)	1.71E-06	1.91E-06	59.5
$K_{CSF-plasma}$ (1/hr)	0.18	0.18	27.3
$K_{plasma-brain}$ (1/hr)	2.42E-03	2.34E-03	31.1
$K_{brain-plasma}$ (1/hr)	0.15	0.14	26.8
$K_{CSF-brain}$ (1/hr)	2.56E-03	0.002779	36.0
$K_{brain-CSF}$ (1/hr)	5.58E-06	4.6E-06	68.2

V$_{brain}$/F (L)	0.037	0.036	21.8
V$_{CSF}$/F (L)	0.015 (fixed)	0.015 (fixed)	-

Humans[2]

Parameter	Geometric Mean	Median	CV%
CL/F (L/hr)	12.37	12.20	58.5
V5/F (L)	155.34	147.25	39.1
Ka (1/hr)	0.135	0.025	94.6
V6/F (L)	405.4	200.05	35.8
Q/F (L/hr)	6.31	28.33	142.0
TAU (1/hr)	1.00	1.95	27.8
K$_{plasma-CSF}$ (1/hr)	4.27E-06	4.11E-06	88.8
K$_{CSF-plasma}$ (1/hr)	0.244	0.244	26.0
K$_{plasma-brain}$ (1/hr)	2.00E-03	2.00E-03	30.2
K$_{brain-plasma}$ (1/hr)	0.175	0.175	31.2
K$_{CSF-brain}$ (1/hr)	3.00E-03	3.00E-03	40.2
K$_{brain-CSF}$ (1/hr)	2.41E-06	2.41E-06	70.5
V$_{brain}$/F (L)	0.514	0.514	25.1
V$_{CSF}$/F (L)	0.15 (Fixed)	0.15 (Fixed)	-

[1]M was not incorporated on the clearance term in the human EFV PK model
[2]The human pharmacokinetic model was developed by a sequential estimation method where the plasma was initially estimated, followed by the CSF and brain tissue distributional parameters

From the final model, the r^2 value for the line of individual conditional model predictions *versus* observations in the plasma (overall, minimum-maximum individual value)

was 0.96 (0.91 – 0.99; **Figure 4.4**). The overall r^2 value for the individual conditional model predictions versus observations in the CSF and the brain tissue was 0.91 and 0.99 respectively. The overlay between observations and individual model predictions for the eight macaques in the plasma are shown in **Figure 4.5.** The data file used in the final IT2S estimation and model code are provided in **Appendix 4.2**.
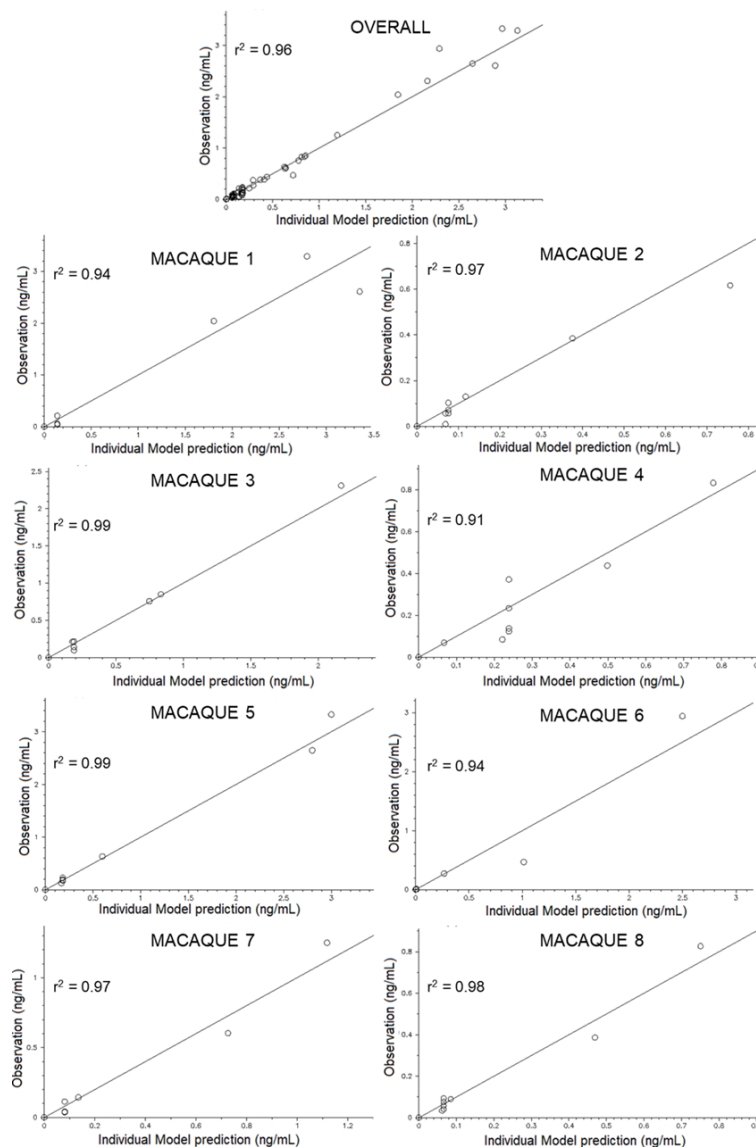
Figure 4.4. Goodness of fit plots for individual model predictions versus observations in the plasma in rhesus macaques for the final PK model. The diagnostic plots are shown overall in the 8 macaques and in each individual macaque. The overall r^2 value was 0.95 and ranged from 0.91 to 0.99 in the individual macaques.
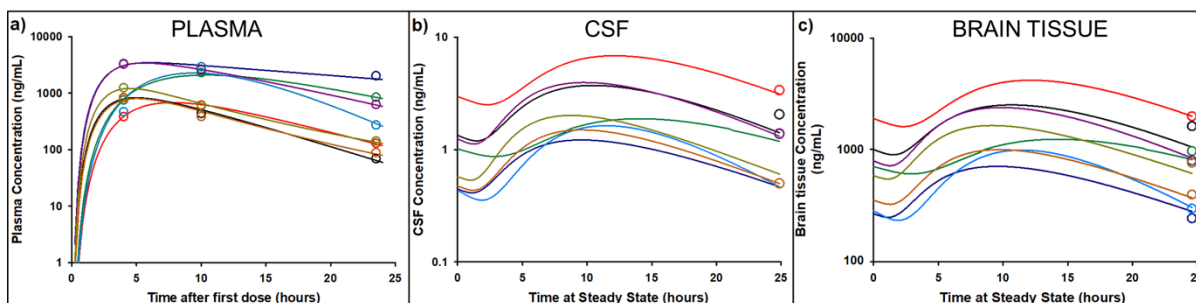
Figure 4.5. Goodness-of-fit spaghetti plots for the rhesus macaque efavirenz PK model. Spaghetti plots of the individual model predictions are shown for the eight individual macaques with observations overlaid in the open circles in the (a) plasma (b) CSF and (c) brain tissue. Each color represents one individual macaque. In the CSF compartment, four animals had undetectable EFV concentrations in the CSF and these values were imputed at 0.5 ng/mL (half of the LLOQ value). Legend – CSF: cerebrospinal fluid. LLOQ – lower limit of quantification.

4.4.2. Clinical study demographics:

Of the 109 HIV-positive men and women who enrolled into the study across both cohorts, twenty-six subjects were on EFV-based regimens. Atripla® was the most commonly prescribed regimen (n=22, 92%). Five participants (18%) were in cohort A (naïve to ARV therapy before study enrollment, and five (18%) were women. One of the subjects enrolled in the treatment-naïve cohort provided study measurements at baseline and week two but was lost to follow-up for the remainder of the study. Another treatment-naïve subject switched ARV regimens after the first two-week study visit and was not on an EFV-based regimen at the one-year PK visit. The EFV concentrations in the plasma and CSF from the two-week samples were below the LLOQ for both of these participants. Therefore, these participants were determined to not be adherent to therapy, and their PK samples were excluded from the final analysis. The complete study demographics for the participants included in the final analysis are listed in **Table 4.4**.

Table 4.4. Demographic Characteristics of the THINC study population

Demographic characteristic	Cohort A – treatment naïve (n=3)	Cohort B – treatment experienced (n=21)
Sex, female	0 (0%)	4 (19%)
Age, years	32 (19 – 53)	54 (42 – 66)
Weight, kg	65.8 (56.7 – 110.2)	71.0 (45.4 – 136.1)
BMI[1]	18.5 (17.2 – 31.2)	21.8 (15.3 – 48.4)
Race		
White	0 (0%)	13 (62%)
African American	3 (100%)	8 (38%)
Combination Regimen		
Atripla	3 (100%)	16 (76%)
Other three-drug regimen	0 (0%)	1 (5%)
Other three+ drug regimen	0 (0%)	4 (19%)
Time on efavirenz treatment[2], years	<1	5 (3-12)
Entry CD4 count, cells/mm^3	303 (158 – 354)	594 (198 – 1,251)
Entry plasma viral load[3], copies/mL	95,870 (18,334-176,506)	BLQ
Entry CSF viral load[3], copies/mL	15,118 (355-38,400)	BLQ
Entry neurocognitive score Z-score	-0.8 (-1.3-0.13)	-0.43 (-2.8-0.86)

Demographic characteristic	Cohort A – treatment naïve (n=3)	Cohort B – treatment experienced (n=21)
Global Deficit Score (GDS)	0.88 (0.125-1.31)	0.44 (0.0-3.27)

Data are expressed as median value (range) or number (%) of subjects.
[1]Body mass index (BMI) is calculated as the weight in kilograms divided by the height in square meters
[2]Information was available for 16/24 patients
[3]The lower limit of quantification for HIV RNA in the plasma and CSF was 40 copies/mL

4.4.3. Pharmacokinetics of efavirenz in the plasma, cerebrospinal fluid and brain tissue of HIV-positive participants:

A total of twenty-nine paired EFV concentration measurements were available from the plasma and CSF to develop the clinical PK model. Similar to the rhesus macaques, the disposition of EFV in the plasma, CSF and brain tissue in humans was described by an eight-compartment model which included three transit absorption compartments to account for the delayed absorption of EFV. The structure of the final model for EFV distribution in the plasma, CSF and brain tissue in rhesus macaques and humans is shown in **Figure 4.2**. In humans, the V_{brain} conditioned on the CSF volume was 0.51 L. The geometric mean CL/F was 12.4 L/hr, V5/F was 155 L and ka was 0.135 1/hr. Individual estimates of the model parameters were generally estimated with high precision (overall r^2, for plasma and for CSF, was 0.97 and 0.92, respectively). **Table 4.3** summarizes the sample statistics for the PK parameters. The median RSE was high (>50%) for Ka, Q/F and $K_{brain-CSF}$. For the remaining parameters, the median RSE varied between 12 and 40%. The goodness-of-fit diagnostic plots for the individual and population predicted values for plasma and CSF are shown in **Figure 4.6.**
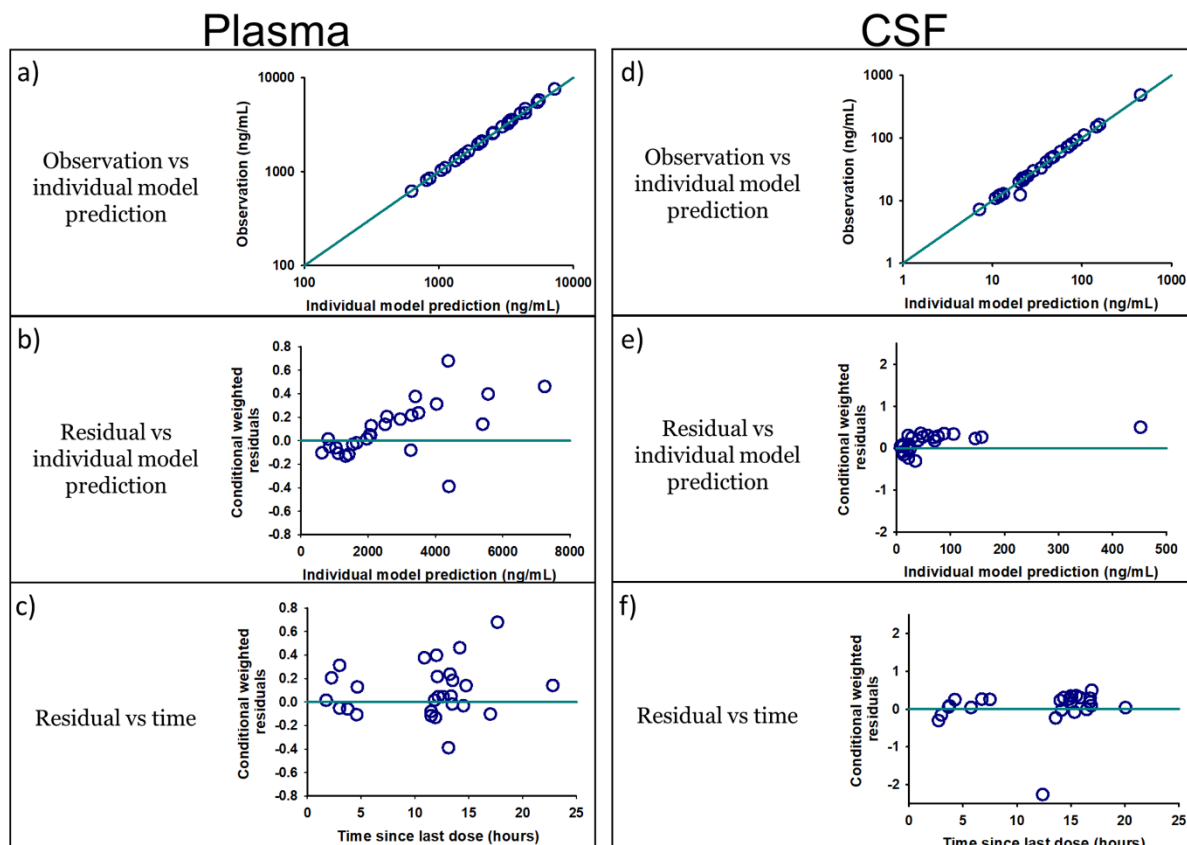
Figure 4.6. Goodness-of-fit diagnostic plots for the final clinical PK model in the plasma and CSF. The light blue solid lines represent the zero lines (b, c, e and f) or the lines of unity (a and d). Observations versus individual predictions in the double logarithmic scale in the plasma (a) and the CSF (d) are shown in the purple open circles. Conditional weighted residuals (CWRES) versus individual model predictions in the linear scale in the plasma (b) and CSF (e) and CWRES versus time after last dose in the plasma (c) and the CSF (f) are shown in the purple open circles.

The implications of the final model in the plasma and CSF, as well as the predicted EFV concentration-time profile in the brain tissue are shown in **Figure 4.7**. The 5th to 95th percentile of the 1000 model replicates of the ms captured 88% and 96% of all EFV observations in the plasma and CSF respectively**,** suggesting that the model was able to sufficiently describe the observations in both matrices, with reasonable partitioning between residual and inter-subject variability. The model-predicted concentration-time profiles in the

CSF and brain tissue were flat, with a median EFV concentration in the CSF and brain tissue of 31 ng/ml (6 to 170 ng/ml) and 8,000 ng/ml (2,300 to 29,000 ng/ml), respectively. The ratio of predicted EFV AUC_{0-24h} in the brain tissue to plasma was 3.6 (3.2 to 3.8) while the ratio of AUC_{0-24h} in the brain tissue to the CSF was 213 (23 to 834). The data file used in the final IT2S estimation and model code are provided in **Appendix 4.3**.

Demographic information for the three HIV-positive patients from the NNTC repository, from whom EFV concentrations in the brain tissue were available for model validation are presented in **Table 4.5**. Model overlay with the external dataset observations (black triangles, **Figure 4.7**) showed that the model predictions adequately captured the observed brain tissue data (ranging from 1,800 ng/mL to 8,000 ng/mL).
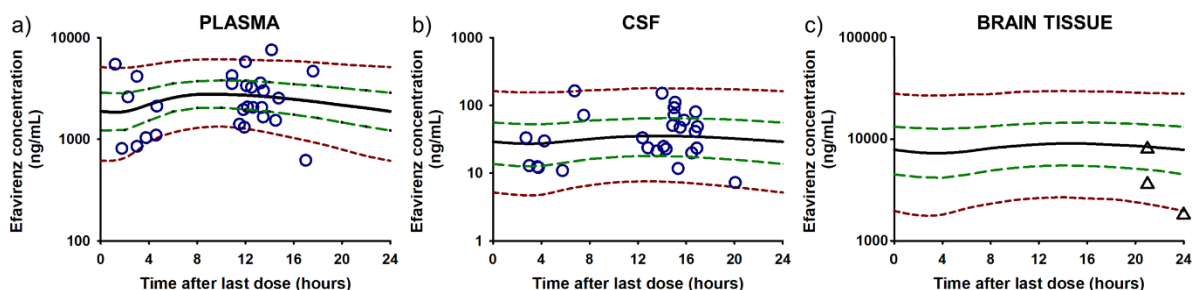
Figure 4.7. Graphical overlay of the implications of the final PK model in the (a) plasma, (b) CSF, and (c) brain tissue. The purple open circles represent the observations from the THINC study and the black open triangles represent observations from our external dataset. The dashed red lines represent the 5th and 95th percentiles of the 1000-replicate simulations, the dashed green lines represent the 25th and 75th percentiles while the thick solid black line is the median concentration. The 5th to 95th percentile captured 88% of the THINC study observations in the plasma and 96% of the observations in the CSF while the brain tissue predictions showed good agreement with the concentrations available from the external dataset.

Table 4.5: Demographic information from the HIV-positive patients in the National Neuro-AIDS Tissue Consortium (NNTC) repository from whom efavirenz brain tissue concentrations were available.

ID	Sex	ARV regimen	Brain tissue collection time post-dose (hours)[1]	EFV concentration (ng/mL)		
				Plasma[2]	CSF[3]	Brain tissue
10015	Male	600 mg EFV + 300 mg lamivudine + 80 mg stavudine	? (trough)	-	16.9	1,800
716	Male	600 mg EFV + 200 mg emtriva + 300 mg tenofovir	21	-	-	8,000
725	Male	600 mg EFV + 100 mg lamivudine + 100 mg zidovudine	21	-	-	3,600

[1]For ID 10015, no information was available from the NNTC repository on the exact time of brain tissue collection post-dose. This value was imputed as a trough concentration for the overlay with the model predictions
[2]No plasma concentration data were available for the three individuals at the time of autopsy
[3]CSF concentration data were only available from ID 10015 at the time of autopsy

Generally, the model-predicted EFV C24h in all three matrices showed a stronger correlation to each other than did the model-predicted AUC_{0-24h} parameters, as shown in **Figure 4.8**. The model-predicted brain tissue C24h and AUC_{0-24h} showed stronger correlation with the respective parameters in the plasma (rho = 0.99, p < 0.001 and rho = 0.99, p < 0.001) than with the respective parameters in the CSF (rho = 0.42, p = 0.04 and rho = 0.36, p = 0.09).
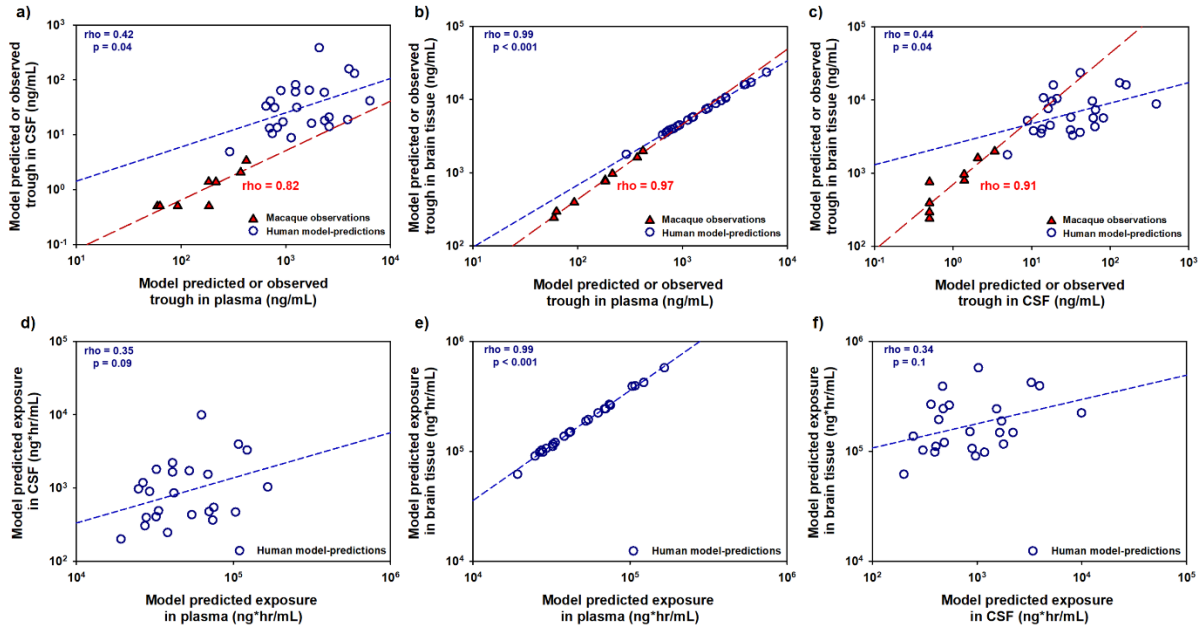
Figure 4.8. Correlation analysis between model-predicted efavirenz concentration at 24 hours (C24h) post-dose and AUC$_{0-24h}$ in the plasma, cerebrospinal fluid (CSF) and brain tissue in humans and observed concentrations at 24 hours in rhesus macaques. The top panels show correlation plots between the model-predicted C24h in humans and observed C24h in macaques for the (a) plasma and CSF, (b) plasma and brain tissue, and (c) CSF and brain tissue. The bottom panels show correlation plots between the model-predicted AUC in humans for the (d) plasma and CSF, (e) plasma and brain tissue, and (f) CSF and brain tissue. The open blue circles represent the predicted C24h and AUC parameters in humans while the filled red triangles represent observed C24h in the rhesus macaques. The red long dashed lines and blue short dashed lines represent the regression lines for the observed macaque data and the predicted human data, respectively. Brain tissue C24h and AUC parameters showed better correlation with the plasma parameters (rho= 0.99, p<0.001 and rho=0.99, p<0.001) than with the CSF (rho= 0.44, p=0.04 and rho=0.34, p=0.1).

4.4.4. Pharmacokinetic/pharmacodynamic correlation analysis:

The Z-score and the GDS did not show any correlation with the model-predicted exposure of EFV in the brain tissue as shown in **Figure 4.9** (rho = 0.005, p = 1.0 and rho = 0.045, p = 0.8) or with the model-predicted EFV exposure in the CSF (rho = 0.05, p = 0.8 and rho = 0.005, p = 1.0; data are not shown).

160
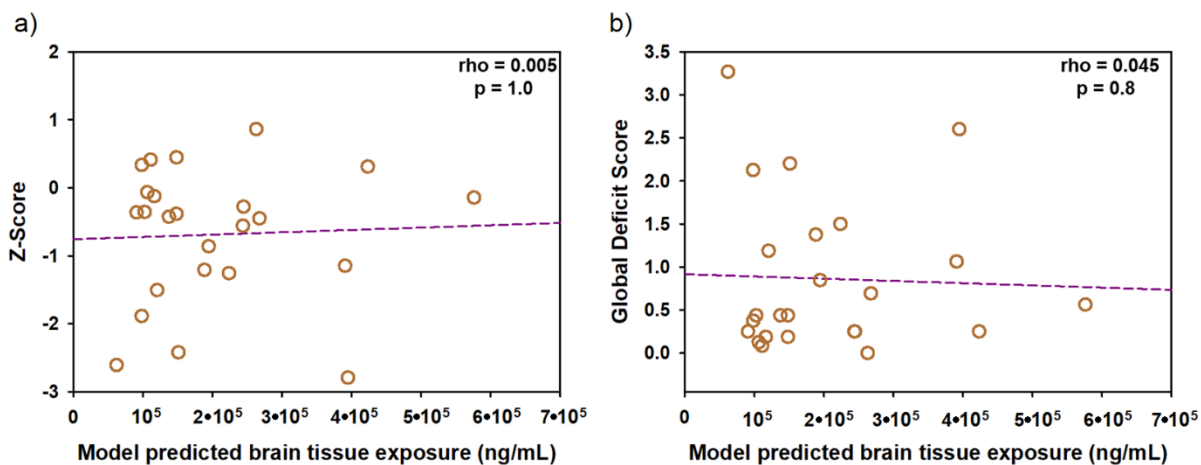
Figure 4.9. Correlation analysis between model-predicted efavirenz exposure (AUC$_{0-24h}$) in the brain tissue in humans and the (a) Z-score and (b) global deficit score (GDS) neurocognitive scores. The correlation analysis is shown between the model predicted exposure of EFV in the brain tissue and (a) Z-scores and (b) GDS. No relationship was noted with either neurocognitive score measurement.

4.5. Discussion

In this analysis, we present a novel framework for analyzing sparse PK data of EFV in preclinical species and translating the model to humans in order to predict drug exposure in the human brain tissue. Since sparse data were available from the rhesus macaques and humans, we chose to develop a PK model for EFV with the prior knowledge that this drug reaches high concentrations in the brain tissue(36). Our analysis showed that the observed C24h in the plasma and brain tissue of macaques were highly correlated (rho = 0.97, p < 0.001), as were C24h in CSF and brain tissue (rho = 0.91, p < 0.001). Similarly, model-predicted EFV AUC$_{0-24h}$ and C24h in human brain tissue were highly correlated with the plasma parameters. These results add credence to previous analyses(37,38) where EFV plasma concentrations may be sufficient to predict brain tissue exposure.

Our data predicted a ten-fold range in EFV exposure in the plasma (median exposure of 41,365 ng•hr/mL and range of 19.223-165,487 ng•hr/mL) and in the brain tissue (149,549 ng•hr/mL [61,908-576,048 ng•hr/mL]) and an almost 50-fold range of exposure in the CSF (875 ng•hr/mL [200-9,940 ng•hr/mL]). The wide range in predicted CSF exposures reflects the high variability of observed CSF data in our participants (90% CV). This high variability resulted in the wide range in AUC_{brain}/AUC_{CSF} values, and the lack of correlation between brain tissue and CSF exposure despite a flat EFV profile in both matrices. High inter-individual variability in plasma concentrations of EFV has been demonstrated previously(39–41) and our brain tissue concentration data from our external dataset were also highly variable (72% CV). This variability is helpful to quantify, as it is not evident within an approach such as the CPE, where a particular ARV regimen has a score equivalent to the sum of the scores of the individual drugs and is the same in all individuals on the same drug regimen.

The observed CSF EFV concentrations in humans (30 ng/mL) were 15-fold higher than the CSF concentrations in the rhesus macaques (~2 ng/mL). These differences in concentrations appear to be driven primarily by the approximately ten-fold higher plasma EFV concentrations in humans (2,100 ng/mL) compared to the macaques (200 ng/mL). These species differences were also reflected in the brain tissue, and the macaque EFV brain tissue concentrations (775 ng/mL) were approximately ten-fold lower than our model-predicted EFV brain tissue concentrations (8,000 ng/mL) in humans. These model-predicted brain tissue concentrations were 267-fold higher than CSF, four-fold higher than plasma, and 15,000-fold higher than the protein-adjusted IC90 of 0.22 ng/ml(42). A 2017 PBPK model(43) predicted that EFV accumulated in the brain tissue with a steady-state concentration of 50,000 ng/ml which is ~ten-fold higher than our model predictions. However, the brain tissue PK data

recently presented by Nicol(44) were within two- to four-fold of our predictions and the brain tissue concentration data from our external NNTC repository dataset showed good agreement with our model. As a result, we believe our PK model predictions are biologically plausible.

In this analysis, our PD measure for the degree of HAND impairment were scores obtained from neurocognitive testing, considered to be the gold standard diagnostic tool(45,46). The lack of relationship between the model-predicted exposure in brain tissue and neurocognitive impairment scores may have been due to the limited range of neurocognitive testing scores in our study participants. Further, we had a small sample size for this analysis and our PK model predicted a narrow range of EFV drug exposures in the plasma and brain tissue. In fact, for 20/24 of our study participants, the model-predicted EFV exposures in the plasma were in the optimal range of exposure previously defined in a population PK analysis by Csjaka(47) as the EFV plasma exposure required for a high probability of viral suppression and a low probability of CNS toxicity. Given the insensitivity of neurocognitive tests to discern milder forms of impairment, future PK/PD studies that explore the relationship between ARV exposure and quantifiable biomarkers of CNS disease may be useful. Several biomarkers have been discovered for events such as underlying inflammation and immune activation in the CNS (neopterin)(48) or neuronal injury (neurofilament light chain)(49). In our analysis, greater EFV exposure in the brain tissue was modestly associated (r=0.7, p=0.04) with lower CSF concentration of neurofilament light chain but not neopterin (data are not shown). While these biomarkers are not routinely used in the clinic, validation of sensitive biomarkers in large trials of HAND in the CSF or plasma may add to the predictability of PK/PD analyses in this setting.

The approach we used in the macaques allowed us to estimate the plasma PK parameters with high precision (high r^2 values for the individual macaque fits) and leverage

data from all animals to estimate CSF and brain tissue profile. We considered simpler CNS model structures, such as the use of inter-compartmental clearance values. However, because of the high variability in CSF and brain tissue concentrations, restricting the distribution to clearance values led to model instability and failure of the covariance matrix to converge. Further, characterizing drug distribution into the CNS by rate constants was biologically relevant since different processes govern EFV movement into (passive diffusion) and out of (active efflux by BCRP) the CNS. Similarly, we also tried multiple modeling approaches for the clinical PK model. Initially, we considered a MAP-Bayesian estimation from a literature model to describe the plasma(32). However, since this model did not adequately capture the observed plasma concentrations **(Figure 4.10)**, it gave us limited confidence to predict brain tissue concentrations. Instead, we performed model fitting using the IT2S estimation method. Given that this tool is also Bayesian in nature and provides valuable individual estimates(33), IT2S is an appropriate method for analyzing sparse data. An important consideration for the use of this method is the accuracy of the initial parameter estimates. For this purpose, we used the published population PK model(32) for obtaining the initial plasma parameter estimates, and refined the parameters to better describe the plasma concentrations in our study subjects.

Given the small number of rhesus macaques and humans for model development, we had limited ability to draw population inferences from our data. The results that we present here used population tools to better characterize individual PK profiles, but are not a substitute for population PK analyses. Indeed, the information gained from prior population PK analyses was invaluable to characterize plasma distribution in our clinical model. Our analysis provides an important proof of concept for the enrichment of sparse data (such as in the setting of therapeutic drug monitoring) with information from data-rich population PK models. Such an

approach allows for the better description of the individual profile and provides the ability to predict PK at otherwise inaccessible sites. Our external validation dataset was a unique data source to compare with our model predictions in the brain tissue. While the observed brain tissue data were all either at, or below, the median concentration of our model predictions, this is not indicative of model misspecification. There were very few brain tissue observations to conclude differences in distribution of the external dataset observations and our model predictions, and most importantly there were no population inferences drawn from our model to assume that the distributions of the external dataset and the model predictions had to be similar. Rather, the external data highlight the strength of our approach to predict hard-to-obtain clinical data, as well as the accuracy of our individual predictions. Ultimately, high individual precision and satisfactory plasma fit in both macaques and humans were leveraged to estimate CSF and brain tissue PK, and provides a novel approach to handle sparse data.
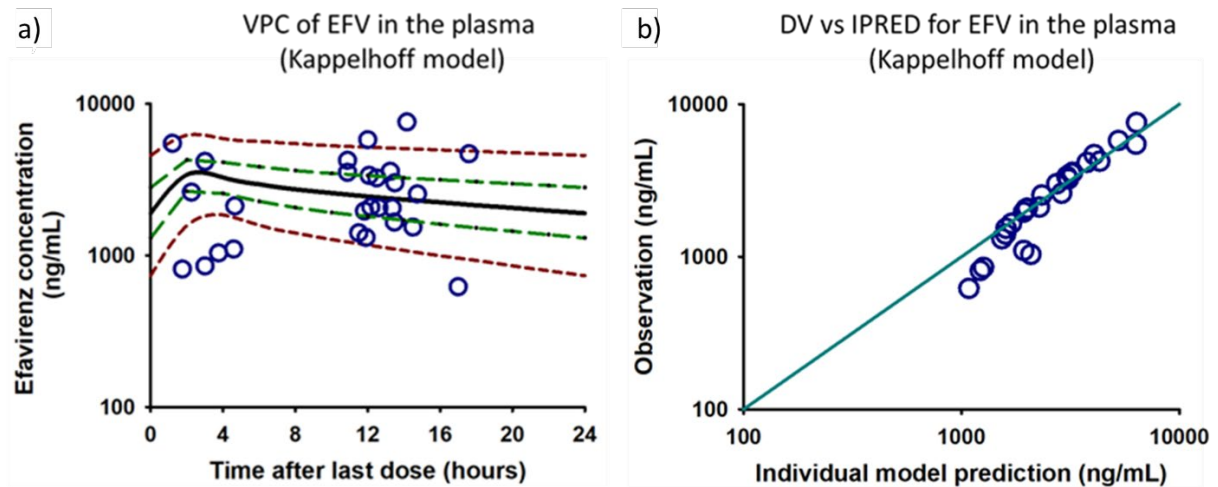
Figure 4.10. Diagnostic plots showing model fit by MAP-Bayesian analysis with the Kappelhoff model. On performing a MAP-Bayesian estimation and performing model diagnostics with (a) VPC and (b) DV vs IPRED plot, it was apparent that the model did not adequately capture the lower plasma EFV concentrations. Furthermore, the VPC indicated model misspecification (only 67% of the data were captured in the 90-percentile interval).

We had a limited ability to identify the mechanism for the increase in CL/F, noted in four macaques, and opted for a parsimonious, empiric structural model that fit the data well. Of note, the lowered plasma concentrations were observed after 96 hours of the first dose. This is early for EFV auto-induction (predicted to occur in humans after a week of dosing(55)), although early auto-induction effect has been shown for some other drugs(56). The four animals that showed lower C24h were predicted to have higher peak concentration after the first dose compared to the other animals (>2,200 ng/mL versus <1,500 ng/mL) and auto-induction may occur earlier with higher concentration of the inducing agent. The faster autoinduction in macaques compared to humans could be attributed to the high variability in CYP2C9 oxidation in macaques(57) and differential drug-enzyme interaction across both species. For example, EFV is also a potent inhibitor of CYP2B6 (Ki=1.68 µm)(58) but CYP2C9 is only moderately inhibited by EFV (Ki=19.46 µm)(58). In our clinical model, since we often had only one plasma concentration per individual collected at steady state, we were not able to estimate the effect of auto-induction.

Another limitation of our approach is the assumption of the same EFV structural model in both macaques and humans. This approach has been demonstrated to work best for drugs that do not undergo active influx or efflux by drug transporters and for drugs that are not highly protein bound(36,37). However, EFV is highly protein bound and is a substrate of the active efflux transporter BCRP(38), which is highly expressed on the blood brain barrier(39,40). Regardless, macaques and humans have similar EFV plasma protein binding (99.4% vs 99.5%)(16) and abundance of BCRP on the blood brain barrier(39,40). These characteristics make our approach suitable.

Finally, the CSF and brain tissue concentrations in the macaques were only collected at the end of the dosing interval at necropsy and this prevented us from estimating the volume of distribution in the CSF and brain tissue due to identifiability issues. Since we had an estimate for the physiologic volume of CSF(30) but had limited data on the physiologic brain tissue volume, we conditioned brain tissue volume on a fixed CSF volume in the macaques. For similar reasons, the CSF volume was also fixed in humans. This resulted in the low values of distributional rate constants describing EFV movement into the CSF. Since only trough concentration data were available from the CSF and brain tissue, we made limited inferences on time-dependent EFV PK profile and performed PK/PD analyses with brain tissue exposure as a more stable model estimate. However, our model-predicted EFV PK profile in these matrices (no distinction between Cmax and C24h) agrees with the relatively flat EFV PK profile observed in the CSF(35), and previously predicted in the brain tissue(43), and highlights the utility of EFV C24h measurements in the CSF and brain tissue.

4.6. Conclusions

In conclusion, an eight-compartment PK model was developed in rhesus macaques and the structural model was translated to humans in order to predict the CSF and brain tissue exposure of EFV. EFV showed first-order absorption and linear elimination from the central compartment and three transit compartments were utilized in order to describe the delay in EFV peak concentrations in the plasma. The PK model predicted the median brain tissue concentration of EFV to be 8,000 ng/ml with median brain tissue AUC_{0-24h} to be 150,000 ng•hr/ml. The 5th to 95th percentile of the 1000 Monte-Carlo replicates of our final model predictions adequately described the plasma and CSF data and captured the post-mortem brain

tissue concentration data, that were available from three HIV-positive individuals from an external validation dataset. The AUC_{0-24h} ratio of brain tissue to plasma was 3.6 while the AUC_{0-24h} ratio of brain tissue to CSF was 212. The brain tissue C24h and AUC_{0-24h} were highly correlated (rho=0.99, p<0.001) with their respective parameters in the plasma but were poorly correlated with the CSF parameters (rho= 0.44, p=0.04 and rho=0.34, p=0.09). The individual predictions of EFV AUC_{0-24h} and C24h in the brain tissue did not correlate with the neurocognitive impairment scores of the study participants, indicating that in this small study there may be factors other than PK that are responsible for influencing neurological outcomes in individuals with HAND.

4.7.   REFERENCES

1.   Marra CM. HIV-associated neurocognitive disorders and central nervous system drug penetration: what next? Antivir Ther. 2015;20(4):365–7.

2.   Tan IL, McArthur JC. HIV-associated neurological disorders: A guide to pharmacotherapy. CNS Drugs. 2012;26(2):123–34.

3.   Letendre S. Central Nervous System Complications in HIV Disease : HIV-Associated Neurocognitive Disorder. Top Antivir Med. 2011;19(4):137–42.

4.   Marra CM, Zhao Y, Clifford DB, Letendre S, Evans S, Henry K, et al. Impact of combination antiretroviral therapy on cerebrospinal fluid HIV RNA and neurocognitive performance. AIDS. 2009;23(11):1359–66.

5.   Robertson K, Liner J, Meeker RB. Antiretroviral neurotoxicity. J Neurovirol. 2012;18(5):388–99.

6.   Ellis RJ, Letendre S, Vaida F, Haubrich R, Heaton RK, Sacktor N, et al. Randomized Trial of Central Nervous System-Targeted Antiretrovirals for HIV-Associated Neurocognitive Disorder. Clin Infect Dis. 2014;58:1015–22.

7.   Caniglia EC, Cain LE, Justice A, Tate J, Logan R, Sabin C, et al. Antiretroviral penetration into the CNS and incidence of AIDS-defining neurologic conditions. Neurology. 2014;83(2):134–41.

8.   Scott Lentendre. Randomized Clinical Trial of Antiretroviral Therapy for Prevention of Hand (Abstract no. 56). In: Conference on Retroviruses and Opportunistic Infections (CROI) Seattle, Washington. 2015.

9.   Letendre S. Validation of the CNS Penetration-Effectiveness Rank for Quantifying Antiretroviral Penetration Into the Central Nervous System. Arch Neurol. 2008;65(1):65–70.

10.   Standing JF. Understanding and applying pharmacometric modelling and simulation in clinical practice and research. Br J Clin Pharmacol. 2017;83(2):247–54.

11.   WHO Model List of Essential Medicines (19th List). World Health Organization http://www.who.int/topics/essential_medicines/en/ Last Accessed June 20th, 2018.

12.   Gannon P, Khan M, Kolson D. Current understanding of HIV-associated neurocognitive disorders pathogenesis. Curr Opin Neurol. 2011;24(3):275–83.

13.   Ciccarelli N, Fabbiani M, Baldonero E. Efavirenz associated with cognitive disorders in otherwise asymptomatic HIV- infected patients. Neurology. 2011;76:1403–9.

14.   Wilkinson G. Wide Range Achievement Test - 3rd Edition. 1993.

15.   Benedict RH, Schretlen D, Groninger L, Brandt J. Hopkins Verbal Learning Test – Revised: Normative Data and Analysis of Inter-Form and Test-Retest Reliability. Clin Neuropsychol. 1998;12(1).

16. Reitan R, Davison L. Clinical Neuropsychology: Current Status and Applications. 1974.

17. Army Individual Test Battery, 1944. 1944.

18. Stroop J. Studies of Interference in Serial Verbal Reaction. J Exp Psychol. 1935;18(6):643–62.

19. Wechsler D. Wechsler adult intelligence scale–Third Edition (WAIS–III). San Antonio, Texas; 1999.

20. Klove H. Clinical Neuropsychology. Med Clin North Am. 1963;47:1647–58.

21. Robertson K, Parsons T, Sidtis J, Hanlon Inman T, Robertson W, Hall C, et al. Timed Gait test: Normative data for the assessment of the AIDS dementia complex. J Clin Exp Neuropsychol. 2006;28(7):1053–64.

22. Gladsjo J, Schuman C, Evans J, Peavy G, Miller S, Heaton R. Norms for Letter and Category Fluency: Demographic Corrections for Age, Education and Ethnicity. Psychol Assess. 1999;6(2):147–78.

23. Heaton R, Miller S, Taylor M, Grant I. Revised Comprehensive Norms for an Expanded Halstead Reitan Battery: Demographically Adjusted Neuropsychological Norms for African American and Caucasian Adults. Lutz: Psychological Assessment Resources, Inc. 2004.

24. Blackstone K, Moore D, Franklin D, Clifford D, Collier A, Marra C. Defining Neurocognitive Impairment in HIV: Deficit Scores versus Clinical Ratings. Clin Neuropsychol. 2012;26(6):894–908.

25. Carey CL, Woods SP, Gonzalez R, Conover E, Marcotte TD, Grant I, et al. Predictive Validity of Global Deficit Scores in Detecting Neuropsychological Impairment in HIV Infection Predictive Validity of Global Deficit Scores in Detecting Neuropsychological Impairment in HIV Infection. J Clin Exp Neuropsychol. 2004;26(3):307–19.

26. Thompson CG, Fallon JK, Mathews M, Charlins P, Remling-Mulder L, Kovarova M, et al. Multimodal analysis of drug transporter expression in gastrointestinal tissue. AIDS. 2017;31(12):1669–78.

27. Rezk NL, Tidwell RR, Kashuba ADM. High-performance liquid chromatography assay for the quantification of HIV protease inhibitors and non-nucleoside reverse transcriptase inhibitors in human plasma. J Chromatogr B Anal Technol Biomed Life Sci. 2004;805(2):241–7.

28. D'Argenio DZ, Schumitzky A, Wang X. ADAPT 5 User's Guide: Pharmacokinetic/Pharmacodynamic Systems Analysis Software. Biomedical Simulations Resource, Los Angeles, 2009.

29. Balani SK, Kauffman LR, Deluna FA, Lin JH. Nonlinear pharmacokinetics of efavirenz (DMP-266), a potent HIV-1 reverse transcriptase inhibitor, in rats and monkeys. Drug Metab Dispos. 1999;27(1):41–5.

30. Barten DM, Cadelina GW, Weed MR. Dosing, collection and quality control issues in cerebrospinal fluid research in animal models. In: Cerebrospinal Fluid in Neurologic Disorders, Volume 146. 2017. p. 47–65.

31. Yamaoka K, Nakagawa T, Uno T. Application of Akaike's information criterion (AIC) in the evaluation of linear pharmacokinetic equations. J Pharmacokinet Pharmacodyn. 1978;6(2):165–75.

32. Kappelhoff BS, Huitema ADR, Yalvaç Z, Prins JM, Mulder JW, Meenhorst PL, et al. Population pharmacokinetics of efavirenz in an unselected cohort of HIV-1-infected individuals. Clin Pharmacokinet. 2005;44(8):849–61.

33. Steimer J-L, Mallet A, Golmard J-L, Boisvieux J-F. Alternative Approaches to Estimation of Population Pharmacokinetic Parameters: Comparison with the Nonlinear Mixed-Effect Model. Drug Metab Rev. 1984;15(1–2):265–92.

34. Sheiner LB. The population approach to pharmacokinetic data analysis: Rationale and standard data analysis methods. Drug Metab Rev. 1984;15(1–2):153–71.

35. Yilmaz A, Watson V, Dickinson L, Back D. Efavirenz pharmacokinetics in cerebrospinal fluid and plasma over a 24-hour dosing interval. Antimicrob Agents Chemother. 2012;56(9):4583–5.

36. Thompson CG, Bokhart MT, Sykes C, Adamson L, Fedoriw Y, Luciw PA, et al. Mass spectrometry imaging reveals heterogeneous efavirenz distribution within putative HIV reservoirs. Antimicrob Agents Chemother. 2015;59(5):2944–8.

37. Marzolini C, Telenti A, Decosterd L, Biollaz J, Buclin T. Efavirenz plasma levels can predict treatment failure and central nervous system side effects in HIV-1-infected patients. AIDS. 2001;15(9):1193–4.

38. Gutiérrez F, Navarro A, Padilla S, Antón R, Masiá M, Borrás J, et al. Prediction of neuropsychiatric adverse events associated with long-term efavirenz therapy, using plasma drug level monitoring. Clin Infect Dis. 2005;41(11):1648–53.

39. Ståhle L, Moberg L, Svensson J-O, Sönnerborg A. Efavirenz plasma concentrations in HIV-infected patients: inter- and intraindividual variability and clinical effects. Ther Drug Monit. 2004;26(3):267–70.

40. Dhoro M, Zvada S, Ngara B, Nhachi C, Kadzirange G, Chonzi P, et al. CYP2B6*6, CYP2B6*18, Body weight and sex are predictors of efavirenz pharmacokinetics and treatment response: population pharmacokinetic modeling in an HIV/AIDS and TB cohort in Zimbabwe. BMC Pharmacol Toxicol. 2015;16(1):4.

41. Peroni RN, Di Gennaro SS, Hocht C, Chiappetta D a, Rubio MC, Sosnik A, et al. Efavirenz is a substrate and in turn modulates the expression of the efflux transporter ABCG2/BCRP in the gastrointestinal tract of the rat. Biochem Pharmacol. 2011;82(9):1227–33.

42. Albright A V, Erickson-Viitanen S, O'Connor M, Frank I, Rayner MM, Gonzalez-Scarano F. Efavirenz is a potent nonnucleoside reverse transcriptase inhibitor of HIV type 1 replication in microglia in vitro. AIDS Res HumRetroviruses.

2000;16(15):1527–37.

43.   Curley P, Rajoli RKR, Moss DM, Liptrott NJ, Letendre S, Owen A. Efavirenz Is Predicted To Accumulate in Brain Tissue: and In Silico, In Vitro and In Vivo Investigation. Antimicrob Agents Chemother. 2017;61(1):1–10.

44.   Nicol M, Taylor J, Pastick K, Fisher J, Karuganda C, Rhein J, et al. Differential Brain Tissue Penetration of Antiretrovirals and Fluconazole. In: Conference on Retroviruses and Opportunistic Infections (CROI); Abtract number: 474; Available from: https://www.croiconference.org/sessions/differential-brainissue- penetration-antiretrovirals-and-fluconazole [Accessed 10 August 2018]. Boston, Massachusetts; 2018.

45.   Carroll A, Brew B. HIV-associated neurocognitive disorders: recent advances in pathogenesis, biomarkers, and treatment. F1000Research. 2017;6:312.

46.   Antinori A, Arendt G, Becker JT, Brew BJ, Byrd DA, Cherner M, et al. Updated research nosology for HIV-associated neurocognitive disorders. Neurology. 2007;69(18):1789–99.

47.   Csajka C, Marzolini C, Fattinger K, Décosterd L, Fellay J, Telenti A, et al. Population pharmacokinetics and effects of efavirenz in patients with human immunodeficiency virus infection. Clin Pharmacol Ther. 2003;73(1):20–30.

48.   Hagberg L, Cinque P, Gisslen M, Brew BJ, Spudich S, Bestetti A, et al. Cerebrospinal fluid neopterin: An informative biomarker of central nervous system immune activation in HIV-1 infection. AIDS Res Ther. 2010;7:1–12.

49.   McGuire JL, Gill AJ, Douglas SD, Kolson DL. Central and peripheral markers of neurodegeneration and monocyte activation in HIV-associated neurocognitive disorders. J Neurovirol. 2015;21(4):439–48.

50.   Sharma V, McNeill JH. To scale or not to scale: The principles of dose extrapolation. Br J Pharmacol. 2009;157(6):907–21.

51.   Zou P, Yu Y, Zheng N, Yang Y, Paholak HJ, Yu LX, et al. Applications of Human Pharmacokinetic Prediction in First-in-Human Dose Estimation. AAPS J. 2012;14(2):262–81.

52.   Ito K, Uchida Y, Ohtsuki S, Aizawa S, Kawakami H, Katsukura Y, et al. Quantitative membrane protein expression at the blood-brain barrier of adult and younger cynomolgus monkeys. J Pharm Sci. 2011;100(9):3939–50.

53.   Uchida Y, Ohtsuki S, Katsukura Y, Ikeda C, Suzuki T, Kamiie J, et al. Quantitative targeted absolute proteomics of human blood-brain barrier transporters and receptors. J Neurochem. 2011;117(2):333–45.

54.   Zhao R, Raub TJ, Sawada GA, Kasper SC, Bacon JA, Bridges AS, et al. Breast cancer resistance protein interacts with various compounds in vitro, but plays a minor role in substrate efflux at the blood-brain barrier. Drug Metab Dispos. 2009;37(6):1251–8.

55.   Ke A, Barter Z, Rowland-Yeo K, Almond L. Towards a Best Practice Approach in

PBPK Modeling: Case Example of Developing a Unified Efavirenz Model Accounting for Induction of CYPs 3A4 and 2B6. CPT Pharmacometrics Syst Pharmacol. 2016;5(7):367–76.

56. Shimizu T, Akimoto K, Yoshimura T, Niwa T, Kobayashi K, Tsunoo M, et al. Autoinduction of MKC-963 [(R)-1-(1-Cyclohexylethylamino)-4- Phenylphthalazine] Metabolism in Healthy Volunteers and its Retrospective Evaluation Using Primary Human Hepatocytes and CDNA-Expressed Enzymes. Drug Metab Dispos. 2006;34(6):950–4.

57. Iwasaki K, Kitsugi Y, Ikeda K, Yoshikawa T, Hosaka S, Uehara S, et al. In vivo individual variations in pharmacokinetics of efavirenz in cynomolgus monkeys genotyped for cytochrome P450 2C9. Biopharm Drug Dispos. 2016;37:379–83.

58. Xu C, Desta Z. In Vitro Analysis and Quantitative Prediction of Efavirenz Inhibition of Eight Cytochrome P450 (CYP) Enzymes: Major Effects on CYPs 2B6, 2C8, 2C9 and 2C19. Drug Metab Pharmacokinet. 2013;28(4):362–71.

CHAPTER-V: IMPACT AND FUTURE DIRECTIONS

In the past two decades, the widespread use of antiretroviral (ARV) therapy has considerably changed the landscape of the treatment of human immunodeficiency virus (HIV) infection. However, despite many important advances in HIV therapy, the treatment of comorbidities such as HIV-associated neurocognitive disorder (HAND) still remains challenging. While the incidence rate of HIV-associated dementia (HAD), the most debilitating form of neurocognitive impairment due to HIV, dropped from 80% to 30% in patients with a CD4+ T-cell count <200 cell/mm^3 after the introduction of highly active antiretroviral therapy (HAART)(1), the reduction in HAD incidence has come with the increased incidence and prevalence of milder forms of HAND. Currently, the less severe forms of HAND such as asymptomatic neurocognitive impairment (ANI) remain highly prevalent in the HIV-positive population (50-60%)(2). Though there are few studies that have measured the incidence of mild forms of HAND, one longitudinal study showed that the incidence of mild impairment in individuals on ARV treatment was also high at 20%(3).

Limited information on ARV drug distribution within the CNS and the exact mechanism for HAND pathogenesis creates obstacles for the treatment of HIV in the brain. The increased knowledge on ARV drug distribution in the cerebrospinal fluid (CSF) has led to some important advances in the field. In particular, the development of CNS penetration effectiveness (CPE) scores to qualify ARV penetration into the CNS was monumental in providing a simple approach to guide

the choice of ARV regimens with improved CNS efficacy(4,5). However, despite a strong association between higher CPE scores and reduced viral replication in the CSF(6), the relationship between CPE and the degree of neurocognitive impairment is still not clearly defined(7). This lack of relationship may be because the CPE scores are developed using CSF PK and the PK of ARVs are not measured in the brain tissue, which is the relevant target site for ARVs in the CNS. Since studies that measure ARV concentrations in the brain tissue are difficult to perform premortem in humans, the CSF drug concentration measurements are considered to be a surrogate of brain tissue concentrations. However, studies across multiple classes of drugs acting in the CNS have shown that this is often an incorrect assumption(8,9), particularly if the drug is a substrate for active drug transporters such as P-gp and BCRP. The scope of this dissertation project was to address these pertinent questions by providing a comprehensive overview of ARV drug concentrations in the brain tissue across three commonly used preclinical models, quantifying the gene and protein expression of relevant drug transporters in the brain tissue, and examining the relationship between model-predicted ARV PK in the human brain tissue and neurocognitive scores in HIV-positive patients. These results were synthesized with the use of several clinical pharmacology tools such as preclinical models, drug transporter measurements, and pharmacometric modeling and simulation.

5.1.   Clinical pharmacology tools can be used to address critical gaps in CNS drug development

As discussed in *Chapter I*, CNS drug development is particularly challenging due to difficulties in predicting the first-in-human dose required for drug efficacy. A comprehensive review of CNS targeting drugs revealed that the high attrition rate (50-70%)(10) in CNS drug

development was mainly driven by the poor translation of PK/PD from animal models to humans due to some critical knowledge gaps that are discussed in this section. The studies presented in this dissertation aimed to address these critical gaps in order to improve treatment strategies for HAND.

The first critical gap is the limited knowledge of CNS target site PK of ARVs in preclinical models of HIV infection. To address this gap, a comprehensive analysis of brain tissue ARV concentrations was performed across three commonly used preclinical models for HIV infection in *Chapter II*, and surrogate efficacy measures at the target site were evaluated in the nonhuman primate (NHP) model due to the close resemblance to humans. This work highlighted important differences in ARV PK between the CSF and brain tissue and is critical to the field to rethink the current method of evaluating the extent of ARV penetration and efficacy in the CNS. This work also serves as an important foundation for future studies to explore the efficacy and toxicity of ARVs within the brain tissue.

A second important critical gap is the limited understanding of differences among animal models that could lead to differences in CNS target site PK and poor clinical predictions. In *Chapter II*, we explored differences in ARV concentrations in the brain tissue due to sex and infection status. In *Chapter III,* we quantified transporter expression in the brain tissue across preclinical species to evaluate if these factors contributed to differences in ARV brain tissue penetration. While the data generated in *Chapter II* suggested that differences in sex and infection status are not crucial to inform ARV concentrations in the brain tissue, the transporter data generated in *Chapter III* suggested that transporter concentrations were variable among preclinical models. Therefore, using mechanistic models that capture these differences may be valuable to aid in the clinical prediction of ARV concentrations in the brain tissue.

Finally, the last critical gap addressed within this dissertation is the limited ability to predict ARV PK in human brain tissue using animal models. To address this gap, we developed a novel posterior Bayesian modeling approach in *Chapter IV* to predict clinical brain tissue PK using sparse data available from preclinical models (NHPs) and humans. This method was used to predict efavirenz (EFV) concentrations in the human brain tissue in a cohort of HIV-infected participants and closely captured observed human brain tissue concentration data available from an external dataset. Further, we used this method to perform target site exposure-response analyses using neurocognitive score data collected from the study participants. Such an approach could not only find utility in predicting the extent of CNS penetration of drugs that have already been approved (similar to the context presented here), but could also improve the predictions of human brain tissue PK earlier in the drug development pipeline for novel therapeutics (Phase II) to aid in dose optimization for further clinical studies.

While the work presented here could be used to address several key gaps highlighted in *Chapter I*, there are two important gaps that we were unable to address within the scope of this dissertation. First, clinical PK/PD translation could be greatly improved by the use of animal models that closely mimic the human form of the disease with relevant targets. However, the work presented here was performed in commonly used animal models of HIV infection and not in a specific "HAND" rodent or NHP model. The second caveat was that we were not able to explore the use of biomarkers to aid in PK/PD assessment, although such an approach holds considerable promise for improving CNS drug development(11). However, the development of animal models that mimic mild neurocognitive disorders due to HIV infection(12,13), and biomarker discovery for underlying HAND pathogenesis(14) are fields of study that are still evolving with our increased understanding of HAND etiology. Therefore, future work integrating the clinical pharmacology

tools discussed in this thesis along with refined animal models/biomarker tools could further improve clinical PK/PD assessments in the brain tissue. The following sections provide a detailed discussion of the knowledge gaps covered by this dissertation and a critical evaluation of future studies needed to further advance the field.

5.2. ARV brain tissue concentrations in preclinical models and surrogate measures of efficacy in the CNS

In *Chapter II*, we demonstrated that ARV brain tissue:plasma concentration ratios were markedly variable across the three different preclinical models for all drugs except raltegravir (RAL). Brain tissue concentrations of the ARVs showed a general increase in penetration rank order from hu-HSC-RAG mice<BLT mice<NHPs, while the plasma concentrations were largely overlapping for all drugs except RAL (rank order in concentrations in the plasma was also hu-HSC-RAG mice<BLT mice<NHPs). Therefore, the increase in brain tissue concentrations of RAL across the preclinical models was driven by a proportional increase in plasma concentrations. However, for the other ARVs in our analysis, alternative factors appeared to be driving the inter-species differences in brain tissue concentrations. The high variability in ARV concentrations in the brain tissue may be a result of drug-drug interactions and drug-transporter interactions. For example, in the hu-HSC-RAG mice, tenofovir (TFV) and emtricitabine (FTC) were administered along with raltegravir (RAL) and maraviroc (MVC), while in the BLT mice and the NHPs, these drugs were administered along with EFV or atazanavir (ATZ), two ARVs that inhibit P-gp and BCRP efflux transporters at the blood-brain-barrier (BBB)(15,16). While we had a limited number of BLT mice and NHPs to dose ARVs individually in these models as dosed in the hu-HSC-RAG mice, the potential for drug-drug interactions are clinically unavoidable since HIV regimens are

made up of multiple ARVs. For this reason, the brain tissue concentration data from our BLT mice and NHPs may more closely approximate what would be seen in the human brain tissue, in the setting of combination ARV therapy.

Brain tissue concentrations in the nonhuman primates (NHPs) were >6-fold higher than the cerebrospinal fluid (CSF) concentrations and with the exception of efavirenz (EFV), the CSF concentrations of ARVs were not an appropriate surrogate for the brain tissue concentrations. These data indicate that CSF concentrations of ARVs alone may not be a good predictor of the extent of drug penetration into the CNS, and this has important implications for drug efficacy. For example, FTC concentrations in the brain tissue (25 ng/g) showed a modest 6-fold increase relative to the CSF concentrations (6 ng/mL). However, these higher brain tissue concentrations were still below the IC_{90} of FTC in all 17 NHPs(17). The concentrations of the active metabolite of FTC, emtricitabine triphosphate (FTC-tp) were also below the limit of quantification in all of our brain tissue samples. These low concentrations of FTC achieved in the brain tissue may result in reduced FTC efficacy in the CNS. In support of this hypothesis, several studies of HIV-positive patients on ARV treatment who had CSF escape (detectable HIV viral replication in the CSF in the absence of viral replication in the plasma) showed that a common HIV resistance mutation identified in these patients was the M148V mutation(18,19), which reduces the efficacy of FTC. The onset of such resistance mutations is usually linked to limited ARV coverage, and the data from our animal models can be used to make this connection.

In order to examine our PK data in the context of ARV efficacy in the brain tissue, we presented two measures of surrogate ARV efficacy: the 90% inhibitory quotient (IQ_{90}) values that were derived from the protein-unbound ARV LC-MS/MS concentrations of the brain tissue homogenate, and the colocalization of EFV spatial distribution and HIV target-cells distribution

(the microglia and CD4+ T-cells) in brain tissue slices. We were limited to surrogate measures of efficacy due to the considerations of our NHP animal model. All NHPs were infected with the RT-SHIV mac239 strain of virus that shows limited distribution into the brain tissue(20,21). In previous studies performed with these models, RT-SHIV infected animals that were left untreated for an entire year of infection still showed very low viral RNA load (~5 copies/million cells) in the brain tissue collected at necropsy(20). In our study, animals were treated with ARVs for only ten days to maximize the ability to detect virus in all the tissues. However, the viral load was undetectable in most of the samples in the CSF, and ranged from 9-70 copies/million cells in the brain tissue. The copy number in the brain tissue was 10- to 1000-fold lower than in other tissue HIV reservoirs (such as the lymph nodes and spleen). Therefore, the IQ_{90} values were calculated to interpret the PK data and provide useful hypotheses for interpretation in future studies. In order to compute the IQ_{90} values, we performed rapid equilibrium dialysis (RED) to measure the protein-free concentrations of ARVs in the brain tissue, and are among the first to report these values for ARV. Our IQ_{90} data showed that EFV was the only ARV that would achieve concentrations greater than the IC_{90} in the brain tissue(17,22–26), despite the fact that EFV was also the most highly protein-bound ARV in the tissue. Given the high degree of accumulation that we saw for EFV in the brain tissue, these results were not surprising.

An interesting result was the discrepancy between our two surrogate measures of EFV efficacy in the brain tissue: i.e. the IQ_{90} results and the MSI colocalization results. Despite EFV achieving $IQ_{90}>1$ in all of the animals, and brain tissue accumulation that was 1000-fold higher than the CSF, only about 3% of the HIV target cell area across the brain tissue section colocalized with EFV at a concentration above the HIV IC_{50}. This discrepancy can be explained by the heterogenous distribution of EFV within the brain tissue. The white matter concentrations of EFV

were 1.1- to 3-fold higher than in the gray matter where we noted the greater density of the microglia and the CD4+ T-cells. Therefore, despite the tissue homogenate data indicating that there would be adequate EFV exposure in the brain tissue, the MSI results showed that the spatial coverage of EFV over the relevant target cells may be insufficient to prevent viral replication. In fact, these results may help explain the instances of CSF escape that has been observed in patients treated with EFV, despite the high drug concentrations achieved in the CNS(27). Taken together, these data highlight the importance of elucidating brain tissue PK of ARVs and emphasizes the advantage of MSI approaches over conventional LC-MS/MS to spatially quantify drug concentrations in the brain tissue. By using concomitantly sliced tissue for other investigations such as immunohistochemistry (IHC) staining for distinct cell populations (e.g. macrophages, microglia), it is also possible to correlate drug distribution to other variables of interest to provide more information about the drug pharmacology at the target site.

There are, however, important limitations with our approach. Reconsideration of simian model of HIV infection would be very important for future studies. The choice of a model with more pronounced CNS involvement such as SIVmac251(28) virus could provide more insight on the persistence of HIV in the CNS despite therapy and allow us to perform in-situ hybridization or RNA-scope techniques to visualize drug disposition by MSI in relation to the localization of HIV RNA within the brain tissue. While tissue collection is invasive regardless of the sampling location, sampling brain tissue from living patients is virtually impossible unless the patient is undergoing brain surgery. This necessitates the translation of the LC-MS/MS or MSI results from preclinical models to humans. While our results suggest this may be a reasonable approach for most ARVs at the doses chosen in this study due to the similarity in plasma concentrations, the high variability in plasma concentrations across the preclinical models is an important caveat for

consideration. ARV concentrations in the brain tissue could also be quantified from brain tissue samples that are collected post-mortem from individuals with known adherence to therapy prior to death. Though such resources are limited, these data could add valuable information on the appropriateness of preclinical to clinical PK approximations in the brain tissue. While other techniques such as microdialysis have been employed to directly sample the CSF for drug concentrations from living patients, CSF concentrations may not necessarily be a good measure of the target site concentration of ARVs, as we have shown in this work. Finally, while we were able to measure drug concentrations over the total area of HIV target cells, IHC images had to be down-sampled (image quality had to be imported at a lower resolution than the original image generated) because of the colocalization analysis with the lower resolution MSI image. Therefore, we were not able to spatially quantify the intracellular concentrations of EFV, although this holds promise as an exciting avenue for future research in the field.

5.3. Inter-species differences in gene and protein expression of drug transporters and utility in predicting penetration of ARVs into the brain tissue

In Chapter III, we conducted an evaluation of drug transporters in the brain tissue across the preclinical models that were previously evaluated in Chapter II. Across all three animal models, we identified significant differences in the gene expression of all influx and efflux transporters except Slc29a1/SLC29A1. Although we were able to quantify the gene expression of all transporters of interest in the brain tissue, there were fewer transporters for which we could quantify the protein concentrations. Only BCRP and P-gp protein concentrations could be quantified in the majority of our tissue samples, and this suggests that these efflux transporters are

the major constituent of the secondary transporter barrier present on cells in the brain parenchyma(29,30).

One surprising result was that our HIV- and RT-SHIV-infected animals showed a similar profile in transporter expression (gene expression as well as protein concentration and localization) relative to the uninfected animals. This would indicate that ARV disposition should not significantly change with infection status, and uninfected preclinical models can be used as a surrogate for drug disposition studies within the CSF and brain tissue. While our results indicated that there was a trend for increased efflux transporter protein concentration in the infected animals relative to uninfected animals, previous analyses have shown that inflammation generally decreases the gene and protein expression of P-gp and BCRP, although P-gp and BCRP expression at the BBB appears to be upregulated with infection(31,32). Specific to HIV, the Tat protein found on the surface of HIV, has been shown to upregulate both the gene and protein expression of MRP1(33). In humans acutely infected with HIV, the ongoing cascade of inflammatory reactions as soon as HIV enters the CNS can lead to changes in the permeability of the BBB(34), though normal permeability is restored after initiation of therapy for chronic infections(34,35,13). It is yet to be explored how these changes during acute infection would alter ARV disposition, either through alterations in the extent of drug diffusion through the membrane or through an altered profile of transporter expression/function. Alterations in permeability through the BBB may also be an underlying cause for persistent neurocognitive impairment(36) despite therapy, and is contrary to the idea that ARVs with higher CNS penetration would result in a lower degree of neurocognitive impairment.

Neither the protein concentration of BCRP nor P-gp showed correlation with ARV brain tissue:plasma concentration ratios, indicating that drug transporter protein concentrations had

limited utility in predicting ARV penetration into the brain tissue. Although we did not measure the concentration of drug transporters at the blood brain barrier (BBB) in this analysis, we compared the results from previous QTAP analyses performed in the BBB from mice and cynomolgus monkeys to our brain tissue data and noted an imperfect correlation between transporter protein concentrations measured at the BBB and the brain tissue(37,38). P-gp transporter protein in the brain tissue was two- to four-fold lower than the BBB P-gp transporter protein concentrations, while BCRP transporter protein was >7-fold lower in the brain tissue relative to previous BBB analyses. These results may be because P-gp is expressed on the surface of various cell types such as neurons, microglia, and astrocytes in the brain tissue(39,40) and BCRP is only expressed on the microglia cells in the brain parenchyma(39). The consequence of these findings is that while the brain tissue drug transporters provide valuable information on inter-species differences in transporter expression patterns and represent a secondary barrier to drug penetration into the brain cells (component of the neurovascular unit)(29), they are not a correlate for the BBB transporter measurements. Finally, our drug transporter IHC and QTAP results showed good agreement with each other. Both techniques indicated that the brain tissue of NHPs contained a high absolute protein concentration (as measured by QTAP) and fractional area of coverage (as measured by IHC) of the efflux transporter BCRP followed by P-gp, while the expression of the influx transporter OATP1A2 showed minimal expression within the brain. However, the gene expression results showed considerably less agreement with the measures of protein concentration. This observation is in line with the growing body of literature(41–43) that indicates that the downstream measurements of protein expression are more reliable indicators for drug transporter expression.

An important limitation of this investigation was the lack of measures of brain transporter function across the preclinical species. It is well known that transporter function is not always conserved across species. For example, the ratio of maximal velocity (Vmax) to Michalis constant (Km) for the transport of diltiazem by P-gp is similar in humans and monkeys but is 5.6-fold higher than canine P-gp.(44) Though beyond the scope of this project, future work should determine the extent of functional differences in drug-transporters across species for ARV substrates by the use of in-vitro assays(45). If there are pronounced differences in transporter function across species, these changes may also contribute to inter-species differences in the penetration of ARVs into the brain tissue.

5.4. Using sparse data from preclinical models to predict clinical brain tissue concentrations of ARVs and relationship to HAND

In Chapter IV, a PK model was developed to predict the disposition of EFV in the plasma, CSF, and brain tissue of HIV-positive participants in the THINC study. Since we did not have PK measurements for the brain tissue from the THINC study participants, we employed allometric scaling of the CSF and brain tissue volume from a PK model developed in rhesus macaques. We developed a clinical model for EFV distribution in the plasma, CSF and brain tissue by combining our NHP structural model with sparse plasma and CSF data obtained from the THINC study by the iterative two-stage (IT2S) estimation method. The initial estimates for the clinical PK model were from a previously published EFV population PK analysis(46). As discussed in the previous chapter, allometric scaling and preclinical to clinical translation is not always a reliable approach to predict PK profiles of drugs in humans, particularly when the drug disposition is non-linear, mediated by drug transporters or when the drug is highly protein bound, as was the case with EFV.

Regardless, similarities in the protein binding of EFV and concentration of BCRP transporter at the BBB (37,38,47) across macaques and humans gives us more confidence with this translational approach. Since we had sparse PK data in the preclinical species as well as humans, this precluded the use of other techniques such as physiologically-based pharmacokinetic (PBPK) models that rely on more robust data to better characterize drug uptake into tissues.

The modeling methodology that was employed for this analysis showcased a novel approach for the handling of sparse data. The data used to develop the PK model in the NHPs and the HIV-positive participants came from two unique datasets that were originally intended for purposes other than PK modeling. Accordingly, the longitudinal information from these studies was very minimal. Since most of our study participants contributed only one EFV PK concentration in the plasma and CSF at random sampling times (not pre-specified to correspond to certain timepoints along the dosing curve), traditional 'population' PK modeling approaches such as a naïve-pooled data (NPD) analysis could not be utilized to fit the data. Instead, we used a Bayesian posterior approach to fit the data through several estimation steps by the iterative two-stage estimation (IT2S)(48). By this approach, our parameter estimates were updated and refined based on the posterior of the individual fits in the model. Importantly, the estimates that we reported for the final model are the geometric mean of the parameters returned for each individual, and not the "population" estimate, since our data were limited to draw these inferences. Since this analysis was Bayesian in nature, it was imperative that we had robust initial estimates for both the NHP model and the clinical model from the literature to characterize our population. Because the literature data on EFV distribution in the CSF and brain tissue were also quite limited, we had to ensure that our model perfectly fit our plasma concentrations so that the plasma EFV PK profile could serve as a forcing function to adequately predict the EFV time course in the CSF and brain

tissue. Obtaining a perfect plasma fit for the EFV model required adding in more complexity to the model, such as using three transit compartments to capture the absorption phase in NHPs, and describing the decrease in EFV trough concentrations from day one to day four with the use of a semi-empirical clearance model. What is important to note is that these complexities did not affect the excellent precision of our individual PK parameter estimates, and this was our most important consideration for this approach.

A third unique dataset that was available to us for the development of the PK model were EFV human brain tissue concentration data from the National Neuro-AIDS Tissue Consortium (NNTC), which is a repository established for the collection of CSF and postmortem brain tissue samples from HIV-positive participants. While there have been studies that report the use of this repository to answer various questions on HIV involvement in the CNS(49), our study is the first to our knowledge to obtain brain tissue samples in order to quantify the concentrations of ARVs in these samples. The brain tissue concentration data that we measured from three HIV-positive participants served as an important external validation dataset for our final clinical model predictions in the brain tissue. Our final PK model adequately captured the brain tissue concentrations from all three samples and provided important evidence that our PK predictions were biologically plausible.

For our pharmacokinetic/pharmacodynamic (PK/PD) analysis, the model-predicted exposure of EFV in human brain tissue did not show any correlation with the neurocognitive test scores in our study cohort. Since our study looked at a cross-sectional cohort, neurocognitive outcome was only measured at a single time-point, at least one-year after the initiation of drug therapy. Therefore, changes in neurocognitive outcome over time for patients who were on EFV were not captured in our dataset, and this may have been a better PD measure to explore against

our model predictions. The lack of relationship between PK and neurocognitive outcome may also reflect the complex multi-factorial etiology of HAND, as shown previously in larger studies(50,51). In this regard, biomarker-based endpoints such as measurement of neopterin levels in the plasma or CSF may be more reliable measures of disease progression and underlying mechanisms of disease such as a low-level of inflammation(36,52). Future studies should evaluate their utility as a diagnostic marker for HAND severity and examine their relationship to ARV PK at the target site.

5.5. Emerging advances to measure antiretroviral concentrations in the brain tissue and enhance the treatment paradigm of HIV

Important mechanistic studies performed in animal models have helped to advance our understanding of HIV pathogenesis in the brain. For a long time the consensus in the field was that HIV infection in the CNS was initiated by the macrophage/monocyte trafficking into the brain through the BBB ("Trojan-horse mechanism")(53), followed by interruption of the BBB and entry of activated CD4+ T-cells into the CNS. However, the recent discovery of lymph vessels in the meninges(54) shows that an alternate mechanism for the infiltration of HIV-infected CD4+ T-cells into the brain tissue is through the meningeal lymphatic system. Recent analyses using T-cell only BLT mice(55), as well as NHPs infected with a strain of SHIV that more closely approximates the natural course of HIV infection of the brain in humans(13), have been used to confirm that HIV infection of the brain can be maintained with CD4+ T-cells, and that initial HIV-infection in the brain may be mediated by a pronounced CD4+ T-cell response, followed by a sustained and enhanced response of the activated monocyte/macrophage cell population. This discovery provides an important pharmacological consideration. If ARV infection in the CNS proceeds in

such a biphasic manner, it would be important to categorize the differential efficacy of ARVs in these two distinct cell populations of the CD4+ T-cells and the monocytes/macrophages in the CNS. In the acutely infected stage, drugs of the nucleoside reverse transcriptase inhibitor (NRTI) ARV drug class show higher efficacy in the macrophages compared to CD4+ T-cells(56). While the exact mechanism for this is unknown, the hypothesis is that lower cellular deoxyribonucleoside triphosphates (dNTP) pools in the macrophages relative to the CD4+ T-cells results in decreased competition for cellular kinases, and a greater ability of the NRTIs to get phosphorylated to active metabolites and show antiviral activity(56). Similarly, protease inhibitors (PIs) also show greater antiviral activity in macrophages compared to the CD4+ T-cells(56). The consequence of these data are that ARVs may need to have higher intra-cellular concentrations in the CD4+ T-cells relative to the macrophages in order to prevent active viral replication in these cell types. Although our MSI technology currently does not have the sensitivity to address these types of questions, refinement of this technology may hold promise for studies that research this hypothesis further. As mentioned in Section 5.2, as we further develop our MSI tools, this technology may also be used to determine ARV concentrations in the various cells of the brain. In order to get to this stage, the key concerns that are to be addressed include improvement of the sensitivity and resolution of the technology. Some approaches to improve sensitivity include increasing the ionization ability or improving the spot-to-spot resolution of MSI. Improved resolution may be achieved by decreasing the spot-size of the laser pulse for tissue ablation in the MSI workflow, so as to allow for the quantification of intracellular drug concentrations. Though we have some distance to go before we can begin to implement these improvements, it is clear that these tools could play a major role in elucidating intra-cellular pharmacology and activity of ARVs within tissue reservoirs.

As discussed in Chapter IV, another novel tool that holds promise in improving our understanding of ARV concentrations within the brain tissue (and potentially cells) is modeling and simulation. The analysis described in this thesis utilized a novel framework of Bayesian analyses and preclinical translation in order to predict human brain tissue PK, even with sparse data. Another modeling and simulation tool that can be applied in a wide variety of analyses is PBPK modeling, that is recently gaining regulatory attention. While the development of PBPK models require rich data in order to have predictive utility, the detail on physiology and enzyme and transporter mechanisms that can be captured with PBPK models make them an attractive option for predicting changes in PK due to disease or other physiological alterations. These models may also be used to capture complex transport mechanisms throughout the CNS such as active drug efflux by drug transporters. In fact, a recent, innovative modeling approach by Yamamoto and colleagues(57) demonstrated a method to input inter-species differences in transporter expression into PBPK models in order to scale the preclinical to clinical CNS distribution of a diverse set of drugs. The data that we have generated in Chapter III on the inter-species differences in drug transporter protein concentrations in the brain tissue could be an informative and valuable dataset to be used in this manner. The development of a similar PBPK framework could help to mechanistically predict ARV penetration into the brain and characterize underlying factors responsible for inter-species differences in brain tissue distribution of ARVs.

While there may be several novel tools to explore ARV PK in the brain tissue, PK/PD analyses in this matrix are more challenging. For example, our PK/PD analysis in Chapter IV was not able to detect any relationship between model-predicted ARV PK in the brain tissue and neurocognitive scores, and this is reflective of the underlying complex etiology of this disorder. HIV enters the brain tissue early in the course of infection(58) and it is possible that inflammatory

processes lead to unresolved neurological damage that is not reversible even on initiation of therapy(5). Novel biomarker analyses might help quantify underlying processes such as immunological involvement in the CNS. Various biomarkers such as neurofilament light chain (NFL), neopterin, and cytokines have been measured in the plasma and CSF in relation to severity of HAND. While there does not as yet exist an ideal biomarker that is associated with HAND progression that can also be easily measured in the plasma, further development in this area can be conducive to the personalized medicine approach to treat HAND. For example, some patients with HAND may benefit from the addition of neuroprotective therapies such as CCR5 antagonists (intranasal peptide T) or N-methyl-D-aspartate (NMDA) antagonists (memantine)(59). In order for such interventions to be effective, it becomes important to identify appropriate patient populations early in the course of treatment who have underlying neurocognitive disorders and would benefit from the addition of these therapies. Also, this evaluation should not be limited to a one-time assessment as the HIV-positive population will continue to age and become susceptible to age-related neurocognitive decline. Considering all the above, routine screening for HAND in the clinic and measuring biomarker levels in the plasma is a potential first step towards optimizing patient care and drug therapy towards the treatment of HAND.

5.6.   Implications for HIV cure strategies within the CNS

While the framework of this dissertation explored ARV penetration into the brain in relation to HIV persistence within the brain tissue and the treatment of HAND, this work also has implications for the development of cure strategies for HIV. Latency in the CNS has historically been a controversial topic, but recent translational breakthroughs such as the development of a macrophage-only humanized mouse model(60), and optimization of a macrophage-specific

quantitative viral outgrowth assay (QVOA)(61) to determine the size of the latent macrophage reservoir have confirmed that latent HIV reservoirs can be established in a dominant macrophage population as seen in the CNS. While the exact mechanisms behind establishment of such latent reservoirs in the CNS are unclear, they are established very early in infection and are unaffected by ARV therapy(62). Instead, novel strategies such as "shock and kill"(63) are being explored wherein the quiescent latently infected cells are first activated to release virions, followed by treatment with a high dose of ARVs to kill the virus and prevent a new round of HIV replication. While there are significant challenges associated with such therapies in general(64), achieving such a functional cure in the CNS is specifically hindered by a few considerations. The first consideration is the limited entry of the latency reversing agents (LRAs) into the CNS. LRAs(65) are derived from classes of oncology drugs such as histone deacetylase inhibitors and protein kinase C agonists that show the pharmacologic effect of reversing HIV latency, which leads to mass release of virus from quiescent cells. However, not all LRAs may be useful for the reversal of latency in CNS cell types at therapeutic concentrations(66). The use of agents that have a good ability to cross the BBB such as bryostatin-1(65) should be explored further for future CNS cure strategies. In this regard, the MSI technique we have utilized within this dissertation could also be used in preclinical models to study the spatial distribution of such LRAs in the brain tissue. This has been demonstrated previously by our group for other HIV reservoirs such as the lymph node tissue and the gut-associated lymphoid tissue(67,68).

Another potential obstacle for the reversal of latency in the CNS is the limited exposure of ARVs in the brain tissue. If there is inadequate ARV drug exposure within the CNS, then the virions that are released after initial treatment with the LRAs could infect more cells and even increase the size of the latent reservoir(69,70). As discussed in *Chapter II*, we showed that both

EFV and tenofovir (TFV) heterogeneously distributed within the brain tissue by MALDESI and poorly colocalized with the microglia and CD4+ T-cells. The poor CNS coverage of existing therapies indicates that newer agents with enhanced CNS penetration may need to be developed in order to further cure efforts in the CNS. Importantly, since the reactivation of the quiescent reservoir could lead to the stimulation of neurotoxic proteins within the CNS, therapies would need to be developed that are capable of targeting the cellular transcription factor NF-kβ(71) and the viral transactivator Tat(72) since these targets play a central role in neurotoxicity and encephalitis(73). The development of novel targeted immunotherapies for HIV in the brain such as dendritic cell vaccines and T-cell backpacks(74), or agents that specifically target neurotoxic HIV proteins(70) are all promising avenues of future research.

5.7.   Conclusion

This dissertation describes the use of clinical pharmacology tools to aid in our understanding of ARV penetration into the brain tissue. We measured the total concentration, protein binding, and spatial localization of six ARVs within the brain tissue across three commonly used preclinical models, demonstrated that PK measurements made in the CSF do not serve as a surrogate for the brain tissue, and derived surrogate measures of efficacy for ARVs in the brain tissue that may have important implications for the efficacy and toxicity of ARVs in the CNS. We demonstrated that HIV infection did not alter the gene or protein expression of transporters, and showed that transporter protein concentrations measured at the brain tissue showed limited utility in predicting ARV brain tissue penetration. Finally, we developed a PK model to describe the distribution of EFV in the plasma, CSF, and brain tissue of rhesus macaques, and used this model to predict the exposure of EFV in the brain tissue of HIV-positive participants. The model was

adequately able to capture observed plasma and CSF concentrations from our study cohort, and was also able to predict brain tissue concentrations measured from the brain tissue samples from three HIV-positive individuals, post-necropsy, obtained from the NNTC repository. However, our analysis showed that there was no relationship between model-predicted brain tissue exposure and neurocognitive outcome in our cohort, and this may be due to the limited range of EFV exposure in the brain tissue, and limited information on the longitudinal development of HAND in our cohort. These data provide a framework to better inform the neuro-HIV field and can be applied to the study of therapies and personalized medicine approaches for the treatment and cure of HIV in the brain.

5.8. REFERENCES

1. Miller EN, Becker JT, Cohen B, Mcarthur JC. HIV-associated neurologic disease incidence changes: Multicenter AIDS Cohort Study, 1990–1998. Neurology. 2001;56(2):257–60.

2. Marra CM. HIV-associated neurocognitive disorders and central nervous system drug penetration: what next? Antivir Ther. 2015;20(4):365–7.

3. Robertson KR, Smurzynski M, Parsons TD, Wu K, Bosch RJ, Wu J, et al. The prevalence and incidence of neurocognitive impairment in the HAART era. AIDS. 2007;21(14):1915–21.

4. Letendre S. Validation of the CNS Penetration-Effectiveness Rank for Quantifying Antiretroviral Penetration Into the Central Nervous System. Arch Neurol. 2008;65(1):65–70.

5. Letendre S. Central Nervous System Complications in HIV Disease : HIV-Associated Neurocognitive Disorder. Top Antivir Med. 2011;19(4):137–42.

6. Marra CM, Zhao Y, Clifford DB, Letendre S, Evans S, Henry K, et al. Impact of combination antiretroviral therapy on cerebrospinal fluid HIV RNA and neurocognitive performance. AIDS. 2009;23(11):1359–66.

7. Nightingale S, Winsto A, Letendre S, Michael BD, Mcarthur JC, Khoo S, et al. Controversies in HIV-associated neurocognitive disorders. Lancet Neurol. 2015;13(11):1139–51.

8. Liu X, Smith BJ, Chen C, Callegari E, Becker SL, Chen X, et al. Evaluation of cerebrospinal fluid concentration and plasma free concentration as a surrogate measurement for brain free concentration. Drug Metab Dispos. 2006;34(9):1443–7.

9. Rambeck B, Jürgens UH, May TW, Wolfgang Pannek H, Behne F, Ebner A, et al. Comparison of brain extracellular fluid, brain tissue, cerebrospinal fluid, and serum concentrations of antiepileptic drugs measured intraoperatively in patients with intractable epilepsy. Epilepsia. 2006;47(4):681–94.

10. Goetghebeur PJD, Swartz JE. True alignment of preclinical and clinical research to enhance success in CNS drug development : a review of the current evidence. J Psychopharmacol. 2016;586(July 2016):1–9.

11. Safavi M, Sabourian R, Abdollahi M. The development of biomarkers to reduce attrition rate in drug discovery focused on oncology and central nervous system. Expert Opin Drug Discov. 2016;11(10):939–56.

12. Jaeger LB, Nath A. Modeling HIV-associated neurocognitive disorders in mice: new approaches in the changing face of HIV neuropathogenesis. Dis Model Mech. 2012;5(May 2012):313–22.

13. Hsu DC, Sunyakumthorn P, Wegner M, Schuetz A, Silsorn D, Estes JD, et al. Central Nervous System Inflammation and Infection During Early, Non-Accelerated Simian-

Human Immunodeficiency Virus Infection in Rhesus Macaques. J Virol. 2018;92(1):1–14.

14.   Carroll A, Brew B. HIV-associated neurocognitive disorders: recent advances in pathogenesis, biomarkers, and treatment. F1000Research. 2017;6:312.

15.   Kis O, Robillard K, Chan GNY, Bendayan R. The complexities of antiretroviral drug-drug interactions: role of ABC and SLC transporters. Trends Pharmacol Sci. 2010 Jan;31(1):22–35.

16.   Peroni RN, Di Gennaro SS, Hocht C, Chiappetta D a, Rubio MC, Sosnik A, et al. Efavirenz is a substrate and in turn modulates the expression of the efflux transporter ABCG2/BCRP in the gastrointestinal tract of the rat. Biochem Pharmacol. 2011;82(9):1227–33.

17.   Mathez D, Schinazi RF, Liotta DC, Leibowitch J. Infectious amplification of wild-type human immunodeficiency virus from patients' lymphocytes and modulation by reverse transcriptase inhibitors in vitro. Antimicrob Agents Chemother. 1993;37(10):2206–11.

18.   Mukerji SS, Misra V, Lorenz DR, Uno H, Morgello S, Franklin D, et al. Impact of Antiretroviral Regimens on CSF Viral Escape in a Prospective Multicohort Study of ART-Experienced HIV-1 Infected Adults in the United States. Clin Infect Dis [Internet]. 2018; Available from: https://doi.org/10.1093/cid/ciy267 [Epub ahead of print] [Accessed 1 September 2018]

19.   Dravid AN, Natrajan K, Kulkarni MM, Saraf CK, Mahejan US, Kore SD, et al. Discordant CSF/plasma HIV-1 RNA in individuals on virologically suppressive antiretroviral therapy in Western India. Med (United States). 2018;97(8):1–8.

20.   North TW, Higgins J, Deere JD, Hayes TL, Villalobos A, Adamson L, et al. Viral sanctuaries during highly active antiretroviral therapy in a nonhuman primate model for AIDS. J Virol. 2010 Mar;84(6):2913–22.

21.   Matsuda K, Dang Q, Brown CR, Keele BF, Wu F, Ourmanov I, et al. Characterization of Simian Immunodeficiency Virus (SIV) That Induces SIV Encephalitis in Rhesus Macaques with High Frequency: Role of TRIM5 and Major Histocompatibility Complex Genotypes and Early Entry to the Brain. J Virol [Internet]. 2014;88(22):13201–11. Available from: http://jvi.asm.org/cgi/doi/10.1128/JVI.01996-14. Last accessed August 15th, 2018

22.   Song I, Chen S, Piscitelli S. Meta analysis of pharmacokinetic-pharmacodynamic relationship of integrase inhibitors. In: 11th International Workshop on Clinical Pharmacology of HIV Therapy [Internet]. Sorrento, Italy; 2010. Available from: http://regist2.virology-education.com/11th/docs/30_Song.pdf. Last accessed 1 October, 2018

23.   Herrera C, Cranage M, McGowan I, Anton P, Shattock RJ. Reverse transcriptase inhibitors as potential colorectal microbicides. Antimicrob Agents Chemother. 2009;53(5):1797–807.

24.   Ramanathan S, Custodio JM, Wei X, Wang H, Fordyce M, Ling KHJ, et al. Pharmacokinetics of Co-Formulated Elvitegravir / Cobicistat / Emtricitabine / Tenofov ir

Disoproxil Fumarate After Switch From Efavirenz / Emtricitabine / Tenofovir Disoproxil Fumarate in Healthy Subjects. JAIDS J Acquir Immune Defic Syndr. 2016;90(3):281–8.

25. Winston A, Bloch M, Carr A, Amin J, Mallon PWG, Ray J, et al. Atazanavir trough plasma concentration monitoring in a cohort of HIV-1-positive individuals receiving highly active antiretroviral therapy. J Antimicrob Chemother. 2005;56(2):380–7.

26. Dorr P, Westby M, Dobbs S, Griffin P, Irvine B, Macartney M, et al. Maraviroc (UK-427,857), a Potent, Orally Bioavailable, and Selective Small-Molecule Inhibitor of Chemokine Receptor CCR5 with Broad-Spectrum Anti-Human Immunodeficiency Virus Type 1 Activity. Antimicrob Agents Chemother. 2005;49(11):4721–32.

27. Edén A, Fuchs D, Hagberg L, Nilsson S, Spudich S, Svennerholm B, et al. HIV-1 viral escape in cerebrospinal fluid of subjects on suppressive antiretroviral treatment. J Infect Dis. 2010;202(12):1819–25.

28. Yen PJ, Mefford ME, Hoxie JA, Williams KC, Desrosiers RC, Gabuzda D. Identification and characterization of a macrophage-tropic SIV envelope glycoprotein variant in blood from early infection in SIVmac251-infected macaques. Virology. 2014;458–459(1):53–68.

29. Alam C, Whyte-Allman S-K, Omeragic A, Bendayan R. Role and modulation of drug transporters in HIV-1 therapy. Adv Drug Deliv Rev. 2016;103:121–43.

30. Wang Q, Zuo Z. Impact of transporters and enzymes from blood–cerebrospinal fluid barrier and brain parenchyma on CNS drug uptake. Expert Opin Drug Metab Toxicol. 2018;14(9):961–72.

31. Cressman AM, Petrovic V, Piquette-Miller M. Inflammation-mediated changes in drug transporter expression/activity: implications for therapeutic drug response. Expert Rev Clin Pharmacol. 2012;5(1):69–89.

32. Evers R, Piquette-Miller M, Polli JW, Russel FGM, Sprowl JA, Tohyama K, et al. Disease-Associated Changes in Drug Transporters May Impact the Pharmacokinetics and/or Toxicity of Drugs: A White Paper From the International Transporter Consortium. Clin Pharmacol Ther. 2018;104(5):900–15.

33. Hayashi K, Pu H, András IE, Eum SY, Yamauchi A, Hennig B, et al. HIV-TAT protein upregulates expression of multidrug resistance protein 1 in the blood–brain barrier. J Cereb Blood Flow Metab. 2005;26(8):1052–65.

34. Stephens EB, Singh DK, Kohler ME, Jackson M, Pacyniak E, Berman NEJ. The primary phase of infection by pathogenic simian-human immunodeficiency virus results in disruption of the blood-brain barrier. AIDS Res Hum Retroviruses. 2003;19(10):837–46.

35. Rahimy E, Li FY, Hagberg L, Fuchs D, Robertson K, Meyerhoff DJ, et al. Blood-brain barrier disruption is initiated during primary HIV infection and not rapidly altered by antiretroviral therapy. J Infect Dis. 2017;215(7):1132–40.

36. Anesten B, Yilmaz A, Hagberg L, Zetterberg H, Nilsson S, Brew BJ, et al. Blood-brain barrier integrity, intrathecal immunoactivation, and neuronal injury in HIV. Neurol Neuroimmunol NeuroInflammation. 2016;3(6):300–21.

37.   Uchida Y, Ohtsuki S, Katsukura Y, Ikeda C, Suzuki T, Kamiie J, et al. Quantitative targeted absolute proteomics of human blood-brain barrier transporters and receptors. J Neurochem. 2011;117(2):333–45.

38.   Ito K, Uchida Y, Ohtsuki S, Aizawa S, Kawakami H, Katsukura Y, et al. Quantitative membrane protein expression at the blood-brain barrier of adult and younger cynomolgus monkeys. J Pharm Sci. 2011;100(9):3939–50.

39.   Sanchez-Covarrubias L, Slosky L, Thompson B, Davis T, Ronaldson P. Transporters at CNS Barrier Sites: Obstacles or Opportunities for Drug Delivery? Curr Pharm Des. 2014;20(10):1422–49.

40.   Ashraf T, Robillard K, Chan GNY, Bendayan R. Role of CNS transporters in the pharmacotherapy of HIV-1 associated neurological disorders. Curr Pharm Des. 2014;20(10):1543–63.

41.   Thompson CG, Fallon JK, Mathews M, Charlins P, Remling-Mulder L, Kovarova M, et al. Multimodal analysis of drug transporter expression in gastrointestinal tissue. AIDS. 2017;31(12):1669–78.

42.   Ohtsuki S, Schaefer O, Kawakami H, Inoue T, Liehner S, Saito A, et al. Simultaneous absolute protein quantification of transporters, cytochromes P450, and UDP-glucuronosyltransferases as a novel approach for the characterization of individual human liver: comparison with mRNA levels and activities. Drug Metab Dispos. 2012 Jan;40(1):83–92.

43.   Ahlin G, Hilgendorf C, Al-Khalili Szigyarto C, Uhlen M, Karlsson JE, Artursson P. Endogenous gene and protein expression of drug transporting proteins in cell lines routinely used in drug discovery programs. Drug Metab Dispos. 2009;37(12):2275–83.

44.   Katoh M, Suzuyama N, Takeuchi T, Yoshitomi S, Asahi S, Yokoi T. Kinetic analyses for species differences in P-glycoprotein-mediated drug transport. J Pharm Sci. 2006;95(12):2673–83.

45.   Giacomini KM, Huang S, Tweedie DJ, Benet LZ. Membrane transporters in drug development. Nat Rev Drug Discov. 2012;9(3):215–36.

46.   Kappelhoff BS, Huitema ADR, Yalvaç Z, Prins JM, Mulder JW, Meenhorst PL, et al. Population pharmacokinetics of efavirenz in an unselected cohort of HIV-1-infected individuals. Clin Pharmacokinet. 2005;44(8):849–61.

47.   Boffito M, Back DJ, Blaschke TF, Rowland M, Bertz RJ, Gerber JG, et al. Protein binding in antiretroviral therapies. AIDS Res Hum Retroviruses. 2003;19:825–35.

48.   Steimer J-L, Mallet A, Golmard J-L, Boisvieux J-F. Alternative Approaches to Estimation of Population Pharmacokinetic Parameters: Comparison with the Nonlinear Mixed-Effect Model. Drug Metab Rev. 1984;15(1–2):265–92.

49.   Lamers SL, Rose R, Maidji E, Agsalda-Garcia M, Nolan DJ, Fogel GB, et al. HIV DNA is frequently present within pathologic tissues evaluated at autopsy from cART-treated patients with undetectable viral load. J Virol. 2016;90(20):8968–83.

50.	Baker LM, Paul RH, Heaps-Woodruff JM, Chang JY, Ortega M, Margolin Z, et al. The Effect of Central Nervous System Penetration Effectiveness of Highly Active Antiretroviral Therapy on Neuropsychological Performance and Neuroimaging in HIV Infected Individuals. J Neuroimmune Pharmacol. 2015;487–92.

51.	Ellis RJ, Letendre S, Vaida F, Haubrich R, Heaton RK, Sacktor N, et al. Randomized Trial of Central Nervous System-Targeted Antiretrovirals for HIV-Associated Neurocognitive Disorder. Clin Infect Dis. 2014;58:1015–22.

52.	Hagberg L, Cinque P, Gisslen M, Brew BJ, Spudich S, Bestetti A, et al. Cerebrospinal fluid neopterin: An informative biomarker of central nervous system immune activation in HIV-1 infection. AIDS Res Ther. 2010;7:1–12.

53.	Zayyad Z, Spudich S. Neuropathogenesis of HIV: From Initial Neuroinvasion to HIV-Associated Neurocognitive Disorder (HAND). Curr HIV/AIDS Rep. 2015;12(1):16–24.

54.	Absinta M, Ha SK, Nair G, Sati P, Luciano NJ, Palisoc M, et al. Human and nonhuman primate meninges harbor lymphatic vessels that can be visualized noninvasively by MRI. Elife [Internet]. 2017;6. Available from: https://www.ncbi.nlm.nih.gov/pmc/articles/PMC5626482/pdf/elife-29738.pdf. Last accessed May 1st, 2018

55.	Honeycutt JB, Wahl A, Garcia JV, Honeycutt JB, Liao B, Nixon CC, et al. T cells establish and maintain CNS viral infection in HIV-infected humanized mice. J Clin Invest. 2018;128(7):2862–76.

56.	Gavegnano C, Schinazi RF. Antiretroviral therapy in macrophages: Implication for HIV eradication. Antivir Chem Chemother. 2009;20(2):63–78.

57.	Yamamoto Y, Välitalo PA, Wong YC, Huntjens DR, Proost JH, Vermeulen A, et al. Prediction of human CNS pharmacokinetics using a physiologically-based pharmacokinetic modeling approach. Eur J Pharm Sci. 2018;112(1):168–79.

58.	Valcour V, Chalermchai T, Sailasuta N, Marovich M, Lerdlum S, Suttichom D, et al. Central nervous system viral invasion and inflammation during acute HIV infection. J Infect Dis. 2012;206(2):275–82.

59.	Jeffrey A Rumbaugh, MD P. Developing neuroprotective strategies for treatment of HIV-associated neurocognitive dysfunction. Futur HIV Ther. 2008;2(3):271–80.

60.	Honeycutt JB, Wahl A, Baker C, Spagnuolo RA, Foster J, Zakharova O, et al. Macrophages sustain HIV replication in vivo independently of T cells. J Clin Invest. 2016;126(4):1353–66.

61.	Avalos CR, Price SL, Forsyth ER, Pin JN, Shirk EN, Bullock BT, et al. Quantitation of Productively Infected Monocytes and Macrophages of Simian Immunodeficiency Virus-Infected Macaques. J Virol. 2016;90(12):5643–56.

62.	Hellmuth J, Valcour V, Spudich S. CNS reservoirs for HIV: implications for eradication. J Virus Erad. 2015;1(2):67–71.

63.	Deeks SG. HIV: Shock and kill. Nature. 2012;487(7408):439–40.

64. Battivelli E, Dahabieh MS, Abdel-Mohsen M, Svensson JP, Da Silva IT, Cohn LB, et al. Distinct chromatin functional states correlate with HIV latency reactivation in infected primary CD4+T cells. Elife. 2018;7:1–22.

65. Darcis G, Kula A, Bouchat S, Fujinaga K, Corazza F, Ait-Ammar A, et al. An In-Depth Comparison of Latency-Reversing Agent Combinations in Various In Vitro and Ex Vivo HIV-1 Latency Models Identified Bryostatin-1+JQ1 and Ingenol-B+JQ1 to Potently Reactivate Viral Gene Expression. PLoS Pathog. 2015;11(7):1–36.

66. Gray LR, Cowley D, Welsh C, Lu HK, Brew BJ, Lewin SR, et al. CNS-specific regulatory elements in brain-derived HIV-1 strains affect responses to latency-reversing agents with implications for cure strategies. Mol Psychiatry. 2016;21(4):574–84.

67. Rosen EP, Sykes C, Thompson C, Kashuba A. Optimized Detection of Latency Reversing Agents in Tissue by Mass Spectrometry Imaging. In: 4th Annual Collaboratory of AIDS Researchers for Eradication Meeting, San Diego, CA [Internet]. San Diego, California; 2013. Available from: http://delaneycare.org/. Last accessed June 1st, 2018

68. Rosen EP, White N, Sykes C, Adamson L, Mathews M, Fedoriw Y, et al. Panobinostat distribution in rhesus macaque lymph nodes following anti-latency therapy (Abstract WEPEA0221). In: International AIDS Society. Paris, France; 2017. p. 419.

69. Gray LR, Brew BJ, Churchill MJ. Strategies to target HIV-1 in the central nervous system. Curr Opin HIV AIDS. 2016;11(4):371–5.

70. Marban C, Forouzanfar F, Ait-Ammar A, Fahmi F, El Mekdad H, Daouad F, et al. Targeting the brain reservoirs: Toward an HIV cure. Front Immunol. 2016;7(SEP):1–13.

71. Pateras I, Giaginis C, Tsigris C, Patsouris E, Theocharis S. NF-κB signaling at the crossroads of inflammation and atherogenesis: searching for new therapeutic links. Expert Opin Ther Targets. 2014;18(9):1089–101.

72. Teodorof-Diedrich C, Spector S. Human Immunodeficiency Virus Type 1 gp120 and Tat Induce Mitochondrial Fragmentation and Incomplete Mitophagy in Human Neurons. J Virol. 2018;92(22):1–10.

73. Gama L, Abreu CM, Shirk EN, Price SL, Li M, Laird GM, et al. Reactivation of simian immunodeficiency virus reservoirs in the brain of virally suppressed macaques. AIDS. 2017;31(1):5–14.

74. Lyon JG, Mokarram N, Saxena T, Carroll SL, Bellamkonda R V. Engineering challenges for brain tumor immunotherapy. Adv Drug Deliv Rev. 2017;114:19–32.

APPENDIX-1.1: SEARCH STRATEGY EMPLOYED FOR THE LITERATURE REVIEW IN CHAPTER-I

Embase Search

Search	Query	Items Found
#1	(pharmacokinetic OR pharmacokinetics OR pharmacodynamic OR pharmacodynamics) NEAR/5 brain	2,712
#2	(pharmacokinetic OR pharmacokinetics OR pharmacodynamic OR pharmacodynamics) NEAR/5 'central nervous system'	822
#3	(pharmacokinetic OR pharmacokinetics OR pharmacodynamic OR pharmacodynamics) NEAR/5 cns	303
#4	#1 OR #2 OR #3	3,708
#5	trovafloxacin OR nelfinavir OR didanosine OR etravirine OR rilpivirine OR amprenavir OR fosamprenavir OR tipranavir OR maraviroc OR elvitegravir OR dolutegravir OR abacavir OR aciclovir OR albendazole OR amikacin OR amoxicillin OR ampicillin OR atazanavir OR azithromycin OR cefazolin OR cefepime OR cefixime OR cefotaxime OR cefpirome OR ceftazidime OR ceftriaxone OR cefuroxime OR cephaloridine OR chloramphenicol OR cilastatin OR ciprofloxacin OR clarithromycin OR clavulanate OR clindamycin OR cloxacillin OR colistin OR cycline OR dapsone OR darunavir OR doxycycline OR efavirenz OR enfuvirtide OR ethambutol OR ethionamide OR fluconazole OR flucytosin OR foscarnet OR fosfomycin OR fusidic AND acid OR gentamicin OR imipenem OR indinavir OR isoniazid OR itraconazole OR lamivudine OR levofloxacin OR linezolid OR lopinavir OR meropenem OR metronidazole OR mezlocillin OR micafungin OR moxifloxacin OR nafcillin OR netilmicin OR nevirapin OR ofloxacin OR penicillin OR piperacillin OR posaconazole OR praziquantel OR pyrazinamide OR pyrimethamine OR raltegravir OR rifampin OR ritonavir OR saquinavir OR stavudine OR steptomycin OR streptomycin OR sulbactam OR sulfadiazine OR sulfamethoxazole OR tazobactam OR tetroxoprim OR tige OR trimethoprim OR valaciclovi OR vancomycin OR voriconazole OR zidovudine OR levodopa OR bromocriptine OR pergolide OR lisuride OR cabergoline OR pramipexole OR ropinirole OR piribedil OR entacapone OR doripenem OR emtricitabine OR tenofovir OR carbamazepine OR oxcarbazepine OR lamotrigine OR levetiracetam OR topiramate OR clonazepam OR apomorphine OR selegiline OR tolcapone OR amantadine OR donepezil OR rivastigmine OR galantamine OR memantine OR haloperidol OR aripirazole OR perospirone OR lurasidone OR cariprazine OR fluoxetine OR fluvoxamine OR norfluoxetine OR venlafaxine OR duloxetine OR mirtazapine OR citalopram	954,442
#6	#4 AND #5	660

Total screened: 660 + references not located by searches (100)
Total conference abstracts screened: 1
Total journal articles screened: 758

APPENDIX-2.1: COMPARISON OF ANTIRETOVIRAL CONCENTRATIONS IN THE PLASMA, CSF (NHPS) AND BRAIN TISSUE AND ANTIRETROVIRAL BRAIN TISSUE:PLASMA AND CSF:PLASMA PENETRATION RATIOS (NHPS) ACROSS THE THREE PRECLINICAL SPECIES

ARV/ Animal Model	ARV concentration (ng/mL [plasma and CSF] or ng/g [brain tissue])							ARV penetration ratio			
	Plasma			Brain Tissue			CSF	Brain tissue:plasma ratio			CSF:plasma ratio
	Hu-HSC-RAG	BLT	NHP	Hu-HSC-RAG	BLT	NHP	NHP	Hu-HSC-RAG	BLT	NHP	NHP
TFV	150 (77.1, 368)	125 (89.5, 241)	60.3 (47.8, 84.4)	4.49 (0.62, 18.8)	14.3 (11.9, 47.9)	51.3 (34.9, 57.5)	2.04 (1.40, 2.82)	0.02 (0.01, 0.11)	0.11 (0.07, 0.14)	0.75 (0.59, 0.92)	0.035 (0.016, 0.055)
FTC	24.0 (19.8, 68.4)	46.6 (27.8, 79.2)	13.5 (8.46, 20.1)	1.78 (0.20, 2.46)	8.33 (4.29, 14.2)	26.3 (15.9, 31.9)	3.97 (2.50, 6.48)	0.05 (0.01, 0.12)	0.16 (0.10, 0.18)	1.55 (1.20, 2.43)	0.33 (0.17, 0.42)
EFV[1]	2.5 (0.50, 10.7)	-	187 (71.6, 339)	0.58 (0.27, 19.8)	-	775 (318, 1453)	0.94 (0.50, 1.89)	1.14 (0.25, 1.90)	-	4.26 (4.07, 4.54)	0.007 (0.005, 0.008)
RAL	1.81	21.9	157	0.22	2.29	21.8	0.50	0.13	0.13	0.12	0.003

ARV/ Animal Model	ARV concentration (ng/mL [plasma and CSF] or ng/g [brain tissue])							ARV penetration ratio			
	Plasma			Brain Tissue			CSF	Brain tissue:plasma ratio			CSF:plasma ratio
	Hu-HSC-RAG	BLT	NHP	Hu-HSC-RAG	BLT	NHP	NHP	Hu-HSC-RAG	BLT	NHP	NHP
	(78.6, 297)	(10.5, 32.2)	(78.6, 297)	(0.19, 0.26)	(1.53, 3.17)	(14.2, 67.1)	(0.50, 1.05)	(0.05, 0.41)	(0.07, 0.17)	(0.05, 0.21)	(0.001, 0.007)
MVC	1.26 (0.50, 5.73)	5.67 (0.94, 23.4)	31.8 (18.0, 80.6)	0.22 (0.20, 1.16)	12.3 (4.44, 19.7)	57.5 (37.6, 108)	0.50 (0.50, 4.96)	0.39 (0.25, 0.44)	1.86 (0.64, 4.84)	1.81 (0.76, 2.14)	0.030 (0.014, 0.082)
ATZ	9.91 (2.50, 18.7)	9.80 (8.64, 14.4)	2.40 (0.50, 106)	0.98 (0.49, 1.54)	2.10 (0.71, 10.1)	84.1 (47.2, 269)	0.50 (0.50, 4.96)	0.13 (0.06, 0.76)	0.12 (0.04, 0.28)	97.4 (0.41, 166)	0.21 (0.039, 0.98)

APPENDIX-2.2: ANTIRETROVIRAL CONCENTRATIONS IN THE PLASMA, CSF (NHPS) AND BRAIN TISSUE AND ANTIRETROVIRAL BRAIN TISSUE:PLASMA AND CSF:PLASMA PENETRATION RATIOS (NHPS) ACROSS THE INDIVIDUAL ANIMALS

I. **Hu-HSC-RAG mice**
   a) **Tenofovir, emtricitabine, raltegravir, and maraviroc**

Drug	TFV			FTC			RAL			MVC		
Animal ID	Plasma (ng/mL)	Brain Tissue (ng/g)	Brain Tissue:Plasma	Plasma (ng/mL)	Brain Tissue (ng/g)	Brain Tissue: Plasma	Plasma (ng/mL)	Brain Tissue (ng/g)	Brain Tissue: Plasma	Plasma (ng/mL)	Brain Tissue (ng/g)	Brain Tissue: Plasma
Uninfected hu-HSC-RAG												
1686	143	17.23	0.118	9.96	3.20	0.31	0.5	0.22	0.44	0.5	0.22	0.44
1698	114	19.36	0.167	19.9	2.46	0.12	0.5	0.20	0.39	0.5	0.20	0.39
1699	127	1.75	0.013	10.0	2.42	0.24	0.5	0.83	1.63	0.5	0.20	0.38
1712	62.1	7.23	0.114	26.3	1.57	0.06	2.69	0.22	0.08	0.5	0.22	0.44
1713	59.1	0.57	0.009	19.2	0.14	0.01	2.06	0.14	0.07	0.5	0.14	0.28
1649	62.8	0.45	0.007	21.9	0.21	0.01	0.5	0.21	0.41	0.5	0.21	0.41
Infected hu-HSC-RAG												

Drug	TFV			FTC			RAL			MVC		
Animal ID	Plasma (ng/mL)	Brain Tissue (ng/g)	Brain Tissue:Plasma	Plasma (ng/mL)	Brain Tissue (ng/g)	Brain Tissue: Plasma	Plasma (ng/mL)	Brain Tissue (ng/g)	Brain Tissue: Plasma	Plasma (ng/mL)	Brain Tissue (ng/g)	Brain Tissue: Plasma
1756	474	0.43	0.001	109	0.16	0.001	14.8	0.16	0.011	23.3	0.16	0.007
1784	432	23.29	0.053	79.9	3.97	0.049	6.68	0.27	0.039	12.1	2.00	0.162
1803	377	10.10	0.026	25.1	1.98	0.077	2.61	0.24	0.091	3.44	0.88	0.250
2132	151	0.78	0.005	28.7	0.19	0.007	1.17	0.19	0.161	1.98	0.50	0.247
2242	312	1.08	0.003	81.2	0.43	0.005	6.32	0.21	0.032	6.34	3.87	0.598
2244	255	22.31	0.086	20.9	2.46	0.115	1.48	0.26	0.172	2.74	1.25	0.449

b) **Efavirenz and atazanavir**

Drug	EFV			Drug	ATZ		
Animal ID	Plasma (ng/mL)	Brain Tissue (ng/g)	Brain Tissue:Plasma	Animal ID	Plasma (ng/mL)	Brain Tissue (ng/g)	Brain Tissue:Plasma
Uninfected hu-HSC-RAG							
1590	4.23	14.33	3.322	1670	0.5	0.44	0.85
1592	2.74	0.16	0.058	1700	9.75	0.94	0.09

Drug	EFV			Drug	ATZ		
Animal ID	Plasma (ng/mL)	Brain Tissue (ng/g)	Brain Tissue:Plasma	Animal ID	Plasma (ng/mL)	Brain Tissue (ng/g)	Brain Tissue:Plasma
1594	3.57	0.14	0.038	1701	2.5	1.27	0.49
1606	2.27	0.41	0.177	1706	129	7.46	0.06
1628	0.5	0.24	0.476	1707	27.9	0.49	0.02
1641	0.5	0.47	0.915	1708	16.4	1.13	0.07
Infected hu-HSC-RAG							
1831	1.5	5.62	3.670	2097	2610	1.02	0.0004
2110	0.5	0.35	0.682	2108	0.5	122.95	241
2118	12.6	24.51	0.159	2109	1.67	0.50	0.293
2125	0.5	0.70	1.372	2116	1.32	0.21	0.157
2246	724	1458.54	0.165	2255	1.2	1.63	1.335
2254	17.5	34.09	0.159	2256	10.5	0.71	0.066

II.   BLT mice

a) Tenofovir and emtricitabine

Drug	TFV			FTC		
Animal ID	Plasma (ng/mL)	Brain Tissue (ng/g)	Brain Tissue:Plasma	Plasma (ng/mL)	Brain Tissue (ng/g)	Brain Tissue:Plasma
Uninfected hu-HSC-RAG						
BLT A	-	178.90	-	-	14.54	-
BLT B	96.7	123.93	1.256	45.4	13.86	0.30
BLT C	245	11.74	0.047	24.7	2.64	0.10
BLT D	126	14.35	0.112	41.2	7.10	0.17
BLT E	86.6	12.28	0.139	58.4	9.66	0.16
BLT F	65.5	8.56	0.128	21.5	8.33	0.38
Infected hu-HSC-RAG						
BLT G	51	12.09	0.232	20.5	3.83	0.183
BLT H	210	14.64	0.068	59.2	6.45	0.107
BLT I	406	43.33	0.105	111	10.13	0.089
BLT J	91.2	11.96	0.129	83.8	15.65	0.183
BLT K	173	17.40	0.099	45.9	4.75	0.102

Drug	TFV			FTC		
Animal ID	Plasma (ng/mL)	Brain Tissue (ng/g)	Brain Tissue:Plasma	Plasma (ng/mL)	Brain Tissue (ng/g)	Brain Tissue:Plasma
BLT L	119	9.21	0.076	35.1	3.31	0.093
BLT M	1010	52.44	0.051	182	29.08	0.157

b) Raltegravir, maraviroc, and atazanavir

Drug	RAL			MVC			ATZ		
Animal ID	Plasma (ng/mL)	Brain Tissue (ng/g)	Brain Tissue:Plasma	Plasma (ng/mL)	Brain Tissue (ng/g)	Brain Tissue:Plasma	Plasma (ng/mL)	Brain Tissue (ng/g)	Brain Tissue:Plasma
Uninfected hu-HSC-RAG									
BLT A	-	2.90	-	-	23.70	-	-	14.10	-
BLT B	46.7	3.45	0.07	0.5	20.46	40.12	9.61	29.58	3.018
BLT C	32.9	0.92	0.03	0.5	2.40	4.71	9.1	0.69	0.075
BLT D	20.3	1.69	0.08	2.21	3.96	1.76	18.3	2.09	0.112
BLT E	27.9	1.86	0.07	0.5	4.23	8.30	9.72	1.98	0.199
BLT F	5.66	0.99	0.17	3.01	15.00	4.89	2.48	0.72	0.285

Drug	RAL			MVC			ATZ		
Animal ID	Plasma (ng/mL)	Brain Tissue (ng/g)	Brain Tissue:Plasma	Plasma (ng/mL)	Brain Tissue (ng/g)	Brain Tissue:Plasma	Plasma (ng/mL)	Brain Tissue (ng/g)	Brain Tissue:Plasma a
Infected hu-HSC-RAG									
BLT G	4.11	2.45	0.586	5.25	16.73	3.124	8.93	2.34	0.257
BLT H	11.7	2.29	0.192	14.6	5.01	0.336	13.5	7.78	0.565
BLT I	22.9	2.47	0.106	74.5	46.37	0.610	93.6	4.16	0.044
BLT J	22.8	3.45	0.148	25.7	19.03	0.726	14.1	1.96	0.136
BLT K	16.1	2.16	0.131	6.17	12.34	1.961	8.47	0.24	0.028
BLT L	9.89	1.36	0.135	5.87	4.64	0.775	4.03	0.17	0.042
BLT M	48.5	7.35	0.149	50.8	11.87	0.229	434	12.39	0.028

III. Nonhuman primates
a) Tenofovir and emtricitabine

Drug	TFV					FTC				
Animal ID	Plasma (ng/mL)	CSF (ng/mL)	Brain Tissue (ng/g)	CSF:Plasma	Brain Tissue:Plasma	Plasma (ng/mL)	CSF (ng/mL)	Brain Tissue (ng/g)	CSF:Plasma	Brain Tissue:Plasma
Uninfected Macaques										
40905	59.1	0.5	55.8	0.008	0.925	19.2	1.78	34.8	0.091	1.78
41033	91.7	0.5	47.1	0.005	0.504	17.4	3.35	33.4	0.189	1.88
42109	67.6	0.5	54.3	0.007	0.788	16.6	0.5	26.3	0.030	1.55
39510	664	10.4	392	0.015	0.579	73.7	11.7	69.3	0.156	0.92
42528	73.8	4.58	56.7	0.061	0.753	6.17	0.5	26.1	0.079	4.15
40585	63.3	1.68	53.9	0.026	0.835	7.07	2.37	17.1	0.329	2.37
42474	19.2	1.3	25.4	0.066	1.296	4.1	2.84	19.1	0.679	4.58
41735	58.6	2.71	41.0	0.045	0.686	8.37	4.65	22.2	0.545	2.61
Infected Macaques										
40437	31.3	2.04	33.5	0.064	1.050	16.3	7.09	27.1	0.426	1.63
42226	32	2.3	22.7	0.070	0.694	9.98	3.88	14.8	0.381	1.45
42971	50.3	1.84	30.1	0.036	0.587	9.16	2.62	13.9	0.280	1.49

Drug	TFV					FTC				
Animal ID	Plasma (ng/mL)	CSF (ng/mL)	Brain Tissue (ng/g)	CSF:Plasma	Brain Tissue:Plasma	Plasma (ng/mL)	CSF (ng/mL)	Brain Tissue (ng/g)	CSF:Plasma	Brain Tissue:Plasma
42827	43.4	1.49	65.1	0.034	1.470	13.2	5.48	33.6	0.407	2.50
41380	59.4	2.94	36.3	0.049	0.599	20.2	7.33	29.9	0.356	1.45
42966	54.9	2.62	51.3	0.047	0.916	21.9	5.86	29.8	0.262	1.33
42707	52.8	1.72	48.1	0.032	0.892	8.21	3.97	2.1	0.474	0.25
40422	226000	4910	3572	0.021	0.015	1420	163	281	0.113	0.19
42706	136	2.37	58.3	0.017	0.420	10.5	4.21	2.0	0.393	0.19
42350	166	5.93	99.8	0.035	0.589	27.6	7.31	30.3	0.260	1.08

b) Efavirenz and raltegravir

Drug	EFV					RAL				
Animal ID	Plasma (ng/mL)	CSF (ng/mL)	Brain Tissue (ng/g)	CSF:Plasma	Brain Tissue:Plasma	Plasma (ng/mL)	CSF (ng/mL)	Brain Tissue (ng/g)	CSF:Plasma	Brain Tissue:Plasma
Uninfected Macaques										
40905	420	3.38	1983	0.008	4.629	287	1.29	27.7	0.004	0.09

41033	215	1.38	965	0.006	4.401	109	1.21	15.8	0.011	0.14
42109	371	2.06	1615	0.005	4.268	81.2	0.5	78.3	0.007	0.21
42474	62.7	0.5	293	0.008	4.582	1060	0.5	265	0.0005	0.24
Infected Macaques										
40437	59.3	0.5	240	0.008	3.965	1990	0.5	33.6	0.000	0.02
42226	183	1.39	792	0.007	4.245	303	0.5	11.5	0.002	0.04
42971	92.7	0.5	392	0.005	4.141	199	0.5	16.0	0.002	0.08
42707	184	0.5	759	0.003	4.041	64.7	0.5	13.7	0.008	0.21
40422	2280	45.6	5610	0.020	2.412	520	35.4	233	0.067	0.44

c) **Maraviroc and atazanavir**

Drug	MVC					ATZ				
Animal ID	Plasma (ng/mL)	CSF (ng/mL)	Brain Tissue (ng/g)	CSF:Plasma	Brain Tissue:Plasma	Plasma (ng/mL)	CSF (ng/mL)	Brain Tissue (ng/g)	CSF:Plasma	Brain Tissue:Plasma
Uninfected Macaques										
39510	400	12.1	193	0.030	0.473	1760	40.5	554	0.023	0.31
42528	31.2	2.87	57.5	0.090	1.808	0.5	0.5	49.7	0.980	97.44

40585	10.5	0.5	21.9	0.047	2.045	0.5	0.5	84.1	0.980	164.92
41735	82.6	6.24	40.5	0.074	0.481	51.4	1.11	26.5	0.021	0.51
Infected Macaques										
42827	46	0.5	105	0.011	2.23	5.93	0.5	138	0.083	22.8
41380	24.8	0.5	48.7	0.020	1.92	0.5	0.5	133	0.980	261
42966	30.1	0.5	34.7	0.016	1.13	0.5	0.5	59.4	0.980	116
42706	7.29	4.56	110	0.613	14.8	2.35	0.5	399	0.209	166
42350	75.5	0.5	79.2	0.006	1.03	157	8.8	44.8	0.055	0.28

APPENDIX-2.3: BRAIN TISSUE CONCENTRATION OF TENOFOVIR DIPHOSPHATE ACROSS THE INDIVIDUAL ANIMALS

Species/Animal ID	Tenofovir diphosphate concentration (fmol/g)
Uninfected macaques	
41033	35344
42109	30862
40905	45839
42528	21509
39510	178703
40585	34841
42474	25485
41735	120646
Infected macaques	
42226	14996
42971	23685
40437	33910
42827	32965
41380	36272
42966	31537
42707	38348
40422	1379987
42350	75359

42706	44518
Uninfected TFRM hu-HSC-RAG[1]	
1686	-
1698	-
1699	-
1712	-
1713	-
1649	-
Infected TFRM hu-HSC-RAG	
1756	13343
1784	14731
1803	23258
2132	7629
2242	BLQ
2244	15314
Uninfected BLT	
BLT A	-
BLT B	2335
BLT C	1841
BLT D	1963
BLT E	980
BLT F	1195

Infected BLT	
BLT G	851
BLT H	1376
BLT I	10485
BLT J	1510
BLT K	1166
BLT L	852
BLT M	2941

[1] – indicates that the sample was not available

APPENDIX-2.4: INHIBITORY QUOTIENTS IN THE BRAIN TISSUE ACROSS THE INVIDUAL NHPS

Animal/Species ID	Protein-free IC90 for RT-SHIV virus						
	2980	84	3	107	290	12750	169811
	Drug IQ90 (unbound trough concentration/ protein-free IC90)						
	TFV	FTC	EFV	RAL	MVC	ATZ	TFV-dp
Uninfected macaques							
41033	0.016	0.398	9.029	0.150	-	-	0.208
42109	0.018	0.313	15.110	0.698	-	-	0.182
40905	0.019	0.414	18.550	0.519	-	-	0.270
42474	0.009	0.228	2.742	2.471	-	-	0.150
42528	0.019	0.311	-	-	0.193	0.003	0.127
39510	0.132	0.825	-	-	0.648	0.033	1.052
40585	0.018	0.203	-	-	0.074	0.005	0.205
41735	0.014	0.265	-	-	0.136	0.002	0.710
Infected macaques							
42226	0.008	0.176	7.412	0.107	-	-	0.088
42971	0.010	0.165	3.663	0.149	-	-	0.139
40437	0.011	0.323	2.264	0.073	-	-	0.200
42707	0.016	0.025	7.096	0.127	-	-	0.226
40422	1.199	3.343	52.484	2.173	-	-	8.127
42827	0.022	0.400	-	-	0.352	0.008	0.194
41380	0.012	0.355	-	-	0.163	0.008	0.214

42966	0.017	0.354	-	-	0.117	0.004	0.186
42350	0.033	0.361	-	-	0.266	0.003	0.444
42706	0.020	0.024	-	-	0.370	0.024	0.262

APPENDIX-3.1: GENE EXPRESSION ASSAYS

Gene Name	Species	Catalog Number
Abcc1	Mouse	Mm00456156_m1
Abcc2	Mouse	Mm00496899_m1
Abcc4	Mouse	Mm01226381_m1
Abcb1	Mouse	Mm00440736_m1
Abcg2	Mouse	Mm00496364_m1
Slco1a4	Mouse	Mm01267407_m1
Slc29a1	Mouse	Mm01270577_m1
Slc22a2	Mouse	Mm00457295_m1
Slc22a8	Mouse	Mm00459534_m1
GAPDH	Mouse	Mm99999915_g1
ABCC1	Macaque	Hs01561502_m1
ABCC2	Macaque	Rh02788077_m1
ABCC4	Macaque	Rh02858818_m1
ABCB1	Macaque	Rh02788239_m1
ABCG2	Macaque	Rh02788848_m1
SLCO1A2	Macaque	Rh01072345_m1
SLC29A1	Macaque	Rh02794207_m1
SLC22A2	Macaque	Hs01010723_m1
SLC22A8	Macaque	Rh02848022_m1

GAPDH	Macaque	Rh02621745_g1
ABCC1	Human	Hs01561502_m1
ABCC2	Human	Hs00166123_m1
ABCC4	Human	Hs00988717_m1
ABCB1	Human	Hs00184500_m1
ABCG2	Human	Hs01053790_m1
SLCO1A2	Human	Hs00245360_m1
SLC29A1	Human	Hs01085704_g1
SLC22A2	Human	Hs01010723_m1
SLC22A8	Human	Hs00188599_m1
GAPDH	Human	Hs02758991_g1

APPENDIX-3.2: PEPTIDE SEQUENCES FOR THE PROTEOMICS ANALYSIS OF DRUG TRANSPORTERS

BCRP (humanized mice): SSLLDVLAAR

BCRP (macaques): VIQLGDLK

P-gp (humanized mice/macaques): NTTGALTR

Oatp1a4 (humanized mice): IYLGLPAALR

OATP1A2 (macaques): YIYLGLPAALR

APPENDIX-3.3: GENE EXPRESSION OF DRUG TRANSPORTERS IN THE HUMANIZED MICE DOSING COHORTS
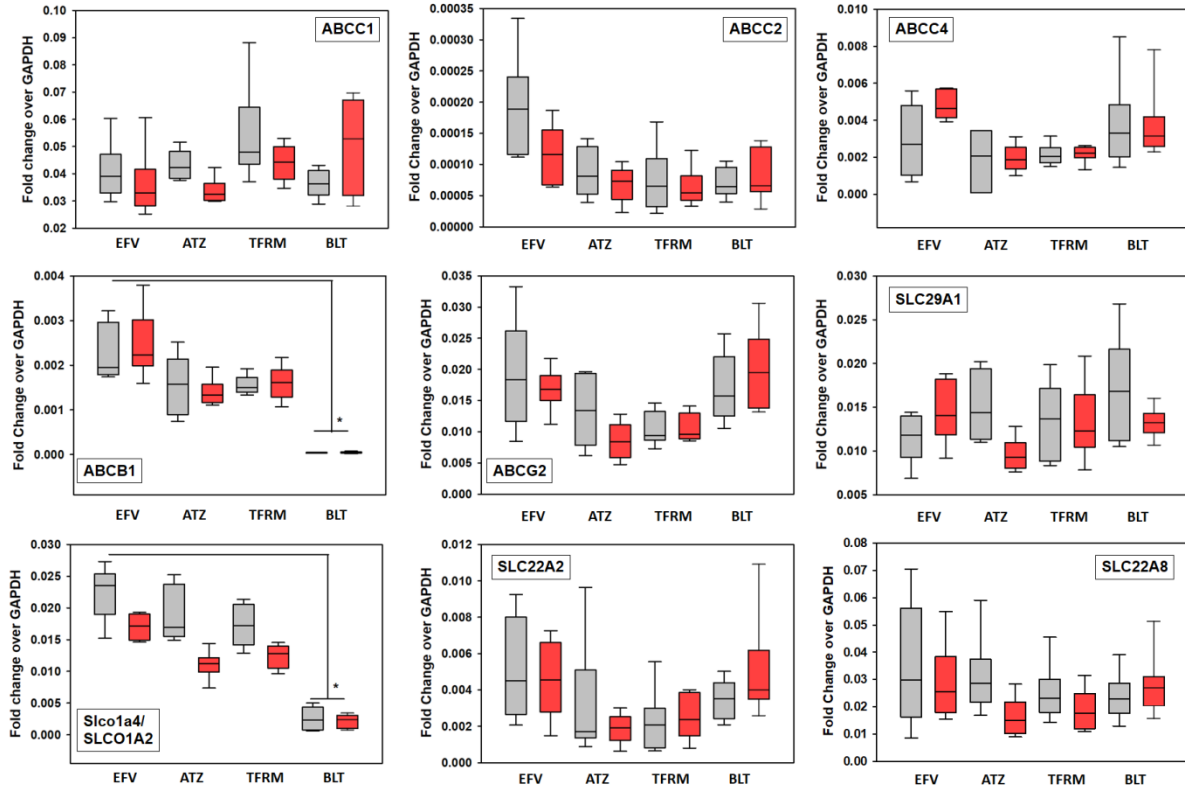
EFV: hu-HS-RAG mice dosed with efavirenz only

ATZ: hu-HSC-RAG mice dosed with atazanavir only

TFRM: hu-HSC-RAG mice dosed with tenofovir, emtricitabine, raltegravir and maraviroc

BLT: BLT mice

Uninfected (gray) and infected (red) cohorts are indicated

APPENDIX-3.4: GENE EXPRESSION OF DRUG TRANSPORTERS ACROSS THE INDIVIDUAL ANIMALS

Specimen/ Animal ID	Gene Expression normalized to GAPDH								
	MRP1	MRP2	MRP4	BCRP	PGP	ENT1	OATP1A2	OAT3	OCT2
Uninfected macaques									
40905	3.98E-03	8.72E-04	7.63E-03	3.46E-03	3.87E-03	7.88E-03	1.29E-02	3.46E-03	-
41033	4.94E-03	5.14E-04	1.71E-03	1.73E-02	3.69E-03	2.99E-02	5.87E-03	5.46E-03	1.01E-08
42109	4.84E-03	2.14E-03	1.12E-02	1.38E-02	6.93E-03	1.33E-02	1.57E-02	1.06E-02	3.74E-08
39510	6.32E-03	4.91E-04	5.82E-03	7.66E-03	1.60E-03	8.84E-03	9.05E-03	2.18E-02	-
42528	9.69E-03	2.16E-03	1.91E-03	1.02E-02	3.68E-03	3.16E-02	3.38E-03	6.14E-04	8.25E-09
40585	5.75E-03	2.88E-04	2.74E-03	9.87E-03	2.05E-03	1.53E-02	4.15E-03	2.20E-03	-
42474	-	6.59E-04	1.04E-03	4.10E-03	1.63E-03	4.28E-03	1.60E-03	8.51E-04	3.11E-06
41735	-	2.07E-04	1.18E-03	4.30E-03	1.44E-03	6.18E-03	1.66E-03	2.33E-04	1.07E-07
Infected macaques									
40437	4.86E-03	9.31E-04	2.82E-03	3.85E-03	2.40E-03	1.22E-02	3.10E-03	6.29E-04	2.12E-08

Specimen/ Animal ID	Gene Expression normalized to GAPDH								
	MRP1	MRP2	MRP4	BCRP	PGP	ENT1	OATP1A2	OAT3	OCT2
42226	5.95E-03	3.88E-04	2.60E-03	1.50E-02	5.34E-03	2.33E-02	7.72E-03	5.69E-03	5.91E-08
42971	4.89E-03	2.75E-04	2.23E-03	7.52E-03	3.36E-03	1.80E-02	3.21E-03	3.92E-04	-
42827	3.82E-03	1.53E-04	1.96E-03	4.60E-03	3.30E-03	1.20E-02	3.26E-03	8.12E-04	3.09E-08
41380	7.11E-03	8.60E-04	8.67E-04	4.88E-03	2.37E-03	1.54E-02	1.37E-03	2.21E-04	-
42966	4.08E-03	1.77E-04	1.25E-03	4.07E-03	2.08E-03	1.05E-02	1.18E-03	1.49E-04	-
42707	-	1.39E-04	1.08E-03	4.77E-03	2.02E-03	5.81E-03	2.14E-03	6.46E-04	2.84E-06
40422	-	8.44E-04	1.71E-03	4.07E-03	1.19E-03	6.68E-03	1.08E-03	4.01E-04	2.25E-08
42706	-	4.56E-04	7.03E-04	3.65E-03	1.73E-03	8.26E-03	2.65E-03	4.44E-04	4.06E-06
42350	-	1.07E-04	9.30E-04	3.09E-03	1.07E-03	5.64E-03	8.86E-04	1.74E-04	5.61E-07
Uninfected EFV hu-HSC-RAG									
1592	8.58E-02	7.17E-04	6.50E-03	1.09E-01	1.08E-02	3.46E-02	3.25E-02	6.21E-02	8.36E-03
1594	8.35E-02	6.95E-04	5.81E-03	8.28E-02	1.07E-02	2.76E-02	2.84E-02	4.33E-02	5.67E-03
1606	6.03E-02	2.01E-04	3.80E-03	2.29E-02	2.03E-03	1.44E-02	2.73E-02	5.14E-02	9.25E-03

Specimen/ Animal ID	Gene Expression normalized to GAPDH								
	MRP1	MRP2	MRP4	BCRP	PGP	ENT1	OATP1A2	OAT3	OCT2
1628	3.74E-02	1.77E-04	4.54E-03	2.38E-02	1.87E-03	1.00E-02	2.32E-02	3.80E-02	4.68E-03
1641	2.97E-02	3.34E-04	5.59E-03	3.33E-02	2.88E-03	6.87E-03	2.39E-02	7.05E-02	7.58E-03
Infected EFV hu-HSC-RAG									
1831	3.53E-02	6.39E-05	4.59E-03	1.81E-02	2.35E-03	1.80E-02	1.90E-02	3.30E-02	4.17E-03
2110	3.22E-02	1.87E-04	3.91E-03	1.63E-02	1.59E-03	1.52E-02	1.76E-02	1.87E-02	3.23E-03
2118	2.92E-02	6.84E-05	4.69E-03	1.73E-02	2.76E-03	1.29E-02	1.46E-02	2.19E-02	1.48E-03
2125	2.52E-02	9.63E-05	5.68E-03	1.12E-02	2.12E-03	9.18E-03	1.50E-02	2.92E-02	4.90E-03
2246	3.37E-02	1.35E-04	4.22E-03	1.63E-02	3.79E-03	1.27E-02	1.67E-02	5.50E-02	6.39E-03
2254	6.07E-02	1.45E-04	5.74E-03	2.18E-02	2.11E-03	1.88E-02	1.93E-02	1.54E-02	7.26E-03
Uninfected TFRM hu-HSC-RAG									
1686	7.19E-02	6.49E-04	4.31E-03	8.71E-02	8.53E-03	4.57E-02	1.95E-02	6.51E-02	8.01E-03
1698	8.89E-02	6.46E-04	4.07E-03	1.05E-01	1.20E-02	4.39E-02	2.60E-02	3.54E-02	3.92E-03
1699	4.96E-02	2.16E-05	2.12E-03	9.12E-03	1.42E-03	1.24E-02	1.46E-02	2.49E-02	2.14E-03

Specimen/ Animal ID	Gene Expression normalized to GAPDH								
	MRP1	MRP2	MRP4	BCRP	PGP	ENT1	OATP1A2	OAT3	OCT2
1712	9.47E-02	9.43E-04	6.26E-03	1.12E-01	1.66E-02	4.65E-02	3.16E-02	5.10E-02	3.46E-03
1713	3.71E-02	8.95E-05	2.32E-03	9.31E-03	1.50E-03	9.00E-03	1.29E-02	1.90E-02	6.47E-04
1649	8.82E-02	1.68E-04	3.14E-03	1.46E-02	1.92E-03	1.99E-02	2.03E-02	4.55E-02	5.55E-03
Infected TFRM hu-HSC-RAG									
1756	4.31E-02	1.23E-04	2.62E-03	1.26E-02	2.18E-03	1.31E-02	1.31E-02	7.95E-04	1.08E-02
1784	3.92E-02	5.76E-05	2.25E-03	9.28E-03	1.47E-03	1.50E-02	9.63E-03	2.07E-02	4.00E-03
1803	5.30E-02	5.19E-05	1.33E-03	9.00E-03	1.07E-03	1.15E-02	1.38E-02	1.24E-02	1.70E-03
2132	3.47E-02	3.30E-05	2.19E-03	1.41E-02	1.80E-03	1.13E-02	1.08E-02	2.98E-03	3.14E-02
2242	4.53E-02	6.78E-05	2.20E-03	8.54E-03	1.76E-03	7.84E-03	1.25E-02	1.77E-03	2.27E-02
2244	4.89E-02	4.60E-05	2.50E-03	9.84E-03	1.35E-03	2.08E-02	1.46E-02	1.47E-02	3.81E-03
Uninfected ATZ hu-HSC-RAG									
1670	8.03E-02	7.15E-04	5.08E-03	7.30E-02	8.73E-03	4.09E-02	2.27E-02	6.63E-02	2.78E-03
1700	1.09E-01	6.86E-04	6.56E-03	1.05E-01	1.05E-02	5.39E-02	3.74E-02	6.04E-02	7.87E-03

Specimen/ Animal ID	Gene Expression normalized to GAPDH								
	MRP1	MRP2	MRP4	BCRP	PGP	ENT1	OATP1A2	OAT3	OCT2
1701	1.26E-01	2.04E-04	4.25E-03	9.20E-02	6.80E-03	7.05E-02	2.90E-02	2.98E-02	2.36E-03
1706	4.36E-02	1.24E-04	3.45E-03	1.73E-02	2.52E-03	1.22E-02	1.82E-02	2.88E-02	1.53E-03
1707	4.09E-02	1.41E-04	3.21E-03	1.93E-02	2.01E-03	1.15E-02	2.52E-02	3.02E-02	1.64E-03
1708	5.16E-02	3.93E-05	3.44E-03	1.96E-02	1.90E-03	2.02E-02	2.32E-02	5.91E-02	9.63E-03
Infected ATZ hu-HSC-RAG									
2097	3.46E-02	8.63E-05	1.49E-03	6.21E-03	1.19E-03	8.18E-03	1.08E-02	8.96E-03	1.98E-03
2108	4.22E-02	7.20E-05	1.82E-03	8.32E-03	1.96E-03	9.14E-03	1.14E-02	3.01E-03	1.95E-02
2109	2.99E-02	5.08E-05	2.35E-03	1.28E-02	1.39E-03	1.28E-02	1.44E-02	1.86E-03	2.83E-02
2116	3.04E-02	2.29E-05	9.96E-04	4.72E-03	1.11E-03	7.61E-03	7.36E-03	6.25E-04	1.05E-02
2255	3.44E-02	7.49E-05	1.89E-03	8.40E-03	1.27E-03	1.03E-02	1.10E-02	1.37E-02	1.42E-03
2256	3.03E-02	1.04E-04	3.11E-03	1.05E-02	1.44E-03	9.41E-03	1.14E-02	1.60E-02	2.36E-03
Uninfected BLT									
BLT A	3.36E-02	5.80E-05	3.57E-03	1.57E-02	4.62E-05	1.14E-02	9.36E-04	1.29E-02	4.19E-03

Specimen/ Animal ID	Gene Expression normalized to GAPDH								
	MRP1	MRP2	MRP4	BCRP	PGP	ENT1	OATP1A2	OAT3	OCT2
BLT B	4.31E-02	3.99E-05	8.50E-03	2.57E-02	4.46E-05	2.68E-02	4.12E-03	3.91E-02	5.03E-03
BLT C	2.88E-02	1.06E-04	3.63E-03	2.08E-02	3.73E-05	1.95E-02	5.01E-03	2.52E-02	4.14E-03
BLT D	3.33E-02	5.76E-05	3.03E-03	1.59E-02	3.37E-05	1.99E-02	3.68E-03	1.92E-02	2.54E-03
BLT E	4.06E-02	7.07E-05	1.45E-03	1.05E-02	2.72E-05	1.05E-02	5.96E-04	2.50E-02	2.90E-03
BLT F	3.91E-02	9.22E-05	2.21E-03	1.32E-02	4.57E-05	1.42E-02	8.28E-04	2.05E-02	2.08E-03
Infected BLT									
BLT G	2.82E-02	5.65E-05	7.81E-03	2.48E-02	4.53E-05	1.27E-02	3.45E-03	3.11E-02	4.23E-03
BLT H	6.71E-02	6.57E-05	2.58E-03	1.38E-02	3.48E-05	1.34E-02	2.72E-03	2.04E-02	3.51E-03
BLT I	5.58E-02	6.65E-05	2.29E-03	1.32E-02	5.75E-05	1.07E-02	3.04E-03	1.57E-02	4.01E-03
BLT J	3.62E-02	1.28E-04	3.51E-03	2.01E-02	3.23E-05	1.60E-02	1.03E-03	2.70E-02	3.90E-03
BLT K	5.29E-02	1.26E-04	4.19E-03	3.06E-02	7.57E-05	1.43E-02	2.40E-03	5.13E-02	1.09E-02
BLT L	3.21E-02	2.92E-05	2.97E-03	1.95E-02	3.92E-05	1.21E-02	1.54E-03	2.65E-02	2.59E-03
BLT M	6.97E-02	1.38E-04	3.15E-03	1.63E-02	2.04E-05	1.32E-02	7.89E-04	2.97E-02	6.18E-03

APPENDIX-3.5: PROTEIN EXPRESSION OF DRUG TRANSPORTERS BY QUANTITATIVE TARGETTED ABSOLUTE PROTEOMICS IN HUMANIZED MICE DOSING COHORTS
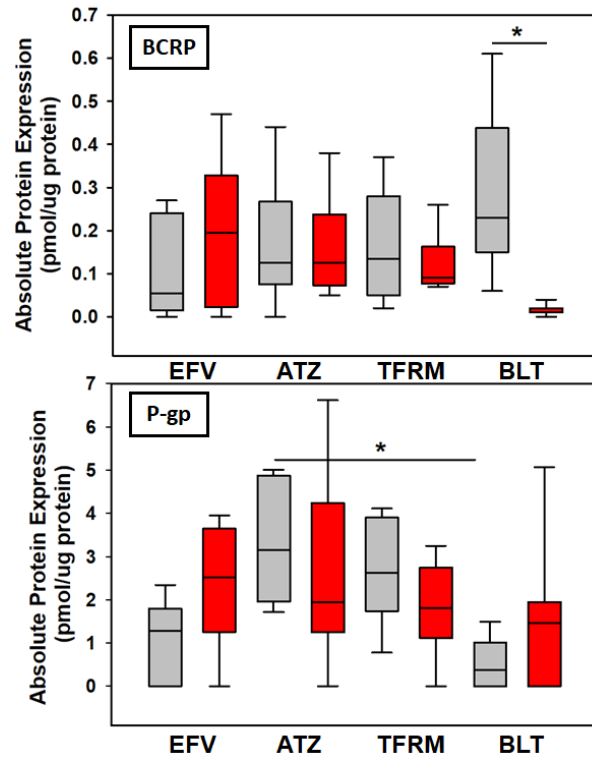
EFV: hu-HS-RAG mice dosed with efavirenz only

ATZ: hu-HSC-RAG mice dosed with atazanavir only

TFRM: hu-HSC-RAG mice dosed with tenofovir, emtricitabine, raltegravir and maraviroc

BLT: BLT mice

Uninfected (gray) and infected (red) cohorts are indicated

* denotes significant differences ($p < 0.05$) with a one-way ANOVA test

APPENDIX-3.6: PROTEIN EXPRESSION OF DRUG TRANSPORTERS BY QUANTITATIVE TARGETTED ABSOLUTE PROTEOMICS ACROSS ALL THE INDIVIDUAL ANIMALS

Specimen/Animal ID	Drug Transporter Protein Concentration (pmol/mg protein)[1]	
	BCRP	PGP
Uninfected Macaques		
40905	0.97	0.21
41033	0.89	0.11
42109	1.15	1.65
39510	1.10	0.85
42528	0.66	0.24
40585	1.88	0.27
42474	2.51	2.38
41735	4.27	4.46
Infected Macaques		
40437	2.40	1.57
42226	1.80	BLQ
42971	1.25	0.26
42827	1.24	0.91
41380	2.37	0.63
42966	2.13	BLQ
42707	2.29	2.29
40422	2.99	2.36

42706	1.71	1.975
42350	2.79	3.36
Uninfected EFV hu-HSC-RAG		
1590	BLQ	BLQ
1592	0.23	2.34
1594	0.27	BLQ
1606	BLQ	1.49
1628	0.11	1.61
1641	BLQ	1.07
Infected EFV hu-HSC-RAG		
1831	BLQ	1.92
2110	0.47	1.97
2118	0.28	6.62
2125	0.25	3.44
2246	0.14	BLQ
2254	BLQ	1.66
Uninfected TFRM hu-HSC-RAG		
1686	BLQ	0.78
1698	0.25	3.07
1699	0.16	3.84
1712	0.37	4.11
1713	BLQ	2.18
1649	BLQ	2.05

Infected TFRM hu-HSC-RAG		
1756	0.26	1.49
1784	0.13	1.58
1803	BLQ	2.58
2132	BLQ	2.03
2242	BLQ	BLQ
2244	BLQ	3.25
Uninfected ATZ hu-HSC-RAG		
1670	BLQ	2.04
1700	0.12	2.24
1701	BLQ	4.06
1706	0.21	1.71
1707	0.13	5.01
1708	0.44	4.83
Infected ATZ hu-HSC-RAG		
2097	0.19	1.92
2108	0.12	1.97
2109	BLQ	6.62
2116	0.11	3.44
2255	0.14	BLQ
2256	0.38	1.66
Uninfected BLT		
BLT A	0.18	BLQ

BLT B	0.24	BLQ
BLT C	0.11	0.76
BLT D	0.38	0.85
BLT E	0.61	1.49
BLT F	0.22	BLQ
Infected BLT		
BLT G	BLQ	1.46
BLT H	BLQ	BLQ
BLT I	0.12	5.07
BLT J	BLQ	1.95
BLT K	BLQ	1.84
BLT L	BLQ	BLQ
BLT M	BLQ	0.65

[1]BLQ indicates that transporter concentration was <0.1 pmol/mg of protein

APPENDIX-4.1: INCLUSION AND EXCLUSION CRITERIA FOR THE THINC CLINICAL STUDY

I.   **Cohort A (Treatment naïve patients)**

Inclusion Criteria

1. Men and women age > 18 years

2. HIV Positive

3. Treatment Naïve*

4. Ability to provide informed consent

5. CD4 count < 400 cells/µL any time prior to study entry

6. Plasma viral load > 5,000 c/mL within 90 days prior to study entry

7. Hemoglobin > 10 Gms/dL within 60 days prior to study entry

8. Neurologic examination by a physician revealing no contraindication to LP (if examination suggests any suspicion of space-occupying brain mass lesion, a cranial computer tomographic (CT) scan without contrast must show no such lesion)

9. Platelet count greater than or equal to 50,000 cells/mm3

10. Prothrombin time (PT) or partial thromboplastin time (PTT): The PT must be documented to be less than or equal to the upper limit of normal or an INR of less than 1.3 prior to study entry. The PTT must be less than or equal to the upper limit of normal.

Exclusion Criteria

1. HIV Negative

2. Allergy to skin numbing medications for LP

3. Any active psychiatric illness including schizophrenia, severe depression, or severe bipolar affective disorder that, in the opinion of the investigator, could confound the analysis of the neurological examination or neuropsychological test results

4. Active drug or alcohol abuse that, in the investigator's opinion, could prevent compliance with study procedures or confound the analysis of study endpoints

5. Active brain infection (except for HIV-1), fungal meningitis, toxoplasmosis, central nervous system (CNS) lymphoma, brain neoplasm, or space-occupying brain lesion requiring acute or chronic therapy

6. Ongoing maintenance treatment for any of the above lesions

---

*HIV subjects naïve to antiretroviral therapy in whom antiretroviral therapy is planned by the treating physician can be enrolled. The study design does not propose to assign study subjects to any specific class or type of antiretroviral therapy.

*Subjects will be considered treatment naïve if they have had NO greater than 7 days of ARVs

*Subjects will be considered treatment naïve if they have had greater than 7 days of ARVs but the period of treatment was at least 12 months before enrolling in the study

II.   Cohort B (Treatment experienced patients)

Inclusion Criteria

1. Men and women age > 18 years

2. HIV positive

3. Ability to provide informed consent

4. CD4 < 400 cells/µL prior to the initiation of cART

5. Hemoglobin > 10gms/dl

6. On stable ARV regimen (no changes in regiment at least 3 months prior to study entry)

7. cART for greater than or equal to 12 months prior to study entry

8. Plasma viral load < 200 c/mL for > 12 months (Must have a minimum of 2 measures before study entry)

9. Neurologic examination by a physician revealing no contraindication to LP (If examination suggests any suspicion of a space-occupying brain mass lesion, a cranial computed tomographic (CT) scan without contrast must show no such lesion)

10. Platelet count greater than or equal to 50,000 cells/mm3

11. Prothrombin time (PT) or partial thromboplastin time (PTT): The PT must be documented to be less than or equal to the upper limit of normal or an INR of less than 1.3 prior to study entry. The PTT must be less than or equal to the upper limit of normal.

Exclusion Criteria

1. HIV Negative

2. Allergy to skin numbing medications for LP

3. Any active psychiatric illness including schizophrenia, severe depression, or severe bipolar affective disorder that, in the opinion of the investigator, could confound the analysis of the neurologic examination or neuropsychological test results

4. Active drug or alcohol abuse that, in the investigator's opinion, could prevent compliance with study procedures or confound the analysis of study endpoints

5. Active brain infection (except for HIV-1), fungal meningitis, toxoplasmosis, central nervous system (CNS) lymphoma, brain neoplasm, or space-occupying brain lesion requiring acute or chronic therapy

6. Ongoing maintenance treatment for any of the above lesions

7. Allergy to skin numbing medications for LP

8. Any active psychiatric illness including schizophrenia, severe depression, or severe bipolar affective disorder that, in the opinion of the investigator, could confound the analysis of the neurological examination or neuropsychological test results.

APPENDIX-4.2: DATASET AND MODEL CODE USED IN THE FINAL RHESUS MACAQUE ITERATIVE TWO-STAGE ESTIMATION PK MODEL

Dataset: Source file – EFV_population_NHP.dat

m40437

7

1

12

0.00000	2.105	7.97	0.167	24.36	4.625	1.462	6.414	200.00
24.0000	2.105	7.97	0.167	24.36	4.625	1.462	6.414	200.00
48.0000	2.105	7.97	0.167	24.36	4.625	1.462	6.414	200.00
72.0000	2.105	7.97	0.167	24.36	4.625	1.462	6.414	200.00
96.0000	2.105	7.97	0.167	24.36	4.625	1.462	6.414	200.00
120.000	2.105	7.97	0.167	24.36	4.625	1.462	6.414	200.00
144.000	2.105	7.97	0.167	24.36	4.625	1.462	6.414	200.00
168.000	2.105	7.97	0.167	24.36	4.625	1.462	6.414	200.00
192.000	2.105	7.97	0.167	24.36	4.625	1.462	6.414	200.00
216.000	2.105	7.97	0.167	24.36	4.625	1.462	6.414	200.00
240.000	2.105	7.97	0.167	24.36	4.625	1.462	6.414	200.00
268.000	2.105	7.97	0.167	24.36	4.625	1.462	6.414	200.00

3

8

0.000000	0.000000	-1.000000	-1.000000
4.000000	3.290000	-1.000000	-1.000000
10.000000	2.610000	-1.000000	-1.000000
23.500000	2.0400000	-1.000000	-1.000000
95.500000	0.2120000	-1.000000	-1.000000
143.500000	0.0466000	-1.000000	-1.000000
216.000000	0.0392000	-1.000000	-1.000000

239.500000   0.0593000   0.0005000   0.2398190

m40905

7

1

12

0.000 18.2 6.61 0.574 14.08 3.601 0.318 0.7983 200.00

24.00 18.2 6.61 0.574 14.08 3.601 0.318 0.7983 200.00

48.00 18.2 6.61 0.574 14.08 3.601 0.318 0.7983 200.00

72.00 18.2 6.61 0.574 14.08 3.601 0.318 0.7983 200.00

96.00 18.2 6.61 0.574 14.08 3.601 0.318 0.7983 200.00

120.0 18.2 6.61 0.574 14.08 3.601 0.318 0.7983 200.00

144.0 18.2 6.61 0.574 14.08 3.601 0.318 0.7983 200.00

168.0 18.2 6.61 0.574 14.08 3.601 0.318 0.7983 200.00

192.0 18.2 6.61 0.574 14.08 3.601 0.318 0.7983 200.00

216.0 18.2 6.61 0.574 14.08 3.601 0.318 0.7983 200.00

240.0 18.2 6.61 0.574 14.08 3.601 0.318 0.7983 200.00

268.0 18.2 6.61 0.574 14.08 3.601 0.318 0.7983 200.00

3

9

0.000000   0.000000   -1.000000   -1.000000

4.000000   0.385000   -1.000000   -1.000000

10.000000   0.616000   -1.000000   -1.000000

23.500000   0.1300000   -1.000000   -1.000000

95.500000   0.0570000   -1.000000   -1.000000

143.500000   0.0709000   -1.000000   -1.000000

191.500000   0.0566000   -1.000000   -1.000000

239.500000   0.1020000   -1.000000   -1.000000

263.500000   0.2870000   0.0033800   1.9829390

m41033

7

1

12

0.000	4.877	6.938	0.4991	15.46	3.603	0.324	2.854	200.00
24.00	4.877	6.938	0.4991	15.46	3.603	0.324	2.854	200.00
48.00	4.877	6.938	0.4991	15.46	3.603	0.324	2.854	200.00
72.00	4.877	6.938	0.4991	15.46	3.603	0.324	2.854	200.00
96.00	4.877	6.938	0.4991	15.46	3.603	0.324	2.854	200.00
120.0	4.877	6.938	0.4991	15.46	3.603	0.324	2.854	200.00
144.0	4.877	6.938	0.4991	15.46	3.603	0.324	2.854	200.00
168.0	4.877	6.938	0.4991	15.46	3.603	0.324	2.854	200.00
192.0	4.877	6.938	0.4991	15.46	3.603	0.324	2.854	200.00
216.0	4.877	6.938	0.4991	15.46	3.603	0.324	2.854	200.00
240.0	4.877	6.938	0.4991	15.46	3.603	0.324	2.854	200.00
268.0	4.877	6.938	0.4991	15.46	3.603	0.324	2.854	200.00

3

9

0.000000	0.000000	-1.000000	-1.000000
4.000000	0.757000	-1.000000	-1.000000
10.000000	2.310000	-1.000000	-1.000000
23.500000	0.851000	-1.000000	-1.000000
95.500000	0.2120000	-1.000000	-1.000000
143.500000	0.1400000	-1.000000	-1.000000
215.500000	0.2120000	-1.000000	-1.000000
263.500000	0.0950000	-1.000000	-1.000000
287.500000	0.2150000	0.0013800	0.9652010

m42109

7

1

12

0.00000	21.15	6.743	0.169	14.42	3.484	1.115	0.41	200.00
24.0000	21.15	6.743	0.169	14.42	3.484	1.115	0.41	200.00
48.0000	21.15	6.743	0.169	14.42	3.484	1.115	0.41	200.00
72.0000	21.15	6.743	0.169	14.42	3.484	1.115	0.41	200.00
96.0000	21.15	6.743	0.169	14.42	3.484	1.115	0.41	200.00
120.000	21.15	6.743	0.169	14.42	3.484	1.115	0.41	200.00
144.000	21.15	6.743	0.169	14.42	3.484	1.115	0.41	200.00
168.000	21.15	6.743	0.169	14.42	3.484	1.115	0.41	200.00
192.000	21.15	6.743	0.169	14.42	3.484	1.115	0.41	200.00
216.000	21.15	6.743	0.169	14.42	3.484	1.115	0.41	200.00
240.000	21.15	6.743	0.169	14.42	3.484	1.115	0.41	200.00
268.000	21.15	6.743	0.169	14.42	3.484	1.115	0.41	200.00

3

9

0.000000	0.000000	-1.000000	-1.000000
4.000000	0.833000	-1.000000	-1.000000
10.000000	0.438000	-1.000000	-1.000000
23.500000	0.0693000	-1.000000	-1.000000
95.500000	0.2340000	-1.000000	-1.000000
143.500000	0.1380000	-1.000000	-1.000000
215.500000	0.0847000	-1.000000	-1.000000
263.500000	0.1240000	-1.000000	-1.000000
287.500000	0.3710000	0.0020600	1.6151680

m42226

7

1

12

0.00000	3.867	7.164	0.453	18.17	4.057	0.782	1.845	200.00

24.0000	3.867	7.164	0.453	18.17	4.057	0.782	1.845	200.00
48.0000	3.867	7.164	0.453	18.17	4.057	0.782	1.845	200.00
72.0000	3.867	7.164	0.453	18.17	4.057	0.782	1.845	200.00
96.0000	3.867	7.164	0.453	18.17	4.057	0.782	1.845	200.00
120.000	3.867	7.164	0.453	18.17	4.057	0.782	1.845	200.00
144.000	3.867	7.164	0.453	18.17	4.057	0.782	1.845	200.00
168.000	3.867	7.164	0.453	18.17	4.057	0.782	1.845	200.00
192.000	3.867	7.164	0.453	18.17	4.057	0.782	1.845	200.00
216.000	3.867	7.164	0.453	18.17	4.057	0.782	1.845	200.00
240.000	3.867	7.164	0.453	18.17	4.057	0.782	1.845	200.00
268.000	3.867	7.164	0.453	18.17	4.057	0.782	1.845	200.00

3

9

0.000000	0.0000000	-1.000000	-1.000000
4.000000	3.3300000	-1.000000	-1.000000
10.000000	2.6500000	-1.000000	-1.000000
23.500000	0.6330000	-1.000000	-1.000000
95.500000	0.2250000	-1.000000	-1.000000
143.500000	0.1880000	-1.000000	-1.000000
191.500000	0.1260000	-1.000000	-1.000000
239.500000	0.1760000	-1.000000	-1.000000
263.500000	0.1830000	0.0013900	0.7922860

m42474

7

1

12

0.00000	6.712	9.827	0.427	7.213	5.23	0.411	13.39	200.00
24.0000	6.712	9.827	0.427	7.213	5.23	0.411	13.39	200.00
48.0000	6.712	9.827	0.427	7.213	5.23	0.411	13.39	200.00

72.0000	6.712	9.827	0.427	7.213	5.23	0.411	13.39	200.00
96.0000	6.712	9.827	0.427	7.213	5.23	0.411	13.39	200.00
120.000	6.712	9.827	0.427	7.213	5.23	0.411	13.39	200.00
144.000	6.712	9.827	0.427	7.213	5.23	0.411	13.39	200.00
168.000	6.712	9.827	0.427	7.213	5.23	0.411	13.39	200.00
192.000	6.712	9.827	0.427	7.213	5.23	0.411	13.39	200.00
216.000	6.712	9.827	0.427	7.213	5.23	0.411	13.39	200.00
240.000	6.712	9.827	0.427	7.213	5.23	0.411	13.39	200.00
268.000	6.712	9.827	0.427	7.213	5.23	0.411	13.39	200.00

3

7

0.000000	0.000000	-1.000000	-1.000000
4.000000	0.4700000	-1.000000	-1.000000
10.000000	2.9400000	-1.000000	-1.000000
23.500000	0.2740000	-1.000000	-1.000000
143.500000	0.0060500	-1.000000	-1.000000
215.500000	0.0092000	-1.000000	-1.000000
263.500000	0.0062700	0.0005000	0.2930570

m42707

7

1

12

0.00000	10.91	6.57	0.832	26.19	4.11	0.462	1.04	200.00
24.0000	10.91	6.57	0.832	26.19	4.11	0.462	1.04	200.00
48.0000	10.91	6.57	0.832	26.19	4.11	0.462	1.04	200.00
72.0000	10.91	6.57	0.832	26.19	4.11	0.462	1.04	200.00
96.0000	10.91	6.57	0.832	26.19	4.11	0.462	1.04	200.00
120.000	10.91	6.57	0.832	26.19	4.11	0.462	1.04	200.00
144.000	10.91	6.57	0.832	26.19	4.11	0.462	1.04	200.00

168.000	10.91	6.57	0.832	26.19	4.11	0.462	1.04	200.00
192.000	10.91	6.57	0.832	26.19	4.11	0.462	1.04	200.00
216.000	10.91	6.57	0.832	26.19	4.11	0.462	1.04	200.00
240.000	10.91	6.57	0.832	26.19	4.11	0.462	1.04	200.00
268.000	10.91	6.57	0.832	26.19	4.11	0.462	1.04	200.00

3

8

0.000000	0.000000	-1.000000	-1.000000
4.000000	1.2500000	-1.000000	-1.000000
10.000000	0.6030000	-1.000000	-1.000000
23.500000	0.1430000	-1.000000	-1.000000
95.500000	0.1130000	-1.000000	-1.000000
167.500000	0.0373000	-1.000000	-1.000000
215.500000	0.0412000	-1.000000	-1.000000
239.500000	0.1840000	0.0005000	0.7585000

m42971

7

1

12

0.00000	14.76	5.75	0.794	16.34	3.26	0.394	1.17	200.00
24.0000	14.76	5.75	0.794	16.34	3.26	0.394	1.17	200.00
48.0000	14.76	5.75	0.794	16.34	3.26	0.394	1.17	200.00
72.0000	14.76	5.75	0.794	16.34	3.26	0.394	1.17	200.00
96.0000	14.76	5.75	0.794	16.34	3.26	0.394	1.17	200.00
120.000	14.76	5.75	0.794	16.34	3.26	0.394	1.17	200.00
144.000	14.76	5.75	0.794	16.34	3.26	0.394	1.17	200.00
168.000	14.76	5.75	0.794	16.34	3.26	0.394	1.17	200.00
192.000	14.76	5.75	0.794	16.34	3.26	0.394	1.17	200.00
216.000	14.76	5.75	0.794	16.34	3.26	0.394	1.17	200.00

240.000	14.76	5.75	0.794	16.34	3.26	0.394	1.17	200.00
268.000	14.76	5.75	0.794	16.34	3.26	0.394	1.17	200.00

3

9

0.000000	0.000000	-1.000000	-1.000000
4.000000	0.827000	-1.000000	-1.000000
10.000000	0.3870000	-1.000000	-1.000000
23.500000	0.0894000	-1.000000	-1.000000
95.500000	0.0750000	-1.000000	-1.000000
143.500000	0.0583000	-1.000000	-1.000000
191.500000	0.0339000	-1.000000	-1.000000
239.500000	0.0409000	-1.000000	-1.000000
263.500000	0.0927000	0.0005000	0.3915840

Model code: Source file – EFV_population_NHP.for

```
C###############################################################
###C

        Subroutine DIFFEQ(T,X,XP)
        Implicit None

        Include 'globals.inc'
        Include 'model.inc'

        Real*8 T,X(MaxNDE),XP(MaxNDE), CL,V2,Ka,V3,CLD,TAU,M,Kpc,Kcp
        Real*8 Kpb,Kbp,Kcb,Kbc,V8

CC
C-------------------------------------------------------------------
---C
C   Enter Differential Equations Below  {e.g.  XP(1) = -P(1)*X(1) }
C
C----c-------------------------------------------------------------
---C


          CL=P(1)
          IF (T.GT.24) CL=(P(7))*CL
          V2=P(2)+0.01
          Ka=P(3)
          V3=P(4)
          CLD=P(5)
          TAU=P(6)
          M=P(7)
          Kpc=P(8) !plasma-CSF rate
          Kcp=P(9) !CSF-plasma rate
          Kpb=P(10) !plasma-brain rate
          Kbp=P(11) !brain-plasma rate
          Kcb=P(12) !CSF-brain rate
          Kbc=P(13) !brain-CSF rate
          V8=P(14)+0.000001 !brain volume


       XP(1) = -TAU*X(1)
      XP(2) = TAU*X(1) -TAU*X(2)
      XP(3) = TAU*X(2) - TAU*X(3)
      XP(4) = TAU*X(3) -Ka*X(4)
       XP(5) = Ka*X(4)- CL*(X(5)/V2)- CLD*(X(5)/V2)
    x      + CLD*(X(6)/V3)
      XP(6) = CLD*(X(5)/V2)- CLD*(X(6)/V3)
      XP(7) = Kpc*X(5) -Kcp*X(7) -Kcb*X(7) +Kbc*X(8) !CSF
      XP(8) = Kcb*X(7) -Kbc*X(7) +Kpb*X(8) -Kbp*X(8) !brain
```

Dataset: Source file – EFV_population_human2.dat

p3006

6

1

31

0.0	14.6561	156.829	0.131	405.579	6.34	1	600
24.0	14.6561	156.829	0.131	405.579	6.34	1	600
48.0	14.6561	156.829	0.131	405.579	6.34	1	600
72.0	14.6561	156.829	0.131	405.579	6.34	1	600
96.0	14.6561	156.829	0.131	405.579	6.34	1	600
120.0	14.6561	156.829	0.131	405.579	6.34	1	600
144.0	14.6561	156.829	0.131	405.579	6.34	1	600
168.0	14.6561	156.829	0.131	405.579	6.34	1	600
192.0	14.6561	156.829	0.131	405.579	6.34	1	600
216.0	14.6561	156.829	0.131	405.579	6.34	1	600
240.0	14.6561	156.829	0.131	405.579	6.34	1	600
264.0	14.6561	156.829	0.131	405.579	6.34	1	600
288.0	14.6561	156.829	0.131	405.579	6.34	1	600
312.0	14.6561	156.829	0.131	405.579	6.34	1	600
336.0	14.6561	156.829	0.131	405.579	6.34	1	600
360.0	14.6561	156.829	0.131	405.579	6.34	1	600
384.0	14.6561	156.829	0.131	405.579	6.34	1	600
408.0	14.6561	156.829	0.131	405.579	6.34	1	600
432.0	14.6561	156.829	0.131	405.579	6.34	1	600
456.0	14.6561	156.829	0.131	405.579	6.34	1	600
480.0	14.6561	156.829	0.131	405.579	6.34	1	600

504.0	14.6561	156.829	0.131	405.579	6.34	1	600
528.0	14.6561	156.829	0.131	405.579	6.34	1	600
552.0	14.6561	156.829	0.131	405.579	6.34	1	600
576.0	14.6561	156.829	0.131	405.579	6.34	1	600
600.0	14.6561	156.829	0.131	405.579	6.34	1	600
624.0	14.6561	156.829	0.131	405.579	6.34	1	600
648.0	14.6561	156.829	0.131	405.579	6.34	1	600
672.0	14.6561	156.829	0.131	405.579	6.34	1	600
696.0	14.6561	156.829	0.131	405.579	6.34	1	600
720.0	14.6561	156.829	0.131	405.579	6.34	1	600

2

2

732.170000	2.0816000	-1.000000
736.780000	-1.000000	0.0804000

p3007

6

1

31

0.0	22.59	160.16	0.12	405.38	6.41	1	600
24.0	22.59	160.16	0.12	405.38	6.41	1	600
48.0	22.59	160.16	0.12	405.38	6.41	1	600
72.0	22.59	160.16	0.12	405.38	6.41	1	600
96.0	22.59	160.16	0.12	405.38	6.41	1	600
120.0	22.59	160.16	0.12	405.38	6.41	1	600
144.0	22.59	160.16	0.12	405.38	6.41	1	600
168.0	22.59	160.16	0.12	405.38	6.41	1	600
192.0	22.59	160.16	0.12	405.38	6.41	1	600
216.0	22.59	160.16	0.12	405.38	6.41	1	600
240.0	22.59	160.16	0.12	405.38	6.41	1	600

264.0	22.59	160.16	0.12	405.38	6.41	1	600
288.0	22.59	160.16	0.12	405.38	6.41	1	600
312.0	22.59	160.16	0.12	405.38	6.41	1	600
336.0	22.59	160.16	0.12	405.38	6.41	1	600
360.0	22.59	160.16	0.12	405.38	6.41	1	600
384.0	22.59	160.16	0.12	405.38	6.41	1	600
408.0	22.59	160.16	0.12	405.38	6.41	1	600
432.0	22.59	160.16	0.12	405.38	6.41	1	600
456.0	22.59	160.16	0.12	405.38	6.41	1	600
480.0	22.59	160.16	0.12	405.38	6.41	1	600
504.0	22.59	160.16	0.12	405.38	6.41	1	600
528.0	22.59	160.16	0.12	405.38	6.41	1	600
552.0	22.59	160.16	0.12	405.38	6.41	1	600
576.0	22.59	160.16	0.12	405.38	6.41	1	600
600.0	22.59	160.16	0.12	405.38	6.41	1	600
624.0	22.59	160.16	0.12	405.38	6.41	1	600
648.0	22.59	160.16	0.12	405.38	6.41	1	600
672.0	22.59	160.16	0.12	405.38	6.41	1	600
696.0	22.59	160.16	0.12	405.38	6.41	1	600
720.0	22.59	160.16	0.12	405.38	6.41	1	600

2

2

731.50000   1.4086000   -1.000000

735.83000   -1.000000   0.0604000

p3013

6

1

31

0.0	14.36	156.39	0.13	405.2	6.37	1	600

24.0	14.36	156.39	0.13	405.2	6.37	1	600
48.0	14.36	156.39	0.13	405.2	6.37	1	600
72.0	14.36	156.39	0.13	405.2	6.37	1	600
96.0	14.36	156.39	0.13	405.2	6.37	1	600
120.0	14.36	156.39	0.13	405.2	6.37	1	600
144.0	14.36	156.39	0.13	405.2	6.37	1	600
168.0	14.36	156.39	0.13	405.2	6.37	1	600
192.0	14.36	156.39	0.13	405.2	6.37	1	600
216.0	14.36	156.39	0.13	405.2	6.37	1	600
240.0	14.36	156.39	0.13	405.2	6.37	1	600
264.0	14.36	156.39	0.13	405.2	6.37	1	600
288.0	14.36	156.39	0.13	405.2	6.37	1	600
312.0	14.36	156.39	0.13	405.2	6.37	1	600
336.0	14.36	156.39	0.13	405.2	6.37	1	600
360.0	14.36	156.39	0.13	405.2	6.37	1	600
384.0	14.36	156.39	0.13	405.2	6.37	1	600
408.0	14.36	156.39	0.13	405.2	6.37	1	600
432.0	14.36	156.39	0.13	405.2	6.37	1	600
456.0	14.36	156.39	0.13	405.2	6.37	1	600
480.0	14.36	156.39	0.13	405.2	6.37	1	600
504.0	14.36	156.39	0.13	405.2	6.37	1	600
528.0	14.36	156.39	0.13	405.2	6.37	1	600
552.0	14.36	156.39	0.13	405.2	6.37	1	600
576.0	14.36	156.39	0.13	405.2	6.37	1	600
600.0	14.36	156.39	0.13	405.2	6.37	1	600
624.0	14.36	156.39	0.13	405.2	6.37	1	600
648.0	14.36	156.39	0.13	405.2	6.37	1	600
672.0	14.36	156.39	0.13	405.2	6.37	1	600
696.0	14.36	156.39	0.13	405.2	6.37	1	600

720.0	14.36	156.39	0.13	405.2	6.37	1	600

2

2

733.350000	2.0585000	-1.000000
736.750000	-1.000000	0.0412000

p3014

6

1

31

0.0	17.99	156.28	0.13	405.47	6.41	1	600
24.0	17.99	156.28	0.13	405.47	6.41	1	600
48.0	17.99	156.28	0.13	405.47	6.41	1	600
72.0	17.99	156.28	0.13	405.47	6.41	1	600
96.0	17.99	156.28	0.13	405.47	6.41	1	600
120.0	17.99	156.28	0.13	405.47	6.41	1	600
144.0	17.99	156.28	0.13	405.47	6.41	1	600
168.0	17.99	156.28	0.13	405.47	6.41	1	600
192.0	17.99	156.28	0.13	405.47	6.41	1	600
216.0	17.99	156.28	0.13	405.47	6.41	1	600
240.0	17.99	156.28	0.13	405.47	6.41	1	600
264.0	17.99	156.28	0.13	405.47	6.41	1	600
288.0	17.99	156.28	0.13	405.47	6.41	1	600
312.0	17.99	156.28	0.13	405.47	6.41	1	600
336.0	17.99	156.28	0.13	405.47	6.41	1	600
360.0	17.99	156.28	0.13	405.47	6.41	1	600
384.0	17.99	156.28	0.13	405.47	6.41	1	600
408.0	17.99	156.28	0.13	405.47	6.41	1	600
432.0	17.99	156.28	0.13	405.47	6.41	1	600
456.0	17.99	156.28	0.13	405.47	6.41	1	600

480.0	17.99	156.28	0.13	405.47	6.41	1	600
504.0	17.99	156.28	0.13	405.47	6.41	1	600
528.0	17.99	156.28	0.13	405.47	6.41	1	600
552.0	17.99	156.28	0.13	405.47	6.41	1	600
576.0	17.99	156.28	0.13	405.47	6.41	1	600
600.0	17.99	156.28	0.13	405.47	6.41	1	600
624.0	17.99	156.28	0.13	405.47	6.41	1	600
648.0	17.99	156.28	0.13	405.47	6.41	1	600
672.0	17.99	156.28	0.13	405.47	6.41	1	600
696.0	17.99	156.28	0.13	405.47	6.41	1	600
720.0	17.99	156.28	0.13	405.47	6.41	1	600

2

2

733.470000	1.6553000	-1.000000
736.880000	-1.000000	0.0234000

p3017

6

1

31

0.0	9.58	154.17	0.14	405.53	6.3	1	600
24.0	9.58	154.17	0.14	405.53	6.3	1	600
48.0	9.58	154.17	0.14	405.53	6.3	1	600
72.0	9.58	154.17	0.14	405.53	6.3	1	600
96.0	9.58	154.17	0.14	405.53	6.3	1	600
120.0	9.58	154.17	0.14	405.53	6.3	1	600
144.0	9.58	154.17	0.14	405.53	6.3	1	600
168.0	9.58	154.17	0.14	405.53	6.3	1	600
192.0	9.58	154.17	0.14	405.53	6.3	1	600
216.0	9.58	154.17	0.14	405.53	6.3	1	600

240.0	9.58	154.17	0.14	405.53	6.3	1	600
264.0	9.58	154.17	0.14	405.53	6.3	1	600
288.0	9.58	154.17	0.14	405.53	6.3	1	600
312.0	9.58	154.17	0.14	405.53	6.3	1	600
336.0	9.58	154.17	0.14	405.53	6.3	1	600
360.0	9.58	154.17	0.14	405.53	6.3	1	600
384.0	9.58	154.17	0.14	405.53	6.3	1	600
408.0	9.58	154.17	0.14	405.53	6.3	1	600
432.0	9.58	154.17	0.14	405.53	6.3	1	600
456.0	9.58	154.17	0.14	405.53	6.3	1	600
480.0	9.58	154.17	0.14	405.53	6.3	1	600
504.0	9.58	154.17	0.14	405.53	6.3	1	600
528.0	9.58	154.17	0.14	405.53	6.3	1	600
552.0	9.58	154.17	0.14	405.53	6.3	1	600
576.0	9.58	154.17	0.14	405.53	6.3	1	600
600.0	9.58	154.17	0.14	405.53	6.3	1	600
624.0	9.58	154.17	0.14	405.53	6.3	1	600
648.0	9.58	154.17	0.14	405.53	6.3	1	600
672.0	9.58	154.17	0.14	405.53	6.3	1	600
696.0	9.58	154.17	0.14	405.53	6.3	1	600
720.0	9.58	154.17	0.14	405.53	6.3	1	600

2

2

733.500000   3.0087000   -1.000000

736.920000   -1.000000   0.4860000

p3019

6

1

31

0.0	8.72	153.38	0.14	405.17	6.31	1	600
24.0	8.72	153.38	0.14	405.17	6.31	1	600
48.0	8.72	153.38	0.14	405.17	6.31	1	600
72.0	8.72	153.38	0.14	405.17	6.31	1	600
96.0	8.72	153.38	0.14	405.17	6.31	1	600
120.0	8.72	153.38	0.14	405.17	6.31	1	600
144.0	8.72	153.38	0.14	405.17	6.31	1	600
168.0	8.72	153.38	0.14	405.17	6.31	1	600
192.0	8.72	153.38	0.14	405.17	6.31	1	600
216.0	8.72	153.38	0.14	405.17	6.31	1	600
240.0	8.72	153.38	0.14	405.17	6.31	1	600
264.0	8.72	153.38	0.14	405.17	6.31	1	600
288.0	8.72	153.38	0.14	405.17	6.31	1	600
312.0	8.72	153.38	0.14	405.17	6.31	1	600
336.0	8.72	153.38	0.14	405.17	6.31	1	600
360.0	8.72	153.38	0.14	405.17	6.31	1	600
384.0	8.72	153.38	0.14	405.17	6.31	1	600
408.0	8.72	153.38	0.14	405.17	6.31	1	600
432.0	8.72	153.38	0.14	405.17	6.31	1	600
456.0	8.72	153.38	0.14	405.17	6.31	1	600
480.0	8.72	153.38	0.14	405.17	6.31	1	600
504.0	8.72	153.38	0.14	405.17	6.31	1	600
528.0	8.72	153.38	0.14	405.17	6.31	1	600
552.0	8.72	153.38	0.14	405.17	6.31	1	600
576.0	8.72	153.38	0.14	405.17	6.31	1	600
600.0	8.72	153.38	0.14	405.17	6.31	1	600
624.0	8.72	153.38	0.14	405.17	6.31	1	600
648.0	8.72	153.38	0.14	405.17	6.31	1	600
672.0	8.72	153.38	0.14	405.17	6.31	1	600

696.0	8.72	153.38	0.14	405.17	6.31	1	600
720.0	8.72	153.38	0.14	405.17	6.31	1	600

2

2

732.080000	3.3657000	-1.000000
735.000000	-1.000000	0.0726000

p3021

6

1

31

0.0	11.46	154.9	0.136	405.47	6.34	1	600
24.0	11.46	154.9	0.136	405.47	6.34	1	600
48.0	11.46	154.9	0.136	405.47	6.34	1	600
72.0	11.46	154.9	0.136	405.47	6.34	1	600
96.0	11.46	154.9	0.136	405.47	6.34	1	600
120.0	11.46	154.9	0.136	405.47	6.34	1	600
144.0	11.46	154.9	0.136	405.47	6.34	1	600
168.0	11.46	154.9	0.136	405.47	6.34	1	600
192.0	11.46	154.9	0.136	405.47	6.34	1	600
216.0	11.46	154.9	0.136	405.47	6.34	1	600
240.0	11.46	154.9	0.136	405.47	6.34	1	600
264.0	11.46	154.9	0.136	405.47	6.34	1	600
288.0	11.46	154.9	0.136	405.47	6.34	1	600
312.0	11.46	154.9	0.136	405.47	6.34	1	600
336.0	11.46	154.9	0.136	405.47	6.34	1	600
360.0	11.46	154.9	0.136	405.47	6.34	1	600
384.0	11.46	154.9	0.136	405.47	6.34	1	600
408.0	11.46	154.9	0.136	405.47	6.34	1	600
432.0	11.46	154.9	0.136	405.47	6.34	1	600

456.0	11.46	154.9	0.136	405.47	6.34	1	600
480.0	11.46	154.9	0.136	405.47	6.34	1	600
504.0	11.46	154.9	0.136	405.47	6.34	1	600
528.0	11.46	154.9	0.136	405.47	6.34	1	600
552.0	11.46	154.9	0.136	405.47	6.34	1	600
576.0	11.46	154.9	0.136	405.47	6.34	1	600
600.0	11.46	154.9	0.136	405.47	6.34	1	600
624.0	11.46	154.9	0.136	405.47	6.34	1	600
648.0	11.46	154.9	0.136	405.47	6.34	1	600
672.0	11.46	154.9	0.136	405.47	6.34	1	600
696.0	11.46	154.9	0.136	405.47	6.34	1	600
720.0	11.46	154.9	0.136	405.47	6.34	1	600

2

2

724.650000	2.1173000	-1.000000
727.500000	-1.000000	0.0715000

p3023

6

1

31

0.0	24.15	159.17	0.12	404.9	6.43	1	600
24.0	24.15	159.17	0.12	404.9	6.43	1	600
48.0	24.15	159.17	0.12	404.9	6.43	1	600
72.0	24.15	159.17	0.12	404.9	6.43	1	600
96.0	24.15	159.17	0.12	404.9	6.43	1	600
120.0	24.15	159.17	0.12	404.9	6.43	1	600
144.0	24.15	159.17	0.12	404.9	6.43	1	600
168.0	24.15	159.17	0.12	404.9	6.43	1	600
192.0	24.15	159.17	0.12	404.9	6.43	1	600

216.0	24.15	159.17	0.12	404.9	6.43	1	600
240.0	24.15	159.17	0.12	404.9	6.43	1	600
264.0	24.15	159.17	0.12	404.9	6.43	1	600
288.0	24.15	159.17	0.12	404.9	6.43	1	600
312.0	24.15	159.17	0.12	404.9	6.43	1	600
336.0	24.15	159.17	0.12	404.9	6.43	1	600
360.0	24.15	159.17	0.12	404.9	6.43	1	600
384.0	24.15	159.17	0.12	404.9	6.43	1	600
408.0	24.15	159.17	0.12	404.9	6.43	1	600
432.0	24.15	159.17	0.12	404.9	6.43	1	600
456.0	24.15	159.17	0.12	404.9	6.43	1	600
480.0	24.15	159.17	0.12	404.9	6.43	1	600
504.0	24.15	159.17	0.12	404.9	6.43	1	600
528.0	24.15	159.17	0.12	404.9	6.43	1	600
552.0	24.15	159.17	0.12	404.9	6.43	1	600
576.0	24.15	159.17	0.12	404.9	6.43	1	600
600.0	24.15	159.17	0.12	404.9	6.43	1	600
624.0	24.15	159.17	0.12	404.9	6.43	1	600
648.0	24.15	159.17	0.12	404.9	6.43	1	600
672.0	24.15	159.17	0.12	404.9	6.43	1	600
696.0	24.15	159.17	0.12	404.9	6.43	1	600
720.0	24.15	159.17	0.12	404.9	6.43	1	600

2

2

731.900000   1.3143000   -1.000000

734.880000   -1.000000   0.0505000

p3027

6

1

31

0.0	14.65	156.56	0.13	405.51	6.31	1	600
24.0	14.65	156.56	0.13	405.51	6.31	1	600
48.0	14.65	156.56	0.13	405.51	6.31	1	600
72.0	14.65	156.56	0.13	405.51	6.31	1	600
96.0	14.65	156.56	0.13	405.51	6.31	1	600
120.0	14.65	156.56	0.13	405.51	6.31	1	600
144.0	14.65	156.56	0.13	405.51	6.31	1	600
168.0	14.65	156.56	0.13	405.51	6.31	1	600
192.0	14.65	156.56	0.13	405.51	6.31	1	600
216.0	14.65	156.56	0.13	405.51	6.31	1	600
240.0	14.65	156.56	0.13	405.51	6.31	1	600
264.0	14.65	156.56	0.13	405.51	6.31	1	600
288.0	14.65	156.56	0.13	405.51	6.31	1	600
312.0	14.65	156.56	0.13	405.51	6.31	1	600
336.0	14.65	156.56	0.13	405.51	6.31	1	600
360.0	14.65	156.56	0.13	405.51	6.31	1	600
384.0	14.65	156.56	0.13	405.51	6.31	1	600
408.0	14.65	156.56	0.13	405.51	6.31	1	600
432.0	14.65	156.56	0.13	405.51	6.31	1	600
456.0	14.65	156.56	0.13	405.51	6.31	1	600
480.0	14.65	156.56	0.13	405.51	6.31	1	600
504.0	14.65	156.56	0.13	405.51	6.31	1	600
528.0	14.65	156.56	0.13	405.51	6.31	1	600
552.0	14.65	156.56	0.13	405.51	6.31	1	600
576.0	14.65	156.56	0.13	405.51	6.31	1	600
600.0	14.65	156.56	0.13	405.51	6.31	1	600
624.0	14.65	156.56	0.13	405.51	6.31	1	600
648.0	14.65	156.56	0.13	405.51	6.31	1	600

672.0	14.65	156.56	0.13	405.51	6.31	1	600
696.0	14.65	156.56	0.13	405.51	6.31	1	600
720.0	14.65	156.56	0.13	405.51	6.31	1	600

2

2

732.620000	2.0606000	-1.000000
735.080000	-1.000000	0.1110000

p304

6

1

31

0.0	18.56	154.76	0.13	405.7	6.39	1	600
24.0	18.56	154.76	0.13	405.7	6.39	1	600
48.0	18.56	154.76	0.13	405.7	6.39	1	600
72.0	18.56	154.76	0.13	405.7	6.39	1	600
96.0	18.56	154.76	0.13	405.7	6.39	1	600
120.0	18.56	154.76	0.13	405.7	6.39	1	600
144.0	18.56	154.76	0.13	405.7	6.39	1	600
168.0	18.56	154.76	0.13	405.7	6.39	1	600
192.0	18.56	154.76	0.13	405.7	6.39	1	600
216.0	18.56	154.76	0.13	405.7	6.39	1	600
240.0	18.56	154.76	0.13	405.7	6.39	1	600
264.0	18.56	154.76	0.13	405.7	6.39	1	600
288.0	18.56	154.76	0.13	405.7	6.39	1	600
312.0	18.56	154.76	0.13	405.7	6.39	1	600
336.0	18.56	154.76	0.13	405.7	6.39	1	600
360.0	18.56	154.76	0.13	405.7	6.39	1	600
384.0	18.56	154.76	0.13	405.7	6.39	1	600
408.0	18.56	154.76	0.13	405.7	6.39	1	600

432.0	18.56	154.76	0.13	405.7	6.39	1	600
456.0	18.56	154.76	0.13	405.7	6.39	1	600
480.0	18.56	154.76	0.13	405.7	6.39	1	600
504.0	18.56	154.76	0.13	405.7	6.39	1	600
528.0	18.56	154.76	0.13	405.7	6.39	1	600
552.0	18.56	154.76	0.13	405.7	6.39	1	600
576.0	18.56	154.76	0.13	405.7	6.39	1	600
600.0	18.56	154.76	0.13	405.7	6.39	1	600
624.0	18.56	154.76	0.13	405.7	6.39	1	600
648.0	18.56	154.76	0.13	405.7	6.39	1	600
672.0	18.56	154.76	0.13	405.7	6.39	1	600
696.0	18.56	154.76	0.13	405.7	6.39	1	600
720.0	18.56	154.76	0.13	405.7	6.39	1	600

2

2

734.500000   1.5370000   -1.000000

735.000000   -1.000000   0.0927000

p305

6

1

31

0.0	4.87	150.6	0.146	404.2	6.34	1	600
24.0	4.87	150.6	0.146	404.2	6.34	1	600
48.0	4.87	150.6	0.146	404.2	6.34	1	600
72.0	4.87	150.6	0.146	404.2	6.34	1	600
96.0	4.87	150.6	0.146	404.2	6.34	1	600
120.0	4.87	150.6	0.146	404.2	6.34	1	600
144.0	4.87	150.6	0.146	404.2	6.34	1	600
168.0	4.87	150.6	0.146	404.2	6.34	1	600

192.0	4.87	150.6	0.146	404.2	6.34	1	600
216.0	4.87	150.6	0.146	404.2	6.34	1	600
240.0	4.87	150.6	0.146	404.2	6.34	1	600
264.0	4.87	150.6	0.146	404.2	6.34	1	600
288.0	4.87	150.6	0.146	404.2	6.34	1	600
312.0	4.87	150.6	0.146	404.2	6.34	1	600
336.0	4.87	150.6	0.146	404.2	6.34	1	600
360.0	4.87	150.6	0.146	404.2	6.34	1	600
384.0	4.87	150.6	0.146	404.2	6.34	1	600
408.0	4.87	150.6	0.146	404.2	6.34	1	600
432.0	4.87	150.6	0.146	404.2	6.34	1	600
456.0	4.87	150.6	0.146	404.2	6.34	1	600
480.0	4.87	150.6	0.146	404.2	6.34	1	600
504.0	4.87	150.6	0.146	404.2	6.34	1	600
528.0	4.87	150.6	0.146	404.2	6.34	1	600
552.0	4.87	150.6	0.146	404.2	6.34	1	600
576.0	4.87	150.6	0.146	404.2	6.34	1	600
600.0	4.87	150.6	0.146	404.2	6.34	1	600
624.0	4.87	150.6	0.146	404.2	6.34	1	600
648.0	4.87	150.6	0.146	404.2	6.34	1	600
672.0	4.87	150.6	0.146	404.2	6.34	1	600
696.0	4.87	150.6	0.146	404.2	6.34	1	600
720.0	4.87	150.6	0.146	404.2	6.34	1	600

2

2

732.000000   5.7878000   -1.000000

734.000000   -1.000000   0.1510000

p306

6

1

31

0.0	21.54	154.58	0.14	405.13	6.16	1	600
24.0	21.54	154.58	0.14	405.13	6.16	1	600
48.0	21.54	154.58	0.14	405.13	6.16	1	600
72.0	21.54	154.58	0.14	405.13	6.16	1	600
96.0	21.54	154.58	0.14	405.13	6.16	1	600
120.0	21.54	154.58	0.14	405.13	6.16	1	600
144.0	21.54	154.58	0.14	405.13	6.16	1	600
168.0	21.54	154.58	0.14	405.13	6.16	1	600
192.0	21.54	154.58	0.14	405.13	6.16	1	600
216.0	21.54	154.58	0.14	405.13	6.16	1	600
240.0	21.54	154.58	0.14	405.13	6.16	1	600
264.0	21.54	154.58	0.14	405.13	6.16	1	600
288.0	21.54	154.58	0.14	405.13	6.16	1	600
312.0	21.54	154.58	0.14	405.13	6.16	1	600
336.0	21.54	154.58	0.14	405.13	6.16	1	600
360.0	21.54	154.58	0.14	405.13	6.16	1	600
384.0	21.54	154.58	0.14	405.13	6.16	1	600
408.0	21.54	154.58	0.14	405.13	6.16	1	600
432.0	21.54	154.58	0.14	405.13	6.16	1	600
456.0	21.54	154.58	0.14	405.13	6.16	1	600
480.0	21.54	154.58	0.14	405.13	6.16	1	600
504.0	21.54	154.58	0.14	405.13	6.16	1	600
528.0	21.54	154.58	0.14	405.13	6.16	1	600
552.0	21.54	154.58	0.14	405.13	6.16	1	600
576.0	21.54	154.58	0.14	405.13	6.16	1	600
600.0	21.54	154.58	0.14	405.13	6.16	1	600
624.0	21.54	154.58	0.14	405.13	6.16	1	600

648.0	21.54	154.58	0.14	405.13	6.16	1	600
672.0	21.54	154.58	0.14	405.13	6.16	1	600
696.0	21.54	154.58	0.14	405.13	6.16	1	600
720.0	21.54	154.58	0.14	405.13	6.16	1	600

2

2

723.000000	0.8521000	-1.000000
723.750000	-1.000000	0.0121000

p316

6

1

31

0.0	20.51	157.76	0.13	405.48	6.19	1	600
24.0	20.51	157.76	0.13	405.48	6.19	1	600
48.0	20.51	157.76	0.13	405.48	6.19	1	600
72.0	20.51	157.76	0.13	405.48	6.19	1	600
96.0	20.51	157.76	0.13	405.48	6.19	1	600
120.0	20.51	157.76	0.13	405.48	6.19	1	600
144.0	20.51	157.76	0.13	405.48	6.19	1	600
168.0	20.51	157.76	0.13	405.48	6.19	1	600
192.0	20.51	157.76	0.13	405.48	6.19	1	600
216.0	20.51	157.76	0.13	405.48	6.19	1	600
240.0	20.51	157.76	0.13	405.48	6.19	1	600
264.0	20.51	157.76	0.13	405.48	6.19	1	600
288.0	20.51	157.76	0.13	405.48	6.19	1	600
312.0	20.51	157.76	0.13	405.48	6.19	1	600
336.0	20.51	157.76	0.13	405.48	6.19	1	600
360.0	20.51	157.76	0.13	405.48	6.19	1	600
384.0	20.51	157.76	0.13	405.48	6.19	1	600

408.0	20.51	157.76	0.13	405.48	6.19	1	600
432.0	20.51	157.76	0.13	405.48	6.19	1	600
456.0	20.51	157.76	0.13	405.48	6.19	1	600
480.0	20.51	157.76	0.13	405.48	6.19	1	600
504.0	20.51	157.76	0.13	405.48	6.19	1	600
528.0	20.51	157.76	0.13	405.48	6.19	1	600
552.0	20.51	157.76	0.13	405.48	6.19	1	600
576.0	20.51	157.76	0.13	405.48	6.19	1	600
600.0	20.51	157.76	0.13	405.48	6.19	1	600
624.0	20.51	157.76	0.13	405.48	6.19	1	600
648.0	20.51	157.76	0.13	405.48	6.19	1	600
672.0	20.51	157.76	0.13	405.48	6.19	1	600
696.0	20.51	157.76	0.13	405.48	6.19	1	600
720.0	20.51	157.76	0.13	405.48	6.19	1	600

2

2

723.750000   1.0382000   -1.000000

724.250000   -1.000000   0.0299000

p327

6

1

31

0.0	21.95	161.75	0.12	405.54	6.18	1	600
24.0	21.95	161.75	0.12	405.54	6.18	1	600
48.0	21.95	161.75	0.12	405.54	6.18	1	600
72.0	21.95	161.75	0.12	405.54	6.18	1	600
96.0	21.95	161.75	0.12	405.54	6.18	1	600
120.0	21.95	161.75	0.12	405.54	6.18	1	600
144.0	21.95	161.75	0.12	405.54	6.18	1	600

168.0	21.95	161.75	0.12	405.54	6.18	1	600
192.0	21.95	161.75	0.12	405.54	6.18	1	600
216.0	21.95	161.75	0.12	405.54	6.18	1	600
240.0	21.95	161.75	0.12	405.54	6.18	1	600
264.0	21.95	161.75	0.12	405.54	6.18	1	600
288.0	21.95	161.75	0.12	405.54	6.18	1	600
312.0	21.95	161.75	0.12	405.54	6.18	1	600
336.0	21.95	161.75	0.12	405.54	6.18	1	600
360.0	21.95	161.75	0.12	405.54	6.18	1	600
384.0	21.95	161.75	0.12	405.54	6.18	1	600
408.0	21.95	161.75	0.12	405.54	6.18	1	600
432.0	21.95	161.75	0.12	405.54	6.18	1	600
456.0	21.95	161.75	0.12	405.54	6.18	1	600
480.0	21.95	161.75	0.12	405.54	6.18	1	600
504.0	21.95	161.75	0.12	405.54	6.18	1	600
528.0	21.95	161.75	0.12	405.54	6.18	1	600
552.0	21.95	161.75	0.12	405.54	6.18	1	600
576.0	21.95	161.75	0.12	405.54	6.18	1	600
600.0	21.95	161.75	0.12	405.54	6.18	1	600
624.0	21.95	161.75	0.12	405.54	6.18	1	600
648.0	21.95	161.75	0.12	405.54	6.18	1	600
672.0	21.95	161.75	0.12	405.54	6.18	1	600
696.0	21.95	161.75	0.12	405.54	6.18	1	600
720.0	21.95	161.75	0.12	405.54	6.18	1	600

2

2

724.580000   1.1000000   -1.000000

725.750000   -1.000000   0.0109000

p1014

6

1

31

0.0	8.57	151.6	0.15	406.57	6.29	1	600
24.0	8.57	151.6	0.15	406.57	6.29	1	600
48.0	8.57	151.6	0.15	406.57	6.29	1	600
72.0	8.57	151.6	0.15	406.57	6.29	1	600
96.0	8.57	151.6	0.15	406.57	6.29	1	600
120.0	8.57	151.6	0.15	406.57	6.29	1	600
144.0	8.57	151.6	0.15	406.57	6.29	1	600
168.0	8.57	151.6	0.15	406.57	6.29	1	600
192.0	8.57	151.6	0.15	406.57	6.29	1	600
216.0	8.57	151.6	0.15	406.57	6.29	1	600
240.0	8.57	151.6	0.15	406.57	6.29	1	600
264.0	8.57	151.6	0.15	406.57	6.29	1	600
288.0	8.57	151.6	0.15	406.57	6.29	1	600
312.0	8.57	151.6	0.15	406.57	6.29	1	600
336.0	8.57	151.6	0.15	406.57	6.29	1	600
360.0	8.57	151.6	0.15	406.57	6.29	1	600
384.0	8.57	151.6	0.15	406.57	6.29	1	600
408.0	8.57	151.6	0.15	406.57	6.29	1	600
432.0	8.57	151.6	0.15	406.57	6.29	1	600
456.0	8.57	151.6	0.15	406.57	6.29	1	600
480.0	8.57	151.6	0.15	406.57	6.29	1	600
504.0	8.57	151.6	0.15	406.57	6.29	1	600
528.0	8.57	151.6	0.15	406.57	6.29	1	600
552.0	8.57	151.6	0.15	406.57	6.29	1	600
576.0	8.57	151.6	0.15	406.57	6.29	1	600
600.0	8.57	151.6	0.15	406.57	6.29	1	600

624.0	8.57	151.6	0.15	406.57	6.29	1	600
648.0	8.57	151.6	0.15	406.57	6.29	1	600
672.0	8.57	151.6	0.15	406.57	6.29	1	600
696.0	8.57	151.6	0.15	406.57	6.29	1	600
720.0	8.57	151.6	0.15	406.57	6.29	1	600

2

4

348.500000	3.2400000	-1.000000
350.330000	-1.000000	0.0227000
730.880000	3.5300000	-1.000000
733.580000	-1.000000	0.0212000

p358

6

1

31

0.0	8.12	158.39	0.13	405.18	6.38	1	600
24.0	8.12	158.39	0.13	405.18	6.38	1	600
48.0	8.12	158.39	0.13	405.18	6.38	1	600
72.0	8.12	158.39	0.13	405.18	6.38	1	600
96.0	8.12	158.39	0.13	405.18	6.38	1	600
120.0	8.12	158.39	0.13	405.18	6.38	1	600
144.0	8.12	158.39	0.13	405.18	6.38	1	600
168.0	8.12	158.39	0.13	405.18	6.38	1	600
192.0	8.12	158.39	0.13	405.18	6.38	1	600
216.0	8.12	158.39	0.13	405.18	6.38	1	600
240.0	8.12	158.39	0.13	405.18	6.38	1	600
264.0	8.12	158.39	0.13	405.18	6.38	1	600
288.0	8.12	158.39	0.13	405.18	6.38	1	600
312.0	8.12	158.39	0.13	405.18	6.38	1	600

336.0	8.12	158.39	0.13	405.18	6.38	1	600
360.0	8.12	158.39	0.13	405.18	6.38	1	600
384.0	8.12	158.39	0.13	405.18	6.38	1	600
408.0	8.12	158.39	0.13	405.18	6.38	1	600
432.0	8.12	158.39	0.13	405.18	6.38	1	600
456.0	8.12	158.39	0.13	405.18	6.38	1	600
480.0	8.12	158.39	0.13	405.18	6.38	1	600
504.0	8.12	158.39	0.13	405.18	6.38	1	600
528.0	8.12	158.39	0.13	405.18	6.38	1	600
552.0	8.12	158.39	0.13	405.18	6.38	1	600
576.0	8.12	158.39	0.13	405.18	6.38	1	600
600.0	8.12	158.39	0.13	405.18	6.38	1	600
624.0	8.12	158.39	0.13	405.18	6.38	1	600
648.0	8.12	158.39	0.13	405.18	6.38	1	600
672.0	8.12	158.39	0.13	405.18	6.38	1	600
696.0	8.12	158.39	0.13	405.18	6.38	1	600
720.0	8.12	158.39	0.13	405.18	6.38	1	600

2

2

722.250000	2.6100000	-1.000000
723.000000	-1.000000	0.0129000

p3036

6

1

31

0.0	15.76	157.14	0.13	406.07	6.34	1	600
24.0	15.76	157.14	0.13	406.07	6.34	1	600
48.0	15.76	157.14	0.13	406.07	6.34	1	600
72.0	15.76	157.14	0.13	406.07	6.34	1	600

96.0	15.76	157.14	0.13	406.07	6.34	1	600
120.0	15.76	157.14	0.13	406.07	6.34	1	600
144.0	15.76	157.14	0.13	406.07	6.34	1	600
168.0	15.76	157.14	0.13	406.07	6.34	1	600
192.0	15.76	157.14	0.13	406.07	6.34	1	600
216.0	15.76	157.14	0.13	406.07	6.34	1	600
240.0	15.76	157.14	0.13	406.07	6.34	1	600
264.0	15.76	157.14	0.13	406.07	6.34	1	600
288.0	15.76	157.14	0.13	406.07	6.34	1	600
312.0	15.76	157.14	0.13	406.07	6.34	1	600
336.0	15.76	157.14	0.13	406.07	6.34	1	600
360.0	15.76	157.14	0.13	406.07	6.34	1	600
384.0	15.76	157.14	0.13	406.07	6.34	1	600
408.0	15.76	157.14	0.13	406.07	6.34	1	600
432.0	15.76	157.14	0.13	406.07	6.34	1	600
456.0	15.76	157.14	0.13	406.07	6.34	1	600
480.0	15.76	157.14	0.13	406.07	6.34	1	600
504.0	15.76	157.14	0.13	406.07	6.34	1	600
528.0	15.76	157.14	0.13	406.07	6.34	1	600
552.0	15.76	157.14	0.13	406.07	6.34	1	600
576.0	15.76	157.14	0.13	406.07	6.34	1	600
600.0	15.76	157.14	0.13	406.07	6.34	1	600
624.0	15.76	157.14	0.13	406.07	6.34	1	600
648.0	15.76	157.14	0.13	406.07	6.34	1	600
672.0	15.76	157.14	0.13	406.07	6.34	1	600
696.0	15.76	157.14	0.13	406.07	6.34	1	600
720.0	15.76	157.14	0.13	406.07	6.34	1	600

2

2

731.820000	1.9600000	-1.000000					
735.330000	-1.000000	0.0117000					

p1011

6

1

31

0.0	3.55	152.12	0.14	401.1	6.39	1	600
24.0	3.55	152.12	0.14	401.1	6.39	1	600
48.0	3.55	152.12	0.14	401.1	6.39	1	600
72.0	3.55	152.12	0.14	401.1	6.39	1	600
96.0	3.55	152.12	0.14	401.1	6.39	1	600
120.0	3.55	152.12	0.14	401.1	6.39	1	600
144.0	3.55	152.12	0.14	401.1	6.39	1	600
168.0	3.55	152.12	0.14	401.1	6.39	1	600
192.0	3.55	152.12	0.14	401.1	6.39	1	600
216.0	3.55	152.12	0.14	401.1	6.39	1	600
240.0	3.55	152.12	0.14	401.1	6.39	1	600
264.0	3.55	152.12	0.14	401.1	6.39	1	600
288.0	3.55	152.12	0.14	401.1	6.39	1	600
312.0	3.55	152.12	0.14	401.1	6.39	1	600
336.0	3.55	152.12	0.14	401.1	6.39	1	600
360.0	3.55	152.12	0.14	401.1	6.39	1	600
384.0	3.55	152.12	0.14	401.1	6.39	1	600
408.0	3.55	152.12	0.14	401.1	6.39	1	600
432.0	3.55	152.12	0.14	401.1	6.39	1	600
456.0	3.55	152.12	0.14	401.1	6.39	1	600
480.0	3.55	152.12	0.14	401.1	6.39	1	600
504.0	3.55	152.12	0.14	401.1	6.39	1	600
528.0	3.55	152.12	0.14	401.1	6.39	1	600

552.0	3.55	152.12	0.14	401.1	6.39	1	600
576.0	3.55	152.12	0.14	401.1	6.39	1	600
600.0	3.55	152.12	0.14	401.1	6.39	1	600
624.0	3.55	152.12	0.14	401.1	6.39	1	600
648.0	3.55	152.12	0.14	401.1	6.39	1	600
672.0	3.55	152.12	0.14	401.1	6.39	1	600
696.0	3.55	152.12	0.14	401.1	6.39	1	600
720.0	3.55	152.12	0.14	401.1	6.39	1	600

2

4

337.200000	5.4800000	-1.000000
338.730000	-1.000000	0.0332000
734.166000	7.5800000	-1.000000
735.500000	-1.000000	0.0475000

p1018

6

1

31

0.0	5.78	165.14	0.11	410.9	6.08	1	600
24.0	5.78	165.14	0.11	410.9	6.08	1	600
48.0	5.78	165.14	0.11	410.9	6.08	1	600
72.0	5.78	165.14	0.11	410.9	6.08	1	600
96.0	5.78	165.14	0.11	410.9	6.08	1	600
120.0	5.78	165.14	0.11	410.9	6.08	1	600
144.0	5.78	165.14	0.11	410.9	6.08	1	600
168.0	5.78	165.14	0.11	410.9	6.08	1	600
192.0	5.78	165.14	0.11	410.9	6.08	1	600
216.0	5.78	165.14	0.11	410.9	6.08	1	600
240.0	5.78	165.14	0.11	410.9	6.08	1	600

264.0	5.78	165.14	0.11	410.9	6.08	1	600
288.0	5.78	165.14	0.11	410.9	6.08	1	600
312.0	5.78	165.14	0.11	410.9	6.08	1	600
336.0	5.78	165.14	0.11	410.9	6.08	1	600
360.0	5.78	165.14	0.11	410.9	6.08	1	600
384.0	5.78	165.14	0.11	410.9	6.08	1	600
408.0	5.78	165.14	0.11	410.9	6.08	1	600
432.0	5.78	165.14	0.11	410.9	6.08	1	600
456.0	5.78	165.14	0.11	410.9	6.08	1	600
480.0	5.78	165.14	0.11	410.9	6.08	1	600
504.0	5.78	165.14	0.11	410.9	6.08	1	600
528.0	5.78	165.14	0.11	410.9	6.08	1	600
552.0	5.78	165.14	0.11	410.9	6.08	1	600
576.0	5.78	165.14	0.11	410.9	6.08	1	600
600.0	5.78	165.14	0.11	410.9	6.08	1	600
624.0	5.78	165.14	0.11	410.9	6.08	1	600
648.0	5.78	165.14	0.11	410.9	6.08	1	600
672.0	5.78	165.14	0.11	410.9	6.08	1	600
696.0	5.78	165.14	0.11	410.9	6.08	1	600
720.0	5.78	165.14	0.11	410.9	6.08	1	600

2

4

346.880000   4.2300000   -1.000000

348.830000   -1.000000   0.0237000

732.380000   -1.000000   0.0123800

737.660000   4.6800000   -1.000000

p336

6

1

31

0.0	11.05	155.45	0.135	405.4	6.32	1	600
24.0	11.05	155.45	0.135	405.4	6.32	1	600
48.0	11.05	155.45	0.135	405.4	6.32	1	600
72.0	11.05	155.45	0.135	405.4	6.32	1	600
96.0	11.05	155.45	0.135	405.4	6.32	1	600
120.0	11.05	155.45	0.135	405.4	6.32	1	600
144.0	11.05	155.45	0.135	405.4	6.32	1	600
168.0	11.05	155.45	0.135	405.4	6.32	1	600
192.0	11.05	155.45	0.135	405.4	6.32	1	600
216.0	11.05	155.45	0.135	405.4	6.32	1	600
240.0	11.05	155.45	0.135	405.4	6.32	1	600
264.0	11.05	155.45	0.135	405.4	6.32	1	600
288.0	11.05	155.45	0.135	405.4	6.32	1	600
312.0	11.05	155.45	0.135	405.4	6.32	1	600
336.0	11.05	155.45	0.135	405.4	6.32	1	600
360.0	11.05	155.45	0.135	405.4	6.32	1	600
384.0	11.05	155.45	0.135	405.4	6.32	1	600
408.0	11.05	155.45	0.135	405.4	6.32	1	600
432.0	11.05	155.45	0.135	405.4	6.32	1	600
456.0	11.05	155.45	0.135	405.4	6.32	1	600
480.0	11.05	155.45	0.135	405.4	6.32	1	600
504.0	11.05	155.45	0.135	405.4	6.32	1	600
528.0	11.05	155.45	0.135	405.4	6.32	1	600
552.0	11.05	155.45	0.135	405.4	6.32	1	600
576.0	11.05	155.45	0.135	405.4	6.32	1	600
600.0	11.05	155.45	0.135	405.4	6.32	1	600
624.0	11.05	155.45	0.135	405.4	6.32	1	600
648.0	11.05	155.45	0.135	405.4	6.32	1	600

672.0	11.05	155.45	0.135	405.4	6.32	1	600
696.0	11.05	155.45	0.135	405.4	6.32	1	600
720.0	11.05	155.45	0.135	405.4	6.32	1	600

2

2

734.750000	2.5400000	-1.000000
736.460000	-1.000000	0.0199000

p353

6

1

31

0.0	18.64	150.11	0.15	404.88	6.17	1	600
24.0	18.64	150.11	0.15	404.88	6.17	1	600
48.0	18.64	150.11	0.15	404.88	6.17	1	600
72.0	18.64	150.11	0.15	404.88	6.17	1	600
96.0	18.64	150.11	0.15	404.88	6.17	1	600
120.0	18.64	150.11	0.15	404.88	6.17	1	600
144.0	18.64	150.11	0.15	404.88	6.17	1	600
168.0	18.64	150.11	0.15	404.88	6.17	1	600
192.0	18.64	150.11	0.15	404.88	6.17	1	600
216.0	18.64	150.11	0.15	404.88	6.17	1	600
240.0	18.64	150.11	0.15	404.88	6.17	1	600
264.0	18.64	150.11	0.15	404.88	6.17	1	600
288.0	18.64	150.11	0.15	404.88	6.17	1	600
312.0	18.64	150.11	0.15	404.88	6.17	1	600
336.0	18.64	150.11	0.15	404.88	6.17	1	600
360.0	18.64	150.11	0.15	404.88	6.17	1	600
384.0	18.64	150.11	0.15	404.88	6.17	1	600
408.0	18.64	150.11	0.15	404.88	6.17	1	600

432.0	18.64	150.11	0.15	404.88	6.17	1	600
456.0	18.64	150.11	0.15	404.88	6.17	1	600
480.0	18.64	150.11	0.15	404.88	6.17	1	600
504.0	18.64	150.11	0.15	404.88	6.17	1	600
528.0	18.64	150.11	0.15	404.88	6.17	1	600
552.0	18.64	150.11	0.15	404.88	6.17	1	600
576.0	18.64	150.11	0.15	404.88	6.17	1	600
600.0	18.64	150.11	0.15	404.88	6.17	1	600
624.0	18.64	150.11	0.15	404.88	6.17	1	600
648.0	18.64	150.11	0.15	404.88	6.17	1	600
672.0	18.64	150.11	0.15	404.88	6.17	1	600
696.0	18.64	150.11	0.15	404.88	6.17	1	600
720.0	18.64	150.11	0.15	404.88	6.17	1	600

2

2

721.750000   0.81300000   -1.000000

723.670000   -1.000000   0.0124000

p328

6

1

31

0.0	7.998	153.22	0.14	405.24	6.3	1	600
24.0	7.998	153.22	0.14	405.24	6.3	1	600
48.0	7.998	153.22	0.14	405.24	6.3	1	600
72.0	7.998	153.22	0.14	405.24	6.3	1	600
96.0	7.998	153.22	0.14	405.24	6.3	1	600
120.0	7.998	153.22	0.14	405.24	6.3	1	600
144.0	7.998	153.22	0.14	405.24	6.3	1	600
168.0	7.998	153.22	0.14	405.24	6.3	1	600

192.0	7.998	153.22	0.14	405.24	6.3	1	600
216.0	7.998	153.22	0.14	405.24	6.3	1	600
240.0	7.998	153.22	0.14	405.24	6.3	1	600
264.0	7.998	153.22	0.14	405.24	6.3	1	600
288.0	7.998	153.22	0.14	405.24	6.3	1	600
312.0	7.998	153.22	0.14	405.24	6.3	1	600
336.0	7.998	153.22	0.14	405.24	6.3	1	600
360.0	7.998	153.22	0.14	405.24	6.3	1	600
384.0	7.998	153.22	0.14	405.24	6.3	1	600
408.0	7.998	153.22	0.14	405.24	6.3	1	600
432.0	7.998	153.22	0.14	405.24	6.3	1	600
456.0	7.998	153.22	0.14	405.24	6.3	1	600
480.0	7.998	153.22	0.14	405.24	6.3	1	600
504.0	7.998	153.22	0.14	405.24	6.3	1	600
528.0	7.998	153.22	0.14	405.24	6.3	1	600
552.0	7.998	153.22	0.14	405.24	6.3	1	600
576.0	7.998	153.22	0.14	405.24	6.3	1	600
600.0	7.998	153.22	0.14	405.24	6.3	1	600
624.0	7.998	153.22	0.14	405.24	6.3	1	600
648.0	7.998	153.22	0.14	405.24	6.3	1	600
672.0	7.998	153.22	0.14	405.24	6.3	1	600
696.0	7.998	153.22	0.14	405.24	6.3	1	600
720.0	7.998	153.22	0.14	405.24	6.3	1	600

2

2

733.250000   3.5800000   -1.000000

734.130000   -1.000000   0.0248000

p3015

6

1

31

0.0	31.22	140.77	0.195	405.24	6.36	1.037	600
24.0	31.22	140.77	0.195	405.24	6.36	1.037	600
48.0	31.22	140.77	0.195	405.24	6.36	1.037	600
72.0	31.22	140.77	0.195	405.24	6.36	1.037	600
96.0	31.22	140.77	0.195	405.24	6.36	1.037	600
120.0	31.22	140.77	0.195	405.24	6.36	1.037	600
144.0	31.22	140.77	0.195	405.24	6.36	1.037	600
168.0	31.22	140.77	0.195	405.24	6.36	1.037	600
192.0	31.22	140.77	0.195	405.24	6.36	1.037	600
216.0	31.22	140.77	0.195	405.24	6.36	1.037	600
240.0	31.22	140.77	0.195	405.24	6.36	1.037	600
264.0	31.22	140.77	0.195	405.24	6.36	1.037	600
288.0	31.22	140.77	0.195	405.24	6.36	1.037	600
312.0	31.22	140.77	0.195	405.24	6.36	1.037	600
336.0	31.22	140.77	0.195	405.24	6.36	1.037	600
360.0	31.22	140.77	0.195	405.24	6.36	1.037	600
384.0	31.22	140.77	0.195	405.24	6.36	1.037	600
408.0	31.22	140.77	0.195	405.24	6.36	1.037	600
432.0	31.22	140.77	0.195	405.24	6.36	1.037	600
456.0	31.22	140.77	0.195	405.24	6.36	1.037	600
480.0	31.22	140.77	0.195	405.24	6.36	1.037	600
504.0	31.22	140.77	0.195	405.24	6.36	1.037	600
528.0	31.22	140.77	0.195	405.24	6.36	1.037	600
552.0	31.22	140.77	0.195	405.24	6.36	1.037	600
576.0	31.22	140.77	0.195	405.24	6.36	1.037	600
600.0	31.22	140.77	0.195	405.24	6.36	1.037	600
624.0	31.22	140.77	0.195	405.24	6.36	1.037	600

648.0	31.22	140.77	0.195	405.24	6.36	1.037	600
672.0	31.22	140.77	0.195	405.24	6.36	1.037	600
696.0	31.22	140.77	0.195	405.24	6.36	1.037	600
720.0	31.22	140.77	0.195	405.24	6.36	1.037	600

2

2

737.000000	0.62090000	-1.000000
740.060000	-1.000000	0.0072499

p3022

6

1

31

0.0	5.54	158.53	0.128	404.69	6.4	1.006	600
24.0	5.54	158.53	0.128	404.69	6.4	1.006	600
48.0	5.54	158.53	0.128	404.69	6.4	1.006	600
72.0	5.54	158.53	0.128	404.69	6.4	1.006	600
96.0	5.54	158.53	0.128	404.69	6.4	1.006	600
120.0	5.54	158.53	0.128	404.69	6.4	1.006	600
144.0	5.54	158.53	0.128	404.69	6.4	1.006	600
168.0	5.54	158.53	0.128	404.69	6.4	1.006	600
192.0	5.54	158.53	0.128	404.69	6.4	1.006	600
216.0	5.54	158.53	0.128	404.69	6.4	1.006	600
240.0	5.54	158.53	0.128	404.69	6.4	1.006	600
264.0	5.54	158.53	0.128	404.69	6.4	1.006	600
288.0	5.54	158.53	0.128	404.69	6.4	1.006	600
312.0	5.54	158.53	0.128	404.69	6.4	1.006	600
336.0	5.54	158.53	0.128	404.69	6.4	1.006	600
360.0	5.54	158.53	0.128	404.69	6.4	1.006	600
384.0	5.54	158.53	0.128	404.69	6.4	1.006	600

408.0	5.54	158.53	0.128	404.69	6.4	1.006	600
432.0	5.54	158.53	0.128	404.69	6.4	1.006	600
456.0	5.54	158.53	0.128	404.69	6.4	1.006	600
480.0	5.54	158.53	0.128	404.69	6.4	1.006	600
504.0	5.54	158.53	0.128	404.69	6.4	1.006	600
528.0	5.54	158.53	0.128	404.69	6.4	1.006	600
552.0	5.54	158.53	0.128	404.69	6.4	1.006	600
576.0	5.54	158.53	0.128	404.69	6.4	1.006	600
600.0	5.54	158.53	0.128	404.69	6.4	1.006	600
624.0	5.54	158.53	0.128	404.69	6.4	1.006	600
648.0	5.54	158.53	0.128	404.69	6.4	1.006	600
672.0	5.54	158.53	0.128	404.69	6.4	1.006	600
696.0	5.54	158.53	0.128	404.69	6.4	1.006	600
720.0	5.54	158.53	0.128	404.69	6.4	1.006	600

2

2

723.000000	4.1626000	-1.000000
726.750000	-1.000000	0.1639999

Model code: Source file – EFV_population_human.for


```
C###############################################################
###C

      Subroutine DIFFEQ(T,X,XP)
      Implicit None

      Include 'globals.inc'
      Include 'model.inc'

      Real*8 T,X(MaxNDE),XP(MaxNDE), CL,V2,Ka,V3,CLD,Ktr,Kpc,Kcp
      Real*8 Kpb,Kbp,Kcb,Kbc,V8
CC
C-------------------------------------------------------------------
---C
C   Enter Differential Equations Below  {e.g.  XP(1) = -P(1)*X(1) }
C
C----c-------------------------------------------------------------
---C
       CL=R(1)
       V2=R(2)+0.01
       Ka=R(3)
       V3=R(4)
       CLD=R(5)
      Ktr=R(6)
      Kpc=P(1)
      Kcp=P(2)
      Kpb=P(3)
      Kbp=P(4)
      Kcb=P(5)
      Kbc=P(6)
      V8=P(7)


      XP(1) = -Ktr*X(1)
       XP(2) = Ktr*X(1) -Ktr*X(2)
       XP(3) = Ktr*X(2) - Ktr*X(3)
       XP(4) = Ktr*X(3) -Ka*X(4)
      XP(5) = Ka*X(4)- CL*(X(5)/V2)- CLD*(X(5)/V2)
    x  +CLD*(X(6)/V3)
      XP(6) = CLD*(X(5)/V2)- CLD*(X(6)/V3)
     XP(7) = Kpc*X(5) -Kcp*X(7) -Kcb*X(7) +Kbc*X(8) !CSF
     XP(8) = Kcb*X(7) -Kbc*X(8) +Kpb*X(5) -Kbp*X(8) !brain
```

APPENDIX-5: RELEVANT PREVIOUSLY PUBLISHED ABSTRACTS

ABSTRACT PRESENTED AT THE AMERICAN SOCIETY OF CLINICAL PHARMACOLOGY AND THERAPEUTICS 2018 CONFERENCE, ORLANDO, FLORIDA

Development and Application of a Population Pharmacokinetic (PK) Model of Maraviroc to Predict HIV Pre-Exposure Prophylaxis (PrEP) Efficacy in Mucosal Tissues

Nithya Srinivas, Mackenzie Cottrell, Nicole White, Craig Sykes, Heather Prince, Daniel Gonzalez & Angela DM Kashuba

Maraviroc (MVC) monotherapy 300 mg daily has been studied in a phase 2 trial as a chemoprophylactic against HIV. Infection occurred in 4 men with low MVC plasma concentrations. Using data from a phase 1 dose-ranging study, we developed a predictive PK model for MVC in plasma, rectal tissue (RT) and female genital tract tissue (FGT) and explored the effect of adherence on efficacy.

PK data were taken from a single-dose study of 24 women given 150, 300 or 600 mg of MVC and sampled in plasma, RT and FGT over 48 h (NCT01330199). A population PK model was developed using NONMEM 7.4. Goodness of fit was assessed by standard diagnostic plots and visual predictive checks. Using the final model, Monte Carlo simulations were performed to simulate 1000 virtual subjects taking 300 mg MVC daily. PrEP efficacy with imperfect adherence was explored by using 2 targets from published tissue explant data: EC80 (1 uM in FGT, 0.63 uM in RT) and complete protection (100 uM).

A 10-compartment linear model captured 90% of the data. 5 transit compartments described accumulation in RT. In simulated subjects, steady state was achieved after a single dose in FGT and 10 doses in RT. Even with 100% adherence, 0% of the virtual subjects achieved protection in FGT using the 2 targets. Adherence had little effect on protection in RT: 100% of population with 30% adherence (2 doses/week) reached the EC80 target, while 0% population with 100% adherence reached the complete inhibition target.

The variable estimates of MVC exposure associated with favorable efficacy identified in literature profoundly affected the outcome of the simulations. However, these data suggest that oral MVC monotherapy may not achieve suitable PrEP efficacy in all populations, and if used, should be combined with other active agents.

Mapping the Distribution of Efavirenz Relative to Brain Tissue Cells

Nithya Srinivas, Elias P Rosen, Gabriela De La Cruz, Craig Sykes, Amanda Schauer, Lourdes Adamson, Paul Luciw & Angela DM Kashuba
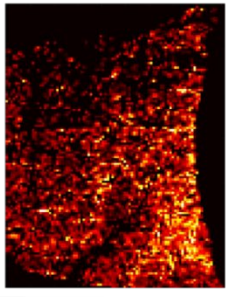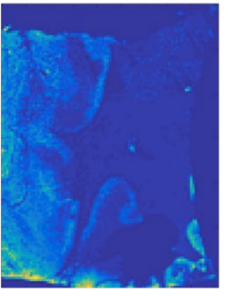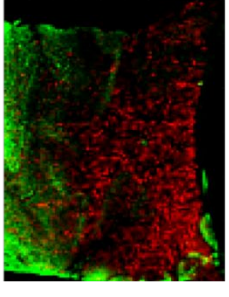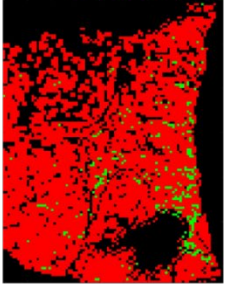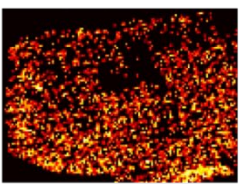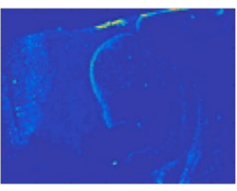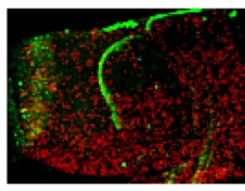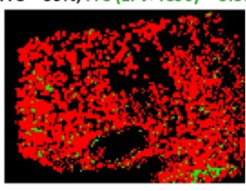
Despite ongoing antiretroviral (ARV) therapy, HIV continues to persist in the central nervous system (CNS), as demonstrated by the establishment of latent microglia reservoirs and HIV-associated neurocognitive disorder. HIV persistence in the brain may be due to inadequate drug exposure in HIV-target cells; however, there is little information on brain distribution of ARVs. In this study, we have quantified the concentration of 4 ARVs in brain tissue by LC-MS/MS and infrared matrix-assisted laser desorption electrospray ionization (IR-MALDESI) while mapping their distribution relative to expression of CD4+ T-cells and CD11b+ microglia.

In 4 male macaques (2 uninfected; 2 SHIV-infected) dosed to steady-state, concentrations of 4 ARVs – tenofovir (TFV), emtricitabine (FTC), efavirenz (EFV), and raltegravir (RAL) were measured in 10-micron cerebellum tissue slices by LC-MS/MS (LLOQ of homogenate ranged from 0.002-0.01 ng/mL). IR-MALDESI mass spectrometry imaging (MSI) was used to characterize drug distribution. Density of 1.06g/cm3 was used to convert tissue concentrations to ng/g. Immunohistochemistry (IHC) staining of CD11b+ microglia and CD4+ T-cells was performed on contiguous slices. Image analysis of co-registered MSI and down-sampled IHC images was performed in MATLAB.

TFV, FTC, and RAL were not detected by MALDESI and were <100 ng/g by LC-MS/MS (range of concentration was 9.4-61.2 ng/g). EFV concentrations by IR-MALDESI had a standard deviation of 663 ng/g for all samples and was 2.2-fold greater in SHIV- than SHIV+ brain (median = 1596 and 723 ng/g, respectively). The fractional coverage of target cells co-localized with EFV (FrC) differed based on infection status: for CD11b FrC = 22-59% (SHIV+) and 76-81% (SHIV-) and for CD4 FrC = 14-59% (SHIV+) and 73-77% (SHIV-). However, the FrC of total CD11b and CD4 cells exposed to EFV concentrations above IC50 (0.5 ng/g) was considerably smaller: 0-3.3%, regardless of infection status (Figure 1, panel IV).

EFV accumulation was 12 to 60-fold greater in brain tissue compared to other ARVs in SHIV+ animals but only 14% to 59% of CD11b and CD4 brain cells in these animals were colocalized with detectable EFV. This suggests that ARV coverage may be incomplete for cell populations that harbor, or can become infected, with HIV. We have shown in this preliminary analysis that this approach has the potential to provide ARV concentration-effect relationships in the brain at the cellular level.

Figure 1

	EFV distribution in cerebellum	CD11b distribution in cerebellum	Overlay of EFV and CD11b distribution in cerebellum	EFV (<IC50, >IC50) colocalization with CD11b
SHIV -ve				FrC = 76%, FrC (EFV>IC50) = 2.6%
SHIV +ve				FrC = 59%, FrC (EFV>IC50) = 3.3%

SHIV Infection and Drug Transporters Influence Brain Tissue Concentrations of Efavirenz

Nithya Srinivas, John K Fallon, Craig Sykes, Nicole White, Amanda Schauer, Michelle Matthews, Lourdes Adamson, Paul Luciw, Phil Smith & Angela DM Kashuba

Despite antiretroviral (ARV) therapy, there is a high prevalence of HIV-associated neurocognitive disorder (HAND) in HIV-infected individuals. Using CSF data, it has been theorized that inadequate ARV concentrations may contribute. However, information on brain tissue concentrations is sparse. This study compared the concentration of ARVs in four regions of brain tissue with CSF in uninfected and SHIV-infected rhesus macaques.

In 12 male macaques (6 uninfected; 6 SHIV-infected) dosed to steady-state, concentrations of 6 ARVs – tenofovir (TFV), emtricitabine (FTC), efavirenz (EFV), raltegravir (RAL), maraviroc (MVC) and atazanavir (ATZ) were measured by LC-MS/MS in the CSF (LLOQ=0.5 ng/mL) and cerebrum, cerebellum, basal ganglia and parietal cortex regions of the brain (LLOQ of homogenate ranged from 0.002-0.01 ng/mL). Tissue concentrations were converted to ng/g using density of 1.06. To assess the influence of drug transporters on ARV concentration, brain tissue was analyzed for P-gp and BCRP efflux transporter proteins by LC-MS proteomics (LLOQ=0.1 pmol/mg protein). Data are presented as median (range); statistical analysis was by Kruskal-Wallis test.

CSF concentrations did not differ by infection status (p>0.1). Since there was no difference in ARV concentration in the various regions of the brain (p>0.1), these data were combined. Concentrations in brain tissue were significantly greater than CSF for TFV, FTC and EFV: ranging from 5-times (FTC) to 769- times (EFV) higher. Brain tissue concentration of EFV was 4.1 times higher in uninfected animals. BCRP concentration was 1.7 times higher in infected animals (p=0.02); P-gp concentration did not differ with infection status (p=0.06).

In this study, brain tissue concentration of EFV was 4-fold lower in infected macaques and this may be due to increased BCRP concentrations. Further, we have shown that ARV CSF concentrations may need cautious interpretation when used as surrogate for brain tissue exposure. Based on these data, further investigations are needed to determine how ARV brain tissue concentrations influence HAND prevalence.

	CSF concentration (ng/mL)		Brain tissue concentration (ng/g)	
	Uninfected	Infected	Uninfected	Infected
TFV	0.8 (0.0, 4.6)	2.2 (1.5, 3)	55.0 (47.1, 392.1)	34.9 (22.7, 65.1)
FTC	2.1 (0.o, 11.7)	5.7 (3.9, 7.3)	29.9 (17.1, 69.2)	28.4 (14.8, 33.6)
EFV	2.1 (1.4, 3.4)	0.5 (0.5, 1.4)	1615.2 (965.2, 1983.0)	391.6 (239.8, 792.3)
RAL	1.2	0.5	27.7	14.7

	(0.6, 1.3)	(0.5, 0.5)	(15.8, 78.3)	(9.7, 21.8)
MVC	2.9 (0.5, 11.1)	0.0 (0.0, 0.0)	57.5 (21.9, 193.0)	48.7 (34.8, 104.8)
ATZ	0.5 (0.0, 40.5)	0.5 (0.5, 0.5)	84.1 (49.7, 554.1)	133.1 (59.4, 138.0)

ABSTRACT PRESENTED AT THE AMERICAN SOCIETY OF CLINICAL PHARMACOLOGY AND THERAPEUTICS 2016 CONFERENCE, SAN DIEGO, CALIFORNIA

Antiretroviral Drug Exposure in Cerebrospinal Fluid (CSF) as a Predictor of Neurocognitive Outcomes in HIV Infected Patients

Nithya Srinivas, Kuo H Yang, John W Collins, Craig Sykes, Sarah-Beth Joseph, Kevin R Robertson, Joseph J Eron, Ronald Swanstrom & Angela DM Kashuba

Neurocognitive impairment in HIV patients remains prevalent despite potent antiretroviral therapy. This may be related to drug penetration into the central nervous system. Here we use a population pharmacokinetic (PK) model to estimate exposure of tenofovir (TFV), emtricitabine (FTC) and darunavir boosted with ritonavir (DRV/r) in CSF over a dosing interval and explore the relationship with neurocognitive outcomes.

In the HIV Tropism, Persistence, Inflammation and Neurocognition in Therapy Initiation Cohort (THINC), we selected 8 subjects on TFV /FTV /DRV /r whose plasma HIV RNA was <40 copies/ml for <'.12mos. One paired plasma and CSF sample was obtained in each subject and analyzed by LC-MS/MS. Published plasma PK models were used for Bayesian posthoc estimates of exposure. CSF data were added and uptake into CSF estimated (NONMEM 7.3). CSF AUC penetration ratio was calculated as (CSF_{AUC}/$plasma_{AUC}$)*100. Neurocognitive impairment was assessed by global deficit score (GDS) and Z test and correlated with CSF drug exposure (R studio). Median data are reported.

The population model captured 99% of observed data. Uptake (mL/h) into CSF was determined to be 14, 164 and 11 for TFV, FTC and DRV and inter individual variability (CV%) was 60, 35 and 84. CSF concentrations (ng/ml) averaged over dosing interval were 7, 103 and 32, respectively. Penetration ratios were 4%, 19% and 1%. Increased DRV exposure in CSF correlated with lower total Z score and worse neurocognitive performance (r=-0.73, p=0.04), whereas TFV and FTC did not.

Quantification of antiretroviral penetration into CSF across the dosing interval is possible with sparse data. In this small study, increased CSF DRV exposure was associated with poorer neurocognition and warrants further investigation.